The Astrophysical Journal, 864:158 (51pp), 2018 September 10 https://doi.org/10.3847/1538-4357/aad8b3

Self-consistent Energetic Particle Acceleration by Contracting and Reconnecting Small-scale Flux Ropes: The Governing Equations

J. A. le Roux[1,2], G. P. Zank[1,2], and O. V. Khabarova[3]
[1] Department of Space Science, University of Alabama in Huntsville, Huntsville, AL 35805, USA
[2] Center for Space Plasma and Aeronomic Research (CSPAR), University of Alabama in Huntsville, Huntsville, AL 35805, USA
[3] Heliophysical Laboratory, Pushkov Institute of Terrestrial Magnetism, Ionosphere and Radiowave Propagation RAS (IZMIRAN), Troitsk, Moscow 142190, Russia
Received 2018 June 11; revised 2018 August 3; accepted 2018 August 4; published 2018 September 12

Abstract

Previous application of our focused transport equation for energetic ion test particle acceleration by numerous active small-scale flux ropes to solar wind conditions near 1 au yielded the formation of hard power-law spectra with high particle pressure. We present an extended theory where the focused transport equation is coupled to a new MHD turbulence transport equation for coherent, quasi-2D magnetic island structures, based on nearly incompressible (N I) MHD turbulence theory. The latter equation includes new expressions for the magnetic island damping/growth rates that enable a self-consistent description of energy exchange between energetic particles and flux ropes during flux-rope acceleration for four flux-rope acceleration scenarios identified in focused transport theory. Revised, more detailed expressions for coherent acceleration in response to mean dynamic flux-rope properties and for stochastic acceleration due to fluctuations in dynamic flux-rope properties are presented. A comparison is made between the efficiencies of the different flux-rope acceleration scenarios for suprathermal protons in the solar wind near 1 au. Dynamic flux-rope-induced pitch-angle scattering and stochastic acceleration rates are compared with the corresponding rates generated by interaction with parallel-propagating Alfvén waves. The results stress the importance of parallel guiding center motion acceleration by the parallel reconnection electric field formed in merging flux ropes, combined curvature drift and generalized betatron acceleration in contracting/merging flux ropes in the compressible limit (flux-rope compression acceleration), and the fluctuating magnetic mirroring force in flux ropes for pitch-angle scattering.

Key words: acceleration of particles – magnetic reconnection – solar wind

1. Energetic Particle Acceleration by Small-scale Flux Ropes near Primary Current Sheets

One of the enduring unsolved problems in heliospheric space physics is the observed formation of energetic ion power-law spectra in the suprathermal energy range of ∼1–100 keV in the solar wind that were found to exist in quiet and turbulent solar wind conditions (e.g., Fisk & Gloeckler 2006; Dayeh et al. 2009; Hill & Hamilton 2010). Besides using diffusive shock acceleration (DSA) theory and modeling at traveling shocks to explain these power laws (e.g., Zank et al. 2000; Giacalone 2005; Kóta et al. 2005; Lee 2005; Li et al. 2005; Ng & Reames 2008; le Roux & Webb 2012; Verkhoglyadova et al. 2015), other earlier attempts involved traditional quasi-linear kinetic theories invoking second-order Fermi acceleration via resonant particle interactions with magnetohydrodynamic (MHD) waves. For example, Fisk (1976) and Schwadron et al. (1996) proposed energetic ion acceleration as a consequence of particles undergoing the magnetic analog of a Landau resonance with obliquely propagating fast-mode magnetosonic waves. Others have considered energetic ion acceleration involving the gyroresonant interaction of particles with parallel-propagating Alfvén waves (e.g., Isenberg 1987; Bogdan et al. 1991; Fichthner et al. 1996). Another possibility is ion acceleration due to nonresonant particle interactions with intermediate-scale compressive solar wind velocity fluctuations (e.g., Fisk & Gloeckler 2008; Fisk et al. 2010; Antecki et al. 2013; Zhang & Lee 2013; Fisk & Gloeckler 2014). The combination of DSA with downstream second-order Fermi acceleration by parallel-propagating Alfvén waves has been considered by Campeanu & Schlickeiser (1992), Vanio & Schlickeiser (1998), and Ng & Reames (2008).

However, in recent years evidence has been accumulating for the existence of small-scale flux ropes with cross sections coinciding with wavelengths of magnetic turbulence in the inertial range (i.e., cross-section scales of ∼0.01 au and less) in the solar wind near Earth. In this paper small-scale flux ropes are considered as coherent, quasi-2D nonlinear structures advected with the large-scale solar wind flow consisting of a twist, or island, magnetic field component in the 2D plane perpendicular to an out-of-plane axial, or guide/background, magnetic field component (e.g., Cartwright & Moldwin 2010). It has been argued that small-scale flux-rope structures are generated locally near 1 au through magnetic reconnection at primary current sheets such as the heliospheric current sheet and primary current sheets associated with interplanetary coronal mass ejections and corotating interaction regions (e.g., Cartwright & Moldwin 2010; Eriksson et al. 2015; Khabarova et al. 2015, 2016). Observational evidence suggests active small-scale flux ropes that merge as a consequence of magnetic reconnection at secondary current sheets formed between neighboring magnetic islands (e.g., Song et al. 2012; Khabarova et al. 2015, 2016; Zheng et al. 2017). In situ observational evidence also supports the idea that solar wind regions containing merging (reconnecting) small-scale flux ropes near primary current sheets in the solar wind are responsible for the energization of electrons and ions (Khabarova et al. 2015, 2016; Khabarova & Zank 2017; Zheng et al. 2017). Furthermore, there are indications that small-scale flux ropes can be especially efficient accelerators when subject to strong plasma compression (Khabarova et al. 2015, 2016; Guidoni et al. 2016). For example, during interaction between the heliospheric current sheet and interplanetary coronal mass ejections, magnetic reconnection becomes more efficient at the disturbed heliospheric

current sheet, and the production of small-scale flux ropes intensifies. In addition, these structures experience strong compression between the converging heliospheric current sheet and the primary current sheets of interplanetary coronal mass ejections, suggesting that island contraction and merging occur in the compressible limit. This provides a possible explanation for the observed strong enhancements in energetic particle fluxes up to MeV energies behind traveling shocks (Khabarova et al. 2015; Khabarova & Zank 2017), which prompted Zank et al. (2015a) and le Roux et al. (2016) to theoretically investigate the combination of DSA of energetic particles at shocks with downstream acceleration of these particles by contracting and merging small-scale flux ropes.

Simultaneous with these observational developments, microscopic kinetic and macroscopic MHD simulations of turbulent magnetic reconnection at single or multiple primary current sheets emphasize that efficient particle energization can occur (e.g., Ambrosiano et al. 1988; Oka et al. 2010; Li et al. 2015; Guo et al. 2016). It appears that acceleration is especially efficient in kinetic simulations when the plasma beta is sufficiently small (Li et al. 2015; Guo et al. 2016). Efficient acceleration is attributed to charged particles interacting with and traversing numerous contracting and merging flux small-scale magnetic islands or flux ropes formed by fast primary current sheet reconnection involving a tearing-mode instability or turbulence (e.g., Ambrosiano et al. 1988; Drake et al. 2006; Oka et al. 2010). These simulations suggest that particles temporary trapped in active small-scale islands are more likely to be energized than particles interacting with the reconnection electric field in the X-point regions between magnetic islands because islands occupy a relative large volume compared to the reconnection sites.

For energetic particles interacting with dynamic small-scale flux ropes, basically three nonresonant acceleration scenarios have emerged from full kinetic simulations as the main contributors to particle energization (e.g., de Gouveia dal Pino & Lazarian 2005; Drake et al. 2006; Oka et al. 2010; Drake et al. 2013; Dahlin et al. 2014; Zank et al. 2014; Li et al. 2015; Dahlin et al. 2016, 2017): (i) Energetic particles gain mainly parallel kinetic energy when following the magnetic field of a contracting magnetic island formed as a product of primary current sheet reconnection. This can be understood in terms of conservation of the second adiabatic invariant when the path length along the magnetic field followed by the particle between the endpoints of the contracting islands shortens with time. Alternatively, and equivalently, acceleration can be thought of as occurring predominantly as a result of curvature drift in the direction of the motional electric field induced at the contracting island endpoints (de Gouveia dal Pino & Lazarian 2005; Drake et al. 2006; Li et al. 2015). (ii) Particles gain mainly parallel kinetic energy when following the magnetic field of two merging (reconnecting) neighboring magnetic field islands. This also involves parallel kinetic energy gain from conservation of the second adiabatic invariant, but in this case the path length along the magnetic field followed by the particle between the endpoints of the merging structure effectively decreases in time because of field-line straightening in the center of the merging structure from the merging process (Drake et al. 2013). Also here the idea of curvature drift acceleration applies because of curvature drift occurring in the direction of the motional electric field induced by the X-point outflow in the merging site. (iii) Parallel kinetic energy gain occurs to the extent that particles temporarily trapped in a merging magnetic island structure experience parallel guiding center motion in the direction of the parallel magnetic reconnection electric field generated in the secondary current sheet diffusion region at the interface of two merging islands (Pritchett 2008; Oka et al. 2010).

These acceleration scenarios were typically considered in the limit of incompressible flux-rope contraction and merging where the parallel kinetic energy gain in cases (i) and (ii) is opposed by perpendicular kinetic energy loss from the betatron acceleration mechanism due to the decrease in the flux-rope magnetic field strength with time. Varying degrees of perpendicular kinetic energy loss have been discussed for case (ii), ranging from negligible loss if the particle distribution maintains a beam-like distribution along the magnetic field, so that acceleration approximates a first-order Fermi process (Drake et al. 2006), to significant loss when the particle distribution is nearly isotropic and acceleration becomes a second-order Fermi process owing to strong particle scattering (Drake et al. 2013; Zank et al. 2014; le Roux et al. 2015a).

The possibility of compressible flux-rope contraction and merging in the solar wind, as suggested by observations (Khabarova et al. 2015, 2016), was considered in Zank et al. (2014) and le Roux et al. (2015a). In this case, both curvature drift and betatron acceleration, due to an increasing flux-rope magnetic field strength, contribute to kinetic energy gain, and the particle acceleration is a first-order Fermi acceleration process when the particle distribution is isotropic or nearly isotropic. In the case of a beam-like particle distribution along the magnetic field the compressible acceleration becomes inefficient. Dmitruk et al. (2004) and Dmitruk & Matthaeus (2006) discuss energetic ion acceleration in 3D MHD weakly compressible turbulence with a strong uniform, out-of-plane guide magnetic field, where it is predominantly perpendicular kinetic energy gain associated with variations in the MHD fields that matters. More recently, the role of compressibility in particle acceleration by contracting and merging small-scale flux ropes was investigated with full 2D kinetic simulations by Li et al. (2018). This was done by comparing drift acceleration due to compression with drift acceleration associated with shear flow. Compression acceleration was found to be especially important in the weak guide field limit, while shear-flow acceleration rivaled compression acceleration when the guide magnetic field becomes comparable to the reconnection magnetic field component because of the increase in the energetic particle anisotropy. In the case of a strong guide field both these mechanisms are suppressed in favor of acceleration by the parallel electric field.

The latter result is consistent with earlier particle simulations where the flux-rope acceleration mechanisms discussed above operate with varying levels of relative efficiency depending on the relative strength of the guide/background magnetic field perpendicular to the in-plane twist/island magnetic field of flux-rope structures (e.g., Dahlin et al. 2014, 2016; Li et al. 2015). From a 2D perspective, both the electric field induced by island contraction and merging and the energetic particle curvature drift velocity (acceleration cases (i) and (ii)), being out-of-plane without a guide field, become predominantly in-plane in the presence of a strong guide field (le Roux et al. 2016). In acceleration case (iii), a significant guide field is beneficial (Dahlin et al. 2016), because then parallel guiding center motion predominantly occurs along the guide field

parallel to the out-of-plane reconnection electric field, thus boosting the efficiency of particle acceleration compared to acceleration cases (i) and (ii). A crucial question is to what extent this 2D view of particle acceleration by small-scale flux ropes will also apply in full 3D simulations in the presence of a significant guide field. There is some support from Birn et al. (1989) and Dmitruk et al. (2004), who found that with a significant guide field magnetic reconnection still mainly occurs in the 2D plane perpendicular to the guide field. However, a key difference in 3D particle simulations with a significant guide field appears to be the enhanced efficiency of acceleration cases (i) and (ii) compared to 2D simulations (Dahlin et al. 2017). This is because particle transport along the guide field allow particles to efficiently exit flux-rope structures to sample new contracting 3D island structures for further acceleration. In 2D simulations particles tend to be trapped in 2D island structures (uniform flux ropes in the guide field direction), where acceleration becomes less efficient as merging and contraction come to an end.

2. Energetic Particle Acceleration by Small-scale Flux Ropes in a Turbulent Plasma

So far, the discussion has emphasized particle energization by local plasma regions of contracting and fast reconnecting (merging) small-scale flux ropes generated in the vicinity of large-scale primary current sheets through turbulent current sheet reconnection. However, one can also approach this topic from the perspective of MHD turbulence theory, simulations, and related solar wind observations. Theoretical considerations and simulations of MHD turbulence in the presence of a significant background/guide magnetic field suggest that solar wind turbulence can to lowest order be modeled in terms of a combination of a dominant quasi-2D turbulence component of coherent structures (small-scale magnetic islands) perpendicular to the background/guide field and a minor parallel-propagating Alfvén wave turbulence component (Shebalin et al. 1983; Zank & Matthaeus 1992, 1993; Dmitruk et al. 2004; Zank et al. 2017), a view that is consistent with analysis of solar wind observations (Matthaeus et al. 1990; Bieber et al. 1996) and with the finding that quasi-2D turbulence alone is not sufficient to explain observed solar wind turbulence (Turner et al. 2012). A recent analysis of *Wind* data to identify inertial-scale flux ropes indicates that these structures are much more commonplace in the solar wind near 1 au than previously thought. Zheng (2017), Zheng et al. (2017), and Zheng & Hu (2018) identified an unprecedented number of small-scale flux ropes at 1 au with scales in the inertial range using the Grad–Shafranov reconstruction approach (~3500 per year on average) with a clear solar cycle dependence, a number that is expected to grow when the data analysis shifts to shorter timescales. Furthermore, an axial (out-of-plane) current density distribution constructed from the Grad–Shafranov-based data analysis yielded a non-Gaussian probability density function (pdf) entirely consistent with the out-of-plane current density pdf produced from compressible 2D MHD turbulence simulations with a strong out-of-plane guide field, in which merging magnetic island structures are a common occurrence (Greco et al. 2009). This result, combined with the sheer number of small-scale flux ropes being identified, suggests that the common occurrence of small-scale flux ropes in the low-latitude solar wind near 1 au is a natural consequence of local MHD turbulence evolution in a highly conductive plasma with a strong guide field, independent of additional flux-rope production at primary current sheets. Furthermore, observational evidence of merging (magnetic reconnection) of neighboring small-scale flux ropes at Earth (Khabarova et al. 2015, 2016), including evidence on the basis of Grad–Shafranov reconstruction of small-scale flux ropes (Zheng & Hu 2016; Zheng 2017; Zheng et al. 2017), is consistent with the concept of quasi-2D turbulence theory of an inverse cascade of magnetic island energy to smaller wavenumbers.

Detailed analyses of high Lindquist number incompressible 2D MHD turbulence simulations revealed the pervasive presence of active multiscale magnetic islands separated by strong magnetic field discontinuities in the form of secondary fast reconnecting current sheets (Servidio et al. 2011). These intermittent discontinuities were found to contribute to pdf's of fluctuations in the field strength that are strongly non-Gaussian on inertial range scales and compare well with observed pdf's in the solar wind near 1 au (Greco et al. 2009; Servidio et al. 2011). Also on this basis one might conclude that a background of small-scale flux-rope structures exists in the solar wind, with additional local sources of production near primary current sheets. In addition, Trenchi et al. (2013) and Tessein et al. (2013, 2016) presented observational evidence connecting energetic particle flux variations to magnetic field discontinuities that can be interpreted as evidence of particle trapping in small-scale flux ropes and of local particle energization at small-scale flux-rope structures, possibly undergoing reconnection with neighboring flux ropes.

Simulations of particle acceleration in incompressible 2D MHD turbulence solutions of highly conductive plasmas with a uniform out-of-plane guide field also show the formation of power-law particle spectra (e.g., Gray & Matthaeus 1992). This is linked to the ubiquitous presence of small-scale magnetic islands undergoing merging through fast reconnection (Servidio et al. 2011). More generally, weakly compressible 3D MHD turbulence simulations that include a strong guide field show that, in the 2D plane perpendicular to the guide field, the 2D MHD turbulence picture of the formation of a "sea" of active multiscale magnetic islands separated by strong magnetic field discontinuities in the form of secondary reconnecting current sheets remains largely intact (Dmitruk et al. 2004). Simulation of ion and electron acceleration using the compressible 3D MHD turbulence solution yields energetic spectra with power laws, just as in the 2D case. This prompted Dmitruk et al. to conclude that the 3D simulation with its strong background/guide field can be interpreted reasonably in terms of a quasi-2D MHD turbulence picture (Shebalin et al. 1983) involving component reconnection (Birn et al. 1989), where secondary current sheets between small-scale flux-rope structures form in the guide field direction and merging or reconnection of small-scale flux ropes mainly involves the magnetic island component in the 2D plane perpendicular to the guide field.

3. Motivation

3.1. Previous Theoretical Development

Based on the growing body of evidence for energetic particle acceleration in solar wind regions with multiple dynamic small-scale flux ropes, it is clear that a deeper theoretical understanding of the observed formation of energetic ion power-law spectra at suprathermal energies in the large-scale solar wind requires investigation of the potential role of these structures. Based on the overview above, we conclude that, irrespective of whether one views the formation of active quasi-2D small-scale flux ropes in

the turbulent solar wind as occurring mainly through reconnection locally at primary current sheets disturbed by solar wind turbulence or as an intrinsic feature of a turbulent solar wind with a significant background/guiding magnetic field, these coherent structures in both cases are subject to the same dynamics of contraction and merging (due to fast magnetic reconnection) that can result potentially in efficient charged particle acceleration according to the three acceleration scenarios outlined above. However, simulation of charged particle transport and acceleration in a "sea" of dynamic small-scale flux ropes using solutions from MHD turbulence or kinetic models is time-consuming. These approaches are currently not feasible for modeling transport and acceleration of suprathermal charged particles in the solar wind on large spatial scales. Thus, recent efforts by us have attempted to unify the three main acceleration scenarios discussed above through a large-scale kinetic focused transport theory for suprathermal particles traversing numerous contracting and merging inertial-scale magnetic islands with a strong prescribed guide/background magnetic field (Zank et al. 2014; le Roux et al. 2015a). This work extended previous steps in this direction (e.g., de Gouveia dal Pino & Lazarian 2005; Drake et al. 2006, 2013; Bian & Kontar 2013). A key characteristic of our transport theory is that a distinction is made between magnetic islands that contract and merge in an incompressible and in a compressible fashion (Zank et al. 2014; le Roux et al. 2015a; see Section 6). This flexibility enables us to investigate observational evidence that suggests that compressible contraction might be an important element in efficient particle acceleration (Khabarova et al. 2015). Furthermore, our transport theory distinguishes between coherent particle acceleration in response to mean flux-rope properties and stochastic acceleration in response to the variance in flux-rope properties such as the contraction/merging flow velocity, the flux-rope magnetic field, and the parallel reconnection electric field generated in merging flux ropes (Bian & Kontar 2013; le Roux et al. 2015a, 2016). Thus, energetic particle acceleration can also be modeled in cases where the statistical probability of flux-rope contraction is balanced by expansion to produce a zero mean contraction electric field, for example (in simulations, alternating contractions and expansions were detected to occur after merging of neighboring flux ropes; Oka et al. 2010). Our theory also includes the option for choosing between a quasi-linear transport limit, where energetic particles propagate with undisturbed guiding center motion (weak scattering limit), and a nonlinear transport limit of diffusive guiding center motion (strong scattering limit) along the magnetic field through small-scale flux-rope structures (le Roux et al. 2015a, 2016).

3.2. New Theoretical Development

Our previous theoretical development efforts were limited to modeling energetic particle acceleration by dynamic small-scale flux ropes in the test particle limit (Zank et al. 2014; le Roux et al. 2015a). However, applications of the theory in solar wind conditions indicated that hard suprathermal power-law spectra might form with high particle pressure (Zank et al. 2014, 2015a, 2015b; le Roux et al. 2015a, 2015b, 2016). This raises the question of how the back-reaction of energetic particles on small-scale flux ropes affects the efficiency of particle acceleration. The main aim of this paper is to extend the kinetic transport formalism of le Roux et al. (2015a) to enable a self-consistent description of energetic particle acceleration by numerous dynamic small-scale flux ropes on macroscopic scales. This is accomplished by (i) deriving new growth/damping rate expressions for the total energy density (kinetic plus magnetic) of the magnetic island component of small-scale flux ropes based on conservation in the exchange of energy between energetic particles and dynamic magnetic island structures (it is assumed that flux-rope dynamics and energy exchange between particles and flux ropes are mainly confined to the magnetic island or twist component in the 2D plane perpendicular to the prescribed strong guide/background magnetic field component as discussed above) and (ii) deriving a new MHD turbulence transport equation for modeling the transport of the total energy density of magnetic islands, using the recently updated, nearly incompressible (NI) MHD theory for turbulence transport in a nonuniform solar wind medium (Zank et al. 2017) as a basis. The island growth/damping rates are included in the MHD magnetic island turbulence transport equation to complete a system of closed equations for modeling self-consistent energetic particle acceleration on large spatial scales in the solar wind.

Furthermore, the kinetic focused transport equation for suprathermal particle transport and acceleration by small-scale flux ropes of le Roux et al. (2015a, 2016) is presented in this paper with revised and more detailed expressions of the Fokker–Planck transport coefficients $D^I_{\mu\mu}$ (pitch-angle scattering caused by small-scale flux ropes), $D^I_{p\mu}$, $D^I_{p\mu}$, and D^I_{pp} (second-order Fermi acceleration due to small-scale flux ropes) for four distinct acceleration cases present in focused transport theory: (i) curvature drift and generalized betatron acceleration (unified betatron and grad-B drift acceleration) in small-scale flux ropes contracting and merging in the compressible limit, (ii) curvature drift and generalized betatron acceleration in small-scale flux ropes contracting and merging in the incompressible limit, (iii) parallel guiding center motion acceleration by the parallel reconnection electric field force formed in merging small-scale flux ropes, and (iv) parallel guiding center motion acceleration by the parallel noninertial force associated with the acceleration of the plasma flow in small-scale flux ropes. The last acceleration mechanism is presented for the first time.

A new analysis is presented comparing the efficiency of the four different flux-rope acceleration scenarios for suprathermal protons with each other (for both coherent and stochastic acceleration) and comparing the stochastic acceleration efficiency of flux ropes with parallel-propagating Alfvén waves in solar wind conditions at 1 au. The strength of pitch-angle scattering for energetic protons at 1 au, induced through the variance in the magnetic mirroring force present in small-scale flux ropes, is compared with earlier estimates of the strength of pitch-angle scattering in quasi-2D MHD turbulence associated with the variance in the 2D turbulence magnetic Lorentz force in prior quasi-linear theory approaches to 2D turbulence (le Roux et al. 2004; le Roux & Webb 2007). Finally, pitch-angle scattering rates by small-scale flux ropes are evaluated against those associated with standard quasi-linear theory for parallel-propagating Alfvén waves.

4. The Reconnection Electric Field and Plasma Drift Velocity of Contracting and Merging Small-scale Flux Ropes on MHD Scales

Our main interest is to use kinetic guiding center and its close equivalent, focused transport theory, to model how highly mobile energetic charged particles are energized on large spatial scales in the solar wind when traversing numerous contracting and reconnecting (merging) small-scale flux ropes

that have turbulence inertial range (MHD) scales. For this purpose our transport theory requires expressions for the parallel electric field and for the plasma drift velocity associated with magnetic flux-rope contraction and merging.

When particle energization by the reconnection electric field is considered on microscopic scales much less than a thermal ion gyroradius, that is, on thermal electron scales, the total electric field $\boldsymbol{E}$ in the observer frame is often modeled using standard MHD theory in terms of a generalized Ohm's law given by

$$\boldsymbol{E} = -\boldsymbol{U}_e \times \boldsymbol{B} + \boldsymbol{E}_{\rm REC}, \tag{1}$$

where the reconnection electric field $\boldsymbol{E}_{\rm REC}$ is the electric field in the plasma electron flow frame moving with a velocity $\boldsymbol{U}_e$ relative to the observer frame. The reconnection electric field is given by the expression

$$\boldsymbol{E}_{\rm REC} = \frac{\boldsymbol{j}}{\sigma} - \frac{1}{en_e}\nabla \cdot \boldsymbol{P}_e + \frac{m_e}{e^2 n_e}\left[\frac{\partial \boldsymbol{j}}{\partial t} + \nabla \cdot \left(\boldsymbol{U}\boldsymbol{j} + \boldsymbol{j}\boldsymbol{U} - \frac{1}{n_e e}\boldsymbol{j}\boldsymbol{j}\right)\right], \tag{2}$$

where σ is the conductivity parameter associated with Coulomb collisions, $\boldsymbol{j}$ is the current density, m_e is the electron mass, n_e is the electron number density, $\boldsymbol{P}_e$ is the electron pressure tensor, and $\boldsymbol{U} \approx \boldsymbol{U}_i$ is the average plasma flow velocity for ions and electrons, typically dominated by ion flow $\boldsymbol{U}_i$ owing to ion inertia. Thus, the induction equation for the evolution of the magnetic field $\boldsymbol{B}$ in the observer frame reads

$$\frac{\partial \boldsymbol{B}}{\partial t} = \nabla \times (\boldsymbol{U}_e \times \boldsymbol{B}) - \nabla \times \boldsymbol{E}_{\rm REC}, \tag{3}$$

where the last term indicates how the terms in the reconnection electric field expression cause magnetic field propagation relative to the plasma flow to enable reconnection at a current sheet. The expression for $\boldsymbol{E}_{\rm REC}$ in Equation (2), simplified for a small electron mass and approximate charge neutrality, contains various nonideal collisionless MHD contributions (electron pressure tensor gradient, and electron inertial terms) and a contribution from the resistivity due to Coulomb collisions, which can for the most part be ignored in our case of a high-conductivity plasma such as the solar wind. A similar expression for $\boldsymbol{E}_{\rm REC}$ can also be found using the electron equation of motion (e.g., Scudder et al. 2015). From the microscopic perspective, the different nonideal collisionless contributions are large and comparable in small-volume current sheet reconnection regions (e.g., Scudder et al. 2015), thus playing a key role in collisionless reconnection in and near primary and secondary current sheet layers, whereas away from the current sheet regions these contributions become small and one recovers the ideal MHD induction equation $\partial \boldsymbol{B}/\partial t \approx \nabla \times (\boldsymbol{U} \times \boldsymbol{B})$ ($\boldsymbol{U}_e \approx \boldsymbol{U}$).

However, our aim is to model energetic particle acceleration by and transport through a "sea" of small-scale flux ropes in the solar wind on inertial range (macroscopic) scales. The flux ropes we consider have cross sections comparable to turbulence wavelengths in the inertial range, as observed (e.g., Cartwright & Moldwin 2010; Khabarova et al. 2015), and are classified as a leading-order component of low-frequency solar wind MHD turbulence in N I MHD theory (e.g., Zank et al. 2017). Viewed on MHD scales, the nonideal collisionless terms that contribute to the reconnection electric field $\boldsymbol{E}_e$ in Equation (2) are all negligible when compared to the motional electric field term ($-\boldsymbol{U}_e \times \boldsymbol{B}$) in Equation (1), and the observer frame electric field simplifies to the standard motional electric field expression

$$\boldsymbol{E} = -\boldsymbol{U}_e \times \boldsymbol{B} \approx -\boldsymbol{U} \times \boldsymbol{B}. \tag{4}$$

We decompose $\boldsymbol{U}$ and $\boldsymbol{B}$ according to

$$\begin{aligned} \boldsymbol{U} &= \boldsymbol{U}_0 + \delta \boldsymbol{U}_I,\ \langle \delta \boldsymbol{U}_I \rangle = 0, \\ \boldsymbol{B} &= \boldsymbol{B}_0 + \delta \boldsymbol{B}_I,\ \langle \delta \boldsymbol{B}_I \rangle = 0, \end{aligned} \tag{5}$$

distinguishing between the large-scale solar wind velocity $\boldsymbol{U}_0$ and magnetic field $\boldsymbol{B}_0$ and the random flux-rope flow velocity $\delta \boldsymbol{U}_I$ and magnetic field $\delta \boldsymbol{B}_I$. After inserting Equation (5) into Equation (4) and doing standard Reynolds averaging, we find that the mean observer frame electric field in the solar wind is

$$\langle \boldsymbol{E} \rangle \approx -\boldsymbol{U}_0 \times \boldsymbol{B}_0 + \langle \boldsymbol{E}_{\rm REC} \rangle, \tag{6}$$

with

$$\langle \boldsymbol{E}_{\rm REC} \rangle = -\langle \delta \boldsymbol{U}_I \times \delta \boldsymbol{B}_I \rangle, \tag{7}$$

so that

$$\frac{\partial \boldsymbol{B}_0}{\partial t} \approx \nabla \times (\boldsymbol{U}_0 \times \boldsymbol{B}_0) - \nabla \times \langle \boldsymbol{E}_{\rm REC} \rangle. \tag{8}$$

The last term in Equation (6), as expressed by Equation (7), represents the magnetic island turbulence induced reconnection electric field on macroscopic (inertial) scales, and the last term in Equation (8) shows how the flux-rope turbulence associated with this electric field causes the large-scale magnetic field to move relative to the large-scale plasma flow to drive magnetic reconnection at current sheets from a macroscopic-scale perspective. Thus, the induction equation simplifies to an ideal MHD induction equation in which a reconnection electric field appears that is predominantly produced by inertial-scale magnetic island turbulence. From this viewpoint, everywhere that flux-rope turbulence exists in the solar wind, the magnetic field is not frozen into the plasma flow. In passing, we note that Eyink (2015) advocates a different averaging approach related to renormalization group theory to avoid scale separation and associated closure issues, which is beyond the scope of this paper.

On MHD scales (scales larger than the ion inertial scale), where the motional electric field predominantly determines the solar wind electric field, the parallel electric field vanishes because

$$\boldsymbol{E}_{\parallel} = \boldsymbol{E} \cdot \boldsymbol{b} = -\boldsymbol{U} \times \boldsymbol{B} \cdot \boldsymbol{b} = 0, \tag{9}$$

where $\boldsymbol{b}$ is the unit vector in the magnetic field direction. However, the parallel electric field effect is retained in our focused transport equation and is introduced by the reconnection electric field in merging flux ropes on MHD scales, which we estimate below to be mainly parallel to the background magnetic field $\boldsymbol{B}_0$ near 1 au.

The existence of such a parallel reconnection electric field can be understood by considering small-scale flux ropes as consisting of a twist (magnetic island component) in the 2D plane perpendicular to the axial component (see solar wind observations by Cartwright & Moldwin 2010). Recent observations at 1 au show that the axial (guide field) component

of small-scale flux ropes is aligned with the Parker spiral magnetic field direction (Zheng 2017). Furthermore, turbulence observations (Smith et al. 2016) show that $\langle \delta B_N^2 \rangle / B_0^2 \approx 0.1$ at 1 au, where δB_N is the magnetic turbulence component perpendicular to the ecliptic plane (meridional component) and B_0 is the magnitude of the background magnetic field interpreted to be consistent with the Parker field model. Assuming axisymmetric magnetic turbulence around $\boldsymbol{B}_0$, and with the observation that ~85% of inertial range magnetic turbulence energy is in a quasi-2D turbulence component in the 2D plane perpendicular to $\boldsymbol{B}_0$ (Bieber et al. 1996; Weygand et al. 2009; MacBride et al. 2010; Oughton et al. 2015; turbulence fluctuation energy is mostly in vector components with quasi-perpendicular wave vectors transverse to $\boldsymbol{B}_0$), we get $\langle \delta B_{2D}^2 \rangle / B_0^2 \approx 0.17$.

These observations can be interpreted in terms of N I MHD theory (Zank et al. 2017), where the equations for the quasi-2D turbulence component allow for solutions of coherent magnetic field structures that can be classified as magnetic islands with plasma flow located in the 2D plane perpendicular to the background magnetic field $\boldsymbol{B}_0$. In the theory $\boldsymbol{B}_0$ acts as a strong axial or guide field component of the magnetic islands in solar wind conditions near 1 au ($\langle \delta B_{2D}^2 \rangle^{1/2} / B_0 = \epsilon$, where ϵ is a smallness parameter). On this basis we interpret small-scale flux ropes at 1 au as having a twist (magnetic island) $\delta \boldsymbol{B}_I$ and flow component component $\delta \boldsymbol{U}_I$ in the 2D plane perpendicular to a relatively strong, locally uniform axial or guide field component represented by the background magnetic field $\boldsymbol{B}_0$ ($\delta \boldsymbol{B}_I \perp \boldsymbol{B}_0$ and $\langle \delta B_I^2 \rangle^{1/2} / B_0 = \epsilon$), so that flux-rope dynamics such as contraction and merging mainly involves the magnetic island and flow component in this 2D plane (Shebalin et al. 1983; Birn et al. 1989; Dmitruk et al. 2004). This implies that the reconnection electric field produced in merging small-scale flux ropes near 1 au should be mainly aligned with the guide or background magnetic field $\boldsymbol{B}_0$ ($\boldsymbol{E}_{\rm REC} \approx \boldsymbol{E}_{{\rm REC}\parallel}$). Furthermore, for such a relatively strong but weakly spatially varying guide field, one can approximate energetic particle guiding center transport at 1 au as occurring mainly along $\boldsymbol{B}_0$, and thus along $\boldsymbol{E}_{{\rm REC}\parallel}$, an ideal situation for particle acceleration by the parallel reconnection electric field.

In our approach to modeling small-scale flux ropes, the magnetic field unit vector $\boldsymbol{b}_0$ along the guide or background magnetic field $\boldsymbol{B}_0$ is also the unit vector along the average magnetic field. This follows because the unit vector along the magnetic field can be approximated as

$$\boldsymbol{b} \approx \boldsymbol{b}_0 + (\delta \boldsymbol{B}_I / B_0) \approx \boldsymbol{b}_0, \tag{10}$$

because $\langle \delta B_I^2 \rangle / B_0^2 \ll 1$ in the strong guide field approximation. Upon taking the ensemble average of $\boldsymbol{b}$, the average field direction becomes $\langle \boldsymbol{b} \rangle \approx \boldsymbol{b}_\circ$ because we assume that $\langle \delta \boldsymbol{B}_I \rangle = 0$ (the assumption of a random distribution of flux-rope structures in the 2D plane perpendicular to $\boldsymbol{B}_0$ in quasi-2D MHD turbulence). Accordingly, we introduce the parallel reconnection electric field by taking first the component of the macroscopic motional electric field $\boldsymbol{E} = -\boldsymbol{U} \times \boldsymbol{B}$ along the average field direction $\boldsymbol{b}_\circ$:

$$\boldsymbol{E}_\parallel = -\boldsymbol{U} \times \boldsymbol{B} \cdot \boldsymbol{b}_\circ. \tag{11}$$

Upon decomposing $\boldsymbol{U}$ and $\boldsymbol{B}$ in Equation (11) according to Equation (5) and doing an ensemble average, we find that the mean parallel electric field is

$$\begin{aligned} \langle \boldsymbol{E}_\parallel \rangle &= -\langle \delta \boldsymbol{U}_I \times \delta \boldsymbol{B}_I \rangle \cdot \boldsymbol{b}_\circ \\ &= -\langle \delta \boldsymbol{U}_I \times \delta \boldsymbol{B}_I \rangle = \langle \boldsymbol{E}_{\rm REC} \rangle, \end{aligned} \tag{12}$$

thus recovering the reconnection electric field expression of Equation (7), because both $\delta \boldsymbol{U}_I$, $\delta \boldsymbol{B}_I \perp \boldsymbol{B}_0$.

When we consider the electric field (plasma) drift velocity on MHD scales by inserting the motional electric field expression (4), we find that

$$\boldsymbol{V}_E = \boldsymbol{b} \times (\boldsymbol{U} \times \boldsymbol{b}) = \boldsymbol{U}_\perp, \tag{13}$$

where $\boldsymbol{U}_\perp$ is the plasma flow perpendicular to the total magnetic field. Upon decomposing $\boldsymbol{b}$ according to Equation (10) and $\boldsymbol{U}$ according to Equation (5), and after applying the strong guide field assumption $\delta B_I / B_0 \ll 1$, we find that

$$\begin{aligned} \boldsymbol{V}_E &= \boldsymbol{V}_{E0} + \delta \boldsymbol{V}_{EI} \\ &\approx \boldsymbol{U}_{0\perp} + \delta \boldsymbol{U}_{I\perp}. \end{aligned} \tag{14}$$

Therefore, the background plasma drift velocity $\boldsymbol{V}_{E0} \approx \boldsymbol{U}_{0\perp}$, where $\boldsymbol{U}_{0\perp}$ is the background solar wind flow perpendicular to the background/guide magnetic field $\boldsymbol{B}_\circ$ and the flux-rope plasma drift velocity $\delta \boldsymbol{V}_{E\perp} \approx \delta \boldsymbol{U}_{I\perp}$, where $\delta \boldsymbol{U}_{I\perp}$ is the flux-rope contraction/merging flow velocity in the 2D plane perpendicular to $\boldsymbol{B}_\circ$.

5. The Role of Compressibility in the Evolution of Flux-rope Magnetic Energy during Flux-rope Contraction and Merging

Following Dahlin et al. (2016), Poynting's theorem in the limit of ideal MHD theory for a high-conductivity plasma can be expressed as

$$\begin{aligned} &\frac{\partial}{\partial t}\left(\frac{B^2}{2\mu_\circ}\right) + \nabla \cdot \left(\frac{B^2}{2\mu_\circ}\boldsymbol{V}_E\right) \\ &\quad = -\boldsymbol{j}_\parallel \cdot \boldsymbol{E}_\parallel - \frac{B^2}{2\mu_\circ}(\nabla \cdot \boldsymbol{V}_E) - \frac{B^2}{\mu_\circ}(\boldsymbol{V}_E \cdot \boldsymbol{\kappa}), \end{aligned} \tag{15}$$

where $\boldsymbol{V}_E$ is the plasma drift velocity, $\boldsymbol{j}$ is the net current density for ions and electrons, and $\boldsymbol{\kappa} = (\boldsymbol{b} \cdot \nabla)\boldsymbol{b}$ is the magnetic field curvature vector. The magnetic tension force $\boldsymbol{F}_{\rm ten}$ exerted on a plasma fluid element is related to magnetic field curvature according to the expression

$$\begin{aligned} \boldsymbol{F}_{\rm ten} &= \frac{1}{\mu_\circ}(\boldsymbol{B} \cdot \nabla)\boldsymbol{B} \\ &= \frac{B^2}{\mu_\circ}\kappa + \frac{B}{\mu_\circ}\boldsymbol{b}(\boldsymbol{b} \cdot \nabla)B. \end{aligned} \tag{16}$$

It then follows that the rate at which work is done by the magnetic tension force on the plasma to advect it at the plasma drift velocity can be expressed as

$$\boldsymbol{V}_E \cdot \boldsymbol{F}_{\rm ten} = \frac{B^2}{\mu_\circ}(\boldsymbol{V}_E \cdot \boldsymbol{\kappa}), \tag{17}$$

which is the last term in Poynting's theorem (15) without a minus sign. When a magnetic flux rope is contracting in the 2D plane perpendicular to a locally uniform guide field, or two such flux ropes with a common guide field are merging, $\boldsymbol{V}_E \cdot \kappa > 0$, so that the magnetic tension force is doing positive

work on a flux-rope plasma fluid element ($(\boldsymbol{V}_E \cdot \boldsymbol{\kappa})B^2/\mu_o > 0$). According to Equation (15), the flux-rope magnetic field loses energy, provided that the contraction or merging process is sufficiently incompressible ($|\boldsymbol{V}_E \cdot \boldsymbol{\kappa}| \gg |\nabla \cdot \boldsymbol{V}_E|$) and the parallel electric field is sufficiently small. Thus, magnetic flux-rope area conservation during contraction or merging in the 2D plane perpendicular to the guide field releases magnetic tension in these structures (circularization of contracting flux ropes or field-line straightening of merging flux ropes in X-point outflow regions in 2D plane as discussed by Drake et al. 2006; Fermo et al. 2010; Drake et al. 2013), for example.

However, if the magnetic curvature contraction term (last term in Equation (15)) is dominated by the compression term (second-to-last term in Equation (15)) so that ($|\boldsymbol{V}_E \cdot \boldsymbol{\kappa}| \ll |\nabla \cdot \boldsymbol{V}_E|$), the contraction or merging is strongly compressible ($\nabla \cdot \boldsymbol{V}_E < 0$), resulting in an increase in flux-rope magnetic energy instead. In this case the plasma environment is doing positive mechanical work on the flux-rope structure, pushing magnetic field lines together to enhance flux-rope magnetic energy. Although it appears that small-scale flux ropes tend to contract or merge predominantly incompressibly in discussions of particle simulations (e.g., Drake et al. 2006; Dahlin et al. 2016), and it is also thought of as intrinsically incompressible in its manifestation as the quasi-2D turbulence component in N I MHD theory of solar wind turbulence (Zank et al. 2017), there is observational evidence to the contrary. For example, when primary current sheets associated with interplanetary coronal mass ejections (ICMEs) interact with the heliospheric current sheet, these structures are disturbed and several small-scale flux-rope structures may be formed when turbulent magnetic reconnection occurs in these structures. The flux ropes, being trapped between the converging heliospheric current sheet and the primary current sheets of ICMEs, experience compression, which may lead to efficient particle acceleration (e.g., Khabarova et al. 2015). However, it is possible that the particles are bounded in space because they cannot escape easily the region filled with small-scale flux ropes, which implies more efficient acceleration. Furthermore, in N I MHD theory of quasi-2D magnetic island turbulence, incompressible flux ropes can be compressed by large-scale density and flow velocity gradients in the nonuniform solar wind (Zank et al. 2017; see also discussion of Equation (69) in Section 8.2). Closer to the Sun, Guidoni et al. (2016) discuss the possibility of strong plasma compression during magnetic island contraction for islands propagating sunward during a solar flare event.

It is interesting to note the relationship $\boldsymbol{V}_E \cdot \kappa = -\boldsymbol{b} \cdot (\boldsymbol{b} \cdot \nabla)\boldsymbol{V}_E = -[b_i b_j \sigma_{ij} + 1/3(\nabla \cdot \boldsymbol{V}_E)]$, where we express the magnetic island curvature advection term $\boldsymbol{V}_E \cdot \kappa$ in terms of the parallel component of the island plasma drift shear flow $-\boldsymbol{b} \cdot (\boldsymbol{b} \cdot \nabla)\boldsymbol{V}_E$. In this expression the shear-flow term has in turn been related to the island plasma drift shear-flow tensor $\sigma_{ij} = 1/2[\partial V_{Ei}/\partial x_j + \partial V_{Ej}/\partial x_i - 2/3(\nabla \cdot \boldsymbol{V}_E)\delta_{ij}]$ with the aid of the Cauchy–Stokes theorem (e.g., le Roux & Webb 2012; Li et al. 2018). In the case of incompressible magnetic island contraction where $|\boldsymbol{V}_E \cdot \boldsymbol{\kappa}| \gg |\nabla \cdot \boldsymbol{V}_E|$, $\boldsymbol{V}_E \cdot \kappa \approx -b_i b_j \sigma_{ij} = -1/2 b_i b_j [\partial V_{Ei}/\partial x_j + \partial V_{Ej}/\partial x_i] = -\boldsymbol{b} \cdot (\boldsymbol{b} \cdot \nabla)\boldsymbol{V}_E > 0$, suggesting that island contraction or merging in this limit can be modeled in terms of a negative parallel component of plasma drift shear flow. For further discussion of the role of shear flow and compression in magnetic island contraction and merging, see Li et al. (2018).

6. A Guiding Center Kinetic Theory Perspective on the Acceleration of Energetic Particles by Contracting and Merging Flux Ropes—Role of Compressibility

Based on standard guiding center kinetic theory (Northrop 1963; Kulsrud 1983; le Roux & Webb 2009), valid for a nearly gyrotropic particle distribution with gyroradii much less than the scale of the electromagnetic field in the plasma, one can express the gyrophase-averaged energetic particle rate of change in kinetic energy as

$$\begin{aligned}\left\langle \frac{dK}{dt} \right\rangle_\phi &\approx \left[q\boldsymbol{E} \cdot \left(v_\parallel \boldsymbol{b} + \frac{m v_\parallel^2}{qB} \boldsymbol{b} \times \kappa \right) \right]_\parallel + \left[M \frac{\partial B}{\partial t} \right. \\ &\quad \left. + q\boldsymbol{E} \cdot \left(\frac{M}{q} \frac{\boldsymbol{B} \times \nabla B}{B^2} + \frac{M}{q} (\nabla \times \boldsymbol{b})_\parallel \boldsymbol{b} \right) \right]_\perp \\ &= [q E_\parallel v_\parallel + m v_\parallel^2 (\boldsymbol{V}_E \cdot \kappa)]_\parallel \\ &\quad + \left[M \left(\frac{\partial B}{\partial t} + (\boldsymbol{V}_E \cdot \nabla) B \right) + B \frac{dM}{dt} \right]_\perp \\ &= [q E_\parallel v \mu + m v^2 \mu^2 (\boldsymbol{V}_E \cdot \kappa)]_\parallel \\ &\quad + \left[-\frac{1}{2} m v^2 (1 - \mu^2)(\nabla \cdot \boldsymbol{V}_E + \boldsymbol{V}_E \cdot \kappa) \right]_\perp, \end{aligned} \quad (18)$$

where M is the magnetic moment of the energetic charged particle, κ is the magnetic field curvature, $\mu = \cos\theta$ is the cosine of the particle pitch angle so that $v_\parallel = v\mu$, and $v_\perp = v(1 - \mu^2)^{1/2}$. Equation (18) has been simplified by assuming fast charged particles ($V_E/v = \epsilon \ll 1$), neglecting terms of higher than first order in V_E/v. Therefore, the effects of polarization drift are not included in the discussion. Terms in square brackets labeled with a "$\parallel$" symbol indicate gyrophase-averaged parallel kinetic energy changes, whereas terms in square brackets labeled with a "$\perp$" symbol are associated with gyrophase-averaged perpendicular kinetic energy changes.

In the first line of Equation (18) it is shown how parallel kinetic energy changes are associated with parallel guiding center motion acceleration by the parallel electric field component (first term) and curvature drift acceleration by the perpendicular electric field component (second term). This is followed by the second line of Equation (18), where perpendicular kinetic energy changes are connected to betatron acceleration by the electric field induced by the time variation in the magnetic field strength B while conserving the magnetic moment of the energetic particle (first term), grad-B drift acceleration by the perpendicular electric field component (second term), and parallel drift acceleration by the parallel electric field component (last term).

Both the curvature drift and grad-B drift acceleration terms in the first two lines of Equation (18) can be expressed in terms of the plasma drift velocity $\boldsymbol{V}_E$ as shown in the third and fourth lines of Equation (18). The second term in the third line of Equation (18) expresses curvature drift acceleration as a consequence of the advection of the flux-rope magnetic

curvature $\kappa = \boldsymbol{b} \cdot (\boldsymbol{b} \cdot \nabla)\boldsymbol{b}$ at the velocity $\boldsymbol{V}_E$ because

$$\left\langle \frac{dK_\parallel}{dt} \right\rangle_\phi = q\boldsymbol{E} \cdot \frac{mv_\parallel^2}{qB}\boldsymbol{b} \times \kappa = mv_\parallel^2(\boldsymbol{V}_E \cdot \kappa). \quad (19)$$

In the case of flux-rope contraction or merging in the 2D plane perpendicular to $\boldsymbol{B}_0$ when $\boldsymbol{V}_E \cdot \kappa > 0$, inevitably curvature drift acceleration by the perpendicular electric field, induced by the contraction or merging process, results in parallel kinetic energy gain. Likewise, the center term in the fourth line of Equation (18) expresses grad-B drift acceleration through the advection of the perpendicular gradient of the flux-rope magnetic field strength at the velocity $\boldsymbol{V}_E$ due to flux-rope contraction or merging processes. Hence,

$$\left\langle \frac{dK_\perp}{dt} \right\rangle_\phi = q\boldsymbol{E} \cdot \frac{M}{q}\frac{\boldsymbol{B} \times \nabla B}{B^2} = M(\boldsymbol{V}_E \cdot \nabla)B, \quad (20)$$

resulting in perpendicular kinetic energy changes. Therefore, perpendicular kinetic energy gain requires that the magnetic field strength gradient have a component in the direction of the contraction or merging velocity $\boldsymbol{V}_E$ in flux ropes. In the fourth line of Equation (18) we also see that the betatron acceleration term $M\partial B/\partial t$ can be unified with the grad-B drift acceleration term given by Equation (20), thus forming a generalized or Lagrangian betatron acceleration term $MdB/dt = M(\partial/\partial t + \boldsymbol{V}_E \cdot \nabla)B$ that, besides describing particle acceleration from the time variation in the flux-rope field strength, also models particle acceleration due to the perpendicular spatial gradient in the flux-rope field strength advected with plasma drift velocity (see discussion by Dahlin et al. 2016).

The last term BdM/dt in the fourth line of Equation (18) is equivalent to the parallel drift acceleration term (last term in the second line) re-expressed in terms of the time variation of the particle's magnetic moment ($BdM/dt = q\boldsymbol{E} \cdot M/q(\nabla \times \boldsymbol{b})_\parallel \boldsymbol{b}$) encountered by the propagating particle guiding center, suggesting that conservation of the particle's magnetic moment (first adiabatic invariant) requires a small parallel electric field. The second adiabatic invariant implies conservation of $v_\parallel s$, where s is distance along the curved magnetic field line (length of curved magnetic field), which can be expressed as $\langle dv_\parallel/dt\rangle_\phi/v_\parallel = -(ds/dt)/s$, thus relating the rate of increase in parallel kinetic energy to the rate of decrease of the length of the curved magnetic field due to flux-rope contraction or merging in the 2D plane perpendicular to $\boldsymbol{B}_0$. In the limit of fast particles ($v_\parallel \gg V_E$), a small parallel electric field, and a magnetic field that is strongly curved $\kappa \gg [(\boldsymbol{b} \cdot \nabla)B]/B$, expression (19) for curvature drift acceleration is a good approximation for the total rate of change in parallel kinetic energy. Accordingly, $\langle dv_\parallel/dt\rangle_\phi/v_\parallel = \boldsymbol{V}_E \cdot \kappa \approx -(ds/dt)/s$, and the condition for the second adiabatic invariant to hold is fulfilled (see also Drake et al. 2006; Dahlin et al. 2017). Zank et al. (2014) combined conservation of the first and second adiabatic invariants as the basis for constructing a simplified flux-rope acceleration model for both compressible and incompressible small-scale flux ropes.

Furthermore, comparing the terms for perpendicular kinetic energy change in the fourth line with the corresponding terms in the sixth line reveals that the generalized betatron acceleration in the fourth line can be related to a combination of the $\boldsymbol{V}_E \cdot \kappa$ and $\nabla \cdot \boldsymbol{V}_E$ terms, assuming approximate magnetic moment conservation (a small $E_\parallel$ value). Thus, generalized betatron acceleration is determined by a competition between incompressible flux-rope contraction or merging ($\boldsymbol{V}_E \cdot \kappa > 0$) and compressible contraction or merging ($\nabla \cdot \boldsymbol{V}_E < 0$). However, such a competition does not appear in the curvature drift acceleration term that depends only on $\boldsymbol{V}_E \cdot \kappa$. To investigate this issue further, it is useful to insert the relationships $\boldsymbol{V}_E \cdot \kappa = -\boldsymbol{b} \cdot (\boldsymbol{b} \cdot \nabla)\boldsymbol{V}_E = -[b_i b_j \sigma_{ij} + 1/3(\nabla \cdot \boldsymbol{V}_E)]$, introduced in the last paragraph of Section 5, into the bottom two lines of Equation (18). We find that

$$\left\langle \frac{dK}{dt} \right\rangle_\phi = qE_\parallel v\mu - \frac{1}{3}mv^2(\nabla \cdot \boldsymbol{V}_E) - \frac{1}{2}mv^2(3\mu^2 - 1)b_i b_j \sigma_{ij}, \quad (21)$$

where the $\nabla \cdot \boldsymbol{V}_E$ term is recognizable as the standard Parker cosmic-ray transport equation term for the combination of curvature drift, grad-B drift, betatron, and parallel drift acceleration that acts collectively as plasma drift compression acceleration and produces net acceleration for the isotropic part of the energetic particle distribution $f_0(p)$ (Kóta 1977; Webb et al. 1981). Similarly, the last term in Equation (21) can be interpreted as a combination of the parallel component of plasma drift shear tensor acceleration associated with curvature drift acceleration with the parallel component of plasma drift shear tensor acceleration associated with unified grad-B drift, betatron, and parallel drift acceleration. This combination can be viewed as the parallel component of shear-flow tensor acceleration yielding net acceleration for the anisotropic part of the particle distribution related to the second moment of the particle distribution $f_2(p)$. Conclusions made about the role of the moments of the energetic particle distribution in acceleration involve (i) taking into account the full transport term $\langle dK/dt\rangle_\phi \partial f/\partial K$ in guiding center kinetic theory, where f is the particle distribution function; (ii) assuming a Legendre moment expansion to the second moment for a nearly isotropic particle distribution (see Equation (164) in Appendix D) in which $f_1(p)$ is the first moment and $f_2(p)$ is the second moment of the anisotropic part of the particle distribution; and (iii) averaging over all μ values.

Upon decomposing the shear-flow tensor according to $\sigma_{ij} = \sigma_{ij}^{\rm sh} - 1/3(\nabla \cdot \boldsymbol{V}_E)\delta_{ij}$, where $b_i b_j \sigma_{ij}^{\rm sh} = 1/2[b_i b_j\, \partial V_{Ei}/\partial x_j + b_j b_i \partial V_{Ej}/\partial x_i] = \boldsymbol{b} \cdot (\boldsymbol{b} \cdot \nabla)\boldsymbol{V}_E$ in Equation (21), we find that

$$\left\langle \frac{dK}{dt} \right\rangle_\phi = qE_\parallel v\mu - \frac{1}{3}mv^2(\nabla \cdot \boldsymbol{V}_E) + \frac{1}{3}mv^2\frac{1}{2}(3\mu^2 - 1)(\nabla \cdot \boldsymbol{V}_E) - \frac{1}{2}mv^2(3\mu^2 - 1)\boldsymbol{b} \cdot (\boldsymbol{b} \cdot \nabla)\boldsymbol{V}_E. \quad (22)$$

In addition to the Parker transport compression term, there is a new compression term (third term in Equation (22)). Just like the Parker compression term, the new term also combines compression acceleration linked to curvature drift acceleration ($-1/3mv^2\mu^2(\nabla \cdot \boldsymbol{V}_E)$) with compression acceleration associated with unified betatron, grad-B drift, and parallel drift acceleration ($-1/3mv^2 1/2(1 - \mu^2)(\nabla \cdot \boldsymbol{V}_E)$). Different from the Parker transport compression term that produces net

acceleration for the isotropic part of the particle distribution $f_0(p)$, the new compression term yields net acceleration for the anisotropic part of the particle distribution related to $f_2(p)$. The last term in Equation (22) combines the parallel component of shear-flow acceleration associated with curvature drift acceleration ($-mv^2\mu^2\boldsymbol{b}\cdot(\boldsymbol{b}\cdot\nabla)\boldsymbol{V}_E$) with the parallel component of shear-flow acceleration linked to unified betatron, grad-B drift, and parallel drift acceleration ($mv^2 1/2(1-\mu^2)\boldsymbol{b}\cdot(\boldsymbol{b}\cdot\nabla)\boldsymbol{V}_E$) to form collectively a shear-flow acceleration term (reduced shear-flow tensor without the compression term) that only yields net acceleration for the anisotropic part of the energetic particle distribution related to $f_2(p)$. Upon combining the two $\nabla\cdot\ \boldsymbol{V}_E$ terms in Equation (22) and doing the substitution $-\boldsymbol{b}\cdot(\boldsymbol{b}\cdot\nabla)\boldsymbol{V}_E=\boldsymbol{V}_E\cdot\kappa$, we find

$$\left\langle\frac{dK}{dt}\right\rangle_\phi = qE_\parallel v\mu+\frac{1}{2}mv^2(3\mu^2-1)(\boldsymbol{V}_E\cdot\kappa) - \frac{1}{2}mv^2(1-\mu^2)(\nabla\cdot\boldsymbol{V}_E). \quad (23)$$

Inspection of Equation (23) reveals that we recovered the expression in the bottom two lines of Equation (18) in a slightly different form. In the process we acquired an alternative interpretation of the plasma drift compression term (center term in Equation (23) and first term in the bottom line of Equation (18)). We have determined that this term can also be interpreted as a combination of curvature drift acceleration with unified betatron, grad-B drift, and parallel drift acceleration acting collectively as plasma drift compression acceleration to yield net acceleration for both the isotropic and the anisotropic parts of the energetic particle distribution. We also found that the $\boldsymbol{V}_E\cdot\kappa$ term in Equation (23) can be viewed as a combination of curvature drift acceleration with unified betatron, grad-B drift, and parallel drift acceleration acting collectively as plasma drift shear-flow acceleration that produces only net acceleration for the anisotropic part of the distribution.

6.1. Curvature Drift and Generalized Betatron Acceleration in Contracting and Merging Small-scale Flux Ropes, the Incompressible Limit

In the limit of incompressible flux-rope contraction or merging (in the strong guide field limit we interpret this to mean magnetic island area conservation during contraction or merging in the 2D plane perpendicular to the guide/background magnetic field) $0<-\nabla\cdot\boldsymbol{V}_E\ll\boldsymbol{V}_E\cdot\kappa=-\boldsymbol{b}\cdot(\boldsymbol{b}\cdot\nabla)\boldsymbol{V}_E>0$. Then, from Equations (18), (22), and (23) it follows that

$$\begin{aligned}\left\langle\frac{dK}{dt}\right\rangle_\phi &= [mv^2\mu^2(\boldsymbol{V}_E\cdot\kappa)]_\parallel \\ &\quad+(1-\mu^2)\left[M'\left(\frac{\partial B}{\partial t}+(\boldsymbol{V}_E\cdot\nabla)B\right)+B\frac{dM'}{dt}\right]_\perp \\ &= [mv^2\mu^2(\boldsymbol{V}_E\cdot\kappa)]_\parallel+\left[-\frac{1}{2}mv^2(1-\mu^2)(\boldsymbol{V}_E\cdot\kappa)\right]_\perp \\ &= [-mv^2\mu^2\boldsymbol{b}\cdot(\boldsymbol{b}\cdot\nabla)\boldsymbol{V}_E]_\parallel \\ &\quad+\left[\frac{1}{2}mv^2(1-\mu^2)\boldsymbol{b}\cdot(\boldsymbol{b}\cdot\nabla)\boldsymbol{V}_E\right]_\perp, \end{aligned} \quad (24)$$

where we expressed the magnetic moment as $M=M'(1-\mu^2)$. For incompressible magnetic island contraction or merging ($\boldsymbol{V}_E\cdot\kappa>0$) it is clear that curvature drift acceleration must result in parallel kinetic energy gain, which is associated with a negative parallel component for flux-rope plasma drift shear flow as stated above (compare the terms in square brackets associated with parallel kinetic energy changes in Equation (24)). However, for generalized (Lagrangian) betatron acceleration the result is perpendicular kinetic energy loss (compare the first two terms in the square brackets in the second line with the term in the second set of square brackets in the third line), assuming approximate conservation of the magnetic moment (neglecting the BdM'/dt term in the square brackets in the second line). This means that $MdB/dt=M(\partial B/\partial t+(\boldsymbol{V}_E\cdot\nabla)B)<0$. In this way we can relate the perpendicular kinetic energy loss to a decreasing magnetic field strength inside flux-rope structures when following the plasma drift $\boldsymbol{V}_E$ during incompressible flux-rope contraction or merging. From Poynting's theorem (Equation (15)) we know that incompressible contraction or merging of the flux-rope curved magnetic field results in $\partial B/\partial t<0$, implying that betatron acceleration should be associated with perpendicular kinetic energy loss. However, because it appears that $M(\boldsymbol{V}_E\cdot\nabla)B>0$ near the endpoints in contracting islands and in the X-point outflow regions of merging islands, grad-B drift acceleration generates perpendicular kinetic energy gain for energetic particles. Thus, $MdB/dt<0$ implies that perpendicular kinetic energy loss from betatron acceleration dominates perpendicular kinetic energy gain from grad-B drift acceleration in contracting and merging flux ropes in the incompressible limit. The conclusion that grad-B drift acceleration is of secondary importance is consistent with the results of Pritchett (2008) and Dahlin et al. (2014), for example.

In conclusion, energetic particle acceleration in incompressible contracting and merging small-scale flux ropes is related to negative parallel plasma drift shear-flow acceleration involving a competition between parallel kinetic energy gain from curvature drift acceleration and perpendicular kinetic energy loss predominantly from betatron acceleration. By combining the competing acceleration terms in each of the bottom two lines of Equation (24), it follows that

$$\begin{aligned}\left\langle\frac{dK}{dt}\right\rangle_\phi &= \frac{1}{2}mv^2(3\mu^2-1)(\boldsymbol{V}_E\cdot\kappa) \\ &= -\frac{1}{2}mv^2(3\mu^2-1)\boldsymbol{b}\cdot(\boldsymbol{b}\cdot\nabla)\boldsymbol{V}_E, \end{aligned} \quad (25)$$

revealing that net acceleration from the combination of the two competing acceleration processes only involves the anisotropic part of the distribution related to $f_2(p)$ when assuming an expansion of the distribution to the second moment (nearly isotropic distribution) and averaging the complete acceleration term including the distribution function over all μ values. This competition is illustrated in diagram form for ions in a contracting small-scale flux-rope ion in Figure 1 and in two neighboring merging flux ropes in Figure 2.

Inspection of Equation (25) reveals that for pitch angles satisfying $\mu^2>1/3$, $\langle dK/dt\rangle_\phi>0$ so that curvature drift

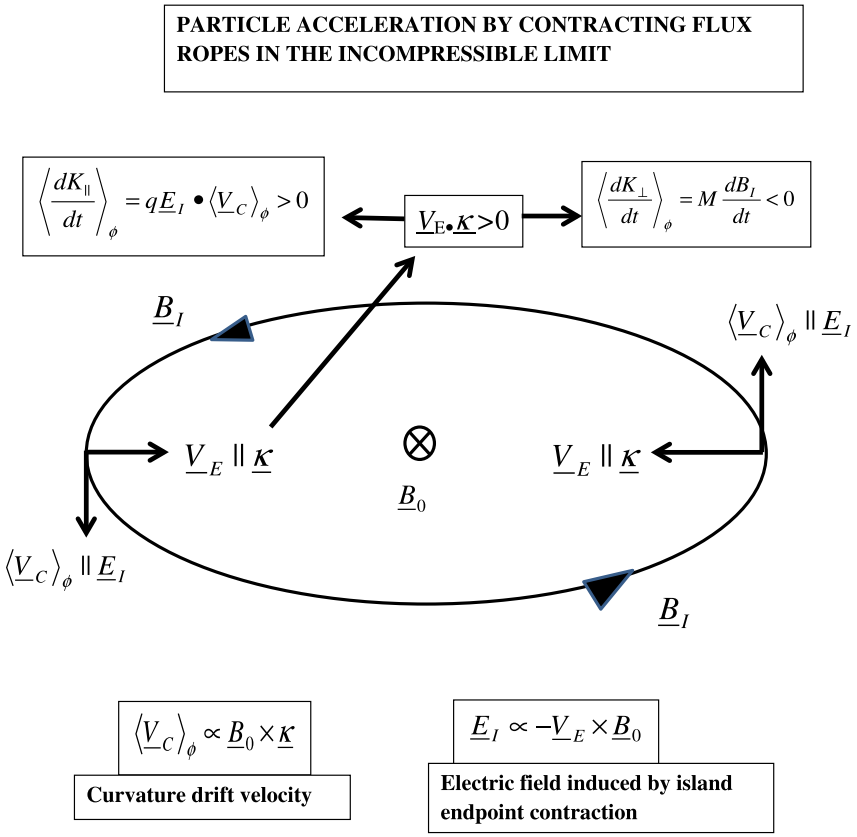

Figure 1. Schematic diagram of energetic ion acceleration by a contracting quasi-2D flux rope in the incompressible limit. Shown is the island (twist) magnetic field component $\boldsymbol{B}_I$ of the flux-rope structure in the 2D plane perpendicular to the locally uniform guide field (axial) component $\boldsymbol{B}_0$ of the flux rope pointing into the page. $\boldsymbol{V}_E$ is the contraction velocity (plasma drift velocity) at the endpoints of the island, and $\kappa = (\boldsymbol{b} \cdot \nabla)\,\boldsymbol{b}$ is the magnetic curvature vector, which points in the same direction as the contraction velocity $\boldsymbol{V}_E$. Thus, for a contracting island $\boldsymbol{V}_E \cdot \kappa > 0$. This ensures parallel kinetic energy gain from curvature drift acceleration by the in-plane electric field $\boldsymbol{E}_I \approx -\boldsymbol{V}_E \times \boldsymbol{B}_0$ induced by contraction because $q\boldsymbol{E}_I \cdot \langle \boldsymbol{V}_C \rangle_{\phi} > 0$, where $\langle \boldsymbol{V}_C \rangle_{\phi}$ is the curvature drift velocity (see Equation (19)), but perpendicular kinetic energy loss from generalized betatron acceleration (combination of betatron and grad-B drift acceleration) because $MdB/dt < 0$ (see Equations (20) and (22)). Since betatron acceleration generates perpendicular kinetic energy loss because of the decreasing magnetic field strength with time during contraction (see Equation (15)) and grad-B drift acceleration results in perpendicular kinetic energy gain at the island endpoints, generalized betatron acceleration is dominated by betatron kinetic energy loss.

energization is more efficient than generalized betatron energy loss during incompressible contraction/merging of small-scale flux ropes. When $\mu^2 < 1/3$, betatron energy loss dominates curvature drift energization. That is why the net acceleration obtained from the two competing acceleration mechanisms depends sensitively on the anisotropy characteristics of the energetic particle pitch-angle distribution as discussed above. Consider the following three possibilities: (1) If energetic particles maintain a highly beamed pitch-angle distribution (which requires negligible pitch-angle scattering), curvature drift energy gain strongly dominates generalized betatron energy loss, and for all practical purposes we have a first-order Fermi acceleration mechanism as a consequence of incompressible contraction or merging of curved flux-rope magnetic fields (de Gouveia dal Pino & Lazarian 2005; Drake et al. 2006, 2010). (2) If the energetic particle distribution stays purely isotropic (extremely strong pitch-angle particle scattering), we can average the last terms in Equation (25) over all μ values to find $\langle dK/dt \rangle_{\phi} = 0$, indicating that the probability for curvature drift energy gain equals the probability for betatron energy loss (Drake et al. 2010). This supports the conclusion made above that net acceleration requires and depends only on the anisotropic part of the distribution. (3) The energetic particle distribution maintains a particle distribution with a small pitch-angle anisotropy (efficient pitch-angle scattering consistent with the diffusion approximation). In this case particle energization by incompressible contraction or merging of curved flux-rope magnetic fields becomes a second-order Fermi acceleration process (Drake et al. 2013; Zank et al. 2014; le Roux et al. 2015a). The small anisotropy option is supported by self-consistent particle simulations of turbulent magnetic reconnection and island formation at stacked primary current sheets in the absence of a guide field (Schoeffler et al. 2011; Drake et al. 2013), because energetic particles are scattered by fluctuations generated by plasma instabilities such as the firehose and magnetic mirror instabilities, resulting in energetic charged particle distributions with small anisotropies. However, in the presence of a strong guide field, particle simulations suggest larger anisotropies owing to weaker instabilities (Dahlin et al. 2017; Li et al. 2018).

6.2. Curvature Drift and Generalized Betatron Acceleration in Contracting and Merging Small-scale Flux Ropes, the Compressible Limit

When flux-rope contraction and merging occur in the compressible limit (area reduction during contraction or merging in 2D magnetic island plane perpendicular to the guide magnetic field) so that $0 < -\nabla \cdot \boldsymbol{V}_E \gg \boldsymbol{V}_E \cdot \kappa = -\boldsymbol{b} \cdot (\boldsymbol{b} \cdot \nabla)\boldsymbol{V}_E > 0$,

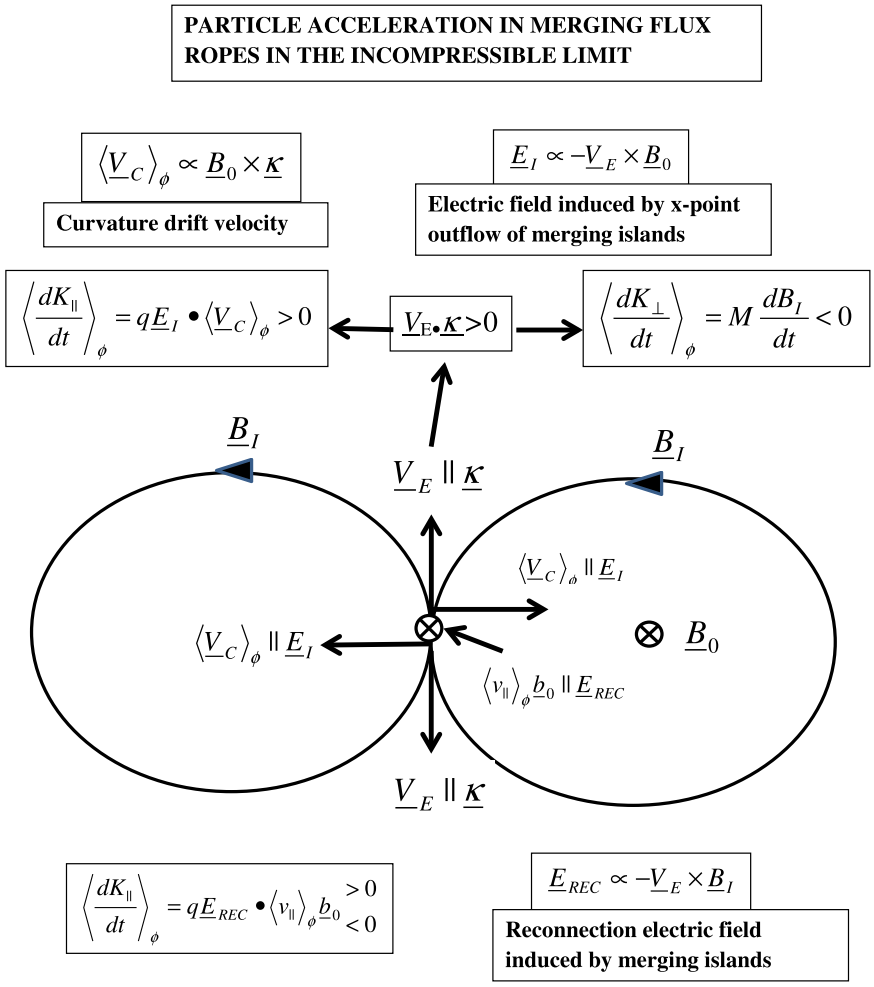

Figure 2. Schematic diagram of ion acceleration by two merging (reconnecting), quasi-2D flux ropes in the incompressible limit. Shown is the island magnetic field $\boldsymbol{B}_I$ in the 2D plane perpendicular to a uniform guide field component $\boldsymbol{B}_0$ pointing into the page. $\boldsymbol{V}_E$ is the X-point plasma outflow drift velocity in the merging area at the center of the merging magnetic islands pointing in the same direction as the magnetic curvature vector κ. Thus, in the merging region (reconnecting area) $\boldsymbol{V}_E \cdot \kappa > 0$, resulting in parallel kinetic energy gain from curvature drift acceleration and perpendicular kinetic energy loss from generalized betatron acceleration. Since betatron acceleration results in perpendicular kinetic energy loss because of the decreasing magnetic field strength with time during the merging process (see Equation (15)) and grad-B drift acceleration results in perpendicular kinetic energy gain in the merging island area, generalized betatron acceleration is dominated by betatron kinetic energy loss. In the center of the merging area, the reconnection electric field $\boldsymbol{E}_{\rm REC} = -\boldsymbol{V}_E \times \boldsymbol{B}_I$ points into the page. Energetic particle guiding center motion along/against $\boldsymbol{B}_0$ will result in parallel kinetic energy gain/loss from the reconnection electric field.

we find from Equations (18) and (22) that

$$\begin{aligned}\left\langle \frac{dK}{dt} \right\rangle_\phi &= [mv^2\mu^2(\boldsymbol{V}_E \cdot \kappa)]_\parallel \\ &+ (1-\mu^2)\left[M'\left(\frac{\partial B}{\partial t} + (\boldsymbol{V}_E \cdot \nabla)B\right) + B\frac{dM'}{dt}\right]_\perp \\ &= \left[-\frac{1}{3}mv^2\mu^2(\nabla \cdot \boldsymbol{V}_E)\right]_\parallel + \left[-\frac{1}{3}mv^2(1-\mu^2)(\nabla \cdot \boldsymbol{V}_E)\right]_\perp \\ &+ \left[\frac{1}{3}mv^2\mu^2(\nabla \cdot \boldsymbol{V}_E)\right]_\parallel + \left[-\frac{1}{6}mv^2(1-\mu^2)(\nabla \cdot \boldsymbol{V}_E)\right]_\perp, \quad (26)\end{aligned}$$

where the two $\nabla \cdot \boldsymbol{V}_E$ terms in the third line of Equation (26) are a decomposition of the compression term $1/3mv^2(\nabla \cdot \boldsymbol{V}_E)$, which yields net acceleration for the isotropic part of the distribution $f_0(p)$ (see Equation (21) and its discussion above), into parallel and perpendicular kinetic energy changes. The two $\nabla \cdot \boldsymbol{V}_E$ terms in the fourth line of Equation (26) are a decomposition of the compression term $1/3mv^2 1/2(3\mu^2 - 1)(\nabla \cdot \boldsymbol{V}_E)$ (see Equation (22) and its discussion above), which produces net acceleration for the second moment of the particle distribution $f_2(p)$, into parallel and perpendicular kinetic energy changes.

Let us first concentrate on the compression terms for $f_0(p)$ (those in the third line of Equation (26)) because they will dominate acceleration for a nearly isotropic energetic particle distribution. During contraction and merging in the compressible limit, the dominant term $\nabla \cdot \boldsymbol{V}_E < 0$ and the relatively small term $\boldsymbol{V}_E \cdot \kappa > 0$. Thus, the term in the square brackets in the first line containing $\boldsymbol{V}_E \cdot \kappa$ and the term in the first set of square brackets in the third line containing $\nabla \cdot \boldsymbol{V}_E$ both suggest that curvature drift acceleration will contribute to parallel kinetic energy gain during flux-rope compression. By comparing the generalized betatron expression consisting of the first two terms in the second line with the compression term in the second set of square brackets in the third line, it follows that the generalized betatron acceleration term will result in perpendicular kinetic energy gain during flux-rope compression ($\nabla \cdot \boldsymbol{V}_E < 0$) assuming approximate conservation of the magnetic moment ($dM/dt \approx 0$). Therefore,

$MdB/dt = M(\partial B/\partial t + (\boldsymbol{V}_E \cdot \nabla)B) > 0$, relating the perpendicular kinetic energy gain to an increasing magnetic field strength with time following the plasma drift flow in flux ropes undergoing compression. Applying $|\nabla \cdot \boldsymbol{V}_E| \gg \boldsymbol{V}_E \cdot \kappa > 0$ and $\nabla \cdot \boldsymbol{V}_E < 0$ in Poynting's theorem (Equation (15)), it follows that $\partial B/\partial t > 0$, so that standard betatron acceleration $M(\partial B/\partial t)$ contributes to perpendicular kinetic energy gain. Therefore, perpendicular kinetic energy gain from generalized betatron acceleration can be explained by standard betatron acceleration if grad-B drift acceleration in contracting and merging magnetic islands is a minor component, as discussed above, suggesting that what matters is the increasing flux-rope field strength with time rather than spatially. The compressible acceleration case is illustrated for ions in a contracting small-scale flux rope in Figure 3.

Consider the compression terms in the bottom line of Equation (26), which collectively yields net acceleration for the relatively small second moment $f_2(p)$ of the particle distribution based on our moment expansion to the second moment for a nearly isotropic particle distribution. For flux-rope compression ($\nabla \cdot \boldsymbol{V}_E < 0$) we find curvature drift acceleration resulting in parallel kinetic energy loss (first term in the bottom line of Equation (26)) and generalized betatron acceleration contributing to perpendicular kinetic energy gain (second term in the bottom line). By combining again the compression acceleration terms for curvature and betatron acceleration in each of the bottom two lines of Equation (26), it follows that for flux-rope compression

$$\left\langle \frac{dK}{dt} \right\rangle_\phi = -\frac{1}{3}mv^2(\nabla \cdot \boldsymbol{V}_E) + \frac{1}{3}mv^2\frac{1}{2}(3\mu^2 - 1)(\nabla \cdot \boldsymbol{V}_E). \quad (27)$$

The first compression term in Equation (27), associated with $f_0(p)$, can be viewed as a first-order Fermi acceleration mechanism because both curvature drift acceleration and generalized betatron acceleration contribute to energy gain. Therefore, net energy gain from the combination of the two acceleration mechanisms occurs for all particle pitch angles during flux-rope compression. The second compression term in Equation (27) associated with $f_2(p)$ predicts net energy loss for pitch angles $\mu^2 > 1/3$ when parallel kinetic energy loss from curvature drift acceleration dominates, and net energy gain for pitch angles $\mu^2 < 1/3$ when perpendicular energy gain from generalized betatron acceleration dominates during flux-rope compression. Consequently, in the case of a nearly isotropic distribution maintained by frequent pitch-angle scattering, particle energization associated with the anisotropic part of the distribution related to $f_2(p)$ becomes a second-order Fermi process (Zank et al. 2014; le Roux et al. 2015a). If the particle distribution stays purely isotropic (extremely strong pitch-angle scattering), we can average the last compression term in Equation (27) over all μ values. This yields zero net energy gain so that energy gain is determined by first-order Fermi acceleration produced by the first compression term in Equation (27) connected to $f_0(p)$.

To summarize, consider the key differences in combined energetic particle curvature drift and generalized betatron acceleration in flux ropes that contract and merge in the compressible and incompressible limits. In the incompressible limit there is a competition between parallel kinetic energy gain from curvature drift acceleration and perpendicular perpendicular kinetic energy loss from generalized betatron acceleration, which acts collectively in terms of a negative parallel component of flux-rope plasma drift shear flow. The combined acceleration only yields net energization when the particle distribution is anisotropic because zero net acceleration occurs for the isotropic part of the distribution. For a nearly isotropic distribution expanded in Legendre polynomial moments to the second moment, only the second moment $f_2(p)$ yields net energization in the form of second-order Fermi or stochastic acceleration due to efficient pitch-angle scattering. In contrast, in the compressible limit there is both parallel kinetic energy gain from curvature drift acceleration and perpendicular kinetic energy gain from generalized betatron acceleration that act collectively as plasma drift compression acceleration to yield net acceleration for the isotropic part of the particle distribution in terms of a first-order Fermi acceleration process. However, additional compression acceleration issues from the anisotropic part of the distribution, where there is a competition between parallel kinetic energy loss from curvature drift acceleration and perpendicular kinetic energy gain from generalized betatron acceleration. In the limit of a nearly isotropic distribution expanded up to the second moment, frequent pitch-angle scattering turns this competition into a second-order Fermi acceleration process, where only the second moment of the particle distribution $f_2(p)$ produces net energization. Since the isotropic part of the distribution is dominant, the probability of first-order Fermi acceleration is higher. For a purely isotropic distribution, there is no net energization from second-order Fermi acceleration during flux-rope compression. Net energization then solely stems from first-order Fermi acceleration involving $f_0(p)$. It appears that if the limit of a nearly isotropic particle distribution holds, one would expect particle energization involving curvature drift and betatron acceleration during compression acceleration to be more efficient compared to when the same acceleration processes are associated with incompressible shear-flow acceleration because (i) first-order Fermi compression acceleration is most likely to occur and (ii) its efficiency is not degraded by energy losses. However, it is less clear whether compression acceleration will be more efficient than incompressible shear-flow acceleration when the particle distribution is strongly anisotropic. For a further discussion of the role of shear flow and compression in small-scale flux-rope acceleration from the viewpoint of full kinetic simulations, see Li et al. (2018).

6.3. Parallel Guiding Center Motion Acceleration by the Reconnection Electric Field of Merging Flux Ropes

Finally, consider the first term in Equation (18), which represents parallel guiding center motion acceleration by the parallel electric field component. We consider this component to be the reconnection electric field generated as a consequence of magnetic reconnection occurring in the 2D plane perpendicular to the guide field at secondary current sheets forming between merging flux ropes, as discussed above. If a strongly beamed ion pitch-angle distribution can be maintained in the direction of the parallel electric field, only energy gain will occur. For a completely isotropic energetic particle distribution, when it is appropriate to average the first term in Equation (18) over all pitch angles, the result is a zero net gain of parallel kinetic energy because of the equal probability of energy gain

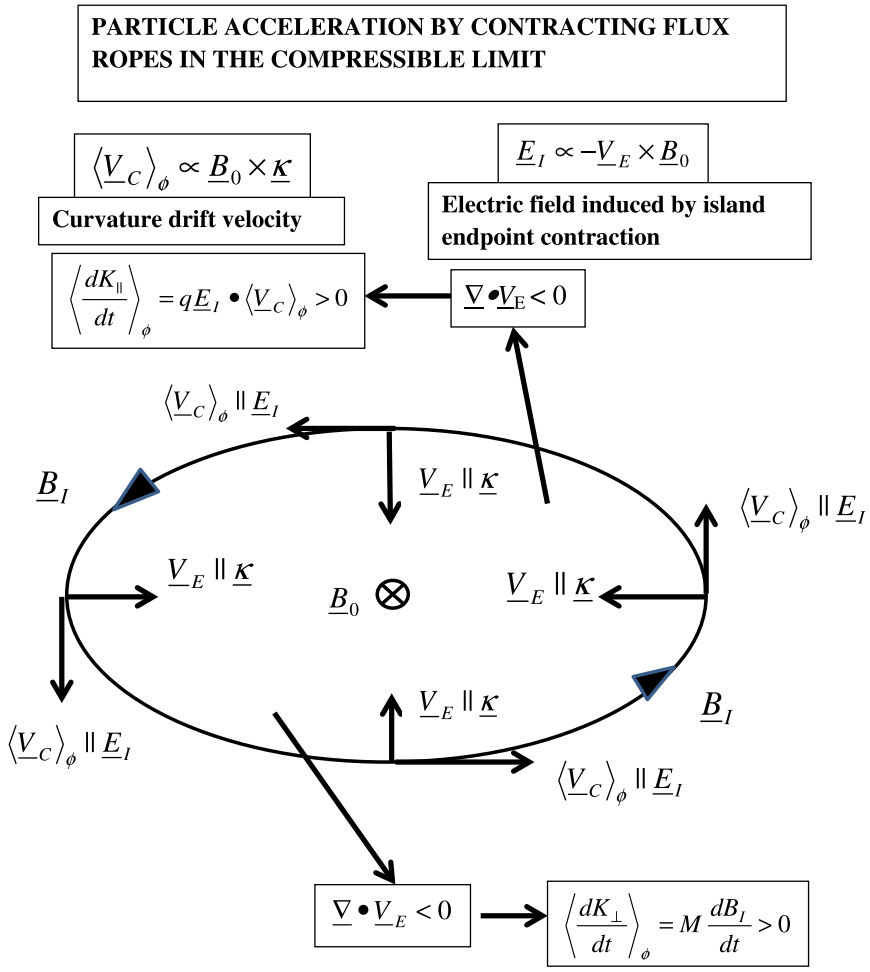

Figure 3. Schematic diagram of ion acceleration in a compressible contracting quasi-2D flux rope. Shown is the island magnetic field (twist component) $\boldsymbol{B_I}$ in the 2D plane perpendicular to a locally uniform guide field component $\boldsymbol{B_0}$ pointing into the page. In the compressible limit the divergence of the contraction velocity $\nabla \cdot \boldsymbol{V}_E < 0$ results in perpendicular kinetic energy gain for energetic particles from the generalized betatron acceleration term $MdB/dt > 0$ (see Equation (24)), which combines the betatron acceleration term with the grad-B drift acceleration term. In this case the flux-rope magnetic field strength increases with time (Equation (15)), so that both betatron and grad-B drift acceleration at the island endpoints contributes to perpendicular kinetic energy gain. Since $\boldsymbol{V}_E \cdot \kappa > 0$ for compressible contraction, there is also parallel kinetic energy gain from curvature drift acceleration, but because $|\nabla \cdot \boldsymbol{V}_E| \gg \boldsymbol{V}_E \cdot \kappa > 0$ in the compressible limit, perpendicular kinetic energy gain from generalized betatron acceleration is dominant.

and loss. In the case of a nearly isotropic distribution, both energy gains and losses occur, and the parallel guiding center motion acceleration by the parallel reconnection electric field in merging flux ropes becomes a second-order Fermi acceleration process. However, the difference is that the particle kinetic energy rate of change for this acceleration mechanism is proportional to particle speed, whereas for the combined curvature drift and generalized betatron acceleration mechanisms it is proportional to particle speed squared. Thus, if acceleration by the parallel reconnection electric field is dominant at lower suprathermal energies, it might not be the case at higher particle energies (e.g., le Roux et al. 2015b; Dahlin et al. 2016).

Note that the discussion about a purely isotropic particle distribution (or the isotropic part of the distribution) yielding zero net particle acceleration for the latter two acceleration cases only considered particle interaction with a single small-scale flux rope. Further below we discuss whether this conclusion also holds when energetic particles respond to numerous contracting and merging magnetic islands. Besides investigating particle acceleration in response to the mean induced electric fields associated with numerous contracting and merging small-scale flux ropes, we also analyze further below how particle acceleration is affected in response to statistical fluctuations of the electric fields (see also Bian & Kontar 2013). These fluctuations are responsible for additional second-order Fermi acceleration for each of the acceleration mechanisms discussed above that should also be investigated. Different from particle interaction with a single flux rope, we find that these additional second-order Fermi acceleration processes can occur for the isotropic part of the distribution for each flux-rope acceleration case.

7. Classification of Flux-rope Acceleration Mechanisms in the Focused Transport Equation

7.1. Relative Rates of Momentum Change

Before introducing our classification for the different flux-rope acceleration mechanisms in focused transport theory, we discuss the transformation of the standard guiding center kinetic transport equation into an equivalent transport equation commonly used in space physics applications, namely, the standard focused transport equation (le Roux & Webb 2009; le Roux et al. 2015a). In this approach, the focus shifts from

describing energy changes in terms of guiding center motion, drifts and particle gyration in the plasma electric fields, or guiding center motion in the magnetic fields advected at the nonuniform plasma drift velocity to energy changes associated with guiding centers propagating in the total nonuniform plasma flow. In the focused transport version, guiding center kinetic theory terms for the rate of change in kinetic energy, as presented in Equations (22) and (23), reappear as part of similar-looking terms referring to the total plasma flow velocity $\boldsymbol{U}$, which we express in terms of a gyrophase-averaged relative momentum rate of change:

$$\frac{1}{p}\left\langle \frac{dp}{dt}\right\rangle_{\phi} = \mu\left(\frac{q\boldsymbol{E}}{p} - \frac{1}{v}\frac{d\boldsymbol{U}}{dt}\right)\cdot\boldsymbol{b} - \frac{1}{2}(3\mu^2-1)\boldsymbol{b}\cdot(\boldsymbol{b}\cdot\nabla)\boldsymbol{U} - \frac{1}{2}(1-\mu^2)(\nabla\cdot\boldsymbol{U}). \quad (28)$$

The complete guiding center kinetic transport equation (not shown) can be transformed into the focused transport equation by (i) assuming the unspecified electric field of the plasma to be the motional electric field $\boldsymbol{E} = -\boldsymbol{U}\times\boldsymbol{B}$, leading to the replacement $\boldsymbol{V}_E = \boldsymbol{U}_\perp$, and (ii) transforming $v_\parallel$ from the observer frame to the plasma flow frame according to $v_\parallel = v'_\parallel + mU_\parallel\boldsymbol{b}$. Consequently, the total plasma flow velocity $\boldsymbol{U} = U_\parallel\boldsymbol{b} + \boldsymbol{U}_\perp$ appears as we move from a description where particle velocity is transformed from the observer frame to the nonuniform plasma drift frame ($\boldsymbol{V}_E$-frame) to one where particle velocity is transformed from the observer frame to the frame of the total nonuniform plasma flow velocity ($\boldsymbol{U}$-frame). In the transformation process an additional acceleration term appears referring to parallel guiding center motion acceleration by the noninertial frame pseudo-force associated with the parallel component of the acceleration of the plasma flow $d\boldsymbol{U}/dt\cdot\boldsymbol{b}$ with $d/dt = \partial/\partial t + (\boldsymbol{U}\cdot\nabla)$ (for more details, see le Roux & Webb 2007, 2009). Therefore, we can recover exactly the guiding center theory expression for the rate of change of kinetic energy given by Equation (23) from the focused transport expression (28) by imposing the limit $U_\parallel = 0$ in Equation (28), replacing $\boldsymbol{U}_\perp$ with $\boldsymbol{V}_E$, converting the shear-flow term to the magnetic curvature advection term according to $-\boldsymbol{b}\cdot(\boldsymbol{b}\cdot\nabla)\boldsymbol{V}_E = \boldsymbol{V}_E\cdot\kappa$, and multiplying Equation (28) by the factor pv to convert the relative momentum rate of change to the rate of change in kinetic energy.

Based on the discussion above of the different flux-rope acceleration mechanisms from the perspective of guiding center kinetic theory, as well as the close relationship between this theory and focused transport theory as presented in Equation (28), we classify and specify the different flux-rope acceleration mechanisms appearing in the focused transport equation using assumptions valid in the solar wind near 1 au discussed in Section 4: (i) $\boldsymbol{U} = \boldsymbol{U}_0 + \delta\boldsymbol{U}_I$ ($\langle\delta\boldsymbol{U}_I\rangle = 0$), $\boldsymbol{B} = \boldsymbol{B}_0 + \delta\boldsymbol{B}_I$ ($\langle\delta\boldsymbol{B}_I\rangle = 0$), where $\boldsymbol{U}_0$ is the background solar wind velocity, $\delta\boldsymbol{U}_I$ is the small-scale flux-rope flow, $\boldsymbol{B}_0$ is the background magnetic field also acting as the flux-rope axial or guide field component (see discussion in Section 4), and $\delta\boldsymbol{B}_I$ is the small-scale flux-rope twist or magnetic island component; (ii) the magnetic field direction $\boldsymbol{b}\approx\boldsymbol{b}_\circ + (\delta\boldsymbol{B}_I/B_0)\approx\boldsymbol{b}_\circ$ assuming the strong guide field limit $\langle\delta B_I^2\rangle^{1/2}/B_0 \ll 1$; (iii) $\langle\delta U_I^2\rangle^{1/2}/U_0 \ll 1$; (iv) $\delta\boldsymbol{U}_I\perp\boldsymbol{B}_0$ and $\delta\boldsymbol{B}_I\perp\boldsymbol{B}_0$ vary spatially predominantly in the 2D plane perpendicular to $\boldsymbol{B}_0$.

On this basis, the relative gyrophase-averaged momentum rate of change of energetic particles is decomposed into two parts:

$$\frac{1}{p}\left\langle\frac{dp}{dt}\right\rangle_{\phi} = \frac{1}{p}\left\langle\frac{dp}{dt}\right\rangle_{\phi}^{\rm SW} + \frac{1}{p}\left\langle\frac{dp}{dt}\right\rangle_{\phi}^{I}, \quad (29)$$

where $(1/p)\langle dp/dt\rangle_\phi^{\rm SW}$ is the rate of momentum change due to particle interaction with the nonuniform background solar wind flow and magnetic field, and $(1/p)\langle dp/dt\rangle_\phi^{I}$ is the rate of momentum change due to particle interaction with the nonuniform flow and magnetic field of contracting and merging active small-scale flux ropes and the nonuniform parallel reconnection electric field formed in merging small-scale flux ropes. Entirely consistent with standard focused transport theory (e.g., Isenberg 1987; le Roux & Webb 2007),

$$\frac{1}{p}\left\langle\frac{dp}{dt}\right\rangle_{\phi}^{\rm SW} = \mu\left(\frac{q\boldsymbol{E}_{\rm surf}}{p} - \frac{1}{v}\frac{d\boldsymbol{U}_0}{dt}\right)\cdot\boldsymbol{b}_0 - \frac{1}{2}(3\mu^2-1)\boldsymbol{b}_0\cdot(\boldsymbol{b}_0\cdot\boldsymbol{\nabla})\boldsymbol{U}_0 - \frac{1}{2}(1-\mu^2)(\boldsymbol{\nabla}\cdot\boldsymbol{U}_0), \quad (30)$$

where $\boldsymbol{E}_{\rm surf}$ refers to a nonmotional electric field component at special surfaces such as the cross-shock electric field at shocks (the background motional electric field is not included because its parallel component $\boldsymbol{E}_0\cdot\boldsymbol{b}_0 = -\boldsymbol{U}_0\times\boldsymbol{B}_0\cdot\boldsymbol{b}_0 = 0$). The small-scale flux-rope acceleration mechanisms are classified according to

$$\frac{1}{p}\left\langle\frac{dp}{dt}\right\rangle_{\phi}^{I} = \mu(\nu_{\rm REC}^I + \nu_{\rm ACC}^I) + \frac{1}{2}(3\mu^2-1)\nu_{\rm INC}^I + \frac{1}{2}(1-\mu^2)\nu_{\rm COM}^I, \quad (31)$$

where

$$\begin{aligned}
\nu_{\rm REC}^I &= \frac{q}{p}\boldsymbol{E}_{\rm REC}\cdot\boldsymbol{b}_\circ = -\frac{q}{p}\delta\boldsymbol{U}_I\times\delta\boldsymbol{B}_I\cdot\boldsymbol{b}_\circ,\\
\nu_{\rm ACC}^I &= -\frac{1}{v}\frac{d\delta\boldsymbol{U}_I}{dt}\cdot\left(\boldsymbol{b}_\circ + \frac{\delta\boldsymbol{B}_I}{B_\circ}\right),\ \left(\frac{d}{dt}\approx\frac{\partial}{\partial t} + (\boldsymbol{U}_\circ\cdot\nabla)\right)\\
\nu_{\rm INC}^I &= -\frac{\delta\boldsymbol{B}_I}{B_\circ}\cdot\left(\frac{\delta\boldsymbol{B}_I}{B_\circ}\cdot\nabla\right)\delta\boldsymbol{U}_I,\\
\nu_{\rm COM}^I &= -(\nabla\cdot\delta\boldsymbol{U}_I).
\end{aligned} \quad (32)$$

In Equation (32), the rate $\nu_{\rm REC}^I$ refers to the relative gyrophase-averaged momentum rate of change sans the μ-dependence due to energetic particle parallel guiding center motion acceleration by the parallel reconnection electric field formed in the reconnection zones of merging magnetic island structures (as discussed in Section 4, in the strong guide field limit both the field-aligned guiding center motion and the reconnection electric field are predominantly along the guide field $\boldsymbol{B}_0$). Consider the rate $\nu_{\rm ACC}$ in the second line of Equation (32). This expression determines the relative gyrophase-averaged rate of momentum change in response to parallel guiding center motion acceleration by parallel noninertial force $\boldsymbol{F}_{\rm ACC}$ associated with the field-aligned

component of the acceleration of the flow $\delta \boldsymbol{U}_I$ of contracting and merging flux ropes. The force has the vector component expression

$$F_{\rm ACC} = m\left\langle \frac{dv_\parallel}{dt}\right\rangle_\phi = -m\frac{d\delta \boldsymbol{U}_I}{dt}\cdot\left(\boldsymbol{b}_0 + \frac{\delta \boldsymbol{B}_I}{B_0}\right). \quad (33)$$

This flux-rope acceleration mechanism is a new addition to our theory not considered in our initial theoretical development (le Roux et al. 2015a). Finally, the rate $\nu^I_{\rm INC}$ determines the relative gyrophase-averaged momentum rate of change for energetic particles experiencing the combined acceleration effect of curvature drift energy gain and generalized betatron energy loss in contracting and merging small-scale flux ropes operating in the incompressible limit (flux-rope parallel shear-flow acceleration), whereas $\nu^I_{\rm COM}$ determines the combined gyrophase-averaged acceleration effect of curvature drift and generalized betatron energy gains when contracting and merging of small-scale flux ropes occur in the compressible limit (flux-rope compression acceleration).

7.2. Rate of Change of Pitch Angle

In the same way, the energetic particle gyrophase-averaged pitch-angle rate of change in focused transport theory, expressed in terms of $\langle d\mu/dt\rangle_\phi$, where $\mu = \cos\theta$ (with θ the particle pitch angle), can be decomposed into two contributions:

$$\left\langle \frac{d\mu}{dt}\right\rangle_\phi = \left\langle \frac{d\mu}{dt}\right\rangle^{\rm SW}_\phi + \left\langle \frac{d\mu}{dt}\right\rangle^{I}_\phi, \quad (34)$$

where $\langle d\mu/dt\rangle^{\rm SW}_\phi$ is related to the rate of pitch-angle change due to particle interaction with the nonuniform background solar wind magnetic field and flow, and $\langle d\mu/dt\rangle^I_\phi$ is connected to the rate of pitch-angle change due to particle interaction with the nonuniform magnetic field and flow of contracting and merging active small-scale flux ropes and the parallel reconnection electric field of merging flux ropes. Their expressions are

$$\left\langle \frac{d\mu}{dt}\right\rangle^{\rm SW}_\phi = \frac{1}{2}(1-\mu^2)(v(\boldsymbol{\nabla}\cdot\boldsymbol{b}_0) + \mu(\boldsymbol{\nabla}\cdot\boldsymbol{U}_0) - 3\mu\boldsymbol{b}_0\cdot(\boldsymbol{b}_0\cdot\boldsymbol{\nabla})\boldsymbol{U}_0 - 2\left(\frac{1}{v}\frac{d\boldsymbol{U}_0}{dt} - \frac{q\boldsymbol{E}_{\rm surf}}{p}\right)\cdot\boldsymbol{b}_0\right) \quad (35)$$

and

$$\left\langle \frac{d\mu}{dt}\right\rangle^{I}_\phi = \frac{1}{2}(1-\mu^2)(\nu^I_{\rm REF} - \mu\nu^I_{\rm COM} + 3\mu\nu^I_{\rm INC} + 2(\nu^I_{\rm ACC} + \nu^I_{\rm REC})). \quad (36)$$

Present in Equation (36) are the expressions $\nu^I_{\rm REC}$, $\nu^I_{\rm ACC}$, $\nu^I_{\rm INC}$, $\nu^I_{\rm COM}$, which, having determined the relative rate of change of p in Equations (31) and (32), are likewise also determining the associated rate of change of μ of energetic particles for the four different flux-rope acceleration cases. However, there is an additional contribution to the pitch-angle rate of change labeled $\nu^I_{\rm REF}$ (first term of Equation (36)) with the approximate expression

$$\nu^I_{\rm REF} \approx \nu\left(\nabla\cdot\frac{\delta \boldsymbol{B}_I}{B_0}\right), \quad (37)$$

in the limit of a strong guide field ($\delta B_I/B_0 \ll 1$). For energetic particles, this term should be the dominant contribution to the total $\langle d\mu/dt\rangle^I_\phi$ because $\nu^I_{\rm REF}\propto v$ is the only term in Equation (36) that increases with particle speed. This term refers to the magnetic mirroring force associated with the nonuniform magnetic island (flux-rope twist) component field strength δB_I acting on energetic particles propagating along the magnetic field, because we can rephrase Equation (37) in terms of a parallel flux-rope mirroring force $\boldsymbol{F}_{\rm REF}$ with a vector component

$$F_{\rm REF} \approx m\left\langle \frac{dv_\parallel}{dt}\right\rangle_\phi = -M_0\left(\frac{\delta \boldsymbol{B}_I}{B_0}\cdot\nabla\right)\delta B_I, \quad (38)$$

where M_0 is the magnetic moment associated with the background magnetic field. As discussed by Guidoni et al. (2016), particles following the magnetic island field inside small-scale flux ropes should encounter maximum field strengths when they reach the center of the magnetic island, resulting potentially in particle reflection in flux-rope center regions.

8. The Coupled Kinetic-MHD Transport Equations for Self-consistent Acceleration of Energetic Particles by Numerous Contracting and Merging (Reconnecting) Small-scale Flux Ropes

In le Roux et al. (2015a) we presented details of a derivation of a focused transport equation with Fokker–Plank terms for energetic charged particle nonresonant interaction with numerous contracting and merging small-scale flux ropes. This was accomplished using the standard guiding center kinetic equation (Kulsrud 1983) as a starting point, followed by transforming this equation into a focused transport equation (le Roux & Webb 2009). We remind the reader that the derived focused transport equation is restricted to particle energies where the particle gyroradii $r_g \ll L_I$ (L_I is the characteristic cross-sectional radius of the small-scale flux ropes considered), which is ideal for studying energetic particles that are quasi-trapped in these structures. Solar wind observations at 1 au show small-scale flux ropes to have a characteristic cross section up to ~0.01 au near the heliospheric current sheet. For comparison a suprathermal 1 keV proton at 1 au has a gyroradius of $\sim 5\times10^{-6}$ au. Thus, the theory applies to a wide range of suprathermal particle energies that easily includes MeV energies, making it suitable for studying acceleration of suprathermal ions as observed in the solar wind. A decomposition of the plasma flow and magnetic field into a background solar wind component and a turbulent magnetic island component was introduced, followed by a perturbation analysis to model particle interaction with numerous dynamic magnetic islands. This involved decomposing the relative particle acceleration rates in Equation (32) and the pitch-angle rates of change in Equation (36) into mean

and random fluctuating parts, that is,

$$\begin{aligned}
\nu^I_{\rm REC} &= \langle \nu^I_{\rm REC}\rangle + \delta\nu^I_{\rm REC},\ \langle \delta\nu^I_{\rm REC}\rangle = 0,\\
\nu^I_{\rm ACC} &= \langle \nu^I_{\rm ACC}\rangle + \delta\nu^I_{\rm ACC},\ \langle \delta\nu^I_{\rm ACC}\rangle = 0,\\
\nu^I_{\rm INC} &= \langle \nu^I_{\rm INC}\rangle + \delta\nu^I_{\rm INC},\ \langle \delta\nu^I_{\rm INC}\rangle = 0,\\
\nu^I_{\rm COM} &= \langle \nu^I_{\rm COM}\rangle + \delta\nu^I_{\rm COM},\ \langle \delta\nu^I_{\rm COM}\rangle = 0,\\
\nu^I_{\rm REF} &= \langle \nu^I_{\rm REF}\rangle + \delta\nu^I_{\rm REF},\ \langle \delta\nu^I_{\rm REF}\rangle = 0.
\end{aligned} \tag{39}$$

By allowing for mean acceleration rates, we can, for example, model the acceleration effect if flux-rope contraction is more probable than expansion (during early-time primary current sheet reconnection), whereas taking the variance of fluctuations, the acceleration rates enable us to simulate acceleration when the probability of flux-rope contraction equals the probability expansion and the mean acceleration rate is zero (during later times when primary current sheet magnetic reconnection gives way to a sea of intermittently merging magnetic islands that expand and contract after merging; Oka et al. 2010). The outcome of the perturbation analysis is a modified focused transport equation that includes transport terms for coherent particle acceleration by flux ropes in response to mean flux-rope properties and Fokker–Planck terms for stochastic particle acceleration due to statistical fluctuations in flux-rope properties for each of the flux-rope acceleration mechanisms. This equation was presented in le Roux et al. (2015a) without the acceleration mechanism associated with the acceleration of the flux-rope flow that we include here. Furthermore, new, more detailed separate expressions for the Fokker–Planck coefficients, for each of the flux-rope acceleration scenarios listed in Equation (32), are presented.

In this paper we extend the focused transport theory to include a transport equation for total energy density (kinetic plus magnetic energy density) of the magnetic island component of small-scale flux ropes in the nonuniform solar wind medium based on N I MHD theory (Zank et al. 2017). The equation includes new expressions for the growth/damping rates of magnetic island energy density, whose derivation is based on total energy conservation in the exchange of energy between energetic particles and flux ropes, thus coupling the flux-rope transport equation to the focused transport equation. We implicitly assume that energy exchange between small-scale flux ropes in the inertial range and particles is dominated by energetic (suprathermal particles) rather than thermal particles. There is support from full particle simulations indicating that, for small enough plasma β values, the magnetic energy in magnetic islands is converted mostly into nonthermal energy for both electrons and protons (Li et al. 2015), but the range of β values for which this holds is not well known. Provided that this condition is fulfilled, we can with this extension simulate energetic particle acceleration by taking into account the back-reaction of the energetic particles on flux ropes, thus improving the estimation of acceleration efficiency in cases where energetic test particle acceleration by flux ropes is very efficient (Zank et al. 2014, 2015a, 2015b; le Roux et al. 2015a, 2015b). To see the basic structure of the two coupled equations, we present them compactly in the following form:

$$\begin{aligned}
\left(\frac{d\langle f\rangle}{dt}\right)_{\rm SW} &= -\left\langle \nabla\cdot\left(\left\langle \frac{d\boldsymbol{x}}{dt}\right\rangle^I_\phi(\epsilon_I)\langle f\rangle\right)\right\rangle\\
&\quad -\frac{1}{p^2}\frac{\partial}{\partial p}\left(p^2\left\langle\left\langle \frac{dp}{dt}\right\rangle^I_\phi\right\rangle(\epsilon_I)\langle f\rangle\right)\\
&\quad -\frac{\partial}{\partial\mu}\left(\left\langle\left\langle \frac{d\mu}{dt}\right\rangle^I_\phi\right\rangle(\epsilon_I)\langle f\rangle\right)\\
&\quad +\frac{\partial}{\partial\mu}\left(D^{\rm eff}_{\mu\mu}(\epsilon_I)\frac{\partial\langle f\rangle}{\partial\mu}+D^I_{\mu p}(\epsilon_I)\frac{\partial\langle f\rangle}{\partial p}\right)\\
&\quad +\frac{1}{p^2}\frac{\partial}{\partial p}\left[p^2\left(D^I_{p\mu}(\epsilon_I)\frac{\partial\langle f\rangle}{\partial\mu}+D^I_{pp}(\epsilon_I)\frac{\partial\langle f\rangle}{\partial p}\right)\right],
\end{aligned}$$

$$\begin{aligned}
\left(\frac{d\epsilon_I}{dt}\right)_{\rm SW} &= \gamma^{\rm coh}_I(\langle f\rangle)\epsilon_I+\gamma^{\rm stoch}_I(\langle f\rangle)\epsilon_I\\
&= \left[-\frac{2\pi}{\epsilon_I}\int_{-1}^1 d\mu\int_0^\infty dpp^2v\left(\left\langle\left\langle\frac{dp}{dt}\right\rangle^I_\phi\right\rangle(\epsilon_I)\langle f\rangle\right)\right]\epsilon_I\\
&\quad +\left[\frac{2\pi}{\epsilon_I}\int_{-1}^1 d\mu\int_0^\infty dpp^2v\left(D^I_{p\mu}(\epsilon_I)\frac{\partial\langle f\rangle}{\partial\mu}\right.\right.\\
&\quad \left.\left.+D^I_{pp}(\epsilon_I)\frac{\partial\langle f\rangle}{\partial p}\right)\right]\epsilon_I,
\end{aligned} \tag{40}$$

where the first equation is the focused transport equation for energetic particles and the second equation is the transport equation for total magnetic island energy density. The average energetic particle distribution $\langle f\rangle(\boldsymbol{x}, p, \mu, t)$ is a function of position $\boldsymbol{x}$, momentum p, cosine of the pitch angle μ, and time t. The distribution function is valid for nearly gyrotropic particle phase-angle distributions in a mixed coordinate system where position and time are measured in the fixed (observer) frame and particle momentum is determined in the plasma flow frame with velocity $\boldsymbol{U} = \boldsymbol{U}_\circ + \delta\boldsymbol{U}_I$. In Equation (40)

$$\epsilon_I = \frac{1}{2}\rho_\circ\langle\delta U_I^2\rangle + \frac{\langle\delta B_I^2\rangle}{8\pi} \tag{41}$$

is the total average magnetic island energy density in the 2D plane perpendicular to axial/guide magnetic field $\boldsymbol{B}_\circ$, consisting of the sum of the mean energy density of the magnetic island flow (first term) and the mean energy density of the island magnetic field (last term) in this plane.

8.1. The Focused Transport Fokker–Planck Equation for Energetic Particle Interaction with Numerous Dynamic Small-scale Flux Ropes

On the left-hand side of the top equation in Equation (40), $(d\langle f\rangle/dt)_{\rm SW}$ refers to the standard focused transport equation for particle transport in a nonuniform background solar wind flow $\boldsymbol{U}_\circ$ and magnetic field $\boldsymbol{B}_\circ$ (e.g., Isenberg 1987; le Roux &

Webb 2007), which, expressed in conservation form, is

$$\left(\frac{d\langle f\rangle}{dt}\right)_{\rm SW} = \frac{\partial\langle f\rangle}{\partial t} + \nabla\cdot\left(\left\langle\frac{d\boldsymbol{x}}{dt}\right\rangle_{\phi}^{\rm SW}\langle f\rangle\right) + \frac{1}{p^2}\frac{\partial}{\partial p}\left(p^2\left\langle\frac{dp}{dt}\right\rangle_{\phi}^{\rm SW}\langle f\rangle\right) + \frac{\partial}{\partial\mu}\left(\left\langle\frac{d\mu}{dt}\right\rangle_{\phi}^{\rm SW}\langle f\rangle\right). \quad (42)$$

Because of the interaction with the nonuniform solar wind flow and magnetic field, particles experience advection in ordinary space ($\langle d\boldsymbol{x}/dt\rangle_{\phi}^{\rm SW}$), in momentum space ($\langle dp/dt\rangle_{\phi}^{\rm SW}$), and in pitch-angle space ($\langle d\mu/dt\rangle_{\phi}^{\rm SW}$). The advection gyrophase-averaged expressions are given by

$$\begin{aligned}
\left\langle\frac{d\boldsymbol{x}}{dt}\right\rangle_{\phi}^{\rm SW} &= \boldsymbol{U}_0 + v\mu\boldsymbol{b}_0,\\
\left\langle\frac{dp}{dt}\right\rangle_{\phi}^{\rm SW} &= p\Bigg(-\frac{1}{2}(1-\mu^2)(\boldsymbol{\nabla}\cdot\boldsymbol{U}_0) - \frac{1}{2}(3\mu^2-1)\boldsymbol{b}_0\cdot(\boldsymbol{b}_0\cdot\boldsymbol{\nabla})\boldsymbol{U}_0 - \mu\left(\frac{1}{v}\frac{d\boldsymbol{U}_0}{dt} - \frac{q\boldsymbol{E}_{\rm surf}}{p}\right)\cdot\boldsymbol{b}_0\Bigg),\\
\left\langle\frac{d\mu}{dt}\right\rangle_{\phi}^{\rm SW} &= \frac{1}{2}(1-\mu^2)\Big(v(\boldsymbol{\nabla}\cdot\boldsymbol{b}_0) + \mu(\boldsymbol{\nabla}\cdot\boldsymbol{U}_0) - 3\mu\boldsymbol{b}_0\cdot(\boldsymbol{b}_0\cdot\boldsymbol{\nabla})\boldsymbol{U}_0 - 2\left(\frac{1}{v}\frac{d\boldsymbol{U}_0}{dt} - \frac{q\boldsymbol{E}_{\rm surf}}{p}\right)\cdot\boldsymbol{b}_0\Big),
\end{aligned} \quad (43)$$

where $\boldsymbol{E}_{\rm surf}$ refers to a nonmotional electric field component at special surfaces such as the cross-shock electric field at shocks.

On the right-hand side of the top equation in Equation (40), $\langle\nabla\cdot\langle d\boldsymbol{x}/dt\rangle_{\phi}^{I}\langle f\rangle\rangle$ is the ensemble average of the divergence of the differential particle flux, $\langle\langle dp/dt\rangle_{\phi}^{I}\rangle$ is the ensemble averaged rate of change of the particle momentum magnitude (kinetic energy), and $\langle\langle d\mu/dt\rangle_{\phi}^{I}\rangle$ is the ensemble averaged rate of change of the cosine of the particle pitch angle in response to mean flux-rope dynamic properties. $D_{\mu\mu}^{I}$, $D_{\mu p}^{I}$, $D_{p\mu}^{I}$, D_{pp}^{I} are Fokker–Planck coefficients indicating the rate of change of the variance of p and μ in response to the statistical fluctuations in flux-rope dynamic properties, based on our assumption of flux-rope activity in the 2D plane perpendicular to $\boldsymbol{B}_0$ as discussed above. Their expressions, which combine all the different flux-rope acceleration mechanisms as defined in Equations (32) and (36), are

$$\begin{aligned}
\left\langle\nabla\cdot\left\langle\frac{d\boldsymbol{x}}{dt}\right\rangle_{\phi}^{I}\right\rangle &= \langle\nabla\cdot(\delta\boldsymbol{U}_I + v\mu\delta\boldsymbol{B}_I/B_0)\rangle,\\
\left\langle\left\langle\frac{dp}{dt}\right\rangle_{\phi}^{I}\right\rangle &= p\Big(\frac{1}{2}(1-\mu^2)\langle\nu_{\rm COM}^{I}\rangle + \frac{1}{2}(3\mu^2-1)\langle\nu_{\rm INC}^{I}\rangle + \mu(\langle\nu_{\rm ACC}^{I}\rangle + \langle\nu_{\rm REC}^{I}\rangle)\Big),\\
\left\langle\left\langle\frac{d\mu}{dt}\right\rangle_{\phi}^{I}\right\rangle &= \frac{1}{2}(1-\mu^2)(\langle\nu_{\rm REF}^{I}\rangle - \mu\langle\nu_{\rm COM}^{I}\rangle + 3\mu\langle\nu_{\rm INC}^{I}\rangle + 2(\langle\nu_{\rm ACC}^{I}\rangle + \langle\nu_{\rm REC}^{I}\rangle)),
\end{aligned} \quad (44)$$

and

$$\begin{aligned}
D_{\mu\mu}^{\rm eff} &= \langle D_{\mu\mu}^{A}\rangle + D_{\mu\mu}^{I},\\
D_{\mu\mu}^{I} &= \Big\langle\Big(\frac{1}{2}(1-\mu^2)(\delta\nu_{\rm REF}^{I} - \mu\delta\nu_{\rm COM}^{I} + 3\mu'\delta\nu_{\rm INC}^{I} + 2(\delta\nu_{\rm ACC}^{I} + \delta\nu_{\rm REC}^{I}))\Big)^2\Big\rangle\tau_{\rm dec},\\
D_{\mu p}^{I} &= p\Big\langle\Big(\frac{1}{2}(1-\mu^2)(\delta\nu_{\rm REF}^{I} - \mu\delta\nu_{\rm COM}^{I} + 3\mu\delta\nu_{\rm INC}^{I} + 2(\delta\nu_{\rm ACC}^{I} + \delta\nu_{\rm REC}^{I}))\Big)\\
&\quad\times\Big(\frac{1}{2}(1-\mu^2)\delta\nu_{\rm COM}^{I} + \frac{1}{2}(3\mu^2-1)\delta\nu_{\rm INC}^{I} + \mu(\delta\nu_{\rm ACC}^{I} + \delta\nu_{\rm REC}^{I})\Big)\Big\rangle\tau_{\rm dec}\\
&= D_{p\mu}^{I},\\
D_{pp}^{I} &= p^2\Big\langle\Big(\frac{1}{2}(1-\mu^2)\delta\nu_{\rm COM}^{I} + \frac{1}{2}(3\mu^2-1)\delta\nu_{\rm INC}^{I} + \mu(\delta\nu_{\rm ACC}^{I} + \delta\nu_{\rm REC}^{I})\Big)^2\Big\rangle\tau_{\rm dec},
\end{aligned} \quad (45)$$

where $D_{\mu\mu}^{\rm eff}$ is the net pitch-angle scattering rate found by adding the pitch-angle scattering rates from particle interaction with Alfvén waves $\langle D_{\mu\mu}^{A}\rangle$ and particle interaction with small-scale flux ropes $D_{\mu\mu}^{I}$. The basic expressions for the different flux-rope-induced relative acceleration and pitch-angle scattering rates $\nu_{\rm REC}^{I}$, $\nu_{\rm ACC}^{I}$, $\nu_{\rm INC}^{I}$, $\nu_{\rm COM}^{I}$, $\nu_{\rm REF}^{I}$ that appear decomposed into mean and fluctuating parts and ensemble averaged in Equations (44) and (45) can be found above in Equations (32) and (37). In the Fokker–Planck coefficient expressions of Equation (45), $\tau_{\rm dec}$ is the energetic particle decorrelation time (the time interval on which propagating energetic particles see decorrelated flux-rope properties, such as the flux-rope flow, magnetic field, and reconnection electric field, when interacting with many flux ropes). The decorrelation time is estimated further below by taking into account the time it takes for a particle to traverse a magnetic flux-rope structure (see Section 9.2, below Equation (73)).

8.2. The N I MHD Magnetic Island Transport Equation with Damping Effects from Acceleration of Energetic Particles by Numerous Dynamic Small-scale Flux Ropes

On the left-hand side of the second equation in Equation (40), $(d\epsilon_I/dt)_{\rm SW}$ refers to a transport equation describing the total small-scale flux-rope energy density ϵ_I (see Equation (41) for definition) in the 2D plane perpendicular to the guide/background magnetic field in the nonuniform background solar wind flowing with velocity $\boldsymbol{U}_0$ (i.e., the total magnetic island or flux-rope twist component energy density). This transport equation was derived on the basis of the quasi-2D magnetic island structure transport equations in Elsässer variables from N I MHD turbulence theory for a nonuniform plasma medium (Zank et al. 2017; see Appendix B for more details). Expressing the derived transport Equation (158) in Appendix B in partial

conservation form, we find

$$\left(\frac{d\epsilon_I}{dt}\right)_{\rm SW} = \frac{\partial \epsilon_I}{\partial t} + \nabla\cdot(\epsilon_I \boldsymbol{U}_0) + \frac{1}{2}(1+(4a-1)\sigma_D^I)(\nabla\cdot\boldsymbol{U}_0)\epsilon_I - \frac{1}{4}[(1+\sigma_C^I)^{3/2} - (1+\sigma_C^I)^{1/2}\sigma_D^I + (1-\sigma_C^I)^{3/2} - (1-\sigma_C^I)^{1/2}\sigma_D^I]\left(\frac{\sqrt{2}}{\rho_0^{3/2}}(\boldsymbol{n}\cdot\nabla)\rho_0\right)\epsilon_I^{3/2} + \frac{(1-(\sigma_C^I)^2)^{1/2}}{L_I}[(1+\sigma_C^I)^{1/2} + (1-\sigma_C^I)^{1/2}]\left(\frac{2}{\rho_0}\right)^{1/2}\epsilon_I^{3/2}, \quad (46)$$

where $\boldsymbol{n}$ is a unit vector along 2D flux-rope turbulence in the 2D plane perpendicular to $\boldsymbol{B}_0$, σ_C^I is the normalized cross helicity of quasi-2D magnetic island structures defined as

$$\sigma_C^I = \frac{2\langle \delta \boldsymbol{U}_I\cdot\delta\boldsymbol{V}_{AI}\rangle}{\langle \delta U_I^2\rangle + \langle \delta V_{AI}^2\rangle} = \frac{2\langle \delta \boldsymbol{U}_I\cdot\delta\boldsymbol{B}_I\rangle}{(r_{\rm A}^I+1)B_0 V_{A0}\langle \delta B_I^2\rangle/B_0^2}, \quad (47)$$

and σ_D^I is the normalized residual magnetic island energy defined according to

$$\sigma_D^I = \frac{\langle \delta U_I^2\rangle - \langle \delta V_{AI}^2\rangle}{\langle \delta U_I^2\rangle + \langle \delta V_{AI}^2\rangle}. \quad (48)$$

The parameter $r_{\rm A}^I = \langle \delta U_I^2\rangle/\langle \delta V_{AI}^2\rangle$ is the Alfvén ratio of the mean flux-rope kinetic energy over the mean flux-rope magnetic energy in the 2D plane perpendicular to $\boldsymbol{B}_0$ ($\langle \delta V_{AI}^2\rangle = \langle \delta B_I^2\rangle/4\pi\rho_0$), L_I is the characteristic size of flux ropes in the 2D plane perpendicular to $\boldsymbol{B}_0$ (average cross-sectional radius of magnetic island), and $V_{A0} = B_0/(4\pi\rho_0)^{1/2}$ is the Alfvén speed associated with the background/guide magnetic field. Thus, $\langle \delta U_I^2\rangle^{1/2} = (r_{\rm A}^I)^{1/2}(\langle \delta B_I^2\rangle^{1/2}/B_0)V_{A0}$.

Equation (46) was derived assuming isotropic 2D turbulence in the 2D plane perpendicular to $\boldsymbol{B}_0$, in which case $a = 1/2$ (see discussion related to Equation (151) in Appendix B). This implies that the unit vector $\boldsymbol{n}$ pointing along 2D turbulence has an arbitrary direction in this 2D plane. Note that the second term on the right-hand side contains the solar wind flow velocity $\boldsymbol{U}_0$ but not the Alfvén velocity. The leading-order description of N I MHD theory thus models 2D magnetic island structures that are advected with the solar wind flow (zero phase velocity), in contrast to previous MHD turbulence models that also included Alfvén wave propagation effects (e.g., Zhou & Matthaeus 1990; Zank et al. 2012). The reason for this change becomes clear by noting that, for plasma beta values appropriate in solar wind conditions ($\beta \sim 1$, $\beta \ll 1$), the leading-order MHD turbulence description of N I MHD theory is a quasi-2D description without the Alfvén velocity (Zank & Matthaeus 1993; Zank et al. 2017). The most widely used MHD turbulence theory, on the other hand, is a 3D incompressible MHD theory that yields a fully 3D description to leading order that includes the Alfvén velocity (e.g., Zhou & Matthaeus 1990; Zank et al. 2012). However, from the perspective of N I MHD theory, this limit can only be recovered when $\beta \gg 1$, thus making it inappropriate for solar wind applications.

Alternatively, we can express Equation (46) as

$$\left(\frac{d\epsilon_I}{dt}\right)_{\rm SW} = \frac{\partial \epsilon_I}{\partial t} + \nabla\cdot(\gamma_I \epsilon_I \boldsymbol{U}_0) - (\boldsymbol{U}_0\cdot\nabla)P_I + NL, \quad (49)$$

where NL denotes the nonlinear terms in the last two lines of Equation (54), and P_I is the pressure of the quasi-2D magnetic island turbulence related to ϵ_I through the relationship $\epsilon_I = P_I/(\gamma_I - 1)$, where

$$\gamma_I = 1 + \frac{1}{2}(1+(4a-1)\sigma_D^I). \quad (50)$$

The combination $\gamma_I\epsilon_I = P_I + \epsilon_I = (\gamma_I/(\gamma_I-1))P_I$ can be viewed as the enthalpy of the quasi-2D magnetic island structures. For magnetic island turbulence that is isotropic in the 2D plane perpendicular to $\boldsymbol{B}_0$ ($a = 1/2$), we find that $\gamma_I = (3+\sigma_D^I)/2$. If, $\sigma_D^I = 0$, we recover the Alfvén wave value $\gamma_I = 3/2$ because then, as for Alfvén waves, $r_{\rm A}^I = 1$ (equipartition between flow and magnetic energy). Solutions of the 2D turbulence transport equations of N I MHD theory for the inner heliosphere (Zank et al. 2017) suggest that $\sigma_D^I \to -1$ with increasing distance from the Sun so that, more realistically, $\gamma_I \to 1$. Equation (54) is valid for a plasma beta of order 1, thus making it suitable for application in the supersonic solar wind. This includes solar wind conditions near 1 au (Zank et al. 2017), which are our main interest in this paper.

To Equation (46) we add an equation from N I MHD theory (Zank et al. 2017). The transport of the variance in the density fluctuations associated with 2D magnetic island turbulence in the nonuniform solar wind is given by

$$\frac{\partial\langle\delta\rho_I^2\rangle}{\partial t} + (\boldsymbol{U}_0\cdot\nabla)\langle\delta\rho_I^2\rangle = -2\langle\delta\rho_I^2\rangle(\nabla\cdot\boldsymbol{U}_0) + 2\langle\delta\rho_I^2\rangle(\langle\delta U_I^2\rangle^{1/2}\boldsymbol{n}\cdot\nabla)\rho_0 - 2\langle\delta\rho_I^2\rangle\frac{\langle\delta U_I^2\rangle^{1/2}}{L_I}. \quad (51)$$

According to the N I MHD theory in its most basic form, quasi-2D flux-rope turbulence is intrinsically incompressible in a uniform plasma medium. However, extended N I MHD theory, as represented by Equations (46) and (51), applies to a nonuniform plasma medium. These equations show how compression of the background solar wind, modeled with the expressions $\nabla\cdot\boldsymbol{U}_0 < 0$ and $\boldsymbol{n}\cdot\nabla\rho_0 > 0$ (see the last two lines of Equation (46) and the first two terms on the right-hand side of Equation (51)), produces a variance in the flux-rope density that contributes to enhancements in the total flux-rope energy density ϵ_I. Just like the magnetic field and plasma flow of flux ropes, the density variations are advected with the solar wind plasma flow. This suggests that wherever the solar wind is compressed strongly enough in regions filled with flux-rope structures, the flux-rope structures themselves will experience compression, resulting in an increase in the strength of the flux-rope field δB_I (see Equation (15)). This also suggests that flow compression across shocks in the solar wind could be a source of compressibility in small-scale flux ropes generated by shocks.

The terms on the right-hand side of the small-scale flux-rope transport equation (second equation in Equation (40)) contain the coefficients $\gamma_I^{\rm coh}(\langle f\rangle)$ and $\gamma_I^{\rm stoch}(\langle f\rangle)$ for modeling the damping/growth of the magnetic island component of small-scale flux ropes when energy is exchanged between energetic particles and these structures. The coefficient

$$\gamma_I^{\rm coh}(\langle f\rangle) = -\frac{2\pi}{\epsilon_I}\int_{-1}^{1} d\mu \int_0^{\infty} dpp^2 v\left(\left\langle \frac{dp}{dt}\right\rangle_{\phi}^{I}(\epsilon_I)\langle f\rangle\right) \quad (52)$$

represents the coherent damping rate of small-scale magnetic islands when energetic particles are coherently accelerated in response to the mean properties of active flux ropes. By contrast,

$$\gamma_I^{\rm stoch}(\langle f\rangle) = \frac{2\pi}{\epsilon_I}\int_{-1}^{1} d\mu \int_0^{\infty} dpp^2 v \times\left(D_{p\mu}^I(\epsilon_I)\frac{\partial\langle f\rangle}{\partial\mu} + D_{pp}^I(\epsilon_I)\frac{\partial\langle f\rangle}{\partial p}\right) \quad (53)$$

denotes the average stochastic damping/growth rate of the magnetic island component of small-scale flux ropes when energetic particles experience stochastic acceleration in response to the fluctuating properties of active magnetic islands (for more details about the derivation of these expressions, see Appendix C). In Equation (53), second-order Fermi acceleration is a combination of D_{pp}^I with $\partial\langle f\rangle/\partial p < 0$ (typical for suprathermal particle spectra), resulting in damping of the magnetic island energy density. However, particle energy change through the combination of $D_{\mu p}^I$ with $\partial\langle f\rangle/\partial\mu$ depends on the sign of $\partial\langle f\rangle/\partial\mu$, thus allowing for the possibility of growth in the magnetic island energy density. It is interesting to note that $\gamma_I^{\rm stoch}$ depends on pitch-angle and momentum gradients of the distribution as in standard quasi-linear theory, but that $\gamma_I^{\rm coh}$ depends only on the particle distribution function. This difference is reminiscent of the discussion in weak plasma turbulence kinetic theory where stimulated radiation emission is driven by momentum and pitch-angle gradients of the particle distribution and spontaneous radiation emission is associated only with the particle distribution itself (e.g., Yoon 2017).

9. Approximate Expressions for Energetic Particle Rates of Momentum Magnitude and Pitch-angle Change for Each Flux-rope Acceleration Case

9.1. Coherent Momentum Magnitude and Pitch-angle Rates of Change

To make our theory useful for application to energetic particle acceleration in dynamic small-scale flux ropes in the solar wind near Earth (see discussions further below), we derived approximate expressions for the average coherent relative acceleration rates (sans the μ-dependence) for each of the four different flux-rope acceleration cases listed in Equation (32) (for more details, see Appendix A). The expressions are

$$\begin{aligned}
\langle\nu_{\rm COM}^I\rangle(\epsilon_I) &\approx \sigma_{\rm COM}^I\left(\frac{r_{\rm A}^I}{r_{\rm A}^I+1}\right)^{1/2}\frac{V_{A0}}{L_I}\left(\frac{\epsilon_I}{\epsilon_{B_0}}\right)^{1/2},\\
\langle\nu_{\rm INC}^I\rangle(\epsilon_I) &\approx \sigma_{\rm INC}^I\frac{(r_{\rm A}^I)^{1/2}}{(r_{\rm A}^I+1)^{3/2}}\frac{V_{A0}}{L_I}\left(\frac{\epsilon_I}{\epsilon_{B_0}}\right)^{3/2},\\
\langle\nu_{\rm ACC}^I\rangle &\approx \sigma_{\rm ACC}^I\frac{(r_{\rm A}^I)^{1/2}}{r_{\rm A}^I+1}\frac{U_\circ}{v}\frac{V_{A0}}{L_{\rm Ir}}\frac{\epsilon_I}{\epsilon_{B_\circ}},\\
\langle\nu_{\rm REC}^I\rangle(\epsilon_I) &\approx \sigma_{\rm REC}^I\frac{(r_{\rm A}^I)^{1/2}}{r_{\rm A}^I+1}\frac{q}{|q|}\frac{Z}{A}\frac{V_{A0}}{v}\frac{V_{A0}}{d_{i/e}}\frac{\epsilon_I}{\epsilon_{B_0}}.
\end{aligned} \quad (54)$$

With the aid of these expressions, approximations for the complete average coherent acceleration rate expressions for each of the four flux-rope acceleration cases listed in the second line of Equation (44) can be found using the relationships

$$\begin{aligned}
\left\langle\left\langle\frac{dp}{dt}\right\rangle_{\phi}^{\rm COM}\right\rangle(\epsilon_I) &= p\frac{1}{2}(1-\mu^2)\langle\nu_{\rm COM}^I\rangle(\epsilon_I),\\
\left\langle\left\langle\frac{dp}{dt}\right\rangle_{\phi}^{\rm INC}\right\rangle(\epsilon_I) &= p\frac{1}{2}(3\mu^2-1)\langle\nu_{\rm INC}^I\rangle(\epsilon_I),\\
\left\langle\left\langle\frac{dp}{dt}\right\rangle_{\phi}^{\rm ACC}\right\rangle(\epsilon_I) &= p\mu\langle\nu_{\rm ACC}^I\rangle(\epsilon_I),\\
\left\langle\left\langle\frac{dp}{dt}\right\rangle_{\phi}^{\rm REC}\right\rangle(\epsilon_I) &= p\mu\langle\nu_{\rm REC}^I\rangle(\epsilon_I).
\end{aligned} \quad (55)$$

In the expression for $\langle\nu_{\rm COM}^I\rangle$, $\sigma_{\rm COM}^I\epsilon[-1, 1]$. When flux ropes experience only compressible contraction or merging, $\sigma_{\rm COM}^I = +1$, whereas $\sigma_{\rm COM} = -1$ when compressible flux ropes expand only. We specify $\sigma_{\rm COM} = 0$ when the probability of contraction is balanced by the probability for expansion. The parameter $r_{\rm A}^I = \langle\delta U_I^2\rangle/\langle\delta V_{AI}^2\rangle$ is the Alfvén ratio of the mean flux-rope kinetic energy over the mean flux-rope magnetic energy in the 2D plane perpendicular to $\boldsymbol{B}_0$ ($\langle\delta V_{AI}^2\rangle = \langle\delta B_I^2\rangle/4\pi\rho_0$), L_I is the characteristic size of flux ropes in the 2D plane perpendicular to $\boldsymbol{B}_0$ (average cross-sectional radius of magnetic island), $V_{A0} = B_0/(4\pi\rho_0)^{1/2}$ is the Alfvén speed associated with background/guide magnetic field, and $\epsilon_{B0} = B_0^2/8\pi$ is the energy density of the background/guide magnetic field. Thus, $\langle\delta B_I^2\rangle/B_0^2 = (\epsilon_I/\epsilon_{B_0})/(r_{\rm A}^I+1)$, and $\langle\delta U_I^2\rangle^{1/2} = (r_{\rm A}^I)^{1/2}(\langle\delta B_I^2\rangle^{1/2}/B_0)V_{A0}$.

In the expression $\langle\nu_{\rm INC}^I\rangle$ (second line of Equation (54)), $\sigma_{\rm INC}^I\epsilon[-1, 1]$ plays exactly the same role as $\sigma_{\rm COM}^I$, but here we refer to flux-rope contraction and merging in the incompressible limit. In $\langle\nu_{\rm ACC}^I\rangle$ (third line of Equation (54)), $\sigma_{\rm ACC}^I\epsilon[-1, 1]$ controls the net magnitude and direction of the average noninertial force associated with the parallel acceleration of the flux-rope flow when energetic particles encounter multiple small-scale flux ropes. For example, if $\sigma_{\rm ACC}^I > 0$, particles with $\mu > 0$ (particles propagating in the direction of $\boldsymbol{B}_0$) will be energized because then the net noninertial force points in the direction of the guiding center motion. Furthermore, $L_{\rm Ir}$ refers to the scale over which $\delta\boldsymbol{U}_I$ varies in the direction of the radial solar wind outflow from the Sun (the sign of $L_{\rm Ir}$ indicates whether the gradient is positive or negative). Also, in $\langle\nu_{\rm REC}^I\rangle$ (fourth line of Equation (54)) $\sigma_{\rm REC}\epsilon$

$[-1, 1]$. When $\sigma^I_{\rm REC} = +1$, the reconnection electric fields of neighboring merging flux-rope pairs all point in the direction of $\boldsymbol{B}_0$; when $\sigma^I_{\rm REC} = -1$, they point in the opposite direction of $\boldsymbol{B}_0$; and $\sigma^I_{\rm REC} = 0$ indicates the reconnection electric fields of multiple merging flux-rope pairs to be pointing randomly along or in the opposite direction of $\boldsymbol{B}_0$. The expression for $\langle \nu^I_{\rm REC}\rangle$ also includes the sign of the net particle charge $q/|q|$, the ratio of the net charge number over the mass number Z/A, and the ion (electron) inertial length $d_{i/e} = m_{p,e}V_{A0}/eB_0$, where $m_{p,e}$ is the proton (electron) mass. For ion acceleration one uses d_i, whereas for electron acceleration one specifies d_e and sets $Z/A = 1$.

The expressions in Equation (54) can also be used to find approximate expressions for the complete average coherent rate of change in the cosine of the pitch angle μ for energetic particles for each of the four different flux-rope acceleration cases listed in the third line of Equation (44) by applying the relationships

$$\begin{aligned}
\left\langle \left\langle \frac{d\mu}{dt} \right\rangle_\phi^{\rm COM} \right\rangle(\epsilon_I) &= -\frac{1}{2}(1-\mu^2)\mu\langle \nu^I_{\rm COM}\rangle(\epsilon_I),\\
\left\langle \left\langle \frac{d\mu}{dt} \right\rangle_\phi^{\rm INC} \right\rangle(\epsilon_I) &= \frac{3}{2}(1-\mu^2)\mu\langle \nu^I_{\rm INC}\rangle(\epsilon_I),\\
\left\langle \left\langle \frac{d\mu}{dt} \right\rangle_\phi^{\rm ACC} \right\rangle(\epsilon_I) &= (1-\mu^2)\langle \nu^I_{\rm ACC}\rangle(\epsilon_I),\\
\left\langle \left\langle \frac{d\mu}{dt} \right\rangle_\phi^{\rm REC} \right\rangle(\epsilon_I) &= (1-\mu^2)\langle \nu^I_{\rm REC}\rangle(\epsilon_I).
\end{aligned} \tag{56}$$

However, for energetic particles, potentially the most important contribution to the rate of change of μ comes from the magnetic mirroring force present in small-scale flux ropes (see Equations (36)–(38) and the related discussion). Taking into account this effect, we derived the following approximate expression for the average coherent pitch-angle rate of change of energetic particles, which, without the μ-dependence, is given by

$$\langle \nu^I_{\rm REF}\rangle(\epsilon_I) \approx -\sigma^I_{\rm REF}\frac{1}{(r^I_{\rm A}+1)^{1/2}}\frac{v}{V_{A0}}\frac{V_{A0}}{L_I}\left(\frac{\epsilon_I}{\epsilon_{B_0}}\right)^{1/2}. \tag{57}$$

This expression models the effect of the average magnetic mirroring force in the 2D plane transverse to $\boldsymbol{B}_0$ that energetic particles encounter when traversing a volume of small-scale flux ropes, assuming $\delta B_I/B_0 \ll 1$ and $\delta\boldsymbol{B}_I \perp \boldsymbol{B}_0$ (see discussion in Section 7.2). In $\langle \nu^I_{\rm REF}\rangle$, $\sigma^I_{\rm REF}\epsilon[-1, 1]$. Thus, when $\sigma^I_{\rm REF} > 0$, the mean magnetic mirroring force particles encounter when traversing numerous flux ropes is such that particles propagating along the magnetic field ($\mu > 0$) will experience a mirroring effect. Those propagating in the opposite direction ($\mu < 0$) will experience a focusing effect. The opposite holds when $\sigma^I_{\rm REF} < 0$. When $\sigma^I_{\rm REF} = 0$, the mean mirroring force encountered by energetic particles crossing numerous flux ropes is zero, resulting in a zero average coherent energetic particle pitch-angle rate of change. The full approximate expression for the average coherent pitch-angle rate of change due to the mean magnetic mirroring force experienced by energetic particles in multiple small-scale flux ropes can be found by applying the relationship in the third line of Equation (44) given by

$$\left\langle \left\langle \frac{d\mu}{dt} \right\rangle_\phi^{\rm REF} \right\rangle(\epsilon_I) = \frac{1}{2}(1-\mu^2)\langle \nu^I_{\rm REF}\rangle(\epsilon_I). \tag{58}$$

9.2. Stochastic Momentum Magnitude and Pitch-angle Rates of Change

For the purpose of application to energetic particle acceleration in dynamic small-scale flux ropes in the solar wind near Earth as discussed below, the Fokker–Planck scattering coefficients defined in Equation (45) were used as a basis for deriving the following approximate expressions (without the μ-dependence) for the variance in the particle relative momentum magnitude/pitch-angle rates of change for each of the flux-rope transport mechanisms listed in Equations (31) and (36) (see Appendix A for further details):

$$\begin{aligned}
\langle(\delta\nu^I_{\rm COM})^2\rangle(\epsilon_I) &\approx C_\delta a\frac{r^I_{\rm A}}{r^I_{\rm A}+1}\frac{V^2_{A0}}{L^2_I}\frac{\epsilon_I}{\epsilon_{B_0}},\\
\langle(\delta\nu^I_{\rm INC})^2\rangle(\epsilon_I) &\approx C_\delta 2a\left[\frac{r^I_{\rm A}+1/4(\sigma^I_C)^2(r^I_{\rm A}+1)^2}{(r^I_{\rm A}+1)^3}\right]\\
&\quad\times\frac{V^2_{A0}}{L^2_I}\left(\frac{\epsilon_I}{\epsilon_{B_0}}\right)^3,\\
\langle(\delta\nu^I_{\rm ACC})^2\rangle(\epsilon_I) &\approx a\frac{r^I_{\rm A}}{r^I_{\rm A}+1}\frac{V^2_{A0}}{L^2_{\rm Ir}}\left(\frac{U_0}{v}\right)^2\frac{\epsilon_I}{\epsilon_{B_0}},\\
\langle(\delta\nu^I_{\rm REC})^2\rangle(\epsilon_I) &\approx C_\delta 4a^2\left[\frac{r^I_{\rm A}-1/4(\sigma^I_C)^2(r^I_{\rm A}+1)^2}{(r^I_{\rm A}+1)^2}\right]\\
&\quad\times\left(\frac{Z}{A}\right)^2\frac{V^2_{A0}}{d^2_{i/e}}\left(\frac{V_{A0}}{v}\right)^2\left(\frac{\epsilon_I}{\epsilon_{B_0}}\right)^2,\\
\langle(\delta\nu^I_{\rm REF})^2\rangle(\epsilon_I) &\approx C_\delta a\frac{1}{r^I_{\rm A}+1}\frac{V^2_{A0}}{L^2_I}\left(\frac{v}{V_{A0}}\right)^2\frac{\epsilon_I}{\epsilon_{B_0}},
\end{aligned} \tag{59}$$

and

$$\begin{aligned}
\langle\delta\nu^I_{\rm COM}\delta\nu^I_{\rm REF}\rangle(\epsilon_I) &\approx -C_\delta\frac{a}{2}\sigma^I_C\frac{V^2_{A0}}{L^2_I}\frac{v}{V_{A0}}\frac{\epsilon_I}{\epsilon_{B_0}},\\
\langle\delta\nu^I_{\rm INC}\delta\nu^I_{\rm REF}\rangle(\epsilon_I) &\approx -C_\delta a\left[\frac{1/2\sigma^I_C(r^I_{\rm A}+1)+(r^I_{\rm A})^{1/2}}{(r^I_{\rm A}+1)^2}\right]\\
&\quad\times\frac{V^2_{A0}}{L^2_I}\frac{v}{V_{A0}}\left(\frac{\epsilon_I}{\epsilon_{B_0}}\right)^2,\\
\langle\delta\nu^I_{\rm ACC}\nu^I_{\rm REF}\rangle(\epsilon_I) &\approx 0,\\
\langle\delta\nu^I_{\rm REC}\delta\nu^I_{\rm REF}\rangle(\epsilon_I) &\approx -C^{1/2}_\delta a\left[\frac{1/2\sigma^I_C(r^I_{\rm A}+1)+(r^I_{\rm A})^{1/2}}{(r^I_{\rm A}+1)^{3/2}}\right]\\
&\quad\times\frac{q}{|q|}\frac{Z}{A}\frac{V^2_{A0}}{L^2_I}\frac{L_I}{d_{i/e}}\left(\frac{\epsilon_I}{\epsilon_{B_0}}\right)^{3/2},
\end{aligned} \tag{60}$$

where σ^I_C is the normalized cross helicity of quasi-2D magnetic island structures (see Equation (47)) and the constant C_δ refers to the assumption introduced by $\langle[\delta(\delta B_I)]^2\rangle = C_\delta\langle\delta B^2_I\rangle$ for

closure purposes (see Appendix A). Furthermore, $a = 1/2$ when making the simplifying assumption that 2D flux-rope turbulence is on average isotropic in the 2D plane perpendicular to $\boldsymbol{B}_0$ (e.g., Zank et al. 2017). Definitions of the rest of the parameters in Equations (59) and (60) can be found in Section 9.1 below Equation (55).

Consider first the basic expressions for the Fokker–Planck coefficients for the case of stochastic flux-rope compression acceleration (combined curvature drift and generalized betatron stochastic acceleration in flux ropes with compressible dynamics) in Equation (45). The stochastic acceleration occurs owing to fluctuations in the contraction/merging velocity and the magnetic field of numerous magnetic islands. The expressions are

$$\begin{aligned}
D_{\mu\mu}^{\rm COM}(\epsilon_I) &= \frac{1}{4}(1-\mu^2)^2\langle(\delta\nu_{\rm REF}^I - \mu\delta\nu_{\rm COM}^I)^2\rangle\tau_{\rm dec},\\
D_{\mu p}^{\rm COM}(\epsilon_I) &= p\frac{1}{4}(1-\mu^2)^2[\langle\delta\nu_{\rm REF}^I\delta\nu_{\rm COM}^I\rangle\\
&\quad - \mu\langle(\delta\nu_{\rm COM}^I)^2\rangle]\tau_{\rm dec}\\
&= D_{p\mu}^{\rm COM}(\epsilon_I),\\
D_{pp}^{\rm COM}(\epsilon_I) &= p^2\frac{1}{4}(1-\mu^2)^2\langle(\delta\nu_{\rm COM}^I)^2\rangle\tau_{\rm dec}.
\end{aligned} \tag{61}$$

By inserting the approximate expressions for $\langle(\delta\nu_{\rm COM}^I)^2\rangle(\epsilon_I)$ in Equation (59) and $\langle\delta\nu_{\rm COM}^I\delta\nu_{\rm REF}^I\rangle(\epsilon_I)$ in Equation (60) into the basic Fokker–Planck coefficient expressions of Equation (61), we find that

$$\begin{aligned}
D_{\mu\mu}^{\rm COM}(\epsilon_I) &\approx \left(1+\mu\sigma_C^I(r_{\rm A}^I+1)\frac{V_{A0}}{v}+\mu^2 r_{\rm A}^I\left(\frac{V_{A0}}{v}\right)^2\right)T_{\mu\mu}^{\rm COM}(\epsilon_I),\\
D_{\mu p}^{\rm COM}(\epsilon_I) &\approx -\left(p\frac{V_{A0}}{v}\right)\left(\frac{1}{2}\sigma_C^I(r_{\rm A}^I+1)+\mu r_{\rm A}^I\frac{V_{A0}}{v}\right)T_{\mu\mu}^{\rm COM}(\epsilon_I)\\
&= D_{p\mu}^{\rm COM}(\epsilon_I),\\
D_{pp}^{\rm COM}(\epsilon_I) &\approx \left(p\frac{V_{A0}}{v}\right)^2 r_{\rm A}^I T_{\mu\mu}^{\rm COM}(\epsilon_I),
\end{aligned} \tag{62}$$

where the average particle pitch-angle scattering rate $T_\mu\mu^{\rm COM}(\epsilon_I)$ (variance in the particle pitch-angle rate of change $\langle\Delta\mu^2\rangle/\Delta t$) is the leading-order term in $D_{\mu\mu}^{\rm COM}$ for energetic particles associated with $\langle(\delta\nu_{\rm REF}^I)^2\rangle$. Thus, $T_{\mu\mu}^{\rm COM}(\epsilon_I)$ can be associated with the variance in the flux-rope mirroring force encountered by energetic particles when interacting with numerous compressible small-scale flux ropes. Its expression is

$$T_{\mu\mu}^{\rm COM}(\epsilon_I) = (1-\mu^2)^2 T_{\mu\mu}(\epsilon_I), \tag{63}$$

with

$$T_{\mu\mu}(\epsilon) = C_\delta\frac{a}{4}\frac{1}{r_{\rm A}^I+1}\frac{v^2}{L_I^2}\frac{\epsilon_I}{\epsilon_{B_0}}\tau_{\rm dec}. \tag{64}$$

Next, we consider the basic expressions for the Fokker–Planck coefficients for the case of stochastic flux-rope parallel shear-flow acceleration (combined curvature drift and generalized betatron stochastic acceleration in flux ropes with incompressible dynamics) in Equation (45). Also in this case the stochastic acceleration occurs owing to fluctuations in the contraction/merging velocity and the magnetic field of numerous magnetic islands. The expressions are

$$\begin{aligned}
D_{\mu\mu}^{\rm INC}(\epsilon_I) &= \frac{1}{4}(1-\mu^2)^2\langle(\delta\nu_{\rm REF}^I + 3\mu\delta\nu_{\rm INC}^I)^2\rangle\tau_{\rm dec},\\
D_{\mu p}^{\rm INC}(\epsilon_I) &= p\frac{1}{4}(3\mu^2-1)(1-\mu^2)\\
&\quad\times[\langle\delta\nu_{\rm REF}^I\delta\nu_{\rm INC}^I\rangle + 3\mu\langle(\delta\nu_{\rm INC}^I)^2\rangle]\tau_{\rm dec}\\
&= D_{p\mu}^{\rm INC}(\epsilon_I),\\
D_{pp}^{\rm INC}(\epsilon_I) &= p^2\frac{1}{4}(3\mu^2-1)^2\langle(\delta\nu_{\rm INC}^I)^2\rangle\tau_{\rm dec}.
\end{aligned} \tag{65}$$

By inserting the approximate expressions for $\langle(\delta\nu_{\rm INC}^I)^2\rangle(\epsilon_I)$ in Equation (59) and $\langle\delta\nu_{\rm INC}^I\delta\nu_{\rm REF}^I\rangle(\epsilon_I)$ in Equation (60) into the basic Fokker–Planck coefficient expressions in Equation (65), we find

$$\begin{aligned}
D_{\mu\mu}^{\rm INC}(\epsilon_I) &\approx \left[1-6\mu\left(\frac{1/2\sigma_C^I(r_{\rm A}^I+1)+(r_{\rm A}^I)^{1/2}}{r_{\rm A}^I+1}\right)\frac{V_{A0}}{v}\frac{\epsilon_I}{\epsilon_{B_0}}\right.\\
&\quad+18\mu^2\left(\frac{r_{\rm A}^I+1/4(\sigma_C^I)^2(r_{\rm A}^I+1)^2}{(r_{\rm A}^I+1)^2}\right)\\
&\quad\left.\times\left(\frac{V_{A0}}{v}\right)^2\left(\frac{\epsilon_I}{\epsilon_{B_0}}\right)^2\right]T_{\mu\mu}^{\rm INC}(\epsilon_I),\\
D_{\mu p}^{\rm INC}(\epsilon_I) &\approx -\left(p\frac{V_{A0}}{v}\right)[(1/2\sigma_C^I(r_{\rm A}^I+1)+(r_{\rm A}^I)^{1/2})\\
&\quad-6\mu\left(\frac{r_{\rm A}^I+1/4(\sigma_C^I)^2(r_{\rm A}^I+1)^2}{r_{\rm A}^I+1}\right)\\
&\quad\left.\times\frac{V_{A0}}{v}\frac{\epsilon_I}{\epsilon_{B_0}}\right]T_{\mu p}^{\rm INC}(\epsilon_I)\\
&= D_{p\mu}^{\rm INC}(\epsilon_I),\\
D_{pp}^{\rm INC}(\epsilon_I) &\approx \left(p\frac{V_{A0}}{v}\right)^2(r_{\rm A}^I+1/4(\sigma_C^I)^2(r_{\rm A}^I+1)^2)T_{pp}^{\rm INC}(\epsilon_I),
\end{aligned} \tag{66}$$

where

$$\begin{aligned}
T_{\mu\mu}^{\rm INC}(\epsilon_I) &= (1-\mu^2)^2 T_{\mu\mu}(\epsilon_I),\\
T_{\mu p}^{\rm INC}(\epsilon_I) &= (1-\mu^2)(3\mu^2-1)\frac{1}{r_{\rm A}^I+1}\frac{\epsilon_I}{\epsilon_{B_0}}T_{\mu\mu}(\epsilon_I),\\
T_{pp}^{\rm INC}(\epsilon_I) &= 2(3\mu^2-1)^2\frac{1}{(r_{\rm A}^I+1)^2}\left(\frac{\epsilon_I}{\epsilon_{B_0}}\right)^2 T_{\mu\mu}(\epsilon_I),
\end{aligned} \tag{67}$$

and $T_{\mu\mu}$ is given by Equation (64). Note that the mean pitch-angle scattering rate $T_{\mu\mu}^{\rm INC} = T_{\mu\mu}^{\rm COM}$ (in the energetic particle limit both expressions refer to the variance in the flux-rope magnetic mirroring force that particles encounter during interaction with multiple small-scale flux-rope structures).

For the case of fluctuations in the particle acceleration rate due to variations in the noninertial force associated with the parallel component of the acceleration of the flux-rope flow, the basic expressions for the Fokker–Planck coefficients as

presented in Equation (45) are

$$
\begin{aligned}
D^{\rm ACC}_{\mu\mu}(\epsilon_I) &= \frac{1}{4}(1-\mu^2)^2\langle(\delta\nu^I_{\rm REF}+2\delta\nu^I_{\rm ACC})^2\rangle\tau_{\rm dec},\\
D^{\rm ACC}_{\mu p}(\epsilon_I) &= p\frac{1}{2}(1-\mu^2)\mu[\langle\delta\nu^I_{\rm REF}\delta\nu^I_{\rm ACC}\rangle\\
&\quad+2\langle(\delta\nu^I_{\rm ACC})^2\rangle]\tau_{\rm dec}=D^{\rm ACC}_{p\mu}(\epsilon_I),\\
D^{\rm ACC}_{pp}(\epsilon_I) &= p^2\mu^2\langle(\delta\nu^I_{\rm ACC})^2\rangle\tau_{\rm dec}.
\end{aligned}
\tag{68}
$$

After inserting the approximate expressions for $\langle(\delta\nu^I_{\rm ACC})^2\rangle(\epsilon_I)$ in Equation (59) and $\langle\delta\nu^I_{\rm ACC}\delta\nu^I_{\rm REF}\rangle(\epsilon_I)$ in Equation (60) into the basic Fokker–Planck coefficient expressions in Equation (68), we find that

$$
\begin{aligned}
D^{\rm ACC}_{\mu\mu}(\epsilon_I) &\approx \left[1+C_\delta^{-1}4r^I_{\rm A}\left(\frac{U_0}{v}\right)^2\left(\frac{V_{A0}}{v}\right)^2\left(\frac{L_I}{L_{\rm Ir}}\right)^2\right]T^{\rm ACC}_{\mu\mu},\\
D^{\rm ACC}_{\mu p}(\epsilon_I) &\approx +\left(p\frac{V_{A0}}{v}\right)C_\delta^{-1}r^I_{\rm A}\frac{V_{A0}}{v}T^{\rm ACC}_{\mu p}(\epsilon_I)=D^{\rm ACC}_{p\mu}(\epsilon_I),\\
D^{\rm ACC}_{pp}(\epsilon_I) &\approx \left(p\frac{V_{A0}}{v}\right)^2C_\delta^{-1}r^I_{\rm A}T^{\rm ACC}_{pp}(\epsilon_I),
\end{aligned}
\tag{69}
$$

where

$$
\begin{aligned}
T^{\rm ACC}_{\mu\mu}(\epsilon_I) &= (1-\mu^2)^2T_{\mu\mu}(\epsilon_I),\\
T^{\rm ACC}_{\mu p}(\epsilon_I) &= 4\mu(1-\mu^2)\left(\frac{U_0}{v}\right)^2\left(\frac{L_I}{L_{\rm Ir}}\right)^2T_{\mu\mu}(\epsilon_I),\\
T^{\rm ACC}_{pp}(\epsilon_I) &= 4\mu^2\left(\frac{U_0}{v}\right)^2\left(\frac{L_I}{L_{\rm Ir}}\right)^2T_{\mu\mu}(\epsilon_I),
\end{aligned}
\tag{70}
$$

and, as before, $T^{\rm ACC}_{\mu\mu}=T^{\rm COM}_{\mu\mu}$ and $T_{\mu\mu}$ is expressed by Equation (64).

Finally, consider fluctuations in the particle acceleration rate associated with variations in the reconnection electric fields in the diffusion regions at the center of merging small-scale flux ropes. In this case the basic Fokker–Planck diffusion coefficient expressions listed in Equation (45) are given by

$$
\begin{aligned}
D^{\rm REC}_{\mu\mu}(\epsilon_I) &= \frac{1}{4}(1-\mu^2)^2\langle(\delta\nu^I_{\rm REF}+2\delta\nu^I_{\rm REC})^2\rangle\tau_{\rm dec},\\
D^{\rm REC}_{\mu p}(\epsilon_I) &= p\frac{1}{2}(1-\mu^2)\mu\\
&\quad\times[\langle\delta\nu^I_{\rm REF}\delta\nu^I_{\rm REC}\rangle+2\langle(\delta\nu^I_{\rm REC})^2\rangle]\tau_{\rm dec},\\
D^{\rm REC}_{\mu p}(\epsilon_I) &= p\frac{1}{2}(1-\mu^2)\mu\\
&\quad\times[\langle\delta\nu^I_{\rm REF}\delta\nu^I_{\rm REC}\rangle+2\langle(\delta\nu^I_{\rm REC})^2\rangle]\tau_{\rm dec},\\
D^{\rm REC}_{pp}(\epsilon_I) &= p^2\mu^2\langle(\delta\nu^I_{\rm REC})^2\rangle\tau_{\rm dec}.
\end{aligned}
\tag{71}
$$

When we insert the approximate expressions for $\langle(\delta\nu^I_{\rm REC})^2\rangle(\epsilon_I)$ in Equation (59) and $\langle\delta\nu^I_{\rm REC}\delta\nu^I_{\rm REF}\rangle(\epsilon_I)$ in Equation (60) into the basic Fokker–Planck coefficient expressions in Equation (71), we find the following:

$$
\begin{aligned}
D^{\rm REC}_{\mu\mu}(\epsilon_I) &\approx \Bigg[1-C_\delta^{-1/2}4\left(\frac{1/2\sigma^I_C(r^I_{\rm A}+1)+(r^I_{\rm A})^{1/2}}{(r^I_{\rm A}+1)^{1/2}}\right)\\
&\quad\times\frac{q}{|q|}\frac{Z}{A}\left(\frac{V_{A0}}{v}\right)^2\frac{L_I}{d_{i/e}}\left(\frac{\epsilon_I}{\epsilon_{B_0}}\right)^{1/2}\\
&\quad+16a\left(\frac{r^I_{\rm A}-1/4(\sigma^I_C)^2(r^I_{\rm A}+1)^2}{r^I_{\rm A}+1}\right)\\
&\quad\times\left(\frac{Z}{A}\right)^2\left(\frac{V_{A0}}{v}\right)^4\left(\frac{L_I}{d_{i/e}}\right)^2\frac{\epsilon_I}{\epsilon_{B_0}}\Bigg]T^{\rm REC}_{\mu\mu}(\epsilon_I),\\
D^{\rm REC}_{\mu p}(\epsilon_I) &\approx -\left(p\frac{V_{A0}}{v}\right)[(1/2\sigma^I_C(r^I_{\rm A}+1)+(r^I_{\rm A})^{1/2})C_\delta^{-1/2}\\
&\quad-8a\left(\frac{r^I_{\rm A}-1/4(\sigma^I_C)^2(r^I_{\rm A}+1)^2}{(r^I_{\rm A}+1)^{1/2}}\right)\\
&\quad\times\frac{q}{|q|}\frac{Z}{A}\left(\frac{V_{A0}}{v}\right)^2\frac{L_I}{d_{i/e}}\left(\frac{\epsilon_I}{\epsilon_{B_0}}\right)^{1/2}\Bigg]T^{\rm REC}_{\mu p}(\epsilon_I)\\
&= D^{\rm REC}_{p\mu}(\epsilon_I),\\
D^{\rm REC}_{pp}(\epsilon_I) &\approx \left(p\frac{V_{A0}}{v}\right)^2(r^I_{\rm A}-1/4(\sigma^I_C)^2(r^I_{\rm A}+1)^2)T^{\rm REC}_{pp}(\epsilon_I),
\end{aligned}
\tag{72}
$$

where

$$
\begin{aligned}
T^{\rm REC}_{\mu\mu}(\epsilon_I) &= (1-\mu^2)^2T_{\mu\mu}(\epsilon_I),\\
T^{\rm REC}_{\mu p}(\epsilon_I) &= \frac{2\mu(1-\mu^2)}{(r^I_{\rm A}+1)^{1/2}}\frac{q}{|q|}\frac{Z}{A}\frac{V_{A0}}{v}\frac{L_I}{d_{i/e}}\left(\frac{\epsilon_I}{\epsilon_{B_0}}\right)^{1/2}T_{\mu\mu}(\epsilon_I),\\
T^{\rm REC}_{pp}(\epsilon_I) &= \frac{16a\mu^2}{r^I_{\rm A}+1}\left(\frac{Z}{A}\right)^2\left(\frac{V_{A0}}{v}\right)^2\left(\frac{L_I}{d_{i/e}}\right)^2\frac{\epsilon_I}{\epsilon_{B_0}}T_{\mu\mu}(\epsilon_I),
\end{aligned}
\tag{73}
$$

where $T^{\rm REC}_{\mu\mu}=T^{\rm COM}_{\mu\mu}$ and $T_{\mu\mu}$ is expressed in Equation (64).

In the Fokker–Planck coefficient expressions above, $T_{\mu\mu}$ contains $\tau_{\rm dec}$, which is the energetic particle decorrelation time (the time interval on which propagating energetic particles see decorrelated flux-rope properties [flux-rope flow, magnetic field, and reconnection electric field] when interacting with many flux ropes). The decorrelation time is estimated by taking into account the time it takes for a particle to traverse a magnetic flux-rope structure (crossing time), which in turn depends on the particle propagation model. We consider two limits. First, consider the weak scattering limit (quasi-linear theory limit) in which a particle's effective scattering time $\tau^{\rm eff}_{\rm sc}\gg\tau_c=L_I/\langle\delta U_I^2\rangle^{1/2}$ (τ_c is the average magnetic island dynamical timescale [nonlinear eddy turnover time or turbulence correlation time]). In this limit we model $\tau_{\rm dec}$ as a competition between the average flux-rope crossing frequency for undisturbed guiding center motion along the flux-rope magnetic field (essentially propagation along the flux-rope axial or guide field because of the strong guide field limit we assume) and the frequency for particle advection by the average magnetic island plasma flow across the guide field.

Thus, the decorrelation time can be expressed approximately as

$$\tau_{\rm dec} \approx \frac{1}{v|\mu|/L_{I\parallel} + \langle \delta U_I^2\rangle^{1/2}/L_I} \approx \frac{1}{v|\mu|/L_{I\parallel} + (V_{A0}/L_I)(r_{\rm A}^I/(r_{\rm A}^I+1))^{1/2}(\epsilon_I/\epsilon_{B_0})^{1/2}}, \quad (74)$$

where $L_{I\parallel}$ is the length of the flux-rope in the guide field direction. $L_\parallel$ is generally thought to be considerably longer than L_I (the cross section of the flux-rope in the 2D plane perpendicular to $\boldsymbol{B}_0$) in the NI MHD theory of quasi-2D magnetic island turbulence (Zank et al. 2017) as observations at 1 au indicate (e.g., Weygand et al. 2011). In Equation (74), the parameter $r_{\rm A}^I = \langle \delta U_I^2\rangle/\langle \delta V_{AI}^2\rangle$ is the Alfvén ratio of the mean flux-rope kinetic energy over the mean flux-rope magnetic energy in the 2D plane perpendicular to $\boldsymbol{B}_0$ ($\langle \delta V_{AI}^2\rangle = \langle \delta B_I^2\rangle/4\pi\rho_0$), $V_{A0} = B_0/(4\pi\rho_0)^{1/2}$ is the Alfvén speed associated with the background/guide magnetic field, and $\epsilon_{B0} = B_0^2/8\pi$ is the energy density of the background/guide magnetic field. Thus, $\langle \delta B_I^2\rangle/B_0^2 = (\epsilon_I/\epsilon_{B_0})/(r_{\rm A}^I+1)$, and $\langle \delta U_I^2\rangle^{1/2} = (r_{\rm A}^I)^{1/2}(\langle \delta B_I^2\rangle^{1/2}/B_0)V_{A0}$.

Assuming the strong scattering limit ($\tau_{\rm sc}^{\rm eff} \ll \tau_c$), we enter the nonlinear transport limit of our theory, where energetic particle guiding centers are assumed to diffuse along the flux-rope magnetic field (mainly along the guide field). Random disturbances in the guiding center trajectory in our theory can be thought of as a product of energetic particles responding to the magnetic mirroring force generated by the field-aligned gradient in the flux-rope magnetic field strength. This can be understood by considering a particle propagating inside a flux rope in which the parallel field strength gradient varies not only as a smooth function on spatial scales $l \gg r_g$ but also randomly on smaller spatial scales $l \leqslant r_g$ owing to the presence of other smaller-scale magnetic islands inside the flux rope that act as magnetic scattering centers (e.g., Ambrosiano et al. 1988). In addition, guiding center trajectories can also be randomly distorted by interaction with other small-scale wave modes present in flux-rope structures, such as Alfvén waves, which we also consider. Thus, the effective particle scattering time $\tau_{\rm sc}^{\rm eff}$ is determined from a competition between the particle scattering frequency due to interaction with gyroscale Alfvén waves $\langle \nu_{\rm sc}^A\rangle$ and the scattering frequency $\langle \nu_{\rm sc}^I\rangle$ due to interaction with fluctuating magnetic mirroring forces generated in small-scale flux ropes, resulting in parallel diffusion. As a result, the particle decorrelation time $\tau_{\rm dec}$ is determined by a competition between the flux-rope crossing frequency due to parallel diffusion mainly along the guide field and the crossing frequency due to particle advection by the magnetic island plasma flow across the guide field. This competition is captured in the expression (for more details, see le Roux et al. 2015a)

$$\tau_{\rm dec} \approx \frac{1}{1/\tau_c + (2/\sqrt{\pi})(1/\sqrt{\tau_c\tau_D})}, \quad (75)$$

where $\tau_D = L_{I\parallel}^2/\kappa_\parallel^{\rm eff1}$ is the flux-rope crossing time for energetic particles diffusing basically along the flux-rope guide field with an effective parallel diffusion coefficient $\kappa_\parallel^{\rm eff1}$. The parallel diffusion coefficient has the expression

$$\kappa_\parallel^{\rm eff1} = \frac{1}{3}\frac{v^2}{\langle \nu_{\rm sc}^{\rm eff1}\rangle}, \quad (76)$$

where the effective scattering frequency is

$$\langle \nu_{\rm sc}^{\rm eff1}\rangle = 2(\langle \nu_{\rm sc}^A\rangle + \langle \nu_{\rm sc}^I\rangle), \quad (77)$$

and $\langle \nu_{\rm sc}^I\rangle = 1/5\langle (\delta\nu_{\rm REF}^I)^2\rangle\tau_{\rm dec}$ (see Equations (169) and (170) in Appendix D, where the diffusion approximation limit of our theory is discussed), reflecting the competition between gyroresonant scattering by Alfvén waves $\langle \nu_{\rm sc}^A\rangle$ and scattering by mirroring forces $\langle \nu_{\rm sc}^I\rangle$ inside flux-rope structures as discussed above.

In the limit of slow diffusion ($\tau_c \ll \tau_D$), when particles are advected with the plasma flow active in magnetic islands,

$$\tau_{\rm dec} \approx \tau_c = \frac{L_I}{\langle \delta U_I^2\rangle^{1/2}} = \frac{(r_{\rm A}^I+1)^{1/2}}{(r_{\rm A}^I)^{1/2}}\frac{L_I}{V_{A0}}\left(\frac{\epsilon_{B_0}}{\epsilon_I}\right)^{1/2}. \quad (78)$$

As discussed in Appendix D.1, we consider this limit to be less likely in the solar wind near 1 au based on our assessment that flux-rope turbulence in these solar wind regions is subject to the strong guide field limit. In the opposite limit of fast diffusion ($\tau_D \ll \tau_c$),

$$\tau_{\rm dec} \approx \frac{\sqrt{\pi}}{2}\sqrt{\tau_c\tau_D}. \quad (79)$$

Assuming $\langle \nu_{\rm sc}^I\rangle \gg \langle \nu_{\rm sc}^A\rangle$, which we find to be plausible in solar wind conditions near 1 au as discussed below in Section 15, and by working in the diffusion approximation, we solved a nonlinear expression for the parallel diffusion coefficient due to scattering by multiple small-scale flux-rope mirroring forces (see Appendix D.1) and found the scattering frequency $\langle \nu_{\rm sc}^I\rangle$ to be

$$\langle \nu_{\rm sc}^I\rangle \approx C_\delta^2\frac{12a^2\pi}{200}\frac{v^2}{\langle \delta U_I^2\rangle^{1/2}}\frac{\langle \delta B_I^2\rangle^2/B_0^4}{L_I^3/L_{I\parallel}^2}. \quad (80)$$

Then the expression for $\tau_{\rm dec}$ finally becomes

$$\tau_{\rm dec} \approx C_\delta\frac{6a\pi}{20}\frac{L_{I\parallel}^2}{L_I}\frac{\langle \delta B_I^2\rangle/B_0^2}{\langle \delta U_I^2\rangle^{1/2}} = C_\delta\frac{6a\pi}{20}\frac{1}{(r_{\rm A}^I+1)^{1/2}(r_{\rm A}^I)^{1/2}}\frac{L_{I\parallel}^2/L_I}{V_{A0}}\left(\frac{\epsilon_I}{\epsilon_{B_0}}\right)^{1/2}, \quad (81)$$

where the ratio C_δ was introduced to enable the simplifying substitution $\langle [\delta(\delta B_I)]^2\rangle = C_\delta\langle \delta B_I^2\rangle$ (see Appendix A). Furthermore, $a = 1/2$ to indicate the assumption that 2D flux-rope turbulence is on average isotropic in the 2D plane perpendicular to $\boldsymbol{B}_0$ (e.g., Zank et al. 2017) as is discussed in Appendix B (see, e.g., Equation (151) and its discussion).

10. Approximate Expressions for the Damping Rates of Small-scale Magnetic Islands for Each Flux-rope Acceleration Case

10.1. Coherent Damping Rates of Small-scale Magnetic Islands

Upon inserting the expression for $\langle\langle dp/dt\rangle_{\phi}^{I}\rangle(\epsilon_I)$ (Equation (44)) into the expression for $\gamma_I^{\rm coh}(\langle f\rangle)$ (Equation (52)), the basic expressions for the total magnetic island energy density coherent damping rate in response to self-consistent coherent particle acceleration by flux ropes for each of the four flux-rope acceleration cases are

$$\begin{aligned}
\gamma_{\rm COM}^{\rm coh}(\epsilon_I) &= \frac{-2\pi}{\epsilon_I} \\
&\quad\times \int_{-1}^{1} d\mu \int_{0}^{\infty} dpp^3 \nu \frac{1}{2}(1-\mu^2)\langle \nu_{\rm COM}^{I}\rangle \langle f\rangle, \\
\gamma_{\rm INC}^{\rm coh}(\epsilon_I) &= \frac{-2\pi}{\epsilon_I} \\
&\quad\times \int_{-1}^{1} d\mu \int_{0}^{\infty} dpp^3 \nu \frac{1}{2}(3\mu^2-1)\langle \nu_{\rm INC}^{I}\rangle \langle f\rangle, \\
\gamma_{\rm ACC}^{\rm coh}(\epsilon_I) &= \frac{-2\pi}{\epsilon_I}\int_{-1}^{1} d\mu \int_{0}^{\infty} dpp^3 \nu\mu \langle \nu_{\rm ACC}^{I}\rangle \langle f\rangle, \\
\gamma_{\rm REC}^{\rm coh}(\epsilon_I) &= \frac{-2\pi}{\epsilon_I}\int_{-1}^{1} d\mu \int_{0}^{\infty} dpp^3 \nu\mu \langle \nu_{\rm REC}\rangle \langle f\rangle.
\end{aligned} \tag{82}$$

After inserting the approximate expressions for the average coherent relative acceleration rates (Equation (54)) into Equation (82), we get the following expressions for the coherent magnetic island energy density damping rates:

$$\begin{aligned}
\gamma_{\rm COM}^{\rm coh}(\epsilon_I) &\approx -\pi\sigma_{\rm COM}^{I}\frac{(r_{\rm A}^{I})^{1/2}}{(r_{\rm A}^{I}+1)^{1/2}}\frac{V_{A0}}{L_I}\left(\frac{\epsilon_{B_0}}{\epsilon_I}\right)^{1/2} \\
&\quad\times \frac{1}{\epsilon_{B_0}}\int_{-1}^{1} d\mu(1-\mu^2)\int_{0}^{\infty} dpp^3\nu\langle f\rangle, \\
\gamma_{\rm INC}^{\rm coh}(\epsilon_I) &\approx -\pi\sigma_{\rm INC}\frac{(r_{\rm A}^{I})^{1/2}}{(r_{\rm A}^{I}+1)^{3/2}}\frac{V_{A0}}{L_I}\left(\frac{\epsilon_I}{\epsilon_{B_0}}\right)^{1/2} \\
&\quad\times \frac{1}{\epsilon_{B_0}}\int_{-1}^{1} d\mu(3\mu^2-1)\int_{0}^{\infty} dpp^3\nu\langle f\rangle, \\
\gamma_{\rm ACC}^{\rm coh}(\epsilon_I) &\approx -2\pi\sigma_{\rm ACC}^{I}\frac{(r_{\rm A}^{I})^{1/2}}{r_{\rm A}^{I}+1}\frac{V_{A0}}{L_{\rm Ir}} \\
&\quad\times \frac{1}{\epsilon_{B0}}\int_{-1}^{1} d\mu\mu\int_{0}^{\infty} dpp^3\nu\frac{U_0}{v}\langle f\rangle, \\
\gamma_{\rm REC}^{\rm coh}(\epsilon_I) &\approx -2\pi\sigma_{\rm REC}^{I}\frac{q}{|q|}\frac{Z}{A}\frac{(r_{\rm A}^{I})^{1/2}}{r_{\rm A}^{I}+1}\frac{V_{A0}}{d_{i/e}} \\
&\quad\times \frac{1}{\epsilon_{B_0}}\int_{-1}^{1} d\mu\mu\int_{0}^{\infty} dpp^3\nu\frac{V_{A0}}{v}\langle f\rangle.
\end{aligned} \tag{83}$$

10.2. Stochastic Damping Rates of Small-scale Magnetic Islands

By inserting the expressions for $D_{p\mu}^{I}(\epsilon_I)$ and $D_{pp}^{I}(\epsilon_I)$ in Equation (45) into the expression for $\gamma_I^{\rm stoch}(\langle f\rangle)$ given by Equation (53), we find the basic expressions for the total magnetic island energy density stochastic damping rate in response to self-consistent stochastic particle acceleration by flux ropes for each of the four flux-rope acceleration cases. They are

$$\begin{aligned}
\gamma_{\rm COM}^{\rm stoch}(\epsilon_I) &= \frac{2\pi}{\epsilon_I}\int_{-1}^{1} d\mu \int_{0}^{\infty} dpp^3\nu\frac{1}{4}(1-\mu^2)^2 \\
&\quad\times\left[(\langle \delta\nu_{\rm COM}^{I}\delta\nu_{\rm REF}^{I}\rangle - \mu\langle(\delta\nu_{\rm COM}^{I})^2\rangle)\frac{\partial\langle f\rangle}{\partial\mu}\right. \\
&\quad\left. + p\langle(\delta\nu_{\rm COM}^{I})^2\rangle\frac{\partial\langle f\rangle}{\partial p}\right]\tau_{\rm dec}, \\
\gamma_{\rm INC}^{\rm stoch}(\epsilon_I) &= \frac{2\pi}{\epsilon_I}\int_{-1}^{1} d\mu \int_{0}^{\infty} dpp^3\nu\frac{1}{4}(3\mu^2-1) \\
&\quad\times\left[(1-\mu^2)(\langle \delta\nu_{\rm INC}^{I}\delta\nu_{\rm REF}^{I}\rangle + 3\mu\langle(\delta\nu_{\rm INC}^{I})^2\rangle)\frac{\partial\langle f\rangle}{\partial\mu}\right. \\
&\quad\left. + p(3\mu^2-1)\langle(\delta\nu_{\rm INC}^{I})^2\rangle\frac{\partial\langle f\rangle}{\partial p}\right]\tau_{\rm dec},
\end{aligned}$$

$$\begin{aligned}
\gamma_{\rm ACC}^{\rm stoch}(\epsilon_I) &= \frac{2\pi}{\epsilon_I}\int_{-1}^{1} d\mu \int_{0}^{\infty} dpp^3\nu\mu \\
&\quad\times\left[\frac{1}{2}(1-\mu^2)(\langle \delta\nu_{\rm ACC}^{I}\delta\nu_{\rm REF}^{I}\rangle + 2\langle(\delta\nu_{\rm ACC}^{I})^2\rangle)\right. \\
&\quad\left.\times\frac{\partial\langle f\rangle}{\partial\mu} + p\mu\langle(\delta\nu_{\rm ACC}^{I})^2\rangle\frac{\partial\langle f\rangle}{\partial p}\right]\tau_{\rm dec}, \\
\gamma_{\rm REC}^{\rm stoch}(\epsilon_I) &= \frac{2\pi}{\epsilon_I}\int_{-1}^{1} d\mu \int_{0}^{\infty} dpp^3\nu\mu \\
&\quad\times\left[\frac{1}{2}(1-\mu^2)(\langle \delta\nu_{\rm REC}^{I}\delta\nu_{\rm REF}^{I}\rangle + 2\langle(\delta\nu_{\rm REC}^{I})^2\rangle)\right. \\
&\quad\left.\times\frac{\partial\langle f\rangle}{\partial\mu} + p\mu\langle(\delta\nu_{\rm REC}^{I})^2\rangle\frac{\partial\langle f\rangle}{\partial p}\right]\tau_{\rm dec}.
\end{aligned} \tag{84}$$

Finally, we insert the approximate expressions for the variance in the relative particle acceleration rates given by Equations (59) and (60) into Equation (84) to acquire the following expressions for the four different stochastic magnetic island energy density growth/damping rates:

$$\begin{aligned}
\gamma_{\rm COM}^{\rm stoch}(\epsilon_I) &\approx -\frac{2\pi}{\epsilon_I}\int_{-1}^{1} d\mu \int_{0}^{\infty} dpp^2\nu\left(\frac{pV_{A0}}{v}\right)T_{\mu\mu}^{\rm COM} \\
&\quad\times\left[\frac{1}{2}\sigma_C^{I}(r_{\rm A}^{I}+1)\frac{\partial\langle f\rangle}{\partial\mu} + r_{\rm A}^{I}\left(\frac{V_{A0}}{v}\right)\right. \\
&\quad\left.\times\left(\mu\frac{\partial\langle f\rangle}{\partial\mu} - p\frac{\partial\langle f\rangle}{\partial p}\right)\right],
\end{aligned} \tag{85}$$

$$\gamma_{\rm INC}^{\rm stoch}(\epsilon_I) \approx -\frac{2\pi}{\epsilon_{B_0}} \times \frac{1}{r_{\rm A}^I+1}\int_{-1}^{1} d\mu \int_0^\infty dpp^2 \nu\left(\frac{pV_{A0}}{\nu}\right)(3\mu^2-1)T_{\mu\mu} \times \left[\left(\frac{1}{2}\sigma_C^I(r_{\rm A}^I+1)+(r_{\rm A}^I)^{1/2}\right)(1-\mu^2)\frac{\partial\langle f\rangle}{\partial\mu} + \frac{r_{\rm A}^I+1/4(\sigma_C^I)^2(r_{\rm A}^I+1)^2}{r_{\rm A}^I+1}\left(\frac{V_{A0}}{\nu}\right)\frac{\epsilon_I}{\epsilon_{B_0}} \times \left(6\mu(1-\mu^2)\frac{\partial\langle f\rangle}{\partial\mu}-2(3\mu^2-1)p\frac{\partial\langle f\rangle}{\partial p}\right)\right], \quad (86)$$

$$\gamma_{\rm ACC}^{\rm stoch}(\epsilon_I) \approx \frac{2\pi}{\epsilon_I}C_\delta^{-1}r_{\rm A}^I\left(\frac{L_I}{L_{\rm Ir}}\right)^2\int_{-1}^{1} d\mu\int_0^\infty dpp^3\nu \times \left(\frac{V_{A0}}{\nu}\right)^2\left(\frac{U_0}{\nu}\right)^2 2\mu T_{\mu\mu} \times \left((1-\mu^2)\frac{\partial\langle f\rangle}{\partial\mu}+\mu p\frac{\partial\langle f\rangle}{\partial p}\right), \quad (87)$$

$$\gamma_{\rm REC}^{\rm stoch}(\epsilon_I) \approx -\frac{2\pi}{\epsilon_I}\frac{1}{(r_{\rm A}^I+1)^{1/2}} \times \left(\frac{\epsilon_I}{\epsilon_{B_0}}\right)^{1/2}\frac{q}{|q|}\frac{Z}{A}\frac{L_I}{d_{i/e}}\int_{-1}^{1} d\mu\int_0^\infty dpp^2\nu\left(p\frac{V_0}{\nu}\right)\frac{V_{A0}}{\nu}2\mu T_{\mu\mu} \times \left[C_\delta^{-1/2}\left(\frac{1}{2}\sigma_C^I(r_{\rm A}^I+1)+(r_{\rm A}^I)^{1/2}\right)(1-\mu^2)\frac{\partial\langle f\rangle}{\partial\mu} - 8a\frac{r_{\rm A}^I-1/4(\sigma_C^I)^2(r_{\rm A}^I+1)^2}{(r_{\rm A}^I+1)^{1/2}}\left(\frac{V_{A0}}{\nu}\right)^2\frac{q}{|q|}\frac{Z}{A}\frac{L_I}{d_{i/e}}\left(\frac{\epsilon_I}{\epsilon_{B_0}}\right)^{1/2} \times \left((1-\mu^2)\frac{\partial\langle f\rangle}{\partial\mu}+\mu p\frac{\partial\langle f\rangle}{\partial p}\right)\right]. \quad (88)$$

11. The Coupled Kinetic-N I MHD Equations in the Diffusion Approximation

As in le Roux et al. (2015a), we consider the possibility that pitch-angle scattering by Alfvén waves and small-scale flux ropes can result in a near-isotropic energetic particle distribution in momentum space for particle transport on large spatial scales (the diffusion approximation). This enables us to write down a pitch-angle-averaged diffusive equation for the large-scale transport of energetic particles in dynamic small-scale flux-rope regions with one less variable, which is useful for computational efficiency. This can be done for either the quasi-linear or nonlinear particle propagation limit of our theory. Here we show only the diffusive approximation for the nonlinear transport limit when the effective timescale for particle scattering is shorter than the magnetic island dynamic timescale ($\tau_{\rm sc}^{\rm eff} \ll \tau_c$), as discussed in Section 8.1 below Equation (46). We think that this limit might be more appropriate for stronger turbulence conditions occurring behind traveling shocks, for example, rather than in quiet solar wind conditions.

The main differences compared to le Roux et al. (2015a) are as follows: (i) more detailed, rederived expressions are presented for the transport coefficients, such as for the stochastic acceleration coefficient D_{pp}^I that includes the acceleration effects of $D_{p\mu}^I$ and $D_{\mu p}^I$ on energetic particles; (ii) a new transport coefficient for stochastic acceleration involving the effect of fluctuations in the noninertial force due to the acceleration of the flux-rope flow; (iii) the spatial transport effects of $D_{p\mu}^I$ and $D_{\mu p}^I$ on energetic particles are considered for the first time; (iv) a new N I MHD equation for transport of the total magnetic island energy density (in the 2D plane perpendicular to $\boldsymbol{B}_0$) in the nonuniform solar wind medium that is coupled to the focused transport equation in the diffusive approximation to facilitate self-consistent energetic particle acceleration. Self-consistency is achieved with the inclusion of flux-rope growth/damping coefficients appropriate for a nearly isotropic energetic particle distribution. For the interested reader, we present the detailed diffusive approximation form of the coupled kinetic-N I MHD equations in Appendices D and E. Specifically, in Appendix D we present the Parker–Gleeson–Axford diffusive transport equation, and in Appendix E we present the N I MHD transport equation with growth/damping coefficients adjusted for nearly isotropic energetic particle distribution functions.

12. Comparing Coherent Energetic Particle Acceleration Rates for Different Small-scale Flux-rope Acceleration Mechanisms

Standard kinetic theories for energetic particle interaction with small-amplitude random wave turbulence (propagating waves with random phases) typically describe the acceleration process as a diffusion process in momentum space. This utilizes Fokker–Planck coefficients that depend on the variance in the electromagnetic fields of the wave turbulence. Usually, acceleration as a coherent process in response to the mean electromagnetic fields, which are assumed to be zero, is not addressed. However, in the case of particle energization by contracting and merging magnetic flux ropes, the possibility exists that multiple flux ropes can have a mean contraction rate. For example, at actively reconnecting primary current sheets in the solar wind one can expect that numerous new contracting flux ropes are being formed intermittently. Khabarova et al. (2015, 2016) discuss how the heliospheric current sheet can act as a source of contracting flux ropes whenever the current sheet is disturbed. Khabarova et al. (2016) and Guidoni et al. (2016) also discuss how magnetic flux ropes can experience continuous compressible contraction at solar flare sites and between the heliospheric current sheet and primary current sheets associated with coronal mass ejections and corotating interaction regions. Furthermore, merging of magnetic flux ropes should produce a finite mean merging rate and perhaps a finite mean reconnection electric field associated with the merging process as well.

Inspection of the approximate expressions of the coherent rates of relative momentum gain for the different flux-rope acceleration cases (Equation (54)) reveals that in some cases a stronger guide magnetic field (reduction in the ratio $\langle\delta B_I^2\rangle^{1/2}/B_0$) will result in less efficient relative momentum gain. Combined curvature drift and betatron momentum gain in small-scale flux ropes that contract or merge in the compressible limit and parallel guiding center motion momentum gain in response to the parallel reconnection electric field force in

merging flux ropes are not sensitive to an increased guide magnetic field. Combined curvature drift and generalized betatron momentum gain in small-scale flux ropes that contract or merge in the incompressible limit ($\langle \dot{p} \rangle^{\rm INC}_{\phi/\mu}/p \propto \langle \delta B_I^2 \rangle / B_0^2$) is the most sensitive to an increased guide magnetic field. Finally, parallel guiding center motion momentum gain in response to the noninertial force associated with the parallel acceleration of the flux-rope flow ($\langle \dot{p} \rangle^{\rm ACC}_{\phi/mu}/p \propto \langle \delta B_I^2 \rangle^{1/2}/B_0$) is sensitive to an intermediate degree to an increase in the guide field strength. This implies that coherent particle parallel guiding center motion acceleration by the parallel reconnection electric field increases in efficiency compared to net particle curvature drift and generalized betatron acceleration in small-scale flux ropes that contract and merge in the incompressible limit when the guide field is increased relative to the magnetic island or twist component consistent with kinetic particle simulations (Dahlin et al. 2017; Li et al. 2018). It also means that combined curvature drift and generalized betatron acceleration in small-scale flux ropes that contract and merge in the compressible limit will become relatively more efficient compared to contraction and merging in the incompressible limit. However, bear in mind that these conclusions are limited in that we do account for a possible increase in the particle anisotropy and a decrease in the level of compressibility with increasing guide field strength (Dahlin et al. 2017; Li et al. 2018).

Comparison of the approximate average coherent energetic particle rates of momentum gain listed in Equations (54) and (55), assuming finite mean values for the contraction, merging, and flow acceleration rates and for the reconnection electric field of numerous contracting and merging small-scale flux ropes, results in the following expressions for the momentum gain rate ratios for the four flux-rope acceleration cases discussed in this paper:

$$
\begin{aligned}
\frac{\langle\langle \dot{p} \rangle^{\rm INC}_{\phi,\mu}\rangle}{\langle\langle \dot{p} \rangle^{\rm COM}_{\phi,\mu}\rangle} &\approx \frac{\langle \nu^I_{\rm INC}\rangle}{\langle \nu^I_{\rm COM}\rangle}\frac{3f_2(p)}{f_0(p)} = \frac{\sigma^I_{\rm INC}}{\sigma^I_{\rm COM}}\frac{\langle \delta B_I^2\rangle}{B_0^2}\frac{3f_2(p)}{f_0(p)},\\
\frac{\langle\langle \dot{p} \rangle^{\rm REC}_{\phi,\mu}\rangle}{\langle\langle \dot{p} \rangle^{\rm COM}_{\phi,\mu}\rangle} &\approx \frac{\langle \nu^I_{\rm REC}\rangle}{\langle \nu^I_{\rm COM}\rangle}\frac{3f_1(p)}{f_0(p)}\\
&= \frac{\sigma^I_{\rm REC}}{\sigma^I_{\rm COM}}\frac{q}{|q|}\frac{Z}{A}\frac{L_I}{d_{i,e}}\frac{V_{A0}}{v}\frac{\langle \delta B_I^2\rangle^{1/2}}{B_0}\frac{3f_1(p)}{f_0(p)},\\
\frac{\langle\langle \dot{p} \rangle^{\rm REC}_{\phi,\mu}\rangle}{\langle\langle \dot{p} \rangle^{\rm INC}_{\phi,\mu}\rangle} &\approx \frac{\langle \nu^I_{\rm REC}\rangle}{\langle \nu^I_{\rm INC}\rangle}\frac{f_1(p)}{f_2(p)}\\
&= \frac{\sigma^I_{\rm REC}}{\sigma^I_{\rm INC}}\frac{q}{|q|}\frac{Z}{A}\frac{L_I}{d_{i,e}}\frac{V_{A0}}{v}\frac{B_0}{\langle \delta B_I^2\rangle^{1/2}}\frac{f_1(p)}{f_2(p)},\\
\frac{\langle\langle \dot{p} \rangle^{\rm ACC}_{\phi,\mu}\rangle}{\langle\langle \dot{p} \rangle^{\rm COM}_{\phi,\mu}\rangle} &\approx \frac{\langle \nu^I_{\rm ACC}\rangle}{\langle \nu^I_{\rm COM}\rangle}\frac{3f_1(p)}{f_0(p)}\\
&= \frac{\sigma^I_{\rm ACC}}{\sigma^I_{\rm COM}}\frac{L_I}{L_{\rm Ir}}\frac{U_0}{v}\frac{\langle \delta B_I^2\rangle^{1/2}}{B_0}\frac{3f_1(p)}{f_0(p)},\\
\frac{\langle\langle \dot{p} \rangle^{\rm ACC}_{\phi,\mu}\rangle}{\langle\langle \dot{p} \rangle^{\rm INC}_{\phi,\mu}\rangle} &\approx \frac{\langle \nu^I_{\rm ACC}\rangle}{\langle \nu^I_{\rm INC}\rangle}\frac{f_1(p)}{f_2(p)} = \frac{\sigma^I_{\rm ACC}}{\sigma^I_{\rm INC}}\frac{L_I}{L_{\rm Ir}}\frac{U_0}{v}\frac{B_0}{\langle \delta B_I^2\rangle^{1/2}}\frac{f_1(p)}{f_2(p)},\\
\frac{\langle\langle \dot{p} \rangle^{\rm ACC}_{\phi,\mu}\rangle}{\langle\langle \dot{p} \rangle^{\rm REC}_{\phi,\mu}\rangle} &\approx \frac{\langle \nu^I_{\rm ACC}\rangle}{\langle \nu^I_{\rm REC}\rangle} = \frac{\sigma^I_{\rm ACC}}{\sigma^I_{\rm REC}}\frac{q}{|q|}\frac{A}{Z}\frac{d_{i,e}}{L_{\rm Ir}}\frac{U_0}{V_{A0}},
\end{aligned}
\tag{89}
$$

where we introduced the simplification $f_0(p) - f_2(p) \approx f_0$. In Equation (89) the expressions for the acceleration rate ratios were derived by including the weighting factor of the pitch-angle anisotropy of the particle distribution function through expansion of the particle distribution function to the second moment in μ-space using Legendre polynomials (see Appendix D, Equation (164) and its discussion), followed by averaging the expressions over all μ values. Thus, in Equation (89) $f_0(p)$ is the isotropic part of the energetic particle distribution, the $f_1(p)$ term is the first-order anisotropy (odd function in μ), and the $f_2(p)$ term is the second-order anisotropy (even function in μ). By cutting off the expansion at the second moment, we are, strictly speaking, limited to nearly isotropic energetic particle distributions in which $f_0(p) \gg f_1(p) \gg f_2(p)$, but in order to discuss the effect of significant particle anisotropy on the acceleration rates, we will allow ourselves the liberty to specify the maximum values $f_{1,2}(p) \lesssim f_0(p)/3$ and $f_2(p) \lesssim f_1(p)$. In the rest of this section we estimate and discuss each of the coherent acceleration rate ratios listed in Equation (89) for energetic protons experiencing acceleration by small-scale flux ropes in solar wind conditions near 1 au. The results are summarized for reference in Table 1.

Consistent with theory and observations for quasi-2D small-scale flux-rope turbulence with cross sections in the inertial range near 1 au (Smith et al. 2016; Zank et al. 2017), we apply the strong guide field limit ($\delta B_I/B_0 = O(\epsilon) \ll 1$). Then, $\langle\langle \dot{p} \rangle^{\rm INC}_{\phi,\mu}\rangle / \langle\langle \dot{p} \rangle^{\rm COM}_{\phi,\mu}\rangle \approx O(\epsilon^2)$ assuming that $\sigma^I_{\rm INC}/\sigma^I_{\rm COM} \approx 1$ and $3f_2(p)/f_0(p) \approx 1$ (anisotropic particle pitch-angle distribution). This implies that, in the test particle limit, coherent energetic particle energization for particles experiencing the effect of a net contraction and merging rate from multiple small-scale flux ropes is much more efficient when these dynamic processes are predominantly compressive ($|\nabla \cdot \boldsymbol{V}_E| \gg \boldsymbol{V}_E \cdot \kappa$) as compared to the case when contraction and merging are mostly incompressible ($|\nabla \cdot \boldsymbol{V}_E| \ll \boldsymbol{V}_E \cdot \kappa$). As discussed above, this makes sense because in the case of compressible flux ropes particles experience energization from both curvature drift acceleration and generalized betatron acceleration, whereas in the case of incompressible flux ropes there is some competition between curvature drift energization and generalized betatron energy loss.

For a nearly isotropic particle pitch-angle distribution, modeled by assuming $f_1(p)/f_0(p) = O(\epsilon)$ and $f_2(p)/f_0(p) = O(\epsilon^2)$, $\langle \dot{p} \rangle^{\rm INC}_{\phi,\mu} / \langle \dot{p} \rangle^{\rm COM}_{\phi,\mu} \approx O(\epsilon^4)$. In this case, the dominance of particle acceleration by compressible flux ropes over incompressible flux ropes is even more pronounced because acceleration by incompressible flux ropes only involves the anisotropic part of the particle distribution, whereas acceleration by compressible flux ropes also involves the isotropic part of the distribution, which in this case is the dominant part of the distribution. In the unlikely situation of a purely isotropic distribution, $f_2(p) = 0$ and acceleration by incompressible flux ropes ceases (the probability of curvature drift momentum gain is balanced by the probability of generalized betatron momentum loss; Drake et al. 2010) when particles traverse numerous flux ropes with a mean contraction and merging rate. According to Equation (89), one way for combined curvature and generalized betatron acceleration in incompressible flux ropes to be competitive with acceleration in compressible flux ropes is to maintain a particle anisotropy of order

Table 1
Ratios of Coherent Small-scale Flux-rope Acceleration Rates for Energetic Protons

Acceleration Ratio	Expression	Value at 1 au
$\langle\dot{p}\rangle_{\phi,\mu}^{\rm INC}/\langle\dot{p}\rangle_{\phi,\mu}^{\rm COM}$	$0.1(3f_2/f_0)$	$\ll 1$
$\langle\dot{p}\rangle_{\phi,\mu}^{\rm REC}/\langle\dot{p}\rangle_{\phi,\mu}^{\rm COM}$	$6\times10^3\left(\frac{V_{A0}}{v}\right)\left(\frac{L_I}{L_c}\right)^{4/3}\left(\frac{3f_1}{f_0}\right)$	>1 if $L_I > 10^{-4}$ au and $3f_1/f_0 \approx 1$
		<1 if $f_1/f_0 \ll 1$
$\langle\dot{p}\rangle_{\phi,\mu}^{\rm REC}/\langle\dot{p}\rangle_{\phi,\mu}^{\rm INC}$	$6\times10^4\left(\frac{V_{A0}}{v}\right)\left(\frac{L_I}{L_c}\right)^{2/3}\left(\frac{f_1}{f_2}\right)$	$\gg 1$ if $L_I \gg d_i$
$\langle\dot{p}\rangle_{\phi,\mu}^{\rm ACC}/\langle\dot{p}\rangle_{\phi,\mu}^{\rm COM}$	$0.32(\frac{U_0}{v})\left(\frac{3f_1}{f_0}\right)$	$\ll 1$
$\langle\dot{p}\rangle_{\phi,\mu}^{\rm ACC}/\langle\dot{p}\rangle_{\phi,\mu}^{\rm INC}$	$3.2(\frac{U_0}{v})\left(\frac{L_c}{L_I}\right)^{1/3}\left(\frac{f_1}{f_2}\right)$	<1 if $L_I \approx L_c$ and $f_1 \approx f_2$
		>1 if $f_2/f_1 \ll 1$
$\langle\dot{p}\rangle_{\phi,\mu}^{\rm ACC}/\langle\dot{p}\rangle_{\phi,\mu}^{\rm REC}$	$5.2\times10^{-4}\left(\frac{L_c}{L_I}\right)$ au	$\ll 1$ if $L_I \gg d_i$

Note. In the table we provide an overview of the simplified expressions and estimated values of ratios of the coherent flux-rope acceleration rates for energetic protons averaged over pitch angle and gyrophase. The estimates were made for protons with kinetic energies $\gtrsim$1 keV ($v > U_0$, where U_0 is the solar wind speed) in solar wind flux-rope regions at 1 au. Flux-rope cross sections L_I were limited to values in the turbulence inertial range ($L_c \gtrsim L_I \gtrsim d_i$, where the turbulence correlation length $L_c \approx 0.01$ au is specified to be the maximum cross section and the ion inertial scale $d_i \approx 6\times10^{-7}$ au is assumed to be the minimum cross section). Energetic particle anisotropies were restricted to intermediate and small values ($3f_{1,2}/f_0 \lesssim 1$, $f_2/f_1 \lesssim 1$, where f_0 is the zeroth moment or isotropic part and $f_{1,2}$ is the first [second] moment belonging to the anisotropic part of the energetic particle distribution function). The distribution function was expanded in terms of Legendre polynomials up to the second moment (see Appendix D, Equation (164)). In the table, V_{A0} is the Alfvén speed associated with the background solar wind magnetic field.

$3f_2(p)/f_0(p) \approx 1$, together with a weaker guide field, $\langle\delta B_I^2\rangle^{1/2}/B_0 \approx 1$. Their is evidence from kinetic particle simulations that for a guide field of approximately this strength the energetic particle anisotropy can be sufficiently large that drift acceleration associated with island flow compression is comparable to drift acceleration associated with island shear flow (Li et al. 2018).

Consider the case of coherent energetic particle parallel guiding center motion energization assuming the existence of a net quasi-parallel reconnection electric field from multiple merging (reconnecting) small-scale flux ropes ($\langle\langle\dot{p}\rangle_{\phi,\mu}^{\rm REC}\rangle$). Compared to the case of combined energetic particle curvature drift and generalized betatron momentum gain by contracting and merging flux ropes in the compressible limit (second line of Equation (89)), we find near Earth that $\langle\langle\dot{p}\rangle_{\phi,\mu}^{\rm REC}\rangle/\langle\langle\dot{p}\rangle_{\phi,\mu}^{\rm COM}\rangle \approx 5.7\times10^3(V_{A0}/v)(L_I/L_c)^{4/3}(3f_1/f_0(p))$ for energetic protons assuming that $\sigma_{\rm REC}^I/\sigma_{\rm COM}^I \approx 1$. The maximum small-scale flux-rope cross section size in the inertial range $L_{I\,\max} \approx L_c \approx 0.01$ au, where L_c is the correlation scale of turbulence at 1 au as discussed above, the ion inertial scale $d_i \approx 5.6\times10^{-7}$ au, and $\langle\delta B_I^2\rangle/B_0^2 \approx 0.1$ at 1 au (Smith et al. 2016). To estimate the ratio, we introduce a Kolmogorov scaling for the total magnetic island energy density $\langle\delta B_I^2\rangle(L_I)$ that decreases in the inertial range as a function of the maximum flux-rope cross section $L_I \leqslant L_c$. This is accomplished according to the relationship $\langle\delta B_I^2\rangle(L_I) = (L_I/L_c)^{(s-1)}\langle\delta B_I^2\rangle(L_c)$, where the index $s = 5/3$ for a Kolmogorov energy density spectrum. The acceleration ratio decreases with increasing particle speed so that combined coherent curvature drift and generalized betatron momentum gain in compressible flux ropes becomes relatively more important at higher suprathermal particle energies. However, domination of acceleration by compressible flux ropes near 1 au depends strongly on the maximum flux-rope cross section under consideration. The energetic proton speed threshold, if combined coherent curvature drift and betatron momentum gain in compressible flux ropes is to dominate coherent parallel guiding center motion momentum gain by the parallel reconnection electric field ($\langle\langle\dot{p}\rangle_{\phi,\mu}^{\rm COM}\rangle \gtrsim \langle\langle\dot{p}\rangle_{\phi,\mu}^{\rm REC}\rangle$), can be determined from $v/U_0 \gtrsim 5.7\times10^2(L_I/L_c)^{4/3})(3f_1(p)/f_0(p))$. If we choose flux-rope cross sections in the inertial range with a maximum value of $L_I = L_c = 0.01$ au and assume that $3f_1(p)/f_0(p) \approx 1$, we find that $\langle\langle\dot{p}\rangle_{\phi,\mu}^{\rm COM}\rangle \gtrsim \langle\langle\dot{p}\rangle_{\phi,\mu}^{\rm REC}\rangle$ when $v/U_0 > 5.7\times10^2$, implying that curvature drift and generalized betatron momentum gain in compressible flux ropes dominates only for high kinetic proton energies $T \gtrsim 325$ MeV. Since the observed suprathermal ion power-law spectra in the inner heliosphere extend to $\lesssim$100 keV nucleon^{-1} (Fisk & Gloeckler 2014), parallel guiding center motion momentum gain by the mean parallel reconnection electric field dominates at all particle speeds of relevance. However, if we consider flux ropes in the inertial range with a smaller maximum cross section $L_I \approx 10^{-4}$ au, that is, a reduction by a factor of a 100, we find that $\langle\langle\dot{p}\rangle_{\phi,\mu}^{\rm COM}\rangle > \langle\langle\dot{p}\rangle_{\phi,\mu}^{\rm REC}\rangle$ when $v/U_0 > 1.2$, that is, for protons with $T > 1.6$ keV. In this case suprathermal energetic proton momentum gain is dominated by curvature drift and generalized betatron acceleration in the compressible limit.

Assuming instead a nearly isotropic particle distribution so that $3f_1(p)/f_0(p) = \epsilon$, and specifying $\epsilon = 0.1$, we find that if the maximum flux-rope cross section $L_I \approx L_c = 0.01$ au, then $\langle\langle\dot{p}\rangle_{\phi,\mu}^{\rm COM}\rangle > \langle\langle\dot{p}\rangle_{\phi,\mu}^{\rm REC}\rangle$ when $v/U_0 \gtrsim 57$ ($T \gtrsim 3.2$ MeV), indicating that coherent proton energization by the mean parallel reconnection electric field dominates in the observed energy range of energetic ions near 1 au. In this regard there is no qualitative change compared to assuming a more strongly anisotropic distribution. However, $\langle\langle\dot{p}\rangle_{\phi,\mu}^{\rm COM}\rangle > \langle\langle\dot{p}\rangle_{\phi,\mu}^{\rm REC}\rangle$ when $v/U_0 \gtrsim 2.6$ ($T > 7$ keV) for all flux-rope cross sections $L_I \lesssim 10^{-3}$ au. Thus, because particle acceleration by the mean parallel electric field is determined by the anisotropic part of the particle distribution related to $f_1(p)$, a small anisotropy results in particle acceleration being dominated by combined curvature drift and generalized betatron momentum gain at suprathermal energies in compressible flux ropes for larger flux-rope cross sections than possible in the case of a strongly anisotropic distribution. Alternatively, considering again the maximum flux-rope cross section $L_I \approx L_c = 0.01$ au, combined with a further reduction in the anisotropy of the particle distribution, then $3f_1(p)/f_0(p) = \epsilon^2 = 0.01$ implies that $\langle\langle\dot{p}\rangle_{\phi,\mu}^{\rm COM}\rangle > \langle\langle\dot{p}\rangle_{\phi,\mu}^{\rm REC}\rangle$ when $v/U_0 \gtrsim 5.7$ ($T \gtrsim 32$ keV) for protons. Then, proton energization by the mean parallel reconnection electric field dominates at lower suprathermal energies, whereas energization involving combined curvature drift and generalized betatron acceleration in the compressible flux-rope limit is more efficient at higher energies $T \gtrsim 32$ keV. For assuming a purely isotropic particle distribution $f_1(p) = 0$, there is no net particle acceleration by the mean parallel reconnection electric field because there is an equal probability for particle

motion along and opposite to the parallel reconnection electric field force.

Using the same values as specified above, we find that $\langle\langle\dot{p}\rangle_{\phi,\mu}^{\rm REC}\rangle/\langle\langle\dot{p}\rangle_{\phi,\mu}^{\rm INC}\rangle \approx 5.7\times10^{4}(V_{A0}/v)(L_I/L_c)^{2/3}(f_1(p)/f_2(p))$ assuming $\sigma^I_{\rm REC}/\sigma_{\rm INC}\approx 1$ (third line of Equation (89)), implying that $\langle\langle\dot{p}\rangle_{\phi,\mu}^{\rm REC}\rangle/\langle\langle\dot{p}\rangle_{\phi,\mu}^{\rm INC}\rangle \lesssim 1$ for $v/U_0 > 5.7\times10^{3}(L_I/L_c)^{2/3}(f_1(p)/f_2(p))$. For the case of an anisotropic energetic distribution with $f_1(p)\approx f_2(p)$, $\langle\langle\dot{p}\rangle_{\phi,\mu}^{\rm REC}\rangle/\langle\langle\dot{p}\rangle_{\phi,\mu}^{\rm INC}\rangle \lesssim 1$ for $v/U_0\gtrsim 2.6$ (energetic protons with $T\gtrsim 7$ keV) for all flux-rope cross sections $L_I\lesssim 10^{-7}$ au. In this case, domination of coherent particle acceleration by combined curvature drift momentum gain and betatron momentum loss in incompressible flux ropes over particle acceleration by the mean parallel reconnection electric field is restricted to considerably smaller flux-rope cross-section sizes compared to compressible contracting and merging flux ropes. Since small-scale flux-rope cross sections in the inertial range vary approximately between $d_i\lesssim L_I\lesssim L_c$ au, where $d_i\approx 5.6\times10^{-6}$, and $L_c\approx 0.01$ au, this implies that $\langle\langle\dot{p}\rangle_{\phi,\mu}^{\rm REC}\rangle$ dominates for energetic protons for flux ropes with cross sections in the inertial range but does not dominate for smaller values in the dissipation range. Assuming instead a nearly isotropic particle distribution with $f_2(p)/f_1(p)=\epsilon=0.1$, $\langle\langle\dot{p}\rangle_{\phi,\mu}^{\rm REC}\rangle/\langle\langle\dot{p}\rangle_{\phi,\mu}^{\rm INC}\rangle\lesssim 1$ for $v/U_0\gtrsim 5.7\times10^{4}(L_I/L_c)^{2/3}$, making it even more unlikely that domination of $\langle\langle\dot{p}\rangle_{\phi,\mu}^{\rm INC}\rangle$ can occur for flux ropes with cross sections in the inertial range. One way for $\langle\langle\dot{p}\rangle_{\phi,\mu}^{\rm INC}\rangle$ to dominate, at least for the smallest flux-rope cross sections in the inertial range, would require maintaining a sufficiently strong particle anisotropy $f_2(p)/f_1(p)\approx 1$ combined with a weaker guide field so that $\langle\delta B_I^2\rangle^{1/2}/B_0\approx 1$. This is in qualitative agreement with kinetic simulation results (Dahlin et al. 2016, 2017; Li et al. 2018).

In the fourth line of Equation (89) we compare the coherent particle momentum gain resulting from the mean parallel acceleration of the flux-rope flow in multiple dynamic flux ropes with the coherent momentum gain from the mean flux-rope contraction and merging rate in the compressible limit. When specifying $L_I\approx L_{\rm Ir}$, $\sigma^I_{\rm ACC}/\sigma^I_{\rm COM}\approx 1$, and $3f_1(p)/f_0(p)\approx 1$, we find $\langle\langle\dot{p}\rangle_{\phi,\mu}^{\rm ACC}\rangle/\langle\langle\dot{p}\rangle_{\phi,\mu}^{\rm COM}\rangle\approx(U_0/v)O(\epsilon)$ assuming the strong guide field limit $\delta B_I/B_0=O(\epsilon)$, where ϵ is a small parameter, at 1 au. This suggests that for suprathermal energetic particles with speeds $v\gtrsim U_0$ (protons with kinetic energy $T\gtrsim 1$ keV), $\langle\langle\dot{p}\rangle_{\phi,\mu}^{\rm ACC}\rangle/\langle\langle\dot{p}\rangle_{\phi,\mu}^{\rm COM}\rangle < O(\epsilon)$. Thus, combined curvature drift and generalized betatron energetic particle energization by compressible flux ropes dominates parallel guiding center motion energization by the parallel acceleration of the flux-rope flow for proton kinetic energies $T>1$ keV, and the dominance increases inversely with particle speed. This domination is further enhanced for a nearly isotropic distribution assuming $3f_1(p)/f_0(p)=O(\epsilon)$. Also in this case, for a purely isotropic particle distribution ($f_1(p)=0$) there is no net momentum gain by energetic particles, because there is an equal probability that energetic particles will propagate in the direction of the noninertial force associated with the parallel acceleration of the mean flux-rope flow and gain momentum, or move in the opposite direction of the force and lose momentum.

If we compare the coherent momentum gain from the mean acceleration of the flux-rope flow with coherent momentum gain due to interaction with contracting and merging flux ropes in the incompressible limit (fifth line of Equation (89)), $\langle\langle\dot{p}\rangle_{\phi,\mu}^{\rm ACC}\rangle/\langle\langle\dot{p}\rangle_{\phi,\mu}^{\rm INC}\rangle\approx(U_0/v)(L_c/L_I)^{1/3}(B_0/\langle\delta B_I^2\rangle^{1/2})(f_1(p)/f_2(p))$ assuming that $\sigma^I_{\rm ACC}/\sigma^I_{\rm INC}\approx 1$ and that $L_{I\max}\approx L_c\approx 0.01$ au, where L_c is the correlation scale of turbulence at 1 au. For a highly anisotropic energetic particle distribution with $f_1(p)/f_2(p)\approx 1$ we find that $\langle\langle\dot{p}\rangle_{\phi,\mu}^{\rm ACC}\rangle/\langle\langle\dot{p}\rangle_{\phi,\mu}^{\rm INC}\rangle\lesssim 1$ for particles with $v/U_0\gtrsim 3.2(L_c/L_I)^{1/3}$ using the observation that $\langle\delta B_I^2\rangle/B_0^2\approx 0.1$ at 1 au. Thus, for $L_I=L_c$, $\langle\langle\dot{p}\rangle_{\phi,\mu}^{\rm INC}\rangle\gtrsim\langle\langle\dot{p}\rangle_{\phi,\mu}^{\rm ACC}\rangle$ when $v/U_0\gtrsim 3.2$ ($T\gtrsim 10$ keV for energetic protons) and already at low suprathermal proton speeds the dominating acceleration rate is $\langle\langle\dot{p}\rangle_{\phi,\mu}^{\rm INC}\rangle$. However, by limiting oneself to smaller maximum flux-rope sizes in the inertial range $L_I\lesssim 10^{-5}$ au, one finds that $\langle\langle\dot{p}\rangle_{\phi,\mu}^{\rm ACC}\rangle\gtrsim\langle\langle\dot{p}\rangle_{\phi,\mu}^{\rm INC}\rangle$ for $v/U_0\gtrsim 3.2$ or $T\gtrsim 10$ keV for energetic protons, so that for the bulk of the observed power-law spectrum of ions at 1 au $\langle\langle\dot{p}\rangle_{\phi,\mu}^{\rm ACC}\rangle$ dominates $\langle\langle\dot{p}\rangle_{\phi,\mu}^{\rm INC}\rangle$. For a nearly isotropic distribution, assuming that $f_2(p)/f_1(p)=\epsilon=0.1$, $\langle\langle\dot{p}\rangle_{\phi,\mu}^{\rm INC}\rangle\gtrsim\langle\langle\dot{p}\rangle_{\phi,\mu}^{\rm ACC}\rangle$ when $v/U_0\gtrsim 32(L_c/L_I)^{1/3}$). Thus, if $L_I=L_c$, $v/U_0\gtrsim 32$, suggesting that $\langle\langle\dot{p}\rangle_{\phi,\mu}^{\rm INC}\rangle\gtrsim\langle\langle\dot{p}\rangle_{\phi,\mu}^{\rm ACC}\rangle$ for energetic protons with $T\gtrsim 1$ MeV. This implies that $\langle\langle\dot{p}\rangle_{\phi,\mu}^{\rm ACC}\rangle\gtrsim\langle\langle\dot{p}\rangle_{\phi,\mu}^{\rm INC}\rangle$ for the bulk of the observed power-law spectrum of ions at 1 au. For smaller L_I values this domination extends to even higher particle speeds, leading to the conclusion that for a nearly isotropic particle distribution $\langle\langle\dot{p}\rangle_{\phi,\mu}^{\rm ACC}\rangle$ is the dominant acceleration rate for all flux-rope sizes in the inertial range and for all proton energies in the observed energy range of the power-law spectrum of energetic ions at 1 au.

Finally, consider the ratio of the rates of momentum gain in the last line of Equation (89), the only ratio that does not depend on the particle distribution. Both acceleration cases depend on the anisotropic part of the energetic particle distribution $f_1(p)$ that cancels out in the ratio. The ratio is independent of particle speed (for nonrelativistic particles) because the relative rates of momentum gain for both cases are inversely proportional to particle speed (see Equation (54)). For energetic protons near 1 au we find that $\langle\langle\dot{p}\rangle_{\phi,\mu}^{\rm ACC}\rangle/\langle\langle\dot{p}\rangle_{\phi,\mu}^{\rm REC}\rangle\approx 5.6\times10^{-4}(L_c/L_I)$ at 1 au assuming that $\sigma^I_{\rm ACC}/\sigma^I_{\rm REC}\approx 1$ and $L_{\rm Ir}\approx L_I$, implying that $\langle\langle\dot{p}\rangle_{\phi,\mu}^{\rm ACC}\rangle > \langle\langle\dot{p}\rangle_{\phi,\mu}^{\rm REC}\rangle$ at all suprathermal proton speeds, independent of the size of the anisotropy in the energetic particle distribution, for $L_I\lesssim 5.6\times10^{-7}$ au. Thus, for all flux-rope cross sections in the inertial range, $\langle\langle\dot{p}\rangle_{\phi,\mu}^{\rm REC}\rangle > \langle\langle\dot{p}\rangle_{\phi,\mu}^{\rm ACC}\rangle$.

13. Comparing Stochastic Energetic Particle Acceleration Rates for Different Small-scale Flux-rope Acceleration Mechanisms

In this section we estimate and compare the Fokker–Planck momentum diffusion coefficients for the four main small-scale flux-rope acceleration cases identified above for suprathermal protons in solar wind turbulence conditions near 1 au. These coefficients arise because energetic particles experience stochastic acceleration when sampling statistical fluctuations in the properties of numerous small-scale flux ropes that they traverse. According to expressions (62), (66), (69), and (72), the approximate expressions for the ratio of

the stochastic acceleration rates are

$$\frac{D_{pp}^{\rm INC}}{D_{pp}^{\rm COM}} \approx \left[1 + \frac{(\sigma_C^I)^2(r_{\rm A}^I+1)^2}{4r_{\rm A}^I}\right]\left(\frac{\langle \delta B_I^2\rangle}{B_0^2}\right)^2,$$

$$\frac{D_{pp}^{\rm REC}}{D_{pp}^{\rm COM}} \approx 8\left[1 - \frac{(\sigma_C^I)^2(r_{\rm A}^I+1)^2}{4r_{\rm A}^I}\right]\left(\frac{L_I}{d_i}\right)^2\left(\frac{V_{A0}}{v}\right)^2\frac{\langle \delta B_I^2\rangle}{B_0^2},$$

$$\frac{D_{pp}^{\rm REC}}{D_{pp}^{\rm INC}} \approx \left[\frac{1 - 1/4(\sigma_C^I)^2(r_{\rm A}^I+1)^2/r_{\rm A}^I}{1 + 1/4(\sigma_C^I)^2(r_{\rm A}^I+1)^2/r_{\rm A}^I}\right]4 \times \left(\frac{L_I}{d_i}\right)^2\left(\frac{V_{A0}}{v}\right)^2\frac{B_0^2}{\langle \delta B_I^2\rangle},$$

$$\frac{D_{pp}^{\rm ACC}}{D_{pp}^{\rm COM}} \approx \frac{4}{C_\delta}\left(\frac{L_I}{L_{\rm Ir}}\right)^2\left(\frac{U_0}{v}\right)^2,$$

$$\frac{D_{pp}^{\rm ACC}}{D_{pp}^{\rm INC}} \approx \frac{2}{C_\delta}\left[1 - \frac{(\sigma_C^I)^2(r_{\rm A}^I+1)^2}{4r_{\rm A}^I}\right]^{-1} \times \left(\frac{L_I}{L_{\rm Ir}}\right)^2\left(\frac{U_0}{v}\right)^2\left(\frac{B_0^2}{\langle \delta B_I^2\rangle}\right)^2,$$

$$\frac{D_{pp}^{\rm ACC}}{D_{pp}^{\rm REC}} \approx \frac{1}{2}\frac{1}{C_\delta}\left[1 - \frac{(\sigma_C^I)^2(r_{\rm A}^I+1)^2}{4r_{\rm A}^I}\right]^{-1} \times \left(\frac{U_0}{V_{A0}}\right)^2\left(\frac{d_i}{L_{\rm Ir}}\right)^2\frac{B_0^2}{\langle \delta B_I^2\rangle}. \quad (90)$$

Note that, different from the case of coherent particle acceleration, particle distribution function information does not feature in the ratios for stochastic acceleration in Equation (90). The reason is that when the stochastic acceleration terms are averaged over all μ values, one finds that all acceleration cases involve both the isotropic (see third line of Equation (165) in Appendix D) and the anisotropic part of the energetic particle distribution function. Thus, in the ratios, the distribution function cancels out. For simplicity, the μ-dependence of the ratio expressions is not shown. Estimates of these expressions near 1 au presented below include the approximation that the expressions in square brackets are ~1. This approximation is supported by solutions of the NI MHD equations for the transport of the leading-order quasi-2D magnetic island turbulence component in the nonuniform solar wind (Zank et al. 2017). According to these solutions, the Alfvén ratio $r_{\rm A}^I \lesssim 0.1$ and the normalized cross helicity $\sigma_C^I \approx 0.3$ near 1 au for the most plausible simulation that includes magnetic-field-dominated 2D turbulence generation by the shear-flow gradient that exists between fast and slow solar wind streams.

Consider first the stochastic acceleration rate ratio $D_{pp}^{\rm INC}/D_{pp}^{\rm COM}$ (first line of Equation (90)). Assuming that near 1 au $\langle \delta B_I^2\rangle/B_0^2 \approx 0.1$ (strong guide field limit) as discussed above, $D_{pp}^{\rm INC}/D_{pp}^{\rm COM} \approx 0.01$. This implies that the second-order Fermi acceleration of energetic protons associated with the variance in the combined curvature drift and generalized betatron acceleration rate due to fluctuations in the contraction and merging rates of numerous contracting and merging flux ropes is far more efficient near 1 au when contraction and merging occur in the compressible limit compared to when these processes occur in the incompressible limit. Comparable acceleration rates would require relaxing the strong guide field limit to $\langle \delta B_I^2\rangle/B_0^2 \approx 1$.

In the second line of Equation (90) we compare the stochastic acceleration rate $D_{pp}^{\rm REC}$ (variance in the parallel guiding center motion acceleration rate) due to fluctuations in the parallel reconnection electric field of numerous merging neighboring small-scale flux ropes with $D_{pp}^{\rm COM}$. Since $D_{pp}^{\rm REC}/D_{pp}^{\rm COM} \propto (L_I/v)^2$, the ratio strongly decreases with increasing particle speed, but it strongly increases with increasing flux-rope cross-sectional size L_I. Assuming a Kolmogorov spectrum for the flux-rope twist component magnetic energy density as a function of L_I, we find that $D_{pp}^{\rm COM} \gtrsim D_{pp}^{\rm REC}$ for particle speeds $v/U_0 \gtrsim 1.6 \times 10^3 (L_I/L_c)^{4/3}$, where $L_c \approx 0.01$ au is the maximum cross section for small-scale flux ropes in the inertial range near 1 au (Cartwright & Moldwin 2010; Khabarova et al. 2015). This implies that $D_{pp}^{\rm COM}$ dominates $D_{pp}^{\rm REC}$ for energetic protons provided that flux-rope cross sections reside approximately in the inertial range with $L_I \lesssim 10^{-4}$ au when $v/U_0 \gtrsim 3.4$ ($T \gtrsim 12$ keV). Thus, for a range of the largest small-scale flux-rope cross sections in the inertial range $10^{-4} \lesssim L_I \lesssim 0.01$ au, $D_{pp}^{\rm REC} \gtrsim D_{pp}^{\rm COM}$ for energetic protons near Earth.

Consider the third line in Equation (90), where we compare $D_{pp}^{\rm REC}$ with $D_{pp}^{\rm INC}$. As in the previous case, this ratio decreases strongly with increasing particle speed and depends sensitively on the value of L_I. The main difference is that whereas $D_{pp}^{\rm REC}/D_{pp}^{\rm COM} \propto \langle \delta B_I^2\rangle/B_0^2$, we now have $D_{pp}^{\rm REC}/D_{pp}^{\rm INC} \propto B_0^2/\langle \delta B_I^2\rangle$, resulting in larger ratios for incompressible flux ropes in the strong guide field limit. We find that $D_{pp}^{\rm INC} \gtrsim D_{pp}^{\rm REC}$ for $v/U_0 \gtrsim 1.1 \times 10^4 (L_I/L_c)^{2/3}$ for energetic protons assuming again a Kolmogorov spectrum for the energy density of the flux-rope magnetic island component as a function of L_I. Compared to $D_{pp}^{\rm COM}$, one has to consider smaller L_I values before reaching a point where $D_{pp}^{\rm INC} \gtrsim D_{pp}^{\rm REC}$ for energetic particles. We have to reduce L_I to $L_I \lesssim 10^{-7}$ au before $D_{pp}^{\rm INC}$ exceeds $D_{pp}^{\rm REC}$ at low suprathermal speeds $v/U_0 \gtrsim 5.1$ or $T \gtrsim 26$ keV. Given that we estimated the ion inertial scale at 1 au to be $d_i \approx 6 \times 10^{-7}$ au, which is approximately the scale at which the turbulence inertial range crosses over to the dissipation range, we conclude that $D_{pp}^{\rm REC}$ dominates $D_{pp}^{\rm INC}$ for suprathermal protons for all small-scale flux-rope cross sections in the inertial range. For domination $D_{pp}^{\rm INC}$ to dominate just inside the inertial range would require relaxing the strong guide field limit to the level $\langle \delta B_I^2\rangle/B_0^2 \approx 1$.

Next, we discuss the ratio $D_{pp}^{\rm ACC}/D_{pp}^{\rm COM}$ in Equation (90), where $D_{pp}^{\rm ACC}$ represents stochastic acceleration of energetic protons (variance in the parallel guiding center motion acceleration rate) in response to statistical fluctuations in the noninertial force associated with the field-aligned acceleration of the flux-rope flow. Just as for $D_{pp}^{\rm REC}/D_{pp}^{\rm COM,INC}$, $D_{pp}^{\rm ACC}/D_{pp}^{\rm COM}$ decreases strongly with increasing particle speed, but unlike the ratios $D_{pp}^{\rm REC}/D_{pp}^{\rm COM,INC}$, this ratio does not depend on L_I because $L_{\rm Ir}$ is the heliocentric radial component of L_I in the ratio $L_I/L_{\rm Ir}$ present in the expression $D_{pp}^{\rm ACC}/D_{pp}^{\rm COM}$. Our estimate at 1 au shows that $D_{pp}^{\rm COM} \gtrsim D_{pp}^{\rm ACC}$ for energetic protons with $v/U_0 \gtrsim 2/C_\delta^{1/2}$ assuming $L_I/L_{\rm Ir} \approx 1$. Upon specifying $C_\delta \approx 1$ (an appropriate choice considering that flux ropes are intermittent nonlinear structures), it implies that $D_{pp}^{\rm COM} \gtrsim D_{pp}^{\rm ACC}$ when $v/U_0 \gtrsim 2$ or $T \gtrsim 4$ keV for protons,

thus largely covering the range of suprathermal energies of accelerated ions in the solar wind near 1 au.

Consider the ratio $D_{pp}^{\rm ACC}/D_{pp}^{\rm INC}$ in the fifth line of Equation (90). This ratio also decreases strongly with increasing particle speed, just as $D_{pp}^{\rm ACC}/D_{pp}^{\rm COM}$, but is comparatively strongly enhanced by the factor $(B_0^2/\langle \delta B_I^2\rangle)^2 \approx 100$ in the strong guide field limit at 1 au. Accordingly, it follows that $D_{pp}^{\rm INC} \gtrsim D_{pp}^{\rm ACC}$ for energetic protons with $v/U_0 \gtrsim 14.1(L_c/L_I)^{2/3}$. For $L_I = L_c \approx 0.01$ au (maximum flux-rope cross-sectional size in the inertial range at 1 au), $D_{pp}^{\rm INC} \gtrsim D_{pp}^{\rm ACC}$ when $v/U_0 \gtrsim 14.1$ or $T \gtrsim 200$ keV. Considering that the observed energetic ion spectra are power laws for $T \lesssim 0.1$–1 MeV at 1 au, it suggests that $D_{pp}^{\rm ACC}$ dominates energization for practically all observed ion energies. This dominance is further increased for smaller-scale flux ropes.

Finally, we estimate the ratio $D_{pp}^{\rm ACC}/D_{pp}^{\rm REC}$. This ratio is independent of particle speed since both stochastic acceleration rates decrease as v^{-2} with increasing particle speed (nonrelativistic particles). Upon assuming $C_\delta \approx 1$, and that at 1 au $U_0/V_{A0} \approx 10$, $\langle \delta B_I^2\rangle/B_0^2 \approx 0.1$, $L_{I\max} = L_c \approx 0.01$ au, and $d_i \approx 6 \times 10^{-7}$ au, we obtain $D_{pp}^{\rm ACC}/D_{pp}^{\rm REC} \approx 1.5 \times 10^{-6}(L_c/L_I)^{8/3}$, after specifying a Kolmogorov spectrum to take into account the reduction in total magnetic island energy density in the inertial range when reducing the maximum considered flux-rope cross section from L_c to a smaller value. This suggests that for $L_I \approx L_c$, $D_{pp}^{\rm REC} \gg D_{pp}^{\rm ACC}$. However, if one restricts oneself to small cross sections in the inertial range $L_I \lesssim 5 \times 10^{-5}$ au, one finds that $D_{pp}^{\rm ACC} \gtrsim D_{pp}^{\rm REC}$.

14. Comparing Second-order Fermi Acceleration Rates for Small-scale Flux Ropes and Parallel-propagating Alfvén Waves

First, we compare the second-order Fermi acceleration rate of energetic protons due to fluctuations of small-scale flux-rope dynamic properties in the quasi-linear limit of our theory with second-order Fermi acceleration by parallel-propagating Alfvén waves based on classical quasi-linear theory (e.g., Schlickeiser 1989; le Roux & Webb 2007) in the solar wind near 1 au. In the quasi-linear limit (undisturbed guiding center motion mainly in the guide field direction), energetic particles see decorrelated flux-rope properties by crossing the flux rope on a timescale $\tau_{\rm dec} \approx L_{I\|}/v|\mu|$, where $L_{I\|}$ is the length of the flux ropes in the guide field direction, assuming that for fast particles $v|\mu| \gg \langle \delta U_I^2\rangle^{1/2}$ (see Equation (74) and its discussion above). We find

$$\begin{aligned}
\frac{D_{pp}^{\rm COM}}{D_{pp}^{A}} &\approx C_\delta \frac{r_{\rm A}^I}{4\pi}\frac{L_{I\|}}{L_I}\left(\frac{l_{\rm A}}{L_I}\right)^{2/3}\left(\frac{r_g}{L_I}\right)^{1/3}\frac{\langle \delta B_I^2\rangle}{\langle \delta B_{\rm A}^2\rangle},\\
\frac{D_{pp}^{\rm INC}}{D_{pp}^{A}} &\approx 2\frac{D_{pp}^{\rm COM}}{D_{pp}^{A}}\left(\frac{\langle \delta B_I^2\rangle}{B_0^2}\right)^2,\\
\frac{D_{pp}^{\rm ACC}}{D_{pp}^{A}} &\approx 4\frac{D_{pp}^{\rm COM}}{D_{pp}^{A}}\left(\frac{L_I}{L_{\rm Ir}}\right)^2\left(\frac{U_0}{v}\right)^2,\\
\frac{D_{pp}^{\rm REC}}{D_{pp}^{A}} &\approx C_\delta \frac{2r_{\rm A}}{\pi}\left(\frac{l_{\rm A}}{r_g}\right)^{2/3}\frac{L_{I\|}}{r_g}\frac{\langle \delta B_I^2\rangle}{\langle \delta B_{\rm A}^2\rangle}\frac{\langle \delta B_I^2\rangle}{B_0^2}\\
&\approx 8\frac{D_{pp}^{\rm COM}}{D_{pp}^{A}}\left(\frac{L_I}{r_g}\right)^2\frac{\langle \delta B_I^2\rangle}{B_0^2},
\end{aligned} \tag{91}$$

where the new parameters related to Alfvén waves are l_A, the bend-over scale separating the inertial range of the Alfvén wave spectral magnetic energy density from the energy-containing range at smaller wavenumbers, and $\langle \delta B_{\rm A}^2\rangle$, a quantity closely related to the average magnetic energy density of Alfvén waves. For simplicity, the μ-dependence of the expressions is not included. Upon specifying $r_{\rm A}^I \approx 0.1$ (Zank et al. 2017), $l_{\rm A} \approx L_{I\|} \approx 3 \times 10^{-2}$ au (Weygand et al. 2011), $\langle \delta B_I^2\rangle/\langle \delta B_{\rm A}^2\rangle \approx 4$ (Bieber et al. 1996; MacBride et al. 2010), $L_{I\|}/L_I \approx 3$ (Weygand et al. 2011), and $C_\delta \approx 1$, we find that $D_{pp}^{\rm COM}/D_{pp}^{A} \approx 0.016$–$0.055$ for 1 keV–1 MeV protons. Thus, stochastic acceleration of energetic protons by Alfvén waves dominates stochastic combined curvature drift and generalized betatron acceleration due to fluctuations in small-scale flux-rope properties in the compressible limit.

In the second line of Equation (91) we compare combined stochastic curvature drift and generalized betatron acceleration driven by fluctuations in small-scale flux-rope dynamics in the incompressible limit with stochastic acceleration by Alfvén waves. Since $\langle \delta B_I^2\rangle/B_0^2 \approx 0.1$ at 1 au (Smith et al. 2016), implying a strong guide field limit, it is clear that stochastic acceleration by Alfvén waves will dominate combined stochastic curvature drift and generalized betatron acceleration in the incompressible flux-rope limit even more strongly compared to the compressible limit. Similarly, analysis of the expression in the third line of Equation (91) shows that stochastic acceleration of energetic protons by Alfvén waves dominates stochastic parallel guiding center motion acceleration, due to fluctuations in the noninertial force associated with the parallel acceleration of the flux-rope flow, more strongly than it dominates combined stochastic curvature drift and generalized betatron acceleration in compressible flux ropes, assuming $L_I \approx L_{\rm Ir}$ and $v \gtrsim U_0$ for suprathermal particles.

Finally, consider $D_{pp}^{\rm REC}/D_{pp}^{A}$ (bottom expression in Equation (91)). We estimate at 1 au that $D_{pp}^{\rm REC}/D_{pp}^{A} \approx 4 \times 10^4$ for 1 keV protons dropping to $D_{pp}^{\rm REC}/D_{pp}^{A} \approx 1.3 \times 10^2$ for 1 MeV protons because $D_{pp}^{\rm REC}/D_{pp}^{A} \propto r_g^{-5/3} \propto p^{-5/3}$. Thus, we find that stochastic parallel guiding center motion acceleration driven by fluctuations in the parallel reconnection electric field in merging small-scale flux ropes strongly dominates stochastic second-order Fermi acceleration by Alfvén waves in the range of suprathermal energies observed for accelerated ion power-law spectra at 1 au, assuming a Kolmogorov spectrum for Alfvén wave magnetic field fluctuations. In conclusion, in the quasi-linear limit of our theory, stochastic acceleration of suprathermal protons by Alfvén waves is estimated to be more efficient for all the small-scale flux-rope acceleration scenarios at 1 au except for stochastic parallel guiding center motion acceleration by fluctuations in the parallel reconnection electric field in merging small-scale flux ropes. Stochastic acceleration by Alfvén waves is comparatively efficient even though we assumed that there is four times more energy in the magnetic island component of small-scale flux ropes than in Alfvén waves at 1 au ($\langle \delta B_I^2\rangle/\langle \delta B_{\rm A}^2\rangle \approx 4$) as indicated by the observations of Bieber et al. (1996) and MacBride et al. (2010), for example.

Let us assume instead that the nonlinear transport limit (strong scattering limit) of our kinetic theory for small-scale flux ropes is more appropriate, considering that the fluctuation energy measured for quasi-2D magnetic island structures far exceeds that observed for Alfvén waves in the quiet solar wind near 1 au as discussed above. After rederiving the ratio

expressions in Equation (91), we find that

$$\frac{D_{pp}^{\rm COM}}{D_{pp}^{A}} \approx C_\delta^2 \frac{3r_{\rm A}^I}{80}\frac{v}{\langle \delta U_I^2\rangle^{1/2}}\left(\frac{r_g}{L_I}\right)^{1/3} \times \left(\frac{l_{\rm A}}{L_I}\right)^{2/3}\left(\frac{L_{I\parallel}}{L_I}\right)^2 \frac{\langle \delta B_I^2\rangle}{\langle \delta B_{\rm A}^2\rangle}\frac{\langle \delta B_I^2\rangle}{B_0^2},$$
$$\frac{D_{pp}^{\rm INC}}{D_{pp}^{A}} \approx 2\frac{D_{pp}^{\rm COM}}{D_{pp}^{A}}\left(\frac{\langle \delta B_I^2\rangle}{B_0^2}\right)^2,$$
$$\frac{D_{pp}^{\rm ACC}}{D_{pp}^{A}} \approx \frac{4}{C_\delta}\frac{D_{pp}^{\rm COM}}{D_{pp}^{A}}\left(\frac{U_0}{v}\right)^2,$$
$$\frac{D_{pp}^{\rm REC}}{D_{pp}^{A}} \approx 8\frac{D_{pp}^{\rm COM}}{D_{pp}^{A}}\left(\frac{L_I}{r_g}\right)^2\frac{\langle \delta B_I^2\rangle}{B_0^2}, \quad (92)$$

having assumed that energetic particles in the strong scattering limit see decorrelated flux-rope magnetic fields in the transport limit of fast diffusion ($\tau_D \ll \tau_c$). In this limit the energetic particle decorrelation timescale $\tau_{\rm dec}$ is determined by expression (81). Upon specifying the same plausible parameter values for 1 au in Equation (92) as we did in Equation (91), we find that $D_{pp}^{\rm COM}/D_{pp}^{A} \approx 0.2$ for 1 keV protons, increasing to ~22.2 at 1 MeV. This indicates that second-order Fermi acceleration of energetic protons might be dominated by Alfvén waves at low suprathermal energies less than ~11 keV based on a Kolmogorov Alfvén wave magnetic energy density spectrum. Combined stochastic curvature drift and generalized betatron acceleration of energetic protons in compressible small-scale flux ropes in response to fluctuations in flux-rope dynamic properties appears to be more important above ~11 keV in 1 au solar wind conditions, thus reversing the result of our kinetic theory in the quasi-linear limit at these energies.

Consider the ratio $D_{pp}^{\rm INC}/D_{pp}^{A}$ for incompressible flux ropes in Equation (92). Assuming that $\langle \delta B_I^2\rangle/B_0^2 \approx 0.1$ at 1 au (strong guide field assumption), $D_{pp}^{\rm INC}/D_{pp}^{A} \approx 0.02$ for 1 keV protons, increasing to ≈2.2 at 1 MeV. Thus, stochastic acceleration by Alfvén waves strongly dominates combined stochastic curvature drift and generalized betatron acceleration in response to fluctuating dynamic properties of incompressible small-scale flux ropes in the nonlinear limit of our theory at low suprathermal proton energies. Combined stochastic curvature drift and generalized betatron acceleration is only competitive at higher particle energies of ~1 MeV, which is in the vicinity of the observed spectral rollover of energetic ions at 1 au. Qualitatively, this result is in agreement with the result using the quasi-linear limit of our kinetic transport theory, but the dominance of stochastic acceleration by Alfvén waves is less strong in the nonlinear limit.

In the third line of Equation (92) we have the ratio $D_{pp}^{\rm ACC}/D_{pp}^{A}$. Assuming $C_\delta \approx 1$, we find for $U_0/v = 1$ ($T \approx$ 1 keV) that $D_{pp}^{\rm ACC}/D_{pp}^{A} \approx 0.8$. The ratio reduces to ≈0.08 at 1 MeV. For this range of suprathermal proton speeds, stochastic acceleration by Alfvén waves is more efficient compared to stochastic acceleration induced by fluctuations in the noninertial force associated with the parallel acceleration of the flux-rope plasma flow. Compared to the result for the quasi-linear limit of our kinetic transport theory, energetic particle stochastic acceleration produced by the acceleration associated with the flux-rope flow is more competitive against stochastic acceleration by Alfvén waves.

For the ratio $D_{pp}^{\rm REC}/D_{pp}^{A}$ we find that $D_{pp}^{\rm REC}/D_{pp}^{A} \approx 5.5 \times 10^5$ for 1 keV protons, which reduces to $D_{pp}^{\rm REC}/D_{pp}^{A} \approx 5.5 \times 10^4$ at 1 MeV. In this case, stochastic parallel guiding center motion acceleration in response to fluctuations in the parallel reconnection electric field generated by merging flux ropes is found to be far more efficient than stochastic acceleration by Alfvén waves at all energies between 1 keV and 1 MeV when applying the nonlinear limit of our kinetic transport theory. This is qualitatively in agreement with our result for the quasi-linear limit of our theory. In the nonlinear limit, however, the dominance is greater overall and continues to higher particle energies.

15. Comparing Energetic Pitch-angle Scattering Rates for Small-scale Flux Ropes and Parallel-propagating Alfvén Waves

In earlier work based on quasi-linear kinetic theory the view has emerged that 2D turbulence is inefficient in scattering energetic particles (Bieber et al. 1994, 1996; le Roux et al. 2004). This can be seen from examining, for example, the quasi-linear theory expressions in Section 4.1 in le Roux & Webb (2007). Assuming a 2D turbulence component with a correlation length scale $l_{2D} \gg r_g$ in those expressions, we find that the effective particle scattering frequency is given by

$$T_{\mu\mu} \approx \frac{2\pi}{3}\frac{\langle \delta B_{2D}^2\rangle}{B_0^2}\frac{1}{\tau_{\rm dec}}, \quad (93)$$

where particles see decorrelated 2D turbulence magnetic fields on a timescale $\tau_{\rm dec} \approx \tau_c = l_{2D}/\langle \delta U_{2D}^2\rangle^{1/2}$. It has often been assumed as a further simplification in quasi-linear kinetic theories that energetic particles see decorrelated turbulence on such short timescales that these particles will perceive the turbulence to be static. Implementation of the static 2D turbulence limit in Equation (93) implies that $T_{\mu\mu} \to 0$ ($\langle \delta U_{2D}^2\rangle \to 0$ so that $\tau_{\rm dec} \to \infty$), suggesting that 2D turbulence cannot result in pitch-angle scattering or parallel diffusion of energetic particles. This occurs because particles in this theory cannot see decorrelated static 2D turbulence if the turbulence, on average, is statistically distributed axisymmetrically around the background magnetic field, and perpendicular particle transport is determined solely by gyromotion around the background field. This explains the absence of gyromotion effects in $\tau_{\rm dec}$ of Equation (93) as an agent for decorrelation. The inclusion of dynamic 2D turbulence in Equation (93) ($\langle \delta U_{2D}^2\rangle \neq 0$), although more realistic, still produced relatively inefficient pitch-angle scattering in 1 au solar wind conditions, because $\langle \delta U_{2D}^2\rangle \ll U_0$. As discussed in le Roux et al. (2004), energetic particle pitch-angle scattering by dynamical 2D turbulence at 1 au is less efficient than gyroresonant scattering by parallel-propagating Alfvén wave turbulence even when the 2D component dominates the Alfvén wave component strongly, as observations near Earth show (Bieber et al. 1994, 1996).

However, in our focused transport approach, where quasi-2D turbulence is represented by quasi-2D small-scale flux ropes, the leading-order term in $D_{\mu\mu}^I$ is determined by the variance in the magnetic mirroring force that energetic particles encounter

when propagating through multiple small-scale flux ropes. In this case we find pitch-angle scattering for energetic particles to be much more efficient compared to the results of previous quasi-linear theory for 2D turbulence, as outlined in le Roux et al. (2004) and le Roux & Webb (2007). This can be seen by calculating the ratio $D^I_{\mu\mu}/D^{2D}_{\mu\mu}$, where $D^I_{\mu\mu}$ refers to pitch-angle scattering by small-scale flux ropes in the quasi-linear limit as modeled in this paper, and $D^{2D}_{\mu\mu}$ refers to quasi-linear pitch-angle scattering in 2D turbulence in le Roux & Webb (2007). We find in the fast particle limit that

$$\frac{D^I_{\mu\mu}}{D^{2D}_{\mu\mu}} \approx \frac{3}{16\pi}\frac{1}{(r^I_{\rm A})^{1/2}}\frac{v}{V_{A0}}\frac{L_\parallel}{L_I}\frac{B_0}{\langle \delta B_I^2\rangle^{1/2}} \times (\tau_{\rm cross} \ll \tau_c = L_I/\langle \delta U_I^2\rangle^{1/2}), \quad (94)$$

where $\tau_{\rm cross} \approx L_{I\parallel}/v|\mu|$ is the particle crossing time of small-scale flux ropes in the guide field direction assuming undisturbed guiding center motion along the flux-rope magnetic field. Upon assuming $r^I_{\rm A} \lesssim 0.1$, $\langle \delta B_I^2\rangle/B_0^2 \approx 0.1$, $L_{I\parallel}/L_I \approx 3$ and specifying fast particles with $v/V_{A0} \gtrsim 10$, we find that $D^I_{\mu\mu}/D^{2D}_{\mu\mu} \gtrsim 18$. Furthermore, assuming that the nonlinear transport regime of our theory is more appropriate in modeling particle scattering by numerous small-scale flux ropes, we find that the particle pitch-angle scattering rate $D^{I,NL}_{\mu\mu}$ is considerably higher than predicted by $D^{I,QLT}_{\mu\mu}$ following from the quasi-linear limit of our theory. In the fast particle limit $D^{I,QLT}_{\mu\mu}/D^{I,NL}_{\mu\mu} \approx (20/3\pi)(r^I_{\rm A})^{1/2}(L_I/L_{I\parallel})\ (B_0/\langle \delta B_I^2\rangle^{1/2})(V_{A0}/v)$. Upon assuming at 1 au that $L_{I\parallel}/L_I \approx 3$, we find for $v/V_{A0} \gtrsim 10$ that $D^{I,QLT}_{\mu\mu}/D^{I,NL}_{\mu\mu} \lesssim 0.07$.

The larger pitch-angle scattering rate predicted with our focused transport theory in comparison to earlier quasi-linear theory predictions is the net result of key differences between the earlier and the current theoretical approaches: (i) In the focused transport theory approach pitch-angle scattering is driven by the variance in the field-aligned spatial gradient of the magnetic field strength in the form of the magnetic mirroring force, whereas in the earlier quasi-linear pitch-angle approach scattering is caused by the variance of the magnetic Lorentz force. Thus, gradients in the magnetic field were not considered. (ii) The energetic particle decorrelation time $\tau_{\rm dec}$ (time needed for energetic particles to experience decorrelated flux-rope magnetic fields) in our focused transport approach is determined by a competition between particle transport along the background/guide field and the turbulence dynamic timescale τ_c. This is because small-scale flux ropes are treated as quasi-2D structures (instead of purely 2D structures) that include a weaker spatial dependence along the guide/background field direction. Therefore, in the strong guide field limit particles tend to follow the guide field to see decorrelated flux-rope magnetic fields in this direction. In earlier quasi-linear theory $\tau_{\rm dec}$ was modeled for a purely 2D turbulence component that is uniform along the uniform background magnetic field. In this case $\tau_{\rm dec}$ is a competition between gyromotion across the magnetic field and the turbulence dynamic timescale τ_c because the option of particles seeing decorrelated magnetic field turbulence along the background field does not exist. Likewise, in earlier versions of N I MHD turbulence theory for a homogeneous background plasma medium the leading-order turbulence component is purely 2D (e.g., Zank & Matthaeus 1993), while in recent, more realistic versions of N I MHD turbulence theory for an inhomogeneous background plasma the leading-order turbulence component is quasi-2D (Hunana & Zank 2010; Zank et al. 2017).

To see how our pitch-angle scattering coefficient for energetic particle interaction with numerous small-scale flux ropes in the quasi-linear limit compares with the standard quasi-linear theory pitch-angle scattering coefficient $D^A_{\mu\mu}$ for gyroresonant interaction with parallel-propagating Alfvén waves (e.g., le Roux & Webb 2007), we derive the ratio

$$\frac{D^I_{\mu\mu}}{D^A_{\mu\mu}} \approx \frac{1}{4\pi}\left(\frac{r_g}{L_I}\right)^{1/3}\left(\frac{l_{\rm A}}{L_I}\right)^{2/3}\frac{L_{I\parallel}}{L_I}\frac{\langle \delta B_I\rangle^2}{\langle \delta B_{\rm A}\rangle^2}, \quad (95)$$

assuming $\tau_{\rm cross} \ll \tau_c$ and $v \gg V_{\rm A}$. In Equation (95), $\langle \delta B_{\rm A}^2\rangle$ is related to the total energy density of Alfvén wave turbulence, and l_A is the value of the bend-over scale in the wave turbulence energy density spectrum, both of which are closely related to the wave turbulence correlation length. Considering conditions in the solar wind near 1 au, we assume as above that $\langle \delta B_{\rm A}^2\rangle/\langle \delta B_{2D}^2\rangle \approx 0.25$ (Bieber et al. 1994, 1996), $L_I \approx 0.01$ au (Cartwright & Moldwin 2010; Khabarova et al. 2015), $l_{\rm A} \approx L_{I\parallel}$, and $L_{I\parallel}/L_I \approx 3$ (Weygand et al. 2009). We find that $D^I_{\mu\mu}/D^A_{\mu\mu} \lesssim 0.16$ for 1 keV protons, increasing to $\sim$0.5 at 1 MeV. The derived ratio is valid for a Kolmogorov Alfvén wave spectrum. This suggests that energetic proton pitch-angle scattering by Alfvén waves dominates pitch-angle scattering by small-scale flux ropes in the quasi-linear limit, especially at lower proton energies.

Note that these conclusions are based on taking the weak scattering (quasi-linear) spatial transport limit of our theory for particle scattering by small-scale flux ropes. Given that observations show that $\langle \delta B_{\rm A}^2\rangle \ll \langle \delta B_{2D}^2\rangle$ at 1 au, one could argue that the strength of particle scattering generated by the variance in the mirroring force in small-scale flux ropes should be estimated in the nonlinear regime of our theory, while retaining the quasi-linear limit for particle scattering by Alfvén waves. Then we find that

$$\frac{D^I_{\mu\mu}}{D^A_{\mu\mu}} \approx \frac{3}{80\pi}\frac{v}{\langle \delta U_I^2\rangle^{1/2}}\left(\frac{r_g}{L_I}\right)^{1/3}\left(\frac{l_{\rm A}}{L_I}\right)^{2/3}\left(\frac{L_{I\parallel}}{L_I}\right)^2\frac{\langle \delta B_I^2\rangle}{\langle \delta B_{\rm A}^2\rangle}\frac{\langle \delta B_I^2\rangle}{B_0^2}, \quad (96)$$

assuming the fast diffusion limit for particle transport through small-scale flux ropes $\tau_D \ll \tau_c$ (see discussion following Equation (75)). We estimated before that the fast diffusion limit holds at 1 au if $\langle \delta B_I^2\rangle/B_0^2 \lesssim 0.2$ (le Roux et al. 2015a). Observations at 1 au suggest that $\langle \delta B_I^2\rangle/B_0^2 \approx 0.1$ (Smith et al. 2016), which supports our choice. Using this observation and estimating that $\langle \delta U^2\rangle^{1/2} = (r^I_{\rm A}\langle \delta B_I^2\rangle/B_0^2)^{1/2}V_{A0} \approx 4\ {\rm km\ s^{-1}}$ for $r^I_{\rm A} \approx 0.1$ and $V_{A0} \approx 40\ {\rm km\ s^{-1}}$, the ratio $D^I_{\mu\mu}/D^A_{\mu\mu}$ varies from $\sim$2.2 for 1 keV protons to $\sim$227 for MeV protons, so that pitch-angle scattering of suprathermal protons by small-scale flux ropes in the nonlinear limit of our theory is more effective than pitch-angle scattering by Alfvén waves at all suprathermal proton energies $\gtrsim$1 keV. This supports earlier work based on nonlinear extensions of quasi-linear theory, not based on focused transport theory as discussed in this paper, that also showed pitch-angle scattering by 2D turbulence to be stronger than pitch-angle scattering by Alfvén waves in 1 au

conditions (le Roux & Webb 2007; Shalchi et al. 2014) when the energy in the 2D component dominates the energy in Alfvén waves (Bieber et al. 1994, 1996). Specifying a steeper Alfvén wave spectrum than the Kolmogorov spectrum assumed, as suggested by some turbulence theories, simulations, and solar wind observations (e.g., Shebalin et al. 1983; Goldreich & Sridhar 1995; Horbury et al. 2008; Forman et al. 2011), proton pitch-angle scattering in the nonlinear limit of our theory is predicted to be strongly dominated by small-scale flux ropes for all proton energies in the suprathermal range 1 keV–1 MeV.

16. Summary and Interpretation

Having extended the previous theoretical development of Zank et al. (2014) and le Roux et al. (2015a), we presented a set of equations that couples a kinetic focused transport equation with Fokker–Planck scattering coefficients for energetic charged particles to an MHD turbulence transport equation based on N I MHD turbulence theory for coherent, quasi-2D magnetic island structures (Zank et al. 2017). The coupled equations enable the modeling of the self-consistent acceleration of suprathermal charged particles interacting with and traversing numerous dynamic (contracting and merging) quasi-2D small-scale flux ropes with cross sections belonging to the inertial range. The theory, despite being limited to energetic particles with gyroradii less than the flux-rope cross section, is ideal for studying ion acceleration by small-scale flux ropes for the full range of suprathermal ion energies observed in the solar wind near 1 au. The flux-rope structures that were modeled comprise a magnetic island or twist component in the 2D plane perpendicular to a strong, axial or guide field component that is aligned with the large-scale magnetic field in the solar wind as observations near 1 au suggest (e.g., Smith et al. 2016; Zheng & Hu 2018). The energetic particle crossing of multiple flux ropes was modeled in terms of guiding center motion predominantly along the guide field direction and includes pitch-angle scattering and parallel diffusion on large spatial scales, thus capturing an important element in 3D simulations of acceleration by small-scale flux ropes (e.g., Dahlin et al. 2017). On more local spatial scales, energetic particle transport in our theory was modeled either in the quasi-linear limit of undisturbed guiding center motion or in the nonlinear limit of diffusive guiding center motion in response to fluctuations in the flux-rope magnetic mirroring force encountered in these structures, depending on the strength of magnetic island turbulence considered. It was assumed that small-scale flux-rope dynamics involving contraction, expansion, and merging through magnetic reconnection and energy exchange between particles and flux ropes involve mainly the magnetic island or twist component in the 2D plane perpendicular to a large-scale guiding magnetic field (Birn et al. 1989; Dmitruk et al. 2004; Hunana & Zank 2010; Zank et al. 2017). Our quasi-2D approach to small-scale flux ropes is consistent with the view that solar wind turbulence is predominantly quasi-2D in the presence of a strong background/guide field as suggested by observations near 1 au, MHD turbulence theory, and simulations (Shebalin et al. 1983; Matthaeus et al. 1990; Zank & Matthaeus 1992, 1993; Bieber et al. 1996; Hunana & Zank 2010; Turner et al. 2012).

Average energetic particle acceleration rate expressions were presented for four small-scale flux-rope acceleration scenarios present in focused transport theory: (1) combined curvature drift and generalized betatron energization in small-scale flux ropes contracting and merging in the compressible limit (flux-rope compression acceleration; Zank et al. 2014; le Roux et al. 2015a), (2) unified curvature drift energization and generalized betatron energy loss in small-scale flux ropes contracting and merging in the incompressible limit (flux-rope parallel shear-flow acceleration; e.g., Drake et al. 2006, 2013), (3) parallel guiding center motion energy gain and loss by the parallel reconnection electric field force generated in merging (reconnecting) flux ropes (e.g., Oka et al. 2010; Zank et al. 2014; Dahlin et al. 2016), and (4) parallel guiding center motion energy gain and loss produced by the parallel noninertial force associated with the parallel acceleration of the plasma flow in dynamic small-scale flux ropes. Whereas the first three acceleration scenarios were discussed previously by us and other authors, the fourth acceleration scenario is presented by us here for the first time. An important element of our theory presented in le Roux et al. (2015a) and in this paper is that a distinction is made between coherent energetic particle acceleration in response to mean dynamic flux-rope properties and stochastic (second-order Fermi) particle acceleration in response to statistical fluctuations in flux-rope dynamic properties (Bian & Kontar 2013).

In this follow-up to le Roux et al. (2015a), we present for the first time the detailed expressions for the four Fokker–Planck coefficients for energetic particle scattering in momentum space ($D^I_{\mu\mu}$ [pitch-angle scattering], $D^I_{\mu p}$, $D^I_{p\mu}$, and D^I_{pp} [stochastic acceleration] for each of the four small-scale flux-rope acceleration scenarios). Furthermore, to enable modeling of self-consistent energetic particle acceleration, total energy conservation in the exchange of energy between energetic particles and magnetic islands was used to derive new expressions for the growth/damping rates of the total flux-rope energy density (kinetic plus magnetic) of magnetic islands. The growth/damping coefficients were included in a new MHD turbulence equation for the transport of the total energy energy density of magnetic islands in a nonuniform solar wind medium. The equation was derived from the quasi-2D magnetic island turbulence transport equations in Elsässer variables published in a recent, updated version of N I MHD turbulence theory by Zank et al. (2017). The two coupled focused transport-N I MHD equations were also derived in the diffusion approximation (near-isotropic particle distribution limit), resulting in a Parker–Gleeson–Axford diffusive transport equation for energetic particles and an N I MHD transport equation for magnetic island structures with growth/damping coefficients adjusted for nearly isotropic energetic particle distributions.

We analyzed our extended theory to determine coherent relative rates of momentum gain for energetic protons in solar wind regions with numerous dynamic small-scale flux ropes near 1 au for all four flux-rope acceleration scenarios, assuming finite mean quantities for their dynamics. Our expressions for momentum gain suggest that combined curvature drift and generalized betatron momentum gain in small-scale flux ropes that contract or merge in the compressible limit and parallel guiding center motion momentum gain in response to the parallel reconnection electric field force in merging flux ropes are not sensitive to an increase in the guide field strength B_0. In contrast, combined curvature drift and generalized betatron momentum gain in small-scale flux ropes that contract or merge

in the incompressible limit is the most sensitive to an increase in B_0 ($\langle \dot{p} \rangle_{\phi/\mu}^{\rm INC}/p \propto \langle \delta B_I^2 \rangle / B_0^2$), whereas parallel guiding center motion momentum gain in response to the noninertial force associated with the parallel acceleration of the flux-rope flow is sensitive to an intermediate degree to such an increase ($\langle \dot{p} \rangle_{\phi/\mu}^{\rm ACC}/p \propto \langle \delta B_I^2 \rangle^{1/2} / B_0$). This implies that coherent particle parallel guiding center motion acceleration by the mean parallel reconnection electric field will gain in relative efficiency compared to coherent particle curvature drift and generalized betatron acceleration in small-scale flux ropes that contract and merge in the incompressible limit when the guide field is increased relative to the magnetic island or twist component (increase in the ratio $\langle \delta B_I^2 \rangle / B_0^2$). It also means that combined curvature drift and generalized betatron acceleration in small-scale flux ropes that contract and merge in the compressible limit will become relatively more efficient compared to contraction and merging occurring in the incompressible limit. However, these conclusions are limited in the sense of not accounting for a possible increase in particle anisotropy and a decrease in the level of compressibility with increasing guide field strength (Dahlin et al. 2017; Li et al. 2018).

A more detailed comparison of the coherent energetic particle acceleration rates was done when accounting for the level of anisotropy in the energetic particle distribution. However, since the comparisons were done for a particle distribution function expanded only to the second moment in pitch-angle space using Legendre polynomials, the results, strictly speaking, only apply to small to moderate anisotropies. These estimates were made in the test particle limit and might change when including a self-consistent exchange of energy between energetic particles and flux ropes. We found the following for energetic protons in the strong guide field limit near Earth: (1) Only combined curvature drift and generalized betatron momentum gain in flux ropes contracting and merging in the compressible limit depends on both the isotropic and anisotropic part of the particle distribution. The other three acceleration scenarios depend solely on the anisotropic part of the particle distribution, so that the coherent rate of momentum gain can be small for a nearly isotropic distribution and is zero for a purely isotropic distribution. (2) Flux ropes with a net mean contraction and merging rate in the compressible limit energize energetic protons coherently through combined curvature drift and generalized betatron momentum gain much more efficiently than flux ropes in the incompressible limit for moderate size particle anisotropies and smaller. In the incompressible limit the momentum gain involves the combined net mean effect of curvature drift energization and generalized betatron energy loss. This dominance is accentuated for a nearly isotropic particle distribution. (3) We concluded that for flux-rope cross sections L_I in the inertial range with $L_I \lesssim 10^{-4}$ au at 1 au, combined curvature drift and generalized betatron coherent momentum gain in compressible flux ropes can be more efficient than parallel guiding center motion momentum gain by a mean parallel reconnection electric field in merging flux ropes for moderate-size pitch-angle anisotropies. However, for the largest small-scale flux-rope cross sections in the range 10^{-4} au $\lesssim L_I \lesssim 0.01$ au, the parallel reconnection electric field is more efficient in accelerating energetic protons. Assuming a nearly isotropic energetic particle distribution, the dominance of combined curvature drift and generalized betatron momentum gain by compressible flux ropes is extended to larger small-scale flux-rope cross sections closer to the maximum size of $\sim$0.01 au in the inertial range. If the pitch-angle anisotropy is small enough, combined curvature drift and generalized betatron momentum gain by compressible flux ropes will be more efficient for all flux-rope cross sections belonging to the inertial range. (4) Coherent energetic proton parallel guiding center motion energization by the mean parallel reconnection electric field dominates coherent energization from combined curvature drift momentum gain and generalized betatron momentum loss in incompressible flux ropes for the full range of flux-rope cross sections in the inertial range. This dominance is further strengthened for nearly isotropic energetic particle distributions. Thus, dominance of combined curvature drift and generalized betatron acceleration over parallel guiding center motion acceleration by the mean parallel reconnection electric field only occurs for inertial-scale flux-rope cross sections when net contraction and merging occur in the compressible limit. (5) Coherent energetic proton parallel guiding center motion momentum gain from the finite mean parallel reconnection electric field generated by multiple merging flux ropes is predicted to be more efficient compared to momentum gain involving the mean parallel noninertial force associated with the parallel component of the acceleration of the flux-rope flow. (6) Energetic particle parallel guiding center motion momentum gain by the finite mean noninertial force associated with the parallel acceleration of the flux-rope flow is less efficient than momentum gain from combined curvature drift and generalized betatron acceleration in compressible flux ropes, and this is even more so in the case of a nearly isotropic particle distribution. (7) Energetic particle momentum gain from the mean flux-rope parallel flow acceleration is estimated to be less efficient than combined curvature drift and generalized betatron acceleration in incompressible flux ropes for protons when $L_I \approx 0.01$ au (maximum value in the inertial range). However, in the case of a nearly isotropic energetic particle distribution, acceleration by the noninertial force dominates acceleration by incompressible flux ropes for suprathermal particle energies for the entire range of flux-rope cross sections in the inertial range.

In conclusion, for coherent energetic proton acceleration associated with mean flux-rope dynamic properties in the strong guide field limit for flux-rope cross sections in the inertial range at 1 au, the two most efficient acceleration scenarios involve combined curvature drift and generalized betatron acceleration in contracting and merging flux ropes in the compressible limit (coherent flux-rope compression acceleration) and parallel guiding center motion acceleration by the parallel reconnection electric field of merging flux ropes. The latter might dominate for the largest magnetic island cross sections in the inertial range if the energetic particle pitch-angle anisotropy is of moderate size, but for sufficiently small anisotropies flux-rope compression acceleration is more efficient for all flux-rope cross sections belonging to the inertial range. In Section 5 observational evidence and arguments were presented for the possibility of compressible behavior imposed externally on small-scale flux ropes by converging primary current sheets in the solar wind behind traveling shocks. It was also argued in Section 8, based on N I MHD theory (Zank et al. 2017), that spatial gradients in the background solar wind flow and density can generate compressibility in small-scale flux ropes, implying that the compression of the solar wind flow across traveling shocks

could result in the emission of compressive small-scale flux ropes by these shocks.

A main difference between the efficiency of coherent acceleration in response to mean flux-rope properties and stochastic acceleration due to fluctuations in flux-rope properties for the four acceleration cases is the role of anisotropy in the energetic particle distribution. In the case of stochastic acceleration, both the isotropic and anisotropic parts of the distribution function play a role in all four acceleration scenarios. Thus, all four acceleration cases contribute to particle acceleration, even when the particle anisotropy is strictly zero in the quasi-linear transport limit of our theory. When comparing ratios of coherent acceleration rates with ratios for stochastic acceleration rates for the different acceleration scenarios for energetic protons in solar wind conditions near 1 au in the strong guide field limit, the results are similar qualitatively for the most part. Quantitative differences in the acceleration ratios are most noticeable when near-isotropic energetic particle distributions are assumed, and when acceleration due to the acceleration of the flux-rope flow is considered. For the latter case the underlying reason appears to be the difference in the expression for the relative coherent rate of momentum gain $\langle \nu^{I}_{\rm ACC} \rangle$, where the $d\delta \boldsymbol{U}_I/dt$ component along $\delta \boldsymbol{B}_I$ is the main contributor, and the expression for the fluctuations in the relative rate of momentum gain $\delta \nu_{\rm ACC}$, where the $d\delta \boldsymbol{U}_I/dt$ component along $\boldsymbol{B}_0$ is the main component.

We find that second-order Fermi parallel guiding center motion acceleration of suprathermal protons at 1 au associated with fluctuations in the parallel reconnection electric field of merging small-scale flux ropes is the only flux-rope acceleration scenario in the quasi-linear spatial transport limit of our theory that is more effective than second-order Fermi acceleration by parallel-propagating Alfvén waves. However, second-order Fermi acceleration by active small-scale flux ropes in the nonlinear transport regime of our kinetic transport theory is significantly more efficient when compared to the quasi-linear limit of our theory. Consequently, in the former limit, combined stochastic curvature drift and generalized betatron acceleration, generated by fluctuations in the properties of small-scale flux ropes in the compressible limit, is more effective than stochastic acceleration by Alfvén waves for a wide range of suprathermal proton kinetic energies $T \gtrsim 11$ keV. The enhanced acceleration efficiency can be attributed to the fact that, in the nonlinear transport regime of our theory, energetic particles are modeled as having diffusively distorted guiding center trajectories in response to fluctuations in the flux-rope magnetic mirroring force encountered during traversal of small-scales flux ropes in the background/guide field direction. Thus, the particles spend more time in each active flux rope (that is, they are quasi-trapped) and can experience more acceleration compared to the quasi-linear regime. In the quasi-linear regime, particles traverse flux ropes in the guide field direction more rapidly owing to undisturbed guiding center motion, providing less magnetic island contact time for acceleration.

In our current focused transport approach, the variance in the magnetic mirroring force present in small-scale flux ropes plays potentially an important role in energetic particle pitch-angle scattering in solar wind conditions at 1 au. This explains our finding that energetic particle pitch-angle scattering by small-scale flux ropes in the quasi-linear spatial transport limit of our theory is more efficient compared to previous quasi-linear kinetic theories for particle interaction with 2D turbulence. This is because previously particle scattering was determined by the variance in the magnetic Lorentz force associated with 2D turbulence (Bieber et al. 1994; le Roux & Webb 2007, 2009; Shalchi et al. 2014). In addition, we found that energetic proton pitch-angle scattering by small-scale flux ropes should be more efficient than pitch-angle scattering by Alfvén waves, provided that the nonlinear spatial transport limit of our theory is applicable, but less efficient than pitch-angle scattering by Alfvén waves when we take the quasi-linear limit. This raises the question of which limit of our theory applies best to solar wind conditions near 1 au. Fits to observed intensity time profiles of solar energetic events at 1 au using focused transport theory suggest that the energetic ion parallel mean free path $\lambda_{\parallel}$ can vary widely between $\sim 2 \times 10^{-2}$ au and 1 au during quiet solar wind conditions in the absence of interplanetary shocks (Dröge 2005). Nonetheless, it appears that $\lambda_{\parallel} \gtrsim L_{I\,\rm max} \approx 0.01$ au, where $L_{I\rm max}$ is the maximum small-scale flux-rope cross section, indicating scatter-free transport of energetic particles through these structures, so that the quasi-linear limit of our theory is more appropriate in quiet solar wind conditions. However, one would expect that the values of $\lambda_{\parallel}$ in the enhanced turbulence levels behind traveling shocks should be significantly smaller, providing potential conditions for the application of the nonlinear transport limit of our theory.

J.A.l.R. and G.P.Z. acknowledge support from NASA grant NNX15AI65G and NSF-DOE grant PHY-1707247. G.P.Z. was also partially supported by the Parker Solar Probe grant sub no. SV4-84017 (Johns Hopkins/APL no. 975569) and acknowledges that this material is based in part on work supported by the NSF EPSCoR RII-Track-1 Cooperative Agreement OIA-1655280.

Appendix A
Energetic Particle Momentum and Pitch-angle Rates of Change during Interaction with Small-scale Flux Ropes

A.1. Energetic Particle Momentum Rates of Change

According to focused transport theory, the relative energetic particle momentum rate of change associated with a compressive plasma flow $\boldsymbol{U}$ (see Equation (28)), omitting the μ-dependence, is determined by the expression

$$\nu_{\rm COM} = -\nabla \cdot \boldsymbol{U}. \tag{97}$$

We may decompose the plasma flow as

$$\boldsymbol{U} = \boldsymbol{U}_0 + \boldsymbol{U}_I, \tag{98}$$

where $\boldsymbol{U}_0$ is the background solar wind flow velocity and $\boldsymbol{U}_I$ is the flux-rope plasma flow velocity associated with the flux-rope dynamics of contraction, expansion, or merging of neighboring flux ropes. Consistent with the discussion in Section 4, assume that small-scale flux-rope dynamics near 1 au are confined mainly to the 2D plane perpendicular to the background magnetic field $\boldsymbol{B}_0$, which also serves as the guide field or axial component/guide magnetic field of flux ropes (Birn et al. 1989; Dmitruk et al. 2004; Hunana & Zank 2010; Zank et al. 2017; Zheng & Hu 2018). If the guide field is specified to be locally aligned with the z-axis ($\boldsymbol{B}_0 = B_0 \boldsymbol{e}_z$), small-scale flux ropes can be modeled as quasi-2D structures with a plasma flow given by $\boldsymbol{U}_I \approx U_{Ix}(x, y)\boldsymbol{e}_x + U_{Iy}(x, y)\boldsymbol{e}_y$. We assume that, statistically, dynamical small-scale flux-rope structures are randomly

distributed in the 2D plane perpendicular to $\boldsymbol{B}_0$, so that $\langle \boldsymbol{U}_I \rangle = \langle \delta \boldsymbol{U}_I \rangle = 0$, which is likely to be consistent with simulations of magnetic flux-rope formation in MHD turbulence models and in kinetic particle simulations initiated with multiple primary current sheet layers in the presence of a strong guide field (Dmitruk et al. 2004; Drake et al. 2010). Then,

$$\begin{aligned} \nu_{\rm COM} &= -(\nabla \cdot \boldsymbol{U}_0) - (\nabla \cdot \boldsymbol{U}_I) \\ &= \nu_{\rm COM}^{\rm SW} + \nu_{\rm COM}^{I}, \end{aligned} \tag{99}$$

where $\boldsymbol{U}_I = \delta \boldsymbol{U}_I$, $\nu_{\rm COM}^{\rm SW}$ is the relative energetic particle momentum rate of change associated with compression of the background solar wind flow, and $\nu_{\rm COM}^{I} = -\nabla \cdot \boldsymbol{U}_I$ is the relative momentum rate of change for energetic particles interacting with compressible quasi-2D small-scale flux ropes. As discussed in Sections 6 and 7, the acceleration involves energetic particles experiencing a combination of curvature drift and generalized betatron energization when flux ropes contract or merge in the compressible limit.

The average (coherent) relative momentum rate of change for energetic particles responding to the mean properties of contracting, expanding, and merging flux ropes in the compressible limit can be expressed as

$$\begin{aligned} \langle \nu_{\rm COM}^{I} \rangle &= -\langle \nabla \cdot \boldsymbol{U}_I \rangle \\ &\approx \sigma_{\rm COM}^{I} \frac{\langle \delta U_I^2 \rangle^{1/2}}{L_I}, \end{aligned} \tag{100}$$

where L_I can be interpreted as the characteristic cross-sectional radius of the flux ropes under consideration, and $\sigma_{\rm COM}^{I} \epsilon [-1, 1]$ is a parameter specifying the statistics of multi-flux-rope contraction, expansion, or merging in the compressible limit. In the case of contraction or expansion, $\sigma_{\rm COM}^{I} = +1$ means that flux ropes only contract (energy gain), $\sigma_{\rm COM}^{I} = 0$ indicates a balance between expanding and contracting flux ropes (no net acceleration), and $\sigma_{\rm COM}^{I} = -1$ implies that flux ropes only expand (energy loss). Upon defining the Alfvén ratio for flux ropes as $r_{\rm A}^{I} = \langle \delta U_I^2 \rangle / \langle \delta V_{AI}^2 \rangle$ ($\langle \delta V_{AI}^2 \rangle = \langle \delta B_I^2 \rangle / 4\pi \rho_0$) for flux-rope energy in the 2D plane perpendicular to the guide field, implying that $\langle \delta U_I^2 \rangle = r_{\rm A}^{I} V_{A0}^2 \langle \delta B_I^2 \rangle / B_0^2$, we find that

$$\begin{aligned} \langle \nu_{\rm COM}^{I} \rangle &= \sigma_{\rm COM}^{I} (r_{\rm A}^{I})^{1/2} \frac{V_{A0}}{L_I} \frac{\langle \delta B_I^2 \rangle^{1/2}}{B_0} \\ &= \sigma_{\rm COM}^{I} \left(\frac{r_{\rm A}^{I}}{r_{\rm A}^{I} + 1} \right)^{1/2} \frac{V_{A0}}{L_I} \left(\frac{\epsilon_I}{\epsilon_{B0}} \right)^{1/2}, \end{aligned} \tag{101}$$

where the relationship

$$\frac{\langle \delta B_I^2 \rangle}{B_0^2} = \frac{1}{r_{\rm A}^{I} + 1} \frac{\epsilon_I}{\epsilon_{B_0}} \tag{102}$$

was introduced to express $\langle \delta B_I^2 \rangle$ in terms of the total flux-rope energy density $\epsilon_I = 1/2 \rho_0 \langle \delta U_I^2 \rangle + \langle \delta B_I^2 \rangle / 8\pi = (r_{\rm A}^{I} + 1) \langle \delta B_I^2 \rangle / 8\pi$ ($\epsilon_{B_0} = B_0^2 / 8\pi$) perpendicular to $\boldsymbol{B}_0$.

Fluctuations in the relative particle momentum rate of change are determined by

$$\begin{aligned} \delta \nu_{\rm COM}^{I} &= \nu_{\rm COM} - \langle \nu_{\rm COM} \rangle \\ &= -\nabla \cdot \boldsymbol{U}_I + \langle \nabla \cdot \boldsymbol{U}_I \rangle \\ &= -\delta (\nabla \cdot \boldsymbol{U}_I). \end{aligned} \tag{103}$$

The variance in the relative momentum rate of change for energetic particles responding to fluctuations in the dynamic properties of numerous small-scale flux ropes in the compressible limit can be expressed as follows:

$$\begin{aligned} \langle (\delta \nu_{\rm COM}^{I})^2 \rangle &= \langle (\delta (\nabla \cdot \boldsymbol{U}_I))^2 \rangle \\ &\approx \frac{\langle \delta U_{Ii} \delta U_{Ij} \rangle}{L_{Ii} L_{I_j}}. \end{aligned} \tag{104}$$

Assuming the flow of numerous small-scale flux ropes to be on average isotropically distributed in the 2D plane perpendicular to the guide field, we specify (Zank et al. 2017)

$$\langle \delta U_{Ii} \delta U_{Ij} \rangle = a \langle \delta \boldsymbol{U}_I \cdot \delta \boldsymbol{U}_I \rangle \delta_{ij}, \tag{105}$$

where $a = 1/2$, and off-diagonal terms, associated with vorticity of the flow, are neglected for simplicity. Then,

$$\langle (\delta \nu_{\rm COM}^{I})^2 \rangle = a r_{\rm A}^{I} \frac{V_{A0}^2}{L_I^2} \frac{\langle \delta B_I^2 \rangle}{B_0^2}. \tag{106}$$

The magnetic field in the plasma is modeled using the decomposition

$$\boldsymbol{B} = \boldsymbol{B}_0 + \boldsymbol{B}_I, \tag{107}$$

where $\boldsymbol{B}_0$ is the axial/background/guide magnetic field component and $\boldsymbol{B}_I$ is the twist/magnetic island component of the flux-rope structure confined to the 2D plane perpendicular to $\boldsymbol{B}_0$ as discussed above. Just as for the flux-rope flow, $\langle \boldsymbol{B} \rangle = \boldsymbol{B}_0$ because we assume that $\langle \boldsymbol{B}_I \rangle = \langle \delta \boldsymbol{B}_I \rangle \approx 0$. This corresponds to considering flux-rope structures that are randomly orientated around $\boldsymbol{B}_0$ as discussed above. Thus, in expression (106), $\langle \delta B_I^2 \rangle = \langle [\delta (\delta B_I)]^2 \rangle$. To maintain simplicity, we assume that $\langle [\delta (\delta B_I)]^2 \rangle = C_\delta \langle \delta B_I^2 \rangle$, where C_δ is a constant. Thus, finally,

$$\begin{aligned} \langle (\delta \nu_{\rm COM}^{I})^2 \rangle &= C_\delta a r_{\rm A}^{I} \frac{V_{A0}^2}{L_I^2} \frac{\langle \delta B_I^2 \rangle}{B_0^2} \\ &= C_\delta a \frac{r_{\rm A}^{I}}{r_{\rm A}^{I} + 1} \frac{V_{A0}^2}{L_I^2} \frac{\epsilon_I}{\epsilon_{B_0}}, \end{aligned} \tag{108}$$

after introducing expression (102).

Next, we consider the relative energetic particle momentum rate of change related to a nonuniform incompressible plasma flow (see discussion in Sections 5, 6.1, and 7.1), which in focused transport theory is expressed as

$$\nu_{\rm INC} = -\boldsymbol{b} \cdot (\boldsymbol{b} \cdot \nabla) \boldsymbol{U}, \tag{109}$$

where $\boldsymbol{b}$ is the unit vector along $\boldsymbol{B}$. Note that the perpendicular flow component $\boldsymbol{U}_\perp = \boldsymbol{V}_E$, where $\boldsymbol{V}_E$ is the plasma drift velocity, so that $\nu_{\rm INC} = \boldsymbol{V}_E \cdot \boldsymbol{\kappa}$ for $\boldsymbol{U}_\perp$, where $\kappa = (\boldsymbol{b} \cdot \nabla) \boldsymbol{b}$ is the magnetic field curvature. Within the context of flux-rope dynamics, Equation (109) refers to the particle acceleration rate in response to the curved magnetic field of the flux-rope structure undergoing incompressible contraction or merging at

the plasma drift velocity $\boldsymbol{V}_E$ (see Section 6.1). Thus, the variance in the relative energetic particle acceleration rate $\nu_{\rm INC}$ can be linked to statistical fluctuations in the flux-rope contraction/merging velocity (Bian & Kontar 2013), as well as variations in the flux-rope magnetic curvature that particles encounter when crossing many active flux ropes, as is discussed further below.

If the magnetic field is decomposed according to Equation (107), the magnetic field unit vector $\boldsymbol{b}$ can be decomposed according to

$$\begin{aligned}\boldsymbol{b} &= \frac{\boldsymbol{B}_0 + \boldsymbol{B}_I}{(B_0^2 + B_I^2)^{1/2}}\\ &\approx \boldsymbol{b}_0 + \frac{\boldsymbol{B}_I}{B_0},\end{aligned} \tag{110}$$

where $\boldsymbol{b}_0$ is the unit vector along $\boldsymbol{B}_0$. The expression in the second line of Equation (110) comes from assuming a strong guide field $B_I/B_0 \ll 1$ and $\boldsymbol{B}_I \perp \boldsymbol{B}_0$, implying that $\boldsymbol{b} \approx \boldsymbol{b}_0$. Upon inserting Equations (98) and (110) into the expression for $\nu_{\rm INC}$,

$$\begin{aligned}\nu_{\rm INC} &= -\left(\boldsymbol{b}_0 + \frac{\boldsymbol{B}_I}{B_0}\right)\cdot\left(\left(\boldsymbol{b}_0 + \frac{\boldsymbol{B}_I}{B_0}\right)\cdot\nabla\right)\boldsymbol{U}_0\\ &\quad - \left(\boldsymbol{b}_0 + \frac{\boldsymbol{B}_I}{B_0}\right)\cdot\left(\left(\boldsymbol{b}_0 + \frac{\boldsymbol{B}_I}{B_0}\right)\cdot\nabla\right)\boldsymbol{U}_I\\ &\approx -\boldsymbol{b}_0\cdot(\boldsymbol{b}_0\cdot\nabla)\boldsymbol{U}_0 - \frac{\boldsymbol{B}_I}{B_0}\cdot\left(\frac{\boldsymbol{B}_I}{B_0}\cdot\nabla\right)\boldsymbol{U}_I\\ &= \nu_{\rm INC}^{\rm SW} + \nu_{\rm INC}^{I},\end{aligned} \tag{111}$$

where $\nu_{\rm INC}^{\rm SW}$ is the relative particle momentum rate of change associated with the incompressible component of the background solar wind flow, and $\nu_{\rm INC}^{I}$ is the relative momentum rate of change of energetic particles undergoing combined curvature drift and generalized betatron acceleration when interacting with quasi-2D small-scale flux ropes contracting and merging in the incompressible limit. The simplified expressions in the third line of Equation (111) result from assuming $B_I/B_0 \ll 1$ in the first line of Equation (111) and assuming, consistent with a quasi-2D flux-rope geometry, that $(\boldsymbol{b}_0\cdot\nabla)\boldsymbol{U}_I \approx \partial/\partial z\boldsymbol{U}_I(x, y) \approx 0$ and $\boldsymbol{b}_0\cdot(\boldsymbol{B}_I\cdot\nabla)\boldsymbol{U}_I = 0$ in the second line of Equation (111), when defining locally that $\boldsymbol{b}_0 \| z$-axis (Hunana & Zank 2010; Zank et al. 2017).

Accordingly, we can express the relative mean (coherent) particle momentum rate of change in response to mean flux-rope dynamical properties in the incompressible limit to be

$$\begin{aligned}\langle\nu_{\rm INC}^{I}\rangle &\approx -\left\langle\frac{\boldsymbol{B}_I}{B_0}\cdot\left(\frac{\boldsymbol{B}_I}{B_0}\cdot\nabla\right)\boldsymbol{U}_I\right\rangle\\ &\approx \sigma_{\rm INC}^{I}\frac{\langle\delta B_I^2\rangle}{B_0^2}\frac{\langle\delta U_I^2\rangle^{1/2}}{L_I}\\ &\approx \sigma_{\rm INC}^{I}(r_{\rm A}^{I})^{1/2}\frac{V_{A0}}{L_I}\left(\frac{\langle\delta B_I^2\rangle}{B_0^2}\right)^{3/2}\\ &= \sigma_{\rm INC}^{I}\frac{(r_{\rm A}^{I})^{1/2}}{(r_{\rm A}^{I}+1)^{3/2}}\frac{V_{A0}}{L_I}\left(\frac{\epsilon_I}{\epsilon_{B_0}}\right)^{3/2},\end{aligned} \tag{112}$$

after applying $\boldsymbol{B}_I = \delta\boldsymbol{B}_I$, $\boldsymbol{U}_I = \delta\boldsymbol{U}_I$, $\langle\delta U_I^2\rangle = r_{\rm A}^{I}V_{A0}^2\langle\delta B_I^2\rangle/B_0^2$, and Equation (102). As for compressible flux ropes, we introduce a parameter $\sigma_{\rm INC}^{I}\epsilon[-1, 1]$ to determine the statistics of multi-flux-rope incompressible contraction and expansion, or merging. In the case of contraction or expansion, $\sigma_{\rm INC}^{I} = +1$ means that flux ropes are contracting only, $\sigma_{\rm INC}^{I} = 0$ indicates a balance between expanding and contracting flux ropes, and $\sigma_{\rm INC}^{I} = -1$ implies that flux ropes are expanding only.

The expression for statistical fluctuations in the relative particle momentum rate of change is determined by

$$\begin{aligned}\delta\nu_{\rm INC}^{I} &= \nu_{\rm INC} - \langle\nu_{\rm INC}\rangle\\ &= -\frac{\boldsymbol{B}_I}{B_0}\cdot\left(\frac{\boldsymbol{B}_I}{B_0}\cdot\nabla\right)\boldsymbol{U}_I + \left\langle\frac{\boldsymbol{B}_I}{B_0}\cdot\left(\frac{\boldsymbol{B}_I}{B_0}\cdot\nabla\right)\boldsymbol{U}_I\right\rangle\\ &= -\delta\left[\frac{\boldsymbol{B}_I}{B_0}\cdot\left(\frac{\boldsymbol{B}_I}{B_0}\cdot\nabla\right)\boldsymbol{U}_I\right].\end{aligned} \tag{113}$$

Therefore, the variance in the relative momentum rate of change for particles responding to fluctuations in the dynamical properties of numerous small-scale flux ropes in the incompressible limit is

$$\begin{aligned}\langle(\delta\nu_{\rm INC}^{I})^2\rangle &= \left\langle\left(\delta\left[\frac{\boldsymbol{B}_I}{B_0}\cdot\left(\frac{\boldsymbol{B}_I}{B_0}\cdot\nabla\right)\boldsymbol{U}_I\right]\right)^2\right\rangle\\ &\approx \frac{1}{L_I^2}\frac{\langle B_I^2\rangle}{B_0^2}\left\langle\delta\left(\frac{B_{Ii}}{B_0}U_{Ii}\right)\delta\left(\frac{B_{Ij}}{B_0}U_{Ij}\right)\right\rangle\\ &= \frac{1}{L_I^2}\frac{\langle B_I^2\rangle}{B_0^4}[\langle\delta B_{Ii}\delta B_{Ij}U_{Ii}U_{Ij}\rangle + \langle B_{Ii}B_{Ij}\delta U_{Ii}\delta U_{Ij}\rangle\\ &\quad + \langle\delta B_{Ii}\delta U_{Ij}U_{Ii}B_{Ij}\rangle + \langle B_{Ii}U_{Ij}\delta U_{Ii}\delta B_{Ij}\rangle].\end{aligned} \tag{114}$$

In Equation (114) we simplified the analysis with the replacement $\boldsymbol{B}_I\cdot\nabla \to \langle B_I^2\rangle^{1/2}/L_I$, thus reducing the number of terms by introducing an estimate of the average magnitude of the gradient of the flux-rope flow along the flux-rope magnetic field in the 2D plane perpendicular to $\boldsymbol{B}_0$. The first term in the third line of Equation (114) can be simplified as follows:

$$\begin{aligned}\langle\delta B_{Ii}\delta B_{Ij}U_{Ii}U_{Ij}\rangle &\approx \langle\delta B_I\delta B_I\rangle\langle U_{Ii}U_{Ij}\rangle\\ &= a\langle\delta\boldsymbol{B}_I\cdot\delta\boldsymbol{B}_I\rangle\langle U_{Ii}U_{Ij}\rangle\delta_{ij}\\ &= ar_{\rm A}^{I}V_{A0}^2\frac{\langle B_I^2\rangle}{B_0^2}\langle\delta B_I^2\rangle.\end{aligned} \tag{115}$$

In Equation (115) we applied the condition for isotropic 2D flux-rope turbulence in the 2D plane perpendicular to $\boldsymbol{B}_0$, $\langle\delta B_{Ii}\delta B_{Ij}\rangle = a\langle\delta\boldsymbol{B}_I\cdot\delta\boldsymbol{B}_I\rangle\delta_{ij}$ $(a = 1/2)$, and used the definition of the Alfvén ratio to specify $\langle U_I^2\rangle = r_{\rm A}^{I}V_{A0}^2\langle B_I^2\rangle/B_0^2$. The first term models the effect of fluctuations in the flux-rope magnetic field curvature on the variance in the acceleration rate. Following the same approach, we can express the second term in the third line of Equation (114) as

$$\langle B_{Ii}B_{Ij}\delta U_{Ii}\delta U_{Ij}\rangle \approx ar_{\rm A}^{I}V_{A0}^2\frac{\langle B_I^2\rangle}{B_0^2}\langle\delta B_I^2\rangle, \tag{116}$$

where we specified $\langle \delta U_{Ii} \delta U_{Ij} \rangle = a \langle \delta \boldsymbol{U}_I \cdot \delta \boldsymbol{U}_I \rangle \delta_{ij}$ ($a = 1/2$) and $\langle \delta U_I^2 \rangle = r_{\rm A}^I V_{A0}^2 \langle \delta B_I^2 \rangle / B_0^2$. Thus, expression (116) equals expression (115), although expression (116) focuses on the contribution of fluctuations in the flux-rope contraction/merging velocity to the variance in the acceleration rate (Bian & Kontar 2013; le Roux et al. 2015a).

Consider the first term in the last line of Equation (114). We find that

$$\begin{aligned}\langle \delta B_{Ii} \delta U_{Ij} U_{Ii} B_{Ij} \rangle &= a \langle \delta \boldsymbol{B}_I \cdot \delta \boldsymbol{U}_I \rangle \langle U_{Ii} B_{Ij} \rangle \delta_{ij} \\ &= a \frac{1}{2} (\sigma_C^I + 1) B_0 V_{A0} \frac{\langle \delta B_I^2 \rangle}{B_0^2} \langle \boldsymbol{U}_I \cdot \boldsymbol{B}_I \rangle \\ &= a \frac{1}{4} (\sigma_C^I)^2 (r_{\rm A}^I + 1)^2 B_0^2 V_{A0}^2 \frac{\langle \delta B_I^2 \rangle}{B_0^2} \frac{\langle B_I^2 \rangle}{B_0^2},\end{aligned} \tag{117}$$

where we applied $\langle \delta B_{Ii} \delta U_{Ij} \rangle = a \langle \delta \boldsymbol{B}_I \cdot \delta \boldsymbol{U}_I \rangle \delta_{ij}$ ($a = 1/2$) and introduced the normalized cross helicity parameter for flux-rope turbulence

$$\sigma_C^I = \frac{2 \langle \delta \boldsymbol{U}_I \cdot \delta \boldsymbol{V}_{AI} \rangle}{\langle \delta U_I^2 \rangle + \langle \delta V_{AI}^2 \rangle} = \frac{2 \langle \delta \boldsymbol{U}_I \cdot \delta \boldsymbol{B}_I \rangle}{(r_{\rm A}^I + 1) B_0 V_{A0} \langle \delta B_I^2 \rangle / B_0^2}. \tag{118}$$

This term is different from the first two terms in that both fluctuations in the flux-rope magnetic curvature and contraction/merging velocity make a contribution to the variance in the acceleration rate. The fourth and last terms in the last line of Equation (114) have the same structure as the third term, thus yielding the same simplified result:

$$\langle B_{Ii} U_{Ij} \delta U_{Ii} \delta B_{Ij} \rangle = a \frac{1}{4} (\sigma_C^I)^2 (r_{\rm A}^I + 1)^2 B_0^2 V_{A0}^2 \frac{\langle \delta B_I^2 \rangle}{B_0^2} \frac{\langle B_I^2 \rangle}{B_0^2}. \tag{119}$$

Combining the simplified expressions (115)–(117) and (119) derived for the four terms in the bottom two lines of Equation (114), we obtain

$$\begin{aligned}\langle (\delta \nu_{\rm INC}^I)^2 \rangle &= 2a \left[r_{\rm A}^I + \frac{1}{4} (\sigma_C^I)^2 (r_{\rm A}^I + 1)^2 \right] \frac{V_{A0}^2}{L_I^2} \frac{\langle B_I^2 \rangle}{B_0^2} \frac{\langle \delta B_I^2 \rangle}{B_0^2} \\ &= C_\delta 2a \left[r_{\rm A}^I + \frac{1}{4} (\sigma_C^I)^2 (r_{\rm A}^I + 1)^2 \right] \frac{V_{A0}^2}{L_I^2} \frac{\langle \delta B_I^2 \rangle^2}{B_0^4} \\ &= C_\delta 2a \left[\frac{r_{\rm A}^I + 1/4 (\sigma_C^I)^2 (r_{\rm A}^I + 1)^2}{(r_{\rm A}^I + 1)^2} \right] \frac{V_{A0}^2}{L_I^2} \left(\frac{\epsilon_I}{\epsilon_{B_0}} \right)^2,\end{aligned} \tag{120}$$

where, after inserting $B_I = \delta B_I$, we enforced closure by assuming that $\langle [\delta (\delta B_I)]^2 \rangle = C_\delta \langle \delta B_I^2 \rangle$, for C_δ a constant, and used expression (102).

We defined the relative energetic particle momentum rate of change associated with the parallel acceleration of the plasma flow in focused transport theory (see Section 7.1) as

$$\nu_{\rm ACC} = -\frac{1}{v} \left(\frac{d\boldsymbol{U}}{dt} \cdot \boldsymbol{b} \right), \tag{121}$$

where the total time derivative following the plasma flow is $d/dt = \partial/\partial t + (\boldsymbol{U} \cdot \nabla)$. After decomposing the plasma flow according to Equation (98) and the magnetic field direction according to Equation (110), Equation (121) becomes

$$\begin{aligned}\nu_{\rm ACC} &= -\frac{1}{v} \left(\frac{\partial}{\partial t} + (\boldsymbol{U}_0 + \boldsymbol{U}_I) \cdot \nabla \right) \boldsymbol{U}_0 \cdot \left(\boldsymbol{b}_0 + \frac{\boldsymbol{B}_I}{B_0} \right) \\ &\quad - \frac{1}{v} \left(\frac{\partial}{\partial t} + (\boldsymbol{U}_0 + \boldsymbol{U}_I) \cdot \nabla \right) \boldsymbol{U}_I \cdot \left(\boldsymbol{b}_0 + \frac{\boldsymbol{B}_I}{B_0} \right) \\ &\approx -\frac{1}{v} \frac{d\boldsymbol{U}_0}{dt} \cdot \boldsymbol{b}_0 - \frac{1}{v} \frac{d\boldsymbol{U}_I}{dt} \cdot \left(\boldsymbol{b}_0 + \frac{\boldsymbol{B}_I}{B_0} \right) \\ &= \nu_{\rm ACC}^{\rm SW} + \nu_{\rm ACC}^I,\end{aligned} \tag{122}$$

where $\nu_{\rm ACC}^I$ is the relative particle acceleration rate caused by parallel guiding center motion acceleration by the noninertial force associated with the parallel component of the acceleration of the flux-rope flow in the 2D plane perpendicular to $\boldsymbol{B}_0$. The simplified expressions in the third line of Equation (122) result from assuming that $U_I/U_0 \ll 1$ (an appropriate assumption for quasi-2D flux-rope turbulence in the supersonic solar wind near 1 au) and $B_I/B_0 \ll 1$ (the strong guide field assumption discussed above) in the first line and that $U_I/U_0 \ll 1$ in the second line of Equation (122).

The average relative energetic particle momentum rate of change, due to the parallel mean acceleration of the flux-rope flow encountered by energetic particles in a region of multiple small-scale flux ropes, is

$$\begin{aligned}\langle \nu_{\rm ACC}^I \rangle &= -\frac{1}{v} \left\langle \frac{d\boldsymbol{U}_I}{dt} \cdot \frac{\boldsymbol{B}_I}{B_0} \right\rangle \\ &\approx -\frac{1}{v} (\boldsymbol{U}_0 \cdot \nabla) \left\langle \boldsymbol{U}_I \cdot \frac{\boldsymbol{B}_I}{B_0} \right\rangle \\ &\approx \sigma_{\rm ACC}^I (r_{\rm A}^I)^{1/2} \frac{V_{A0}}{L_{\rm Ir}} \frac{U_0}{v} \frac{\langle \delta B_I^2 \rangle}{B_0^2} \\ &= \sigma_{\rm ACC}^I \frac{(r_{\rm A}^I)^{1/2}}{r_{\rm A}^I + 1} \frac{V_{A0}}{L_{\rm Ir}} \frac{U_0}{v} \frac{\epsilon_I}{\epsilon_{B_0}},\end{aligned} \tag{123}$$

where $L_{\rm Ir} = L_I (\boldsymbol{n} \cdot \boldsymbol{e}_r)$ ($\boldsymbol{n}$ is the unit vector along $\boldsymbol{U}_I$, and $\boldsymbol{e}_r$ is the unit vector along the background radial solar wind outflow) is the flux-rope cross-sectional radius component in the direction of the background radial solar wind outflow $\boldsymbol{U}_0$. In the case of 2D flux-rope turbulence that is statistically isotropic in the 2D plane perpendicular to $\boldsymbol{B}_0$, unit vector $\boldsymbol{n}$ has an arbitrary direction in this 2D plane. To derive Equation (123), we applied $\langle \boldsymbol{B}_I \rangle = \langle \delta \boldsymbol{B}_I \rangle = 0$, $|\partial \boldsymbol{U}_I / \partial t| \approx U_I^2 / L_I \ll |(\boldsymbol{U}_0 \cdot \nabla) \boldsymbol{U}_I| \approx (U_0/U_I)) U_I^2 / L_I$ because $U_I/U_0 \ll 1$, introduced the Alfvén ratio r_A^I through the relationship $\langle \delta U_I^2 \rangle = r_{\rm A}^I V_{A0}^2 \langle \delta B_I^2 \rangle / B_0^2$, used the substitution (102), and defined a parameter $\sigma_{\rm ACC}^I \epsilon [-1, 1]$ that controls the magnitude and direction of the mean noninertial force associated with the parallel acceleration of the plasma flow in multiple small-scale flux ropes. If $\sigma_{\rm ACC}^I > 0$, particles with $\mu > 0$ (guiding center motion along the magnetic field) will experience energization because the average noninertial force then has a component in the direction of the guiding center motion.

Fluctuations in the relative energetic particle momentum rate of change $\nu^I_{\rm ACC}$ are modeled as

$$\begin{aligned}\delta\nu^I_{\rm ACC} &= \nu_{\rm ACC} - \langle\nu_{\rm ACC}\rangle \\ &= -\frac{1}{v}\frac{d\boldsymbol{U}_I}{dt}\cdot\left(\boldsymbol{b}_0+\frac{\boldsymbol{B}_I}{B_0}\right)+\frac{1}{v}\left\langle\frac{d\boldsymbol{U}_I}{dt}\cdot\left(\boldsymbol{b}_0+\frac{\boldsymbol{B}_I}{B_0}\right)\right\rangle \\ &\approx -\frac{1}{v}(\boldsymbol{U}_0\cdot\nabla)\boldsymbol{U}_I\cdot\boldsymbol{b}_0,\end{aligned} \tag{124}$$

because $B_I/B_0 \ll 1$ and $\langle\boldsymbol{U}_I\rangle=\langle\delta\boldsymbol{U}_I\rangle = 0$. Thus, the variance in the relative particle momentum rate of change due to fluctuations in the flux-rope flow velocity is

$$\begin{aligned}\langle(\delta\nu^I_{\rm ACC})^2\rangle &= \frac{1}{v^2}\langle[(\boldsymbol{U}_0\cdot\nabla)\boldsymbol{U}_I\cdot\boldsymbol{b}_0]^2\rangle \\ &\approx \frac{U_0^2}{v^2}\frac{1}{L^2_{\rm Ir}}\langle U_{Ii}U_{Ij}\rangle b_{0i}b_{0j} \\ &= a r^I_{\rm A}\frac{V^2_{A0}}{L^2_{\rm Ir}}\left(\frac{U_0}{v}\right)^2\frac{\langle\delta B_I^2\rangle}{B_0^2} \\ &= a\frac{r^I_{\rm A}}{r^I_{\rm A}+1}\frac{V^2_{A0}}{L^2_{\rm Ir}}\left(\frac{U_0}{v}\right)^2\frac{\epsilon_I}{\epsilon_{B_0}}.\end{aligned} \tag{125}$$

To derive the expression, we applied the condition for isotropic 2D turbulence in the 2D plane perpendicular to $\boldsymbol{B}_0$, $\langle\delta U_{Ii}\delta U_{Ij}\rangle = a\langle\delta\boldsymbol{U}_I\cdot\boldsymbol{U}_I\rangle\delta_{ij}$, the relationship $\langle\delta U_I^2\rangle = r^I_{\rm A}V^2_{A0}\langle\delta B_I^2\rangle/B_0^2$, and expression (102).

Finally, we consider the relative energetic particle momentum rate of change $\nu_{\rm REC}$ in response to the parallel electric field component. The parallel electric field is considered only in the background/guide magnetic field direction, enabling us to introduce the reconnection electric field that we argued to be mainly in the guide field direction in the solar wind at 1 au (see discussion in Section 4). The expression for $\nu_{\rm REC}$ is

$$\nu_{\rm REC} = \frac{q\boldsymbol{E}}{p}\cdot\boldsymbol{b}_0, \tag{126}$$

where on MHD scales the electric field is defined as $\boldsymbol{E} = -\boldsymbol{U}\times\boldsymbol{B}$ (see discussion in Section 4). Upon decomposing the plasma flow and magnetic field according to Equations (98) and (107),

$$\begin{aligned}\nu_{\rm REC} &= -\frac{q}{p}\boldsymbol{U}_0\times(\boldsymbol{B}_0+\boldsymbol{B}_I)\cdot\boldsymbol{b}_0 \\ &\quad -\frac{q}{p}\boldsymbol{U}_I\times(\boldsymbol{B}_0+\boldsymbol{B}_I)\cdot\boldsymbol{b}_0 \\ &\approx -\frac{q}{p}\boldsymbol{U}_0\times\boldsymbol{B}_I\cdot\boldsymbol{b}_0-\frac{q}{p}\boldsymbol{U}_I\times\boldsymbol{B}_I\cdot\boldsymbol{b}_0 \\ &= \nu^{\rm SW}_{\rm REC}+\nu^I_{\rm REC},\end{aligned} \tag{127}$$

where $\nu^{\rm SW}_{\rm REC}$ is the relative particle momentum rate of change in response to the background electric field. $\nu^I_{\rm REC}$ is the relative particle momentum rate of change due to particle parallel guiding center motion acceleration by the parallel reconnection electric field force generated by the merging of two neighboring flux ropes in the 2D plane perpendicular to $\boldsymbol{B}_0$. Note that, because the parallel component of the background electric field $\boldsymbol{E}_{\rm SW} = -\boldsymbol{U}_0\times\boldsymbol{B}_0$ is zero, $\nu^{\rm SW}_{\rm REC}$ only contributes to the background particle acceleration rate due to fluctuations in the magnetic field $\boldsymbol{B}_I$ generated by flux-rope structures. However, because we neglected in all other flux-rope acceleration cases small fluctuations in the background particle acceleration rates generated by flux-rope structures in favor of the background particle acceleration rates themselves, we set $\nu^{\rm SW}_{\rm REC} = 0$ in our focused transport theory.

The relative average (coherent) energetic particle momentum rate of change for particles responding to a net mean parallel reconnection electric field in numerous merging flux ropes is expressed as

$$\begin{aligned}\langle\nu^I_{\rm REC}\rangle &= -\frac{q}{p}\langle\boldsymbol{U}_I\times\boldsymbol{B}_I\rangle\cdot\boldsymbol{b}_0 \\ &\approx \sigma^I_{\rm REC}\frac{q}{|q|}(r^I_{\rm A})^{1/2}\frac{V_{A0}}{r_g}\frac{\langle\delta B_I^2\rangle}{B_0^2} \\ &= \sigma^I_{\rm REC}\frac{q}{|q|}\frac{Z}{A}\frac{(r^I_{\rm A})^{1/2}}{r^I_{\rm A}+1}\frac{V_{A0}}{d_{i/e}}\frac{V_{A0}}{v}\frac{\epsilon_I}{\epsilon_{B_0}},\end{aligned} \tag{128}$$

where $r_g = p/|q|B_0$ is the energetic particle gyroradius for $\mu = 0$ with q the net energetic particle charge, Z is the atomic number, A is the mass number, $d_{i/e}$ is the proton/electron inertial scale, and $\sigma^I_{\rm REC}\,\epsilon\,[-1,\,1]$ is a parameter that defines the net magnitude and direction of the mean parallel reconnection electric field of numerous merging flux-rope structures. A value of $\sigma^I_{\rm REC} > 0$, for example, implies that the net parallel reconnection electric field force is pointing in the direction of energetic ions propagating along the magnetic field with $\mu > 0$. Equation (128) was derived using the relationships $\langle\delta U_I^2\rangle^{1/2} = (r^I_{\rm A})^{1/2}V_{A0}\langle\delta B_I^2\rangle^{1/2}/B_0$, Equation (102), and $d_{i/e}/r_g = (Z/A)(V_{A0}/v)$ for nonrelativistic particle speeds. For ions we use $d_i/r_g = (Z/A)(V_{A0}/v)$, and for electrons we specify $d_e/r_g = V_{A0}/v$ $(Z/A = 1)$.

Statistical fluctuations in the energetic particle acceleration rate $\nu^I_{\rm REC}$ are determined by the expression

$$\begin{aligned}\delta\nu^I_{\rm REC} &= \nu_{\rm REC} - \langle\nu_{\rm REC}\rangle \\ &\approx -\frac{q}{p}(\boldsymbol{U}_I\times\boldsymbol{B}_I)\cdot\boldsymbol{b}_0+\frac{q}{p}\langle\boldsymbol{U}_I\times\boldsymbol{B}_I\rangle\cdot\boldsymbol{b}_0 \\ &= -\frac{q}{p}\delta(\boldsymbol{U}_I\times\boldsymbol{B}_I)\cdot\boldsymbol{b}_0,\end{aligned} \tag{129}$$

where we assumed $\nu^{\rm SW}_{\rm REC} = 0$ as discussed above. The variance in the relative energetic particle momentum rate of change in response to fluctuations in the dynamic properties of merging flux ropes can be expressed as

$$\begin{aligned}\langle(\delta\nu^I_{\rm REC})^2\rangle &= \frac{q^2}{p^2}\langle[\delta(\boldsymbol{U}_I\times\boldsymbol{B}_I)\cdot\boldsymbol{b}_0]^2\rangle \\ &= \frac{q^2}{p^2}[\epsilon_{ijk}\epsilon_{lmn}\langle\delta U_{Ij}\delta U_{Im}\rangle\langle B_{Ik}B_{In}\rangle b_{0i}b_{0l} \\ &\quad +\epsilon_{ijk}\epsilon_{lmn}\langle U_{Ij}U_{Im}\rangle\langle\delta B_{Ik}\delta B_{In}\rangle b_{0i}b_{0l} \\ &\quad +\epsilon_{ijk}\epsilon_{lmn}\langle\delta U_{Ij}\delta B_{In}\rangle\langle B_{Ik}U_{Im}\rangle b_{0i}b_{0l} \\ &\quad +\epsilon_{ijk}\epsilon_{lmn}\langle U_{Ij}B_{In}\rangle\langle\delta B_{Ik}\delta U_{Im}\rangle b_{0i}b_{0l}].\end{aligned} \tag{130}$$

The term in the second line of Equation (130) can be simplified as follows:

$$\epsilon_{ijk}\epsilon_{lmn}\langle\delta U_{Ij}\delta U_{Im}\rangle\langle B_{Ik}B_{In}\rangle b_{0i}b_{0l} = 2a^2\langle\delta\boldsymbol{U}_I\cdot\delta\boldsymbol{U}_I\rangle\langle\boldsymbol{B}_I\cdot\boldsymbol{B}_I\rangle, \tag{131}$$

by applying the conditions for isotropic 2D flux-rope turbulence in the 2D plane perpendicular to $\boldsymbol{B}_0$, which are $\langle U_{Ij}U_{Im}\rangle = a\langle\delta\boldsymbol{U}_I\cdot\boldsymbol{U}_I\rangle\delta_{jm}$ and $\langle B_{Ik}B_{In}\rangle = a\langle\boldsymbol{B}_I\cdot\boldsymbol{B}_I\rangle\delta_{kn}$, where $a = 1/2$, and using $\epsilon_{imn}\epsilon_{lmn} = \epsilon_{mni}\epsilon_{mnl} = 2\delta_{il}$. Following the same approach, the term in the third line of Equation (130) can be expressed as

$$\epsilon_{ijk}\epsilon_{lmn}\langle U_{Ij}U_{Im}\rangle\langle\delta B_{Ik}\delta B_{In}\rangle b_{0i}b_{0l} = 2a^2\langle\boldsymbol{U}_I\cdot\boldsymbol{U}_I\rangle\langle\delta\boldsymbol{B}_I\cdot\delta\boldsymbol{B}_I\rangle. \tag{132}$$

Consider the term in the fourth line of Equation (130). In this case

$$\begin{aligned}&\epsilon_{ijk}\epsilon_{lmn}\langle\delta U_{Ij}\delta B_{In}\rangle\langle B_{Ik}U_{Im}\rangle b_{0i}b_{0l}\\ &\quad = -2a^2\langle\delta\boldsymbol{U}_I\cdot\delta\boldsymbol{B}_I\rangle\langle\boldsymbol{B}_I\cdot\boldsymbol{U}_I\rangle,\end{aligned} \tag{133}$$

because we specified $\langle\delta U_{Ij}\delta B_{In}\rangle = a\langle\delta\boldsymbol{U}_I\cdot\boldsymbol{B}_I\rangle\delta_{jn}$ and $\langle B_{Ik}U_{Im}\rangle = a\langle\boldsymbol{B}_I\cdot\boldsymbol{U}_I\rangle\delta_{km}$ and applied $\epsilon_{inm}\epsilon_{lmn} = -\epsilon_{imn}\epsilon_{lmn} = -2\delta_{il}$. In the same way we find that the term in the bottom line of Equation (130) becomes

$$\begin{aligned}&\epsilon_{ijk}\epsilon_{lmn}\langle U_{Ij}B_{In}\rangle\langle\delta B_{Ik}\delta U_{Im}\rangle b_{0i}b_{0l}\\ &\quad = -2a^2\langle\boldsymbol{U}_I\cdot\boldsymbol{B}_I\rangle\langle\delta\boldsymbol{B}_I\cdot\delta\boldsymbol{U}_I\rangle.\end{aligned} \tag{134}$$

After inserting expressions (131)–(134) into Equation (130), we obtain

$$\begin{aligned}\langle(\delta\nu^I_{\rm REC})^2\rangle &= 4a^2\left[r^I_{\rm A} - \frac{1}{4}(\sigma^I_C)^2(r^I_{\rm A}+1)^2\right]\frac{V^2_{A0}}{r_g^2}\frac{\langle\delta B_I^2\rangle}{B_0^2}\frac{\langle B_I^2\rangle}{B_0^2}\\ &= C_\delta 4a^2\left[r^I_{\rm A} - \frac{1}{4}(\sigma^I_C)^2(r^I_{\rm A}+1)^2\right]\frac{V^2_{A0}}{r_g^2}\left(\frac{\langle\delta B_I^2\rangle}{B_0^2}\right)^2\\ &= C_\delta 4a^2\left[\frac{r^I_{\rm A} - 1/4(\sigma^I_C)^2(r^I_{\rm A}+1)^2}{(r^I_{\rm A}+1)^2}\right]\frac{V^2_{A0}}{r_g^2}\left(\frac{\epsilon_I}{\epsilon_{B_0}}\right)^2\\ &= C_\delta 4a^2\left[\frac{r^I_{\rm A} - 1/4(\sigma^I_C)^2(r^I_{\rm A}+1)^2}{(r^I_{\rm A}+1)^2}\right]\frac{Z^2}{A^2}\frac{V^2_{A0}}{d^2_{i,e}}\left(\frac{V_{A0}}{v}\right)^2\\ &\quad\times\left(\frac{\epsilon_I}{\epsilon_{B_0}}\right)^2,\end{aligned} \tag{135}$$

after implementing the expression for the normalized cross helicity σ^I_C given by Equation (118), using the relationship involving the Alfvén ratio r^I_A defined by $\langle\delta U_I^2\rangle = r^I_{\rm A}V^2_{A0}\langle B_I^2\rangle/B_0^2$, enforcing the closure assumption $\langle[\delta(\delta B_I)]^2\rangle = C_\delta\langle\delta B_I^2\rangle$ after applying $B_I = \delta B_I$, inserting the expression $1/r_g = (1/d_{i,e})(Z/A)(V_{A0}/v)$, and applying Equation (102).

A.2. Energetic Particle Pitch-angle and Combined Pitch-angle and Momentum Rates of Change

The energetic particle pitch-angle rate of change is expressed in terms of $d\mu/dt$ ($\mu = \cos\theta$, where θ is the particle's pitch angle). In focused transport theory there is a contribution to $d\mu/dt$ from the magnetic mirroring force defined as

$$\nu_{\rm REF} = v(\nabla\cdot\boldsymbol{b}). \tag{136}$$

By decomposing the magnetic field unit vector $\boldsymbol{b}$ according to Equation (110), valid for $B_I/B_0 \ll 1$ (strong guide field assumption), it follows that

$$\begin{aligned}\nu_{\rm REF} &\approx v(\nabla\cdot\boldsymbol{b}_0) + v\left(\nabla\cdot\frac{\boldsymbol{B}_0}{B_0}\right)\\ &= \nu^{\rm SW}_{\rm REF} + \nu^I_{\rm REF},\end{aligned} \tag{137}$$

where $\nu^{\rm SW}_{\rm REF}$ refers to the energetic particle pitch-angle rate of change for particles experiencing the magnetic mirroring force associated with the nonuniform background solar wind magnetic field, which also serves as the axial or guide magnetic field component of flux-rope structures, and $\nu^I_{\rm REF}$ represents the energetic particle pitch-angle rate of change for particles responding to the magnetic mirroring force associated with the nonuniform flux-rope twist (island) magnetic field component.

We express the average (coherent) energetic particle pitch-angle rate of change in response to the mean magnetic mirroring force that particles encounter when traversing numerous flux ropes in the guide field direction as

$$\begin{aligned}\langle\nu^I_{\rm REF}\rangle &= v\left\langle\nabla\cdot\frac{\boldsymbol{B}_I}{B_0}\right\rangle\\ &\approx -\sigma^I_{\rm REF}\frac{v}{L_I}\frac{\langle\delta B_I^2\rangle^{1/2}}{B_0}\\ &\quad - \frac{\sigma^I_{\rm REF}}{(r^I_{\rm A}+1)^{1/2}}\frac{v}{L_I}\frac{\epsilon_I^{1/2}}{\epsilon_{B_0}},\end{aligned} \tag{138}$$

where $\sigma^I_{\rm REF}\epsilon[-1, 1]$. Thus, when $\sigma^I_{\rm REF} > 0$, the mean magnetic mirroring force that particles encounter when traversing numerous flux ropes is such that particles propagating along the magnetic field ($\mu > 0$) will experience a mirroring effect. Those propagating in the opposite direction ($\mu < 0$) will experience a focusing effect. The opposite holds when $\sigma^I_{\rm REF} < 0$. When $\sigma^I_{\rm REF} = 0$, the mean mirroring force encountered by energetic particles crossing numerous flux ropes is zero, resulting in a zero average (coherent) energetic particle pitch-angle rate of change.

Fluctuations in the energetic particle pitch-angle rate of change encountered by particles when traversing numerous flux ropes are determined by

$$\begin{aligned}\delta\nu^I_{\rm REF} &= \nu_{\rm REF} - \langle\nu_{\rm REF}\rangle\\ &= v\left(\nabla\cdot\frac{\boldsymbol{B}_I}{B_0}\right) - v\left\langle\nabla\cdot\frac{\boldsymbol{B}_I}{B_0}\right\rangle\\ &= v\delta\left(\nabla\cdot\frac{\boldsymbol{B}_I}{B_0}\right).\end{aligned} \tag{139}$$

The variance in the energetic particle pitch-angle rate of change due to fluctuations in $\boldsymbol{B}_I$ (fluctuations in the magnetic mirroring force) encountered by energetic particles when traversing

numerous flux ropes can be expressed as

$$\langle(\delta\nu^I_{\rm REF})^2\rangle = v^2\left\langle\left[\delta\left(\nabla\cdot\frac{\boldsymbol{B}_I}{B_0}\right)\right]^2\right\rangle \approx \frac{v^2}{B_0^2}\frac{\langle\delta B_{Ii}\delta B_{Ij}\rangle}{L_{Ii}L_{Ij}} \approx a\frac{v^2}{L_I^2}\frac{\langle\delta B_I^2\rangle}{B_0^2} = \frac{C_\delta a}{r_{\rm A}^I+1}\frac{v^2}{L_I^2}\frac{\epsilon_I}{\epsilon_{B_0}}. \quad (140)$$

Expression (140) was derived by applying the condition for isotropic 2D turbulence in the 2D plane perpendicular to $\boldsymbol{B}_0$, namely, $\langle\delta B_{Ii}\delta B_{Ij}\rangle = a\langle\delta\boldsymbol{B}_I\cdot\delta\boldsymbol{B}_I\rangle\delta_{ij}$ with $a = 1/2$, applying $\boldsymbol{B}_I = \delta\boldsymbol{B}_I$, and using the closure assumption $\langle[\delta(\delta B_I)]^2\rangle = C_\delta\langle\delta B_I^2\rangle$.

Consider now the coupling of terms involving fluctuations in the relative particle momentum rates of change and the particle pitch-angle rates of change for the different flux-rope acceleration mechanisms that appear in our kinetic transport theory. For compressible contracting and merging flux ropes we derive the following approximate expression for the term $\langle\delta\nu^I_{\rm COM}\delta\nu^I_{\rm REF}\rangle$:

$$\langle\delta\nu^I_{\rm COM}\delta\nu^I_{\rm REF}\rangle = -\left\langle\delta(\nabla\cdot\boldsymbol{U}_I)\delta\left(\nabla\cdot\frac{\boldsymbol{B}_I}{B_0}\right)\right\rangle \approx -\frac{1}{B_0}\frac{\langle\delta U_{Ii}\delta B_{Ij}\rangle}{L_{Ii}L_{Ij}} \approx -\frac{a}{2}\sigma_C^I(r_{\rm A}^I+1)\frac{vV_{A0}}{L_I^2}\frac{\langle\delta B_I^2\rangle}{B_0^2} = -\frac{C_\delta a}{2}\sigma_C^I\frac{vV_{A0}}{L_I^2}\frac{\epsilon_I}{\epsilon_{B_0}}, \quad (141)$$

where we specified the condition for isotropic 2D turbulence in the 2D plane perpendicular to $\boldsymbol{B}_0$, namely, $\langle\delta U_{Ii}\delta B_{Ij}\rangle = a\langle\delta\boldsymbol{U}_I\cdot\delta\boldsymbol{B}_I\rangle\delta_{ij}$ with $a = 1/2$, introduced the definition for normalized cross helicity σ_C^I expressed in Equation (118), applied $\boldsymbol{B}_I = \delta\boldsymbol{B}_I$, and used the closure assumption $\langle[\delta(\delta B_I)]^2\rangle = C_\delta\langle\delta B_I^2\rangle$.

For incompressible contracting and merging flux ropes we derived an approximate expression for the term $\langle\delta\nu^I_{\rm INC}\delta\nu^I_{\rm REF}\rangle$ given by

$$\langle\delta\nu^I_{\rm INC}\delta\nu^I_{\rm REF}\rangle = -\left\langle\delta\left[\frac{\boldsymbol{B}_I}{B_0}\cdot\left(\frac{\boldsymbol{B}_I}{B_0}\cdot\nabla\right)\boldsymbol{U}_I\right]\delta\left(\nabla\cdot\frac{\boldsymbol{B}_I}{B_0}\right)\right\rangle$$
$$\approx -\frac{v}{B_0^3}\frac{\langle B_I^2\rangle^{1/2}}{L_I}(\langle\delta B_{Ii}\delta B_{Ij}\rangle\langle U_{Ii}L_{Ij}^{-1}\rangle + \langle B_{Ii}L_{Ij}^{-1}\rangle\langle\delta U_{Ii}\delta B_{Ij}\rangle)$$
$$\approx -a\frac{vV_{A0}}{L_I^2}\frac{\langle B_I^2\rangle}{B_0^2}\frac{\langle\delta B_I^2\rangle}{B_0^2}\left[(r_{\rm A}^I)^{1/2}+\frac{1}{2}\sigma_C^I(r_{\rm A}^I+1)\right]$$
$$\approx -\frac{C_\delta a}{(r_{\rm A}^I+1)^2}\frac{vV_{A0}}{L_I^2}\left(\frac{\epsilon_I}{\epsilon_{B_0}}\right)^2\left[(r_{\rm A}^I)^{1/2}+\frac{1}{2}\sigma_C^I(r_{\rm A}^I+1)\right], \quad (142)$$

where the first term in the last line of Equation (142) represents the effect of fluctuations in the flux-rope magnetic field $\boldsymbol{B}_I$ and the last term in the same line accounts for the effect of fluctuations in the flux-rope contraction/merging velocity $\boldsymbol{U}_I$. In Equation (142) we introduced the replacement $\boldsymbol{B}_I\cdot\nabla\rightarrow\langle B_I^2\rangle^{1/2}/L_I$ in the first line, thus reducing the number of terms by including an estimate of the average magnitude of the gradient of the flux-rope flow along the flux-rope magnetic field in the 2D plane perpendicular to $\boldsymbol{B}_0$. In the second line we assumed isotropic 2D turbulence in the 2D plane perpendicular to $\boldsymbol{B}_0$, namely, $\langle\delta B_{Ii}\delta B_{Ij}\rangle = a\langle\delta\boldsymbol{B}_I\cdot\delta\boldsymbol{B}_I\rangle\delta_{ij}$ and $\langle\delta U_{Ii}\delta B_{Ij}\rangle = a\langle\delta\boldsymbol{U}_I\cdot\delta\boldsymbol{B}_I\rangle\delta_{ij}$ with $a = 1/2$, made use of the definition of normalized cross helicity (118), introduced the approximations $\langle\boldsymbol{U}_I\cdot\boldsymbol{L}_I^{-1}\rangle\rightarrow\langle U_I^2\rangle^{1/2}/L_I$ and $\langle\boldsymbol{B}_I\cdot\boldsymbol{L}_I^{-1}\rangle\rightarrow\langle B_I^2\rangle^{1/2}/L_I$, and used the expression for the magnetic island Alfvén ratio r_A^I given by $\langle U_I^2\rangle^{1/2} = (r_{\rm A}^I)^{1/2}V_{A0}\langle B_I^2\rangle^{1/2}/B_0$. In the third line we applied $\boldsymbol{B}_I = \delta\boldsymbol{B}_I$ and used the closure assumption $\langle[\delta(\delta B_I)]^2\rangle = C_\delta\langle\delta B_I^2\rangle$.

A simplified expression for $\langle\delta\nu^I_{\rm ACC}\nu^I_{\rm REF}\rangle$ can be derived as follows:

$$\langle\delta\nu^I_{\rm ACC}\nu^I_{\rm REF}\rangle = -\left\langle\frac{1}{v}(\boldsymbol{U}_0\cdot\nabla)\boldsymbol{U}_I\cdot\boldsymbol{b}_0 v\delta\left(\nabla\cdot\frac{\boldsymbol{B}_I}{B_0}\right)\right\rangle \approx -\frac{1}{B_0}\frac{U_0}{L_{\rm Ir}}b_{0i}L_{Ij}^{-1}\langle U_{Ii}B_{Ij}\rangle\frac{\langle\delta B_I^2\rangle^{1/2}}{\langle B_I^2\rangle^{1/2}} = -\frac{a}{B_0}\frac{U_0}{L_{\rm Ir}}(\boldsymbol{b}_0\cdot\boldsymbol{L}_I^{-1})\langle\boldsymbol{U}_I\cdot\boldsymbol{B}_I\rangle\frac{\langle\delta B_I^2\rangle^{1/2}}{\langle B_I^2\rangle^{1/2}} = 0. \quad (143)$$

We expressed $\boldsymbol{U}_0\cdot\nabla = U_0/L_{\rm Ir}$ in the first line of Equation (143) because for a radial solar wind outflow the flux-rope cross-sectional radius is $L_{\rm Ir}$. We assumed in the second line of Equation (143) that $\langle\delta U_{Ii}\delta B_{Ij}\rangle = a\langle\delta\boldsymbol{U}_I\cdot\delta\boldsymbol{B}_I\rangle\delta_{ij}$ with $a = 1/2$ to specify isotropic 2D turbulence in the 2D plane perpendicular to $\boldsymbol{B}_0$. This led to the inner product $\boldsymbol{b}_0\cdot\boldsymbol{L}_I^{-1}$ in the third line of Equation (143). However, because $\boldsymbol{L}_I^{-1}\perp\boldsymbol{b}_0$, $\boldsymbol{b}_0\cdot\boldsymbol{L}_I^{-1} = 0$, resulting in $\langle\delta\nu^I_{\rm ACC}\nu^I_{\rm REF}\rangle = 0$.

Finally, the expression for $\langle\delta\nu^I_{\rm REC}\delta\nu^I_{\rm REF}\rangle$ is derived as follows:

$$\langle\delta\nu^I_{\rm REC}\delta\nu^I_{\rm REF}\rangle = -\left\langle\frac{q}{p}\delta(\boldsymbol{U}_I\times\boldsymbol{B}_I)\cdot\boldsymbol{b}_0 v\delta\left(\nabla\cdot\frac{\boldsymbol{B}_I}{B_0}\right)\right\rangle$$
$$\approx -\frac{qv}{pB_0}b_{0i}\epsilon_{ijk}[\langle\delta U_{Ij}\delta B_{Il}\rangle\langle B_{Ik}L_{Il}^{-1}\rangle + \langle\delta B_{Ik}\delta B_{Il}\rangle\langle U_{Ij}L_{Il}^{-1}\rangle]$$
$$= -a\frac{q}{|q|}\frac{v}{r_gL_I}\frac{1}{B_0^2}[\langle\delta\boldsymbol{U}_I\cdot\delta\boldsymbol{B}_I\rangle\langle B_I^2\rangle^{1/2} + \langle\delta\boldsymbol{B}_I\cdot\delta\boldsymbol{B}_I\rangle\langle U_I^2\rangle^{1/2}]$$
$$= -a\frac{vV_{A0}}{r_gL_I}\frac{q}{|q|}\frac{\langle\delta B_I^2\rangle}{B_0^2}\frac{\langle B_I^2\rangle^{1/2}}{B_0}\times\left[(r_{\rm A}^I)^{1/2}+\frac{1}{2}\sigma_C^I(r_{\rm A}^I+1)\right]$$
$$= -\frac{C_\delta^{1/2}a}{(r_{\rm A}^I+1)^{3/2}}\frac{Z}{A}\frac{V_{A0}^2}{d_{i,e}L_I}\left(\frac{\epsilon_I}{\epsilon_{B_0}}\right)^{3/2}\times\left[(r_{\rm A}^I)^{1/2}+\frac{1}{2}\sigma_C^I(r_{\rm A}^I+1)\right], \quad (144)$$

where the first term in the last line of Equation (144) represents the effect of fluctuations in the flux-rope magnetic field $\boldsymbol{B}_I$ and the last term in the same line accounts for the effect of fluctuations in the flux-rope contraction/merging velocity $\boldsymbol{U}_I$. In the second line of Equation (144) we applied the conditions $\langle \delta U_{Ij}\delta B_{Il}\rangle = a\langle \delta \boldsymbol{U}_I\cdot\delta\boldsymbol{B}_I\rangle\delta_{jl}$ and $\langle \delta B_{Ik}\delta B_{Il}\rangle = a\langle \delta\boldsymbol{B}_I\cdot\delta\boldsymbol{B}_I\rangle\delta_{kl}$ with $a = 1/2$ for isotropic 2D turbulence in the 2D plane perpendicular to $\boldsymbol{B}_0$, whereas in the third line of Equation (144) we introduced the definition of normalized cross helicity (118), inserted the approximations $\langle \boldsymbol{L}_I^{-1}\times\boldsymbol{U}_I\rangle\cdot\boldsymbol{b}_0 \rightarrow \langle U_I^2\rangle^{1/2}/L_I$ and $\langle \boldsymbol{L}_I^{-1}\times\boldsymbol{B}_I\rangle\cdot\boldsymbol{b}_0 \rightarrow \langle U_I^2\rangle^{1/2}/L_I$, and used the expression $\langle U_I^2\rangle^{1/2} = (r_{\rm A}^I)^{1/2}V_{A0}\langle B_I^2\rangle^{1/2}/B_0$. In the fourth line we made use of the closure assumption $\langle[\delta(\delta B_I)]^2\rangle = C_\delta\langle\delta B_I^2\rangle$ after applying $B_I = \delta B_I$ and set $1/r_g = (1/d_{i,e})(Z/A)(V_{A0}/v)$.

Appendix B
An N I MHD Transport Equation for the Mean Total Energy Density of the Magnetic Island Component of Small-scale Flux Ropes

The equation for the transport of the total energy density of the magnetic island or twist component of small-scale flux-rope structures in the nonuniform solar wind that we couple to the focused transport equation to model self-consistent particle acceleration is based on nearly incompressible (N I) MHD theory (Zank et al. 2017). This theory, mainly developed in the early 1990s (e.g., Zank & Matthaeus 1992, 1993), was expanded more recently to include the important extension to the inhomogeneous solar wind flow (Hunana & Zank 2010). N I MHD theory addresses the underlying incompressibility of solar wind turbulence. The N I MHD description also relates typical solar wind plasma beta values of order one or less to the observed leading-order quasi-2D turbulence nature of solar wind MHD turbulence (e.g., Matthaeus et al. 1990; Bieber et al. 1994; Zheng & Hu 2018). Zank et al. (2017) continued this work with a detailed application to solar wind turbulence, rewriting the N I MHD system of equations in terms of Elsässer variables in which distinct descriptions of quasi-2D and slab turbulence (parallel-propagating Alfvén waves) emerge naturally, as do the nonlinear couplings between these two turbulence modes. For plasma beta order one or less solar wind regions, an N I MHD formulation describing the transport of majority quasi-2D and minority slab turbulence throughout the nonuniform solar wind was undertaken, and a promising preliminary comparison of theory and observations was accomplished (Adhikari et al. 2017). Zank et al. (2017) also illustrates with a purely 2D solution of the quasi-2D turbulence equations in the 2D plane perpendicular to background magnetic field $\boldsymbol{B}_0$ in a uniform solar wind medium that the quasi-2D component can be linked to nonlinear, dynamic coherent magnetic island structures in this 2D plane advected with the solar wind flow. The solution can be viewed as a small-scale (MHD-scale) flux-rope structure where the magnetic island is the twist component and $\boldsymbol{B}_0$ acts as a large-scale axial or guide field for the flux-rope structure. Observations indicate the apparently ubiquitous existence of such quasi-2D small-scale flux-rope structures in the solar wind, including that the background magnetic field $\boldsymbol{B}_0$ acts as a strong out-of-plane guide field for these structures (e.g., Bieber et al. 1996; Cartwright & Moldwin 2010; Khabarova et al. 2015; Oughton et al. 2015; Smith et al. 2016; Zheng 2017; Zheng & Hu 2018).

To model quasi-2D small-scale (inertial-scale) magnetic island turbulence transport in the nonuniform solar wind medium, including the assumption that the background magnetic field represents a strong guide field component for these structures, we adopt the lowest-order version of N I MHD theory in Elsässer variables presented by Zank et al. (2017). The equation is

$$\frac{\partial \boldsymbol{Z}_I^{\pm}}{\partial t} + (\boldsymbol{U}_0\cdot\nabla)\boldsymbol{Z}_I^{\pm} + (\boldsymbol{Z}_I^{\mp}\cdot\nabla)\boldsymbol{U}_0 + \frac{\boldsymbol{Z}_I^{\pm}-\boldsymbol{Z}_I^{\mp}}{4}(\nabla\cdot\boldsymbol{U}_0) - \frac{\boldsymbol{Z}_I^{\pm}-\boldsymbol{Z}_I^{\mp}}{4}\frac{1}{\rho_0}(\boldsymbol{Z}_I^{\pm}\cdot\nabla)\rho_0 = -(\boldsymbol{Z}_I^{\mp}\cdot\nabla)\boldsymbol{Z}_I^{\pm} - \frac{1}{\rho_0}\nabla\left(\delta P_I + \frac{\delta B_I^2}{8\pi}\right), \tag{145}$$

where the nonuniform Elsässer variables for quasi-2D flux-rope turbulence are defined as

$$\boldsymbol{Z}_I^{\pm} = \delta\boldsymbol{U}_I \pm \frac{\delta\boldsymbol{B}_I}{\sqrt{4\pi\rho_0}} = \delta\boldsymbol{U}_I \pm \delta\boldsymbol{V}_{AI}, \tag{146}$$

restricted locally by $\delta\boldsymbol{B}_I(x,y)$, $\delta\boldsymbol{U}_I(x,y)\perp\boldsymbol{B}_0 = B_0\boldsymbol{e}_z$, approximately, and by $\delta B_I/B_0 \ll 1$.

Following Zank et al. (2017), this equation can be converted into a partially closed transport equation for $\langle \boldsymbol{Z}_I^{\pm}\cdot\boldsymbol{Z}_I^{\pm}\rangle = \langle (Z_I^{\pm})^2\rangle$ by taking the dot product of Equation (145) with respect to $\boldsymbol{Z}_I^{\pm}$ and by specifying the following definitions and approximations: (i) Introduce

$$\langle \boldsymbol{Z}_I^{\pm}\cdot\boldsymbol{Z}_I^{\mp}\rangle = \langle \delta U_I^2\rangle - \langle \delta V_{AI}^2\rangle = E_D^I, \tag{147}$$

where E_D^I is the residual flux-rope energy determining the difference between the average kinetic and magnetic energy of the magnetic island component of small-scale flux ropes. (ii) Replace the two nonlinear terms on the right-hand side of Equation (145) as follows:

$$-(\boldsymbol{Z}_I^{\mp}\cdot\nabla)\boldsymbol{Z}_I^{\pm} - \frac{1}{\rho_0}\nabla\left(\delta P_I + \frac{\delta B_I^2}{8\pi}\right) \rightarrow -\boldsymbol{Z}_I^{\pm}\frac{\langle (Z_I^{\mp})^2\rangle^{1/2}}{L_I^{\pm}}, \tag{148}$$

where

$$(\tau_I)^{-1} = \frac{\langle (Z_I^{\mp})^2\rangle^{1/2}}{L_I^{\pm}} \tag{149}$$

is the average timescale for the nonlinear interaction of magnetic islands resulting in energy loss due to a forward cascade of energy to smaller-scale islands. (iii) Use the result that

$$(\langle \boldsymbol{Z}_I^{\mp}\rangle\cdot\nabla)\boldsymbol{U}_0\cdot\boldsymbol{Z}_I^{\pm} = \langle Z_{Ii}^{\mp}Z_{Ij}^{\pm}\rangle\frac{\partial U_{0j}}{\partial x_i} = a\langle \boldsymbol{Z}_I^{\mp}\cdot\boldsymbol{Z}_I^{\pm}\rangle\delta_{ij}\frac{\partial U_{0}j}{\partial x_i} = aE_D^I(\nabla\cdot\boldsymbol{U}_0) \tag{150}$$

for the third term on the left-hand side of Equation (145) after taking the dot product of this term with respect to $\boldsymbol{Z}_I^{\pm}$. The result (Equation (150)) implies that $\langle Z_{Ii}^{\mp}Z_{Ij}^{\pm}\rangle = a\langle \boldsymbol{Z}_I^{\mp}\cdot\boldsymbol{Z}_I^{\pm}\rangle\delta_{ij}$. This relationship can be found by assuming that 2D magnetic island turbulence is nearly isotropic in the 2D plane

perpendicular to $\boldsymbol{B}_0$ according to the expressions

$$\begin{aligned}\langle \delta U_{Ii}\delta U_{Ij}\rangle &= a\langle \delta \boldsymbol{U}_I\cdot \boldsymbol{U}_I\rangle \delta_{ij},\\ \langle \delta V_{AIi}\delta V_{AIj}\rangle &= a\langle \delta \boldsymbol{V}_{AI}\cdot \boldsymbol{V}_{AI}\rangle \delta_{ij},\\ \langle \delta U_{Ii}\delta V_{AIj}\rangle &= a\langle \delta \boldsymbol{U}_I\cdot \boldsymbol{V}_{AI}\rangle \delta_{ij},\\ \langle \delta V_{AIi}\delta U_{Ij}\rangle &= a\langle \delta \boldsymbol{V}_{AI}\cdot \boldsymbol{U}_I\rangle \delta_{ij},\end{aligned} \tag{151}$$

where $a = 1/2$ for 2D turbulence (Zank et al. 2017). These expressions ignore off-diagonal terms (terms with $i \neq j$), so that magnetic helicity and vorticity effects associated with magnetic island structures are neglected for simplicity. (iv) Introduce a unit vector $\boldsymbol{n} \perp \boldsymbol{B}_0$ in the direction of 2D turbulence and specify in the term in the second line of Equation (145) the replacement

$$\boldsymbol{Z}_I^{\pm}\cdot\nabla \rightarrow \langle (Z_I^{\pm})^2\rangle^{1/2}\boldsymbol{n}\cdot\nabla. \tag{152}$$

Because of the assumption of isotropic 2D turbulence in the 2D plane perpendicular to $\boldsymbol{B}_0$, the direction of $\boldsymbol{n}$ can be considered to be arbitrary in this plane. The transport equations for $\langle (Z_I^{\pm})^2\rangle$ then become

$$\begin{aligned}&\frac{\partial\langle (Z_I^{\pm})^2\rangle}{\partial t} + (\boldsymbol{U}_0\cdot\nabla)\langle (Z_I^{\pm})^2\rangle + \frac{1}{2}\langle (Z_I^{\pm})^2\rangle(\nabla\cdot\boldsymbol{U}_0)\\ &\quad + (2a-1/2)E_D^I(\nabla\cdot\boldsymbol{U}_0)\\ &\quad - \frac{1}{2}(\langle (Z_I^{\pm})^2\rangle - E_D^I)\frac{1}{\rho_0}(\boldsymbol{n}\cdot\nabla)\rho_0\\ &= -2\langle (Z_I^{\pm})^2\rangle\frac{\langle (Z_I^{\mp})^2\rangle^{1/2}}{L_I^{\pm}}.\end{aligned} \tag{153}$$

This equation agrees with Equation (68) in Zank et al. (2017).

Next, we convert the two equations in Equation (153) into a partially closed equation for total magnetic island energy E_T^I (that is, the sum of kinetic and magnetic energy) in the 2D plane perpendicular to $\boldsymbol{B}_0$ by taking the average of the two equations and by introducing

$$\begin{aligned}E_T^I &= \langle \delta U_I^2\rangle + \langle \delta V_{AI}^2\rangle = \frac{1}{2}[\langle (Z_I^{\pm})^2\rangle + \langle (Z_I^{\mp})^2\rangle],\\ E_C^I &= 2\langle \delta\boldsymbol{U}_I\cdot\delta\boldsymbol{V}_{AI}\rangle = \frac{1}{2}[\langle (Z_I^{\pm})^2\rangle - \langle (Z_I^{\mp})^2\rangle],\\ E_T^I &\pm E_C^I = \langle (Z_I^{\pm})^2\rangle,\\ \sigma_C^I &= \frac{E_C^I}{E_T^I},\ \ \sigma_D^I = \frac{E_D^I}{E_T^I},\end{aligned} \tag{154}$$

where E_C^I is the cross helicity of 2D flux-rope turbulence, σ_C^I is cross helicity normalized to E_T^I, and σ_D^I is residual flux-rope energy E_D^I (see Equation (147)), also normalized to E_T^I. The resultant transport equation for total 2D magnetic island energy is

$$\begin{aligned}&\frac{\partial E_T^I}{\partial t} + (\boldsymbol{U}_0\cdot\nabla)E_T^I + \frac{1}{2}(1+(4a-1)\sigma_D^I)(\nabla\cdot\boldsymbol{U}_0)E_T^I\\ &\quad - \frac{1}{4}[(1+\sigma_C^I)^{3/2} - (1+\sigma_C^I)^{1/2}\sigma_D^I + (1-\sigma_C^I)^{3/2}\\ &\quad - (1-\sigma_C^I)^{1/2}\sigma_D^I]\left(\frac{1}{\rho_0}(\boldsymbol{n}\cdot\nabla)\rho_0\right)(E_T^I)^{3/2}\\ &\quad + (1-(\sigma_C^I)^2)^{1/2}\left[\frac{(1+\sigma_C^I)^{1/2}}{L_I^+}\right.\\ &\quad \left. + \frac{(1-\sigma_C^I)^{1/2}}{L_I^-}\right](E_T^I)^{3/2}.\end{aligned} \tag{155}$$

Finally, we convert Equation (155) into a transport equation for the total magnetic island energy density ϵ_I in the 2D plane perpendicular to $\boldsymbol{B}_0$ by multiplying Equation (155) by $1/2\rho_0$, by defining

$$\epsilon_I = \frac{1}{2}\rho_0 E_T^I, \tag{156}$$

and by simplifying the ensuing equation with the continuity equation for the background solar wind

$$\frac{\partial\rho_0}{\partial t} + \nabla\cdot\rho_0\boldsymbol{U}_0 = 0. \tag{157}$$

Then,

$$\begin{aligned}&\frac{\partial\epsilon_I}{\partial t} + (\boldsymbol{U}_0\cdot\nabla)\epsilon_I + \frac{1}{2}(3+(4a-1)\sigma_D^I)(\nabla\cdot\boldsymbol{U}_0)\epsilon_I\\ &\quad - \frac{1}{4}[(1+\sigma_C^I)^{3/2} - (1+\sigma_C^I)^{1/2}\sigma_D^I + (1-\sigma_C^I)^{3/2}\\ &\quad - (1-\sigma_C^I)^{1/2}\sigma_D^I]\left(\frac{\sqrt{2}}{\rho_0^{3/2}}(\boldsymbol{n}\cdot\nabla)\rho_0\right)\epsilon_I^{3/2}\\ &= -(1-(\sigma_C^I)^2)^{1/2}\left[\frac{(1+\sigma_C^I)^{1/2}}{L_I^+} + \frac{(1-\sigma_C^I)^{1/2}}{L_I^-}\right]\\ &\quad \times\left(\frac{2}{\rho_0}\right)^{1/2}\epsilon_I^{3/2}.\end{aligned} \tag{158}$$

Appendix C
The Energy Exchange Rate between the Magnetic Island Component of Small-scale Flux Ropes and Energetic Charged Particles

Here we derive the growth/damping rate of small-scale flux-rope energy in the 2D plane perpendicular to $\boldsymbol{B}_0$ based on the assumption of total energy conservation in the energy exchange between the magnetic island component of flux ropes and energetic charged particles. Following the approach of Ng et al. (2003), we express the focused transport Equation (40) in

Fokker–Planck notation:

$$\frac{d\langle f\rangle_{\rm SW}}{dt} = -\nabla\cdot\left(\left\langle\frac{\Delta \boldsymbol{x}}{\Delta t}\right\rangle_I\langle f\rangle\right) - \frac{\partial}{\partial\mu}\left(\left\langle\frac{\Delta\mu}{\Delta t}\right\rangle_I\langle f\rangle\right) - \frac{1}{p^2}\frac{\partial}{\partial p}\left(p^2\left\langle\frac{\Delta p}{\Delta t}\right\rangle_I\langle f\rangle\right), \quad (159)$$

where

$$\left\langle\frac{\Delta \boldsymbol{x}}{\Delta t}\right\rangle_I\langle f\rangle = \left\langle\frac{d\boldsymbol{x}}{dt}\right\rangle_\phi^I\langle f\rangle,$$
$$\left\langle\frac{\Delta\mu}{\Delta t}\right\rangle_I\langle f\rangle = \left\langle\frac{d\mu}{dt}\right\rangle_\phi^I\langle f\rangle - D^{\rm eff}_{\mu\mu}\frac{\partial\langle f\rangle}{\partial\mu} - D^I_{\mu p}\frac{\partial\langle f\rangle}{\partial p},$$
$$\left\langle\frac{\Delta p}{\Delta t}\right\rangle_I\langle f\rangle = \left\langle\frac{dp}{dt}\right\rangle_\phi^I\langle f\rangle - D^I_{p\mu}\frac{\partial\langle f\rangle}{\partial\mu} - D^I_{pp}\frac{\partial\langle f\rangle}{\partial p}. \quad (160)$$

Thus, the average kinetic energy rate of change of energetic particles interacting with the magnetic island component of small-scale flux ropes $\langle\Delta T/\Delta t\rangle_I$ is governed by

$$\left\langle\frac{\Delta T}{\Delta t}\right\rangle_I\langle f\rangle = v\left(\left\langle\frac{dp}{dt}\right\rangle_\phi^I\langle f\rangle - D^I_{p\mu}\frac{\partial\langle f\rangle}{\partial\mu} - D^I_{pp}\frac{\partial\langle f\rangle}{\partial p}\right). \quad (161)$$

On assuming total energy conservation in the energy exchange between energetic particles and small-scale magnetic islands, the average rate of change of total magnetic island energy density $d\epsilon_I/dt$ is determined by

$$\frac{d\epsilon_I}{dt} = -\frac{d\epsilon_c}{dt} = -\int d^3p\langle f\rangle\frac{\langle\Delta T\rangle}{\Delta t} = -2\pi\int_{-1}^{1}d\mu\int_0^\infty dpp^2v\left\langle\frac{dp}{dt}\right\rangle_\phi^I(\epsilon_I)\langle f\rangle + 2\pi\int_{-1}^{1}d\mu\int_0^\infty dpp^2v\left(D^I_{p\mu}(\epsilon_I)\frac{\partial\langle f\rangle}{\partial\mu} + D^I_{pp}(\epsilon_I)\frac{\partial\langle f\rangle}{\partial p}\right), \quad (162)$$

where $d\epsilon_c/dt$ is the average rate of change of energetic particle energy density found after integrating over particles distributed in nested spherical shells in momentum space. In Equation (162), the term in the second line refers to the energy exchange rate associated with coherent energetic particle acceleration in response to mean flux-rope dynamic properties, whereas the last two terms in the bottom line refer to the energy exchange rate generated by stochastic energetic particle acceleration in response to statistical fluctuations in flux-rope dynamics. On the basis of Equation (162) we express the average, relative damping/growth rate of total magnetic island flux-rope energy density as

$$\gamma_I^{\rm coh}(\langle f\rangle) = -\frac{2\pi}{\epsilon_I}\int_{-1}^{1}d\mu\int_0^\infty dpp^2v\left(\left\langle\frac{dp}{dt}\right\rangle_\phi^I(\epsilon_I)\langle f\rangle\right),$$
$$\gamma_I^{\rm stoch}(\langle f\rangle) = \frac{2\pi}{\epsilon_I}\int_{-1}^{1}d\mu\int_0^\infty dpp^2v \times\left(D^I_{p\mu}(\epsilon_I)\frac{\partial\langle f\rangle}{\partial\mu} + D^I_{pp}(\epsilon_I)\frac{\partial\langle f\rangle}{\partial p}\right), \quad (163)$$

where $\gamma_I^{\rm coh}$ refers to the flux-rope growth/damping rate in response to coherent particle acceleration and $\gamma_{\rm stoch}$ indicates the flux-rope growth/damping rate due to stochastic particle acceleration.

Appendix D
The Parker–Gleeson–Axford Transport Equation for Energetic Particle Interaction with Small-scale Flux Ropes

To derive the focused transport Equation (40) in the diffusive limit, we apply the standard technique of expanding the energetic particle distribution function in terms of moments in μ-space involving Legendre polynomials in $\mu = \cos\theta$, where θ is the energetic particle pitch angle. Expanded up to the second moment, the distribution function is

$$\langle f\rangle(\boldsymbol{x}, p, \mu, t) \approx f_0(\boldsymbol{x}, p, t) + 3\mu f_1(\boldsymbol{x}, p, t) + \frac{5}{2}(3\mu^2 - 1)f_2(\boldsymbol{x}, p, t), \quad (164)$$

allowing us to derive the zeroth, first, and second moments of the focused transport equation. In this paper, both the zeroth and first moments of the focused transport equations are extended to include the spatial transport and acceleration effects of $D^I_{p\mu}$ and $D^I_{\mu p}$ on energetic particles in the diffusion approximation (compare with Equations (39)–(47) of le Roux et al. 2015a). The moment expressions are

$$\frac{\partial f_0}{\partial t} + (\boldsymbol{U}_0\cdot\nabla)f_0 + \langle\delta\boldsymbol{U}_I\cdot\nabla\rangle f_0 - (\nabla\cdot\boldsymbol{U}_0 - \langle\nu^I_{\rm COM}\rangle)\frac{p}{3}\frac{\partial f_0}{\partial p} + \langle\nu^I_{\rm REF}\rangle f_1 = -\nabla\cdot(v\boldsymbol{b}_0 f_1)$$
$$+ \frac{1}{p^2}\frac{\partial}{\partial p}\left[p^4\left(\frac{2}{15}\langle(\delta\nu^I_{\rm COM})^2\rangle + \frac{1}{5}\langle(\delta\nu^I_{\rm INC})^2\rangle + \frac{1}{3}(\langle(\delta\nu^I_{\rm ACC})^2\rangle + \langle(\delta\nu^I_{\rm REC})^2\rangle)\right)\tau_{\rm dec}\frac{\partial f_0}{\partial p}\right]$$
$$+ \frac{1}{p^2}\frac{\partial}{\partial p}\left[p^3\left(\frac{2}{5}\langle\delta\nu^I_{\rm COM}\delta\nu^I_{\rm REF}\rangle - \frac{1}{5}\langle\delta\nu^I_{\rm INC}\delta\nu^I_{\rm REF}\rangle\right)\tau_{\rm dec}f_1\right]$$
$$+ \frac{1}{p^2}\frac{\partial}{\partial p}\left[p^3\left(\left(\frac{1}{v}\frac{d\boldsymbol{U}_0}{dt} - \frac{q\boldsymbol{E}_{\rm surf}}{p}\right)\cdot\boldsymbol{b}_0 - \langle\nu^I_{\rm ACC}\rangle - \langle\nu^I_{\rm REC}\rangle\right)f_1\right]$$
$$+ \frac{1}{p^2}\frac{\partial}{\partial p}\left[p^3\left(\boldsymbol{b}_0\boldsymbol{b}_0 : \underline{\sigma}^{\rm sh} + \frac{1}{3}\langle\nu^I_{\rm COM}\rangle - \langle\nu^I_{\rm INC}\rangle\right)f_2\right], \quad (165)$$

$$f_1(p) \approx -\frac{1}{3}\frac{v}{\langle \nu_{\rm sc}^{\rm eff1}\rangle}\boldsymbol{b}_0\cdot\nabla f_0 - \frac{1}{\langle \nu_{\rm sc}^{\rm eff1}\rangle}\left[-\left(\frac{1}{v}\frac{d\boldsymbol{U}_0}{dt} - \frac{q\boldsymbol{E}_{\rm surf}}{p}\right)\cdot\boldsymbol{b}_0 + \langle \nu_{\rm ACC}^I\rangle + \langle \nu_{\rm REC}^I\rangle + \frac{1}{5}(2\langle \delta\nu_{\rm REF}^I \delta\nu_{\rm COM}^I\rangle - \langle \delta\nu_{\rm REF}^I \delta\nu_{\rm INC}^I\rangle)\tau_{\rm dec}\right]\frac{p}{3}\frac{\partial f_0}{\partial p}, \quad (166)$$

$$f_2(p) \approx \left(\frac{1}{15}\frac{\boldsymbol{b}_0\boldsymbol{b}_0\colon \underline{\underline{\sigma}}^{\rm sh} + 1/3\langle \nu_{\rm COM}^I\rangle - \langle \nu_{\rm INC}\rangle^I}{\langle \nu_{sc2}^{\rm eff}\rangle}\right)p\frac{\partial f_0}{\partial p}, \quad (167)$$

where the fourth line of the zeroth moment (Equation (165)) and the third line of the first moment (Equation (166)) contain new terms related to the coefficients $D_{p\mu}^I$ and $D_{\mu p}^I$ for both incompressible and compressible contracting and merging small-scale flux ropes that were omitted in le Roux et al. (2015a; see their Equations (49) and (51)). The first- and second-moment expressions are simplified to enable simple closure in the zeroth-moment equation in terms of a diffusive transport equation. After inserting the expressions for $f_1(p)$ and $f_2(p)$ into the zeroth-moment equation, one finds a closed, extended Parker transport equation for the isotropic part of the energetic particle distribution function $f_0(\boldsymbol{x}, p, t) = (1/2)\int_{-1}^{1} d\mu\, \langle f\rangle(\boldsymbol{x}, p, \mu, t)$ given by

$$\begin{aligned}\frac{\partial f_0}{\partial t} &+ \left(\boldsymbol{U}_0 - \frac{1}{3p^2}\frac{\partial}{\partial p}[p^3(U_{\rm RECU}^I - U_{p\mu}^I)\boldsymbol{b}_0] + \frac{1}{3}U_{\rm REF}^I\boldsymbol{b}_0\right)\cdot\nabla f_0 + \langle \delta\boldsymbol{U}_I\cdot\nabla\rangle f_0 \\ &- [\nabla\cdot\boldsymbol{U}_0 - \langle \nu_{\rm COM}^I\rangle + \nabla\cdot(U_{\rm RECU}^I + U_{p\mu}^I)\boldsymbol{b}_0 + \frac{\langle \nu_{\rm REF}^I\rangle}{v}(U_{\rm RECU}^I + U_{\mu p}^I)\Big]\frac{p}{3}\frac{\partial f_0}{\partial p} \\ &= \nabla\cdot(\kappa_\parallel^{\rm eff1}\boldsymbol{b}_0\boldsymbol{b}_0\cdot\nabla f_0) + \frac{1}{p^2}\frac{\partial}{\partial p}\left(p^2 D_{pp}^I\frac{\partial f_0}{\partial p}\right) + \frac{2}{3}pU_{\rm RECU}^I(\boldsymbol{b}_0\cdot\nabla)\frac{\partial f_0}{\partial p}, \end{aligned} \quad (168)$$

where

$$U_{\rm RECU}^I(\epsilon_I) = \frac{3\kappa_\parallel^{\rm eff1}}{v}(\langle \nu_{\rm ACC}^I\rangle + \langle \nu_{\rm REC}^I\rangle - \left(\frac{1}{v}\frac{d\boldsymbol{U}_0}{dt} - \frac{q\boldsymbol{E}_{\rm surf}}{p}\right)\cdot\boldsymbol{b}_0\Big),$$

$$U_{\rm REF}^I(\epsilon_I) = \frac{3\kappa_\parallel^{\rm eff1}}{v}\langle \nu_{\rm REF}^I\rangle,$$

$$U_{p\mu}^I(\epsilon_I) = \frac{3\kappa_\parallel^{\rm eff1}}{v}\frac{1}{5}(2\langle \delta\nu_{\rm REF}^I\delta\nu_{\rm COM}^I\rangle - \langle \delta\nu_{\rm REF}^I\delta\nu_{\rm INC}^I\rangle)\tau_{\rm dec} = U_{\mu p}^I(\epsilon_I),$$

$$\kappa_\parallel^{\rm eff1}(\epsilon_I) = \frac{1}{3}\frac{v^2}{\langle \nu_{\rm sc}^{\rm eff1}\rangle};\ \ \langle \nu_{\rm sc}^{\rm eff1}\rangle = 2(\langle \nu_{\rm sc}^A\rangle + \langle \nu_{\rm sc}^{I1}\rangle),$$

$$\kappa_\parallel^{\rm eff2}(\epsilon_I) = \frac{1}{3}\frac{v^2}{\langle \nu_{\rm sc}^{\rm eff2}\rangle};\ \ \langle \nu_{\rm sc}^{\rm eff2}\rangle = 2(\langle \nu_{\rm sc}^A\rangle + \langle \nu_{\rm sc}^{I2}\rangle),$$

$$\begin{aligned}D_{pp}^I(\epsilon_I) &= p^2\frac{1}{5}\left(\boldsymbol{b}_0\boldsymbol{b}_0\colon \underline{\underline{\sigma}}^{\rm sh} + \frac{1}{3}\langle \nu_{\rm COM}^I\rangle - \langle \nu_{\rm INC}^I\rangle\right)^2\frac{\kappa_\parallel^{\rm eff2}}{v^2} \\ &+ p^2(\langle \nu_{\rm ACC}^I\rangle + \langle \nu_{\rm REC}^I\rangle - \left(\frac{1}{v}\frac{d\boldsymbol{U}_0}{dt} - \frac{q\boldsymbol{E}_{\rm surf}}{p}\right)\cdot\boldsymbol{b}_0\Big)^2\frac{\kappa_\parallel^{\rm eff1}}{v^2} \\ &+ p^2\Big[\frac{2}{15}\langle(\delta\nu_{\rm COM}^I)^2\rangle + \frac{1}{5}\langle(\delta\nu_{\rm INC}^I)^2\rangle - \left(\frac{2}{5}\langle \delta\nu_{\rm COM}^I\delta\nu_{\rm REF}^I\rangle - \frac{1}{5}\langle \delta\nu_{\rm INC}^I\delta\nu_{\rm REF}^I\rangle\right)^2 \\ &\times \tau_{\rm dec}\frac{\kappa_\parallel^{\rm eff1}}{v^2} + \frac{1}{3}(\langle \delta\nu_{\rm ACC}^I\rangle^2 + \langle \delta\nu_{\rm REC}^I\rangle^2)\Big]\tau_{\rm dec}, \end{aligned} \quad (169)$$

where $\kappa_\parallel^{\rm eff1}$ and $\kappa_\parallel^{\rm eff2}$ are parallel diffusion coefficients that combine energetic particle pitch-angle scattering by Alfvén waves ($\langle \nu_{\rm sc}^A\rangle$ is the mean scattering frequency of energetic particles caused by gyroresonant interaction of particles with parallel-propagating Alfvén waves) and by small-scale flux ropes ($\langle \nu_{\rm sc}^{I1}\rangle$ and $\langle \nu_{\rm sc}^{I2}\rangle$ are the mean scattering frequencies of energetic particles interacting with multiple small-scale flux ropes). In our theory, the leading-order effect that contributes to energetic particle pitch-angle scattering is the variance in the magnetic mirroring force that particles encounter when interacting with numerous small-scale flux ropes (see discussion below Equation (62) in Section 9.2). Thus, the expressions for the flux-rope-induced particle scattering frequencies are

$$\langle \nu_{\rm sc}^{I1}\rangle = \frac{1}{5}\langle(\delta\nu_{\rm REF}^I)^2\rangle\tau_{\rm dec},$$

$$\langle \nu_{\rm sc}^{I2}\rangle = \frac{1}{7}\langle(\delta\nu_{\rm REF}^I)^2\rangle\tau_{\rm dec}. \quad (170)$$

In the last line of Equation (165), Equation (167), and the first line of D_{pp}^I in Equation (169) the matrix $\underline{\underline{\sigma}}^{\rm sh}$ represents the large-scale plasma shear-flow tensor (e.g., Earl et al. 1988), which can be expressed in index notation as

$$\sigma_{ij}^{\rm sh} = \frac{1}{2}\left(\frac{\partial U_{0i}}{\partial x_j} + \frac{\partial U_{0j}}{\partial x_i} - \frac{2}{3}\frac{\partial U_{0k}}{\partial x_k}\delta_{ij}\right). \quad (171)$$

Compared to le Roux et al. (2015a; see their Equations (55)–(56)), there are new energetic particle large-scale spatial advection and adiabatic energy change terms containing the average speeds $U_{p\mu}^I$ and $U_{\mu p}^I$ (first and second lines of Equation (168)), and the momentum diffusion coefficients D_{pp}^I are extended (see new additions to D_{pp}^I in the second line from the bottom of Equation (169)), all involving the effects of small-scale magnetic islands through the Fokker–Planck scattering coefficients $D_{p\mu}^I = D_{\mu p}^I$. Energetic particle large-scale spatial advection and adiabatic energy change terms containing the average speeds $U_{\rm RECU}^I$ and $U_{\rm REF}^I$ were defined previously in le Roux et al. (2015a) in their Equations (55)–(56), although

the expression for $U^I_{\rm RECU}$ is extended in this paper. The expanded speed expression $U^I_{\rm RECU}$ includes the effects of the parallel components of both the mean reconnection electric field in merging flux ropes and the mean acceleration of the flux-rope magnetic island flow and of the parallel components of the nonmotional electric field across special surfaces in the solar wind and of the acceleration of the solar wind flow.

Assuming $U^I_{\rm REF} = \langle \nu^I_{\rm REF}\rangle = 0$, one can express the Parker transport Equation (169) in conservation form as a Gleeson–Axford transport equation

$$\begin{aligned}&\frac{\partial f_0}{\partial t} + \nabla\cdot(C[\boldsymbol{U}_0 + (U^I_{\rm RECU} + U^I_{p\mu})\boldsymbol{b}_0]f_0)\\ &\quad + \langle \nabla\cdot(C\delta\boldsymbol{U}_I f_0)\rangle - \kappa_\parallel^{\rm eff1}\boldsymbol{b}_0\boldsymbol{b}_0\cdot\nabla f_0)\\ &\quad + \frac{1}{3p'^2}\frac{\partial}{\partial p'}(p'^3[\boldsymbol{U}_0\cdot\nabla + \langle\,\delta\boldsymbol{U}_I\cdot\nabla\rangle\\ &\quad - (U^I_{\rm RECU} - U^I_{p\mu})\boldsymbol{b}_0\cdot\nabla)]f_0)\\ &= \frac{1}{p'^2}\frac{\partial}{\partial p'}\left(p'^2 D^I_{pp}\frac{\partial f_0}{\partial p'}\right),\end{aligned} \tag{172}$$

where

$$C = -\frac{1}{3}\frac{p'}{f_0}\frac{\partial f_0}{\partial p'} \tag{173}$$

is the Compton–Getting factor for transforming the differential current density between inertial frames (e.g., Gleeson & Axford 1968). If we also put $U^I_{\rm RECU} = 0$, use the fact that $U^I_{p\mu}$ is independent of p in the nonlinear spatial transport limit of our theory, and assume that $\langle \nu^I_{\rm sc}\rangle \gg \langle \nu^A_{\rm sc}\rangle$ (pitch-angle scattering of energetic particles by magnetic islands dominates pitch-angle scattering by parallel-propagating Alfvén waves in the nonlinear transport limit of our theory as discussed in Section 15), an alternative conservation form of Equation (168) (Parker transport equation in conservation form) is

$$\begin{aligned}&\frac{\partial f_0}{\partial t} + \nabla\cdot[(\boldsymbol{U}_0 + U^I_{p\mu}\boldsymbol{b}_0)f_0] + \langle\nabla\cdot(\delta\boldsymbol{U}_I f_0)\rangle\\ &\quad - \frac{1}{3p^2}\frac{\partial}{\partial p}(p^3[\nabla\cdot\boldsymbol{U}_0 - \langle\nu^I_{\rm COM}\rangle + \nabla\cdot U^I_{p\mu}\boldsymbol{b}_0]f_0)\\ &\quad = \nabla\cdot(\kappa_\parallel^{\rm eff1}\boldsymbol{b}_0\boldsymbol{b}_0\cdot\nabla f_0) + \frac{1}{p^2}\frac{\partial}{\partial p}\left(p^2 D^I_{pp}\frac{\partial f_0}{\partial p}\right).\end{aligned} \tag{174}$$

D.1. Parallel Diffusion Induced by Fluctuating Magnetic Mirroring Forces in Small-scale Flux Ropes

When pitch-angle scattering of energetic particles is dominated by small-scale flux ropes rather than by Alfvén waves ($\langle\nu^I_{\rm sc}\rangle \gg \langle\nu^A_{\rm sc}\rangle$), the effective particle scattering frequency $\langle\nu^{\rm eff1(2)}_{\rm sc}\rangle$ in Equation (169) simplifies to $\langle\nu^{\rm eff1(2)}_{\rm sc}\rangle = 2\langle\nu^{I1(2)}_{\rm sc}\rangle$ with $\langle\nu^{I1(2)}_{\rm sc}\rangle$ defined by Equation (170). Then, the expression for the parallel diffusion coefficient is

$$\begin{aligned}\kappa_\parallel^{\rm eff1(2)} &\approx \frac{5(7)}{6}\frac{v^2}{\langle(\delta\nu^I_{\rm REF})^2\rangle\tau_{\rm dec}},\\ &\approx \frac{5(7)}{6C_\delta a}\frac{L_I^2}{\langle\delta B_I^2\rangle/B_0^2}\frac{1}{\tau_{\rm dec}},\end{aligned} \tag{175}$$

where we inserted the approximate expression for $\langle(\delta\nu^I_{\rm REF})^2\rangle$ given by Equation (140) in Appendix A, the ratio C_δ was introduced to enable the simplifying substitution $\langle[\delta(\delta B_I)]^2\rangle = C_\delta\langle\delta B_I^2\rangle$ (see Appendix A), and $a = 1/2$ for isotropic flux-rope turbulence in the 2D plane perpendicular to $\boldsymbol{B}_0$.

In the limit of slow diffusion ($\tau_c \ll \tau_D$, where $\tau_c = L_I/\langle\delta U_I^2\rangle^{1/2}$ is the mean magnetic island flow crossing time in the 2D plane perpendicular to the guide field and $\tau_D = L_{I\parallel}^2/\kappa_\parallel^{\rm eff1(2)}$ is the mean energy particle parallel diffusion crossing time of flux ropes in the guide field direction, approximately), when particles are advected with the magnetic island flow (see discussion below Equation (75) in Section 9.2) so that the particle decorrelation time is $\tau_{\rm dec} \approx \tau_c = L_I/\langle\delta U_I^2\rangle^{1/2}$, we find that

$$\kappa_\parallel^{\rm eff1(2)} \approx \frac{5(7)}{6C_\delta a}\frac{L_I\langle\delta U_I^2\rangle^{1/2}}{\langle\delta B_I^2\rangle/B_0^2}. \tag{176}$$

However, the condition for this expression to apply ($\tau_c \ll \tau_D$) requires that $\langle\delta B_I^2\rangle/B_0^2 \gg (5(7)/3)(L_I/L_{I\parallel})^2$. Since $L_{I\parallel}/L_I \approx 3$ in the solar wind near Earth (Weygand et al. 2011), the requirement is $\langle\delta B_I^2\rangle/B_0^2 \gg 0.19(0.26)$. Based on our observational estimate in Section 4 that $\langle\delta B_I^2\rangle/B_0^2 \approx 0.1$–$0.2$ in the solar wind near Earth (strong guide field limit), we conclude that the slow diffusion limit is probably not applicable in solar wind conditions near Earth.

In the opposite and more likely limit of fast diffusion ($\tau_D \ll \tau_c$), when $\tau_{\rm dec} \approx \sqrt{(\pi/2)\tau_c\tau_D}$ (see discussion below Equation (74) in Section 9.2), we have to solve a nonlinear expression for $\kappa_\parallel^{\rm eff1(2)}$, which yields

$$\begin{aligned}\kappa_\parallel^{\rm eff1(2)} &\approx \frac{100(196)}{36C_\delta^2 a^2\pi}\frac{L_I^3}{L_{I\parallel}^2}\frac{\langle\delta U_I^2\rangle^{1/2}}{(\langle\delta B_I^2\rangle/B_0^2)^2}\\ &= \frac{100(196)}{36C_\delta^2 a^2\pi}\frac{L_I^3}{L_{I\parallel}^2}\frac{(r_{\rm A}^I+1)^{3/2}(r_{\rm A}^I)^{1/2}V_{A0}}{(\epsilon_I/\epsilon_{B0})^{3/2}}.\end{aligned} \tag{177}$$

This implies that the scattering frequency of energetic particles by flux ropes $\langle\nu^{I1(2)}_{\rm sc}\rangle$ has the expression

$$\langle\nu^{I1(2)}_{\rm sc}\rangle \approx C_\delta^2\frac{12a^2\pi}{200(392)}\frac{v^2}{\langle\delta U_I^2\rangle^{1/2}}\frac{\langle\delta B_I^2\rangle^2/B_0^4}{L_I^3/L_{I\parallel}^2}, \tag{178}$$

resulting in an expression for the particle decorrelation time given by

$$\begin{aligned}\tau_{\rm dec} &\approx C_\delta\frac{6a\pi}{20(28)}\frac{L_{I\parallel}^2}{L_I}\frac{\langle\delta B_I^2\rangle/B_0^2}{\langle\delta U_I^2\rangle^{1/2}}\\ &= C_\delta\frac{6a\pi}{20(28)}\frac{1}{(r_{\rm A}^I+1)^{1/2}(r_{\rm A}^I)^{1/2}}\frac{L_{I\parallel}^2/L_I}{V_{A0}}\left(\frac{\epsilon_I}{\epsilon_{B_0}}\right)^{1/2}.\end{aligned} \tag{179}$$

In Equations (177) and (179) the parameter $r_{\rm A}^I = \langle\delta U_I^2\rangle/\langle\delta V_{AI}^2\rangle$ is the Alfvén ratio of the mean flux-rope kinetic energy over the mean flux-rope magnetic energy in the 2D plane perpendicular to $\boldsymbol{B}_0$ ($\langle\delta V_{AI}^2\rangle = \langle\delta B_I^2\rangle/4\pi\rho_0$), $V_{A0} = B_0/(4\pi\rho_0)^{1/2}$ is the Alfvén speed associated with the background/guide magnetic field, and $\epsilon_{B0} = B_0^2/8\pi$ is the energy density of the background/guide magnetic field. Thus, $\langle\delta B_I^2\rangle/B_0^2 = (\epsilon_I/\epsilon_{B_0})/(r_{\rm A}^I+1)$, and $\langle\delta U_I^2\rangle^{1/2} = (r_{\rm A}^I)^{1/2}(\langle\delta B_I^2\rangle^{1/2}/B_0)V_{A0}$.

D.2. Second-order Fermi Acceleration by Small-scale Flux Ropes in the Diffusion Approximation

Consider now the expressions for second-order Fermi acceleration in response to fluctuations in the magnetic field and plasma flow of the magnetic island component of small-scale flux ropes for each acceleration scenario. We find that

$$
\begin{aligned}
D_{pp}^{\rm COM} &= p^2\Bigg[\frac{2}{15}\langle(\delta\nu^I_{\rm COM})^2\rangle\tau_{\rm dec} \\
&\quad - \left(\frac{2}{5}\langle\delta\nu^I_{\rm COM}\delta\nu^I_{\rm REF}\rangle\right)^2\tau^2_{\rm dec}\frac{\kappa_\parallel^{\rm eff1}}{v^2}\Bigg] \\
&\approx p^2 C_\delta\frac{2a}{15}\left[\frac{r_{\rm A}^I - 1/4(\sigma_C^I)^2(r_{\rm A}^I+1)^2}{r_{\rm A}^I+1}\right]\frac{V_{A0}^2}{L_I^2}\frac{\epsilon_I}{\epsilon_{B_0}}\tau_{\rm dec}, \\
D_{pp}^{\rm INC} &= p^2\left[\frac{1}{5}\langle(\delta\nu^I_{\rm INC})^2\rangle\tau_{\rm dec} - \left(\frac{1}{5}\langle\delta\nu^I_{\rm INC}\delta\nu^I_{\rm REF}\rangle\right)^2\tau^2_{\rm dec}\frac{\kappa_\parallel^{\rm eff1}}{v^2}\right] \\
&\approx p^2 C_\delta\frac{2a}{5}\Bigg[\frac{(r_{\rm A}^I + 1/4(\sigma_C^I)^2(r_{\rm A}^I+1)^2)}{(r_{\rm A}^I+1)^3} \\
&\quad - \frac{1/12(1/2\sigma_C^I(r_{\rm A}^I+1)+(r_{\rm A}^I)^{1/2})^2}{(r_{\rm A}^I+1)^3}\Bigg]\frac{V_{A0}^2}{L_I^2}\left(\frac{\epsilon_I}{\epsilon_{B_0}}\right)^3\tau_{\rm dec}, \\
D_{pp}^{\rm ACC} &= p^2\frac{1}{3}\langle(\delta\nu^I_{\rm ACC})^2\rangle\tau_{\rm dec} \\
&\approx p^2\frac{a}{3}\frac{r_{\rm A}^I}{r_{\rm A}^I+1}\frac{V_{A0}^2}{L_{\rm Ir}^2}\left(\frac{U_0}{v}\right)^2\frac{\epsilon_I}{\epsilon_{B_0}}\tau_{\rm dec}, \\
D_{pp}^{\rm REC} &= p^2\frac{1}{3}\langle(\delta\nu^I_{\rm REC})^2\rangle\tau_{\rm dec} \\
&\approx p^2 C_\delta\frac{4a^2}{3}\left[\frac{r_{\rm A}^I - 1/4(\sigma_C^I)^2(r_{\rm A}^I+1)^2}{(r_{\rm A}^I+1)^2}\right] \\
&\quad\times\left(\frac{Z}{A}\right)^2\frac{V_{A0}^2}{d_{i/e}^2}\left(\frac{V_{A0}}{v}\right)^2\left(\frac{\epsilon_I}{\epsilon_{B_0}}\right)^2\tau_{\rm dec}.
\end{aligned}
\tag{180}
$$

These expressions have been derived in the nonlinear transport limit of our theory by assuming the strong scattering limit ($\tau_{\rm sc}^{\rm eff} \ll \tau_c$), fast diffusion ($\tau_D \ll \tau_c$), and that $\langle\nu^I_{\rm sc}\rangle \gg \langle\nu^A_{\rm sc}\rangle$ as estimated in Section 15. Accordingly, the expression for $\tau_{\rm dec}$ is determined by Equation (179).

In the case of $D_{pp}^{\rm COM}$ (combined energetic particle stochastic curvature drift and generalized betatron acceleration by compressible small-scale flux ropes), the second term in the first line of Equation (174), or equivalently the second term in the square brackets of the second line of Equation (174), represents the contribution of $D_{\mu p}^{\rm COM}$ in the diffusion approximation to the acceleration. The expression in square brackets in the second line predicts that $D_{pp}^{\rm COM} = 0$ if the Alfvén ratio $r_{\rm A}^I = 1$ and the normalized cross helicity $\sigma_C^I = \pm 1$ for the magnetic island component of small-scale flux ropes. This agrees with earlier kinetic theories for energetic particle interaction with 2D turbulence not based on focused transport theory (e.g., le Roux et al. 2004; le Roux & Webb 2007). The conditions for $D_{pp}^{\rm COM} = 0$ also correspond to the requirements for $D_{pp}^A = 0$ in kinetic theory for particle gyroresonant interaction with parallel-propagating Alfvén waves in the diffusion approximation (e.g., Schlickeiser 1989; le Roux & Webb 2007). In the Alfvén wave case $\sigma_C^A = \mp 1$ refers to Alfvén waves propagating forward or backward along the background magnetic field and $r_{\rm A}^A = 1$ holds for Alfvén waves. However, as discussed in Section 11, probably more appropriate values for small-scale magnetic island turbulence near 1 au are $r_{\rm A}^I \approx 0.1$ and $\sigma_C^I \approx 0.3$ based on N I MHD theory simulations of quasi-2D turbulence transport in the supersonic solar wind (Zank et al. 2017). Then, in the numerator of the expression in square brackets in the second line of Equation (174) the first term r_A^I dominates. Thus, at 1 au the contribution of $D_{\mu p}^I$ to second-order Fermi acceleration in $D_{pp}^{\rm COM}$ can be neglected.

Consider the second stochastic acceleration case $D_{pp}^{\rm INC}$ in Equation (174) (stochastic curvature drift and generalized betatron acceleration by incompressible small-scale flux ropes), where a new second term appears in the square brackets in the first line of $D_{pp}^{\rm INC}$ and in the square brackets in the second and third lines of $D_{pp}^{\rm INC}$ owing to $D_{\mu p}^{\rm INC}$. As before, when $r_{\rm A}^I \approx 0.1$ and $\sigma_C^I \approx 0.3$, the first term r_A^I in the numerator of the square brackets dominates, so that the contribution of $D_{\mu p}^{\rm INC}$ to $D_{pp}^{\rm INC}$ is negligible. The last two stochastic acceleration cases in Equation (174) ($D_{pp}^{\rm ACC}$ and $D_{pp}^{\rm REC}$) do not contain new contributions from $D_{\mu p}^I$. Nonetheless, $D_{pp}^{\rm REC} = 0$ if $r_{\rm A}^I = 1$ and $\sigma_C^I = \pm 1$, just as was found on the focused transport level (see Equation (72)). Also here the numerator of the expression in square brackets can be approximated by the first term r_A^I assuming $r_{\rm A}^I \approx 0.1$ and $\sigma_C^I \approx 0.3$.

D.3. Energetic Particle Advection and Adiabatic Energy Changes Induced by Small-scale Flux Ropes in the Diffusion Approximation

Consider the new advection speed terms $U_{p\mu}^I = U_{\mu p}^I$ in the Parker transport Equation (168) generated by fluctuations in small-scale flux-rope properties. The expressions of these terms, which depend on whether we consider stochastic curvature drift and generalized betatron acceleration in compressible or incompressible small-scale flux-rope turbulence, are

$$
\begin{aligned}
U_{\mu p}^{\rm COM} &= \frac{2}{5}\langle\delta\nu^I_{\rm REF}\delta\nu^I_{\rm COM}\rangle\tau_{\rm dec}\frac{3\kappa_\parallel^{\rm eff1}}{v} \\
&= U_{p\mu}^{\rm COM} = -\frac{1}{2}\sigma_C^I(r_{\rm A}^I+1)V_{A0} \\
U_{\mu p}^{\rm INC} &= -\frac{1}{5}\langle\delta\nu^I_{\rm REF}\delta\nu^I_{\rm INC}\rangle\tau_{\rm dec}\frac{3\kappa_\parallel^{\rm eff1}}{v} \\
&= U_{p\mu}^{\rm INC} = \frac{1}{2}\left[\frac{1/2\sigma_C^I(r_{\rm A}^I+1)+(r_{\rm A}^I)^{1/2}}{r_{\rm A}^I+1}\right]\frac{\epsilon_I}{\epsilon_{B_0}}V_{A0}.
\end{aligned}
\tag{181}
$$

If one assumes values for compressible small-scale flux ropes also applicable to parallel Alfvén waves propagating mainly along or in the opposite direction of the magnetic field ($r_{\rm A}^I = 1$ and $\sigma_C^I = \mp 1$) and applies the limit that $\langle\nu^I_{\rm sc}\rangle \gg \langle\nu^A_{\rm sc}\rangle$ (particle scattering by small-scale flux ropes dominates scattering by Alfvén waves), we find $U_{p\mu}^{\rm COM} = U_{\mu p}^{\rm COM} = \pm V_{A0}$ in the nonlinear spatial transport limit of our theory. This suggests that energetic particles tend to be advected at the background

Alfvén speed in the guide field direction by small-scale flux ropes just as one would get for energetic particle gyroresonant interaction with parallel-propagating Alfvén waves. However, inserting the more appropriate values $r_{\rm A}^I \approx 0.1$ and $\sigma_C^I \approx 0.3$ at 1 au (Zank et al. 2017), we find that $U_{p\mu}^{\rm COM} = U_{\mu p}^{\rm COM} \approx -0.17 V_{A0} \approx -0.017 U_0 \approx -7\,{\rm km\,s^{-1}}$, which is considerably less than the background Alfvén speed (weak advection effect). Inserting the same more plausible values for r_A^I and σ_C^I into the advection speed expression associated with incompressible flux ropes (last line of Equation (181)) and specifying $\langle \delta B_I^2 \rangle / B_0^2 \approx 0.1$ (strong guide field limit appropriate at 1 au), the advection speed drops by an order of magnitude compared to the compressible flux-rope limit, becoming insignificant.

Let us also analyze the advection speed $U_{\rm RECU}^I$ (see Equation (169)) imparted to energetic particles when these particles respond to the average properties of numerous small-scale flux ropes. Since we estimated at 1 au that $\langle \nu_{\rm REC}^I \rangle \gg \langle \nu_{\rm ACC}^I \rangle$ in Section 10.1,

$$U_{\rm RECU}^I \approx \frac{3\kappa_\parallel^{\rm eff1}}{v} \langle \nu_{\rm REC} \rangle \approx \frac{100}{3\pi} \sigma_{\rm REC}^I r_{\rm A}^I \left[\left(\frac{L_I}{L_{I\parallel}} \right)^2 \frac{L_I}{d_i} \left(\frac{V_{A0}}{v} \right)^2 \frac{B_0}{\langle \delta B_I^2 \rangle^{1/2}} \right] V_{A0}. \quad (182)$$

Inserting the usual 1 au values as above, we find that $U_{\rm RECU}^I \approx 75.5 (V_{A0}/v)^2 V_{A0}$ for the most optimistic case when $\sigma_{\rm REC}^I \approx 1$ (all the parallel reconnection electric fields of merging flux ropes pointing in the same direction along the magnetic field). Then, for protons at 1 keV, $U_{\rm RECU}^I \approx 0.76 V_{A0}$. Because of the strong inverse speed dependence of the expression, already at ~10 keV, the advection speed drops to a value of $U_{\rm RECU}^I \approx 0.08 V_{A0} \approx 3\,{\rm km\,s^{-1}}$, indicating that at higher proton energies the advection speed will become insignificant.

Finally, there is the advection speed $U_{\rm REF}^I$ associated with the average mirroring force that particles encounter when crossing numerous small-scale flux ropes (see Equation (169)). The expression is

$$U_{\rm REF}^I = \frac{3\kappa_\parallel^{\rm eff1}}{v} \langle \nu_{\rm REF}^I \rangle \approx -\left[\frac{100}{3\pi} \sigma_{\rm REF}^I (r_{\rm A}^I)^{1/2} \frac{B_0^2}{\langle \delta B_I^2 \rangle} \right] V_{A0}. \quad (183)$$

Assuming that $\sigma_{\rm REF}^I \approx 1$, we find that $U_{\rm REF}^I \approx -34 V_{A0}$, thus yielding an unphysically large advection speed, much larger than the background Alfvén speed. A sensible advection speed $U_{\rm REC}^I < V_{A0}$ requires setting $\sigma_{\rm REF}^I \lesssim 0.03$, perhaps indicating the unlikeliness of energetic particles traversing numerous flux ropes experiencing a significant mean mirroring force. The rms of the magnetic island dynamic velocity $\langle \delta U_I^2 \rangle^{1/2} = [r_{\rm A}^I (\langle \delta B_I^2 \rangle / B_0^2) V_{A0}]^{1/2} \approx 4\,{\rm km\,s^{-1}}$ at 1 au. This value appears to be a sensible upper bound for the different flux-rope-induced advection velocities estimated above for energetic particles (except for the last case, which appears to be unphysical).

Appendix E
The N I MHD Transport Equation for the Magnetic Island Component of Small-scale Flux Ropes with Magnetic Island Growth/Damping Rates in the Diffusion Approximation

By inserting the moment expansion expression for the distribution function (Equation (164)) into the expression for $\gamma_I^{\rm coh}$ given by Equation (163) or Equation (52) (the damping rate for the magnetic island component of small-scale flux ropes associated with coherent particle acceleration) and integrating Equation (163) over all particle pitch angles, we find that

$$\gamma_I^{\rm coh}(\langle f \rangle) = -\frac{4\pi}{\epsilon_I} \int_0^\infty dp p^3 v \times \left[\frac{1}{3} \langle \nu_{\rm COM}^I \rangle (f_0(p) - f_2(p)) + \langle \nu_{\rm INC}^I \rangle f_2(p) + (\langle \nu_{\rm ACC}^I \rangle + \langle \nu_{\rm REC}^I \rangle) f_1(p) \right]. \quad (184)$$

More detailed expressions follow when inserting the expressions for the moments f_1 and f_2 (Equations ((166) and (167))) and for the coherent relative acceleration rates (see Equation (54) or Appendix A) into Equation (183). The damping rate expressions for each of the four coherent flux-rope acceleration cases are

$$\begin{aligned}
\gamma_{\rm COM}^{\rm coh}(\langle f \rangle) &= -\frac{4\pi}{\epsilon_I} \frac{\langle \nu_{\rm COM}^I \rangle}{3} \int_0^\infty dp p^3 v (f_0(p) - f_2(p)) \\
&= -\langle \nu_{\rm COM}^I \rangle \frac{P_c}{\epsilon_I} + \frac{1}{5} (\boldsymbol{b}_0 \boldsymbol{b}_0 : \underline{\underline{\sigma}}^{\rm sh} + \frac{1}{3} \langle \nu_{\rm COM}^I \rangle) \langle \nu_{\rm COM}^I \rangle \\
&\times \frac{\kappa_\parallel^{\rm eff2}(\epsilon_I)}{\epsilon_I} \left[\frac{4\pi}{3} \int_0^\infty dp \frac{p^4}{v} \frac{\partial f_0(p)}{\partial p} \right] \\
&\approx -\sigma_{\rm COM}^I \frac{(r_{\rm A}^I)^{1/2}}{(r_{\rm A}^I + 1)^{1/2}} \frac{V_{A0}}{L_I} \frac{\epsilon_{B_0}^{1/2}}{\epsilon_I^{1/2}} \frac{P_c}{\epsilon_{B_0}} \\
&+ \frac{1}{C_\delta^2 a^2} \frac{49}{45\pi} \left[\boldsymbol{b}_0 \boldsymbol{b}_0 : \underline{\underline{\sigma}}^{\rm sh} + \frac{1}{3} \sigma_{\rm COM}^I \left(\frac{r_{\rm A}^I}{r_{\rm A}^I + 1} \right)^{1/2} \right. \\
&\times \left. \frac{V_{A0}}{L_I} \frac{\epsilon_I^{1/2}}{\epsilon_{B_0}^{1/2}} \right] \sigma_{\rm COM}^I r_{\rm A}^I (r_{\rm A}^I + 1) \left(\frac{L_I}{L_{I\parallel}} \right)^2 \\
&\times \left(\frac{\epsilon_{B_0}}{\epsilon_I} \right)^2 \frac{1}{\epsilon_{B_0}} \left[\frac{4\pi}{3} \int_0^\infty dp p^4 v \left(\frac{V_{A0}}{v} \right)^2 \frac{\partial f_0(p)}{\partial p} \right],
\end{aligned} \quad (185)$$

$$\begin{aligned}
\gamma_{\rm INC}^{\rm coh}(\langle f \rangle) &= -\frac{4\pi}{\epsilon_I} \langle \nu_{\rm INC}^I \rangle \int_0^\infty dp p^3 v f_2(p) \\
&= -\frac{3}{5} (\boldsymbol{b}_0 \boldsymbol{b}_0 : \underline{\underline{\sigma}}^{\rm sh} - \langle \nu_{\rm INC}^I \rangle) \langle \nu_{\rm INC}^I \rangle \frac{\kappa_\parallel^{\rm eff2}(\epsilon_I)}{\epsilon_I} \\
&\times \left[\frac{4\pi}{3} \int_0^\infty dp \frac{p^4}{v} \frac{\partial f_0(p)}{\partial p} \right] \\
&\approx -\frac{1}{C_\delta^2 a^2} \frac{49}{15\pi} \left[\boldsymbol{b}_0 \boldsymbol{b}_0 : \underline{\underline{\sigma}}^{\rm sh} \frac{\epsilon_{B_0}}{\epsilon_I} \right. \\
&- \left. \sigma_{\rm INC}^I \frac{(r_{\rm A}^I)^{1/2}}{(r_{\rm A}^I + 1)^{3/2}} \frac{V_{A0}}{L_I} \frac{\epsilon_I^{1/2}}{\epsilon_{B_0}^{1/2}} \right] \sigma_{\rm INC}^I r_{\rm A}^I \left(\frac{L_I}{L_{I\parallel}} \right)^2 \\
&\times \frac{1}{\epsilon_{B_0}} \left[\frac{4\pi}{3} \int_0^\infty dp p^4 v \left(\frac{V_{A0}}{v} \right)^2 \frac{\partial f_0(p)}{\partial p} \right],
\end{aligned} \quad (186)$$

$$\gamma_{\rm ACC}^{\rm coh}(\langle f\rangle) = -\frac{4\pi}{\epsilon_I}\int_0^\infty dpp^3 v\,\langle \nu_{\rm ACC}^I\rangle f_1(p)$$
$$= 3\langle \overline{\nu}_{\rm ACC}^I\rangle \frac{\kappa_\parallel^{\rm eff1}}{\epsilon_I}(\boldsymbol{b}_0\cdot\nabla)\left[\frac{4\pi}{3}\int_0^\infty dpp^3\frac{U_0}{v}f_0(p)\right]$$
$$+ 3\left[\langle \overline{\nu}_{\rm ACC}^I\rangle - \frac{1}{U_0}\left(\frac{d\boldsymbol{U}_0}{dt} - \frac{v}{p}q\boldsymbol{E}_{\rm surf}\right)\cdot\boldsymbol{b}_0\right]\langle \overline{\nu}_{\rm ACC}^I\rangle\frac{\kappa_\parallel^{\rm eff1}}{\epsilon_I}$$
$$\times\left[\frac{4\pi}{3}\int_0^\infty dp\frac{p^4}{v}\left(\frac{U_0}{v}\right)^2\frac{\partial f_0(p)}{\partial p}\right]$$
$$\approx \frac{1}{C_\delta^2 a^2}\frac{25}{3\pi}\sigma_{\rm ACC}^I r_{\rm A}^I(r_{\rm A}^I+1)^{1/2}V_{A0}\frac{L_I^3}{L_{\rm Ir}L_\parallel^2}\left(\frac{\epsilon_{B_0}}{\epsilon_I}\right)^{3/2}$$
$$\times\frac{1}{\epsilon_{B_0}}(\boldsymbol{b}_0\cdot\nabla)\times\left[\frac{4\pi}{3}\int_0^\infty dpp^3 v\frac{U_0}{v}\frac{V_{A0}}{v}f_0(p)\right]$$
$$\approx -\frac{1}{C_\delta^2 a^2}\frac{25}{3\pi}\sigma_{\rm ACC}^I r_{\rm A}^I(r_{\rm A}^I+1)^{1/2}\frac{L_I^3}{L_{\rm Ir}L_\parallel^2}\frac{\epsilon_{B_0}^{1/2}}{\epsilon_I^{1/2}}$$
$$\times\left[\frac{1}{U_0}\left(\frac{d\boldsymbol{U}_0}{dt} - \frac{v}{p}q\boldsymbol{E}_{\rm surf}\right)\cdot\boldsymbol{b}_0\frac{\epsilon_{B_0}}{\epsilon_I} - \sigma_{\rm ACC}^I\frac{(r_{\rm A}^I)^{1/2}}{r_{\rm A}^I+1}\frac{V_{A0}}{L_I}\frac{L_I}{L_{\rm Ir}}\right]$$
$$\times\left[\frac{4\pi}{3}\int_0^\infty dpp^4 v\left(\frac{U_0}{v}\right)^2\left(\frac{V_{A0}}{v}\right)^2\frac{\partial f_0(p)}{\partial p}\right], \quad (187)$$

$$\gamma_{\rm REC}^{\rm coh}(\langle f\rangle) = -\frac{4\pi}{\epsilon_I}\int_0^\infty dpp^3 v\,\langle \nu_{\rm REC}^I\rangle f_1(p)$$
$$= 3\langle \overline{\nu}_{\rm REC}^I\rangle \frac{\kappa_\parallel^{\rm eff1}}{\epsilon_I}(\boldsymbol{b}_0\cdot\nabla)\left[\frac{4\pi}{3}\int_0^\infty dpp^3\frac{V_{A0}}{v}f_0(p)\right]$$
$$+ 3\left[\langle \overline{\nu}_{\rm REC}^I\rangle - \frac{1}{V_{A0}}\left(\frac{d\boldsymbol{U}_0}{dt} - \frac{v}{p}q\boldsymbol{E}_{\rm surf}\right)\cdot\boldsymbol{b}_0\right]\langle \overline{\nu}_{\rm REC}^I\rangle\frac{\kappa_\parallel^{\rm eff1}}{\epsilon_I}$$
$$\times\left[\frac{4\pi}{3}\int_0^\infty dp\frac{p^4}{v}\left(\frac{V_{A0}}{v}\right)^2\frac{\partial f_0(p)}{\partial p}\right]$$
$$\approx C_\delta^{-2}\frac{100}{3\pi}\sigma_{\rm REC}^I\frac{q}{|q|}\frac{Z}{A}r_{\rm A}^I(r_{\rm A}^I+1)^{1/2}V_{A0}\frac{L_I^3}{d_{i/e}L_\parallel^2}\left(\frac{\epsilon_{B_0}}{\epsilon_I}\right)^{3/2}$$
$$\times\frac{(\boldsymbol{b}_0\cdot\nabla)}{\epsilon_{B_0}}\left[\frac{4\pi}{3}\int_0^\infty dpp^3 v\left(\frac{V_{A0}}{v}\right)^2 f_0(p)\right]$$
$$- C_\delta^{-2}\frac{100}{3\pi}\sigma_{\rm REC}^I\frac{q}{|q|}\frac{Z}{A}r_{\rm A}^I(r_{\rm A}^I+1)^{1/2}\frac{L_I^3}{d_{i/e}L_\parallel^2}\left(\frac{\epsilon_{B_0}}{\epsilon_I}\right)^{1/2}$$
$$\times\left[\frac{1}{V_{A0}}\left(\frac{d\boldsymbol{U}_0}{dt} - \frac{v}{p}q\boldsymbol{E}_{\rm surf}\right)\cdot\boldsymbol{b}_0\frac{\epsilon_{B_0}}{\epsilon_I}\right.$$
$$\left. - \sigma_{\rm REC}^I\frac{q}{|q|}\frac{(r_{\rm A}^I)^{1/2}}{r_{\rm A}^I+1}\frac{L_I}{d_{i/e}}\frac{V_{A0}}{L_I}\right]$$
$$\times\frac{1}{\epsilon_{B_0}}\left[\frac{4\pi}{3}\int_0^\infty dpp^4 v\left(\frac{V_{A0}}{v}\right)^4\frac{\partial f_0(p)}{\partial p}\right], \quad (188)$$

where $P_c = (4\pi/3)\int_0^\infty dpp^3 v f_0(p)$ is the energetic particle pressure, $\langle \nu_{\rm ACC}^I\rangle = (U_0/v)\langle \overline{\nu}_{\rm ACC}^I\rangle$, and $\langle \nu_{\rm REC}^I\rangle = (V_{A0}/v)\langle \overline{\nu}_{\rm REC}^I\rangle$. As before, $\tau_D \ll t_c$, and $\langle \nu_{\rm sc}^I\rangle \gg \langle \nu_{\rm sc}^A\rangle$.

Similarly, by inserting the moment expansion expression (164) for the distribution function and the expressions for $D_{p\mu}^I$ and D_{pp}^I, given by Equations (62), (66), (69), and (72), into the expression for $\gamma_I^{\rm stoch}$ given by Equation (53) (the damping rate for small-scale flux ropes associated with energetic particle stochastic acceleration in response to fluctuations in flux-rope properties), integrating Equation (53) over all particle pitch angles, and finally inserting the expressions for the moments $f_1(p)$ and $f_2(p)$ given by Equations (166) and (167) into Equation (53), we find that the flux-rope damping rates for the four flux-rope acceleration cases are

$$\gamma_{\rm COM}^{\rm stoch}(\langle f\rangle) = \frac{2\pi}{\epsilon_I}\frac{48}{15}\int_0^\infty dpp^3 v\,\langle \delta\nu_{\rm COM}^I\delta\nu_{\rm REF}^I\rangle\tau_{\rm dec}f_1(p)$$
$$+\frac{2\pi}{\epsilon_I}\frac{16}{15}\int_0^\infty dpp^4 v\,\langle(\delta\nu_{\rm COM}^I)^2\rangle\tau_{\rm dec}\frac{\partial f_0(p)}{\partial p}$$
$$= \frac{2\pi}{\epsilon_I}\frac{8}{15}\int_0^\infty dpp^2 v\left(p\frac{V_{A0}}{v}\right)[-3\sigma_C^I(r_{\rm A}^I+1)f_1(p)$$
$$+ 2r_{\rm A}^I\left(p\frac{V_{A0}}{v}\right)\frac{\partial f_0(p)}{\partial p}]T_{\mu\mu}(\epsilon_I)$$
$$= +\frac{1}{2}\sigma_C^I(r_{\rm A}^I+1)V_{A0}\frac{\epsilon_{B_0}}{\epsilon_I}\frac{1}{\epsilon_I}[(\boldsymbol{b}_0\cdot\nabla)P_c$$
$$-\left(\frac{d\boldsymbol{U}_0}{dt} - \frac{v}{p}q\boldsymbol{E}_{\rm surf}\right)\cdot\boldsymbol{b}_0\frac{4\pi}{3}\int_0^\infty dp\frac{p^4}{v}\frac{\partial f_0(p)}{\partial p}]$$
$$+ C_\delta\frac{2a}{5}\frac{V_{A0}^2}{L_I^2}\tau_{\rm dec}\left[\frac{r_{\rm A}^I - 1/4(\sigma_C^I)^2(r_{\rm A}^I+1)^2}{r_{\rm A}^I+1}\right]$$
$$\times\frac{1}{\epsilon_{B_0}}\left[\frac{4\pi}{3}\int_0^\infty dpp^4 v\frac{\partial f_0(p)}{\partial p}\right], \quad (189)$$

where $T_{\mu\mu}(\epsilon_I)$ is defined by Equation (64);

$$\gamma_{\rm INC}^{\rm stoch}(\langle f\rangle) = -\frac{2\pi}{\epsilon_I}\frac{8}{5}\int_0^\infty dpp^3 v\,\langle \delta\nu_{\rm INC}^I\delta\nu_{\rm REF}^I\rangle\tau_{\rm dec}f_1(p)$$
$$+\frac{2\pi}{\epsilon_I}\frac{8}{5}\int_0^\infty dpp^4 v\,\langle(\delta\nu_{\rm INC}^I)^2\rangle\tau_{\rm dec}\frac{\partial f_0(p)}{\partial p}$$
$$= \frac{2\pi}{\epsilon_I}\frac{8}{5}\int_0^\infty dpp^2 v\left(p\frac{V_{A0}}{v}\right)[((r_{\rm A}^I)^{1/2}$$
$$+ 1/2\sigma_C^I(r_{\rm A}^I+1))\overline{T}_{p\mu}^{\rm INC}(\epsilon_I)f_1(p)$$
$$+\left(p\frac{V_{A0}}{v}\right)(r_{\rm A}^I+1/4(\sigma_C^I)^2(r_{\rm A}^I+1)^2)\overline{T}_{pp}^{\rm INC}(\epsilon_I)\frac{\partial f_0(p)}{\partial p}]$$
$$= -V_{A0}\left[\frac{(r_{\rm A}^I)^{1/2} + 1/2\sigma_C^I(r_{\rm A}^I+1)}{r_{\rm A}^I+1}\right]\frac{1}{\epsilon_{B_0}}[(\boldsymbol{b}_0\cdot\nabla)P_c$$
$$-\left(\frac{d\boldsymbol{U}_0}{dt} - \frac{v}{p}e\boldsymbol{E}_{\rm surf}\right)\cdot\boldsymbol{b}_0\frac{4\pi}{3}\int_0^\infty dp\frac{p^4}{v}\frac{\partial f_0(p)}{\partial p}]$$
$$+ C_\delta\frac{6a}{5}\frac{V_{A0}^2}{L_I^2}\left(\frac{\epsilon_I}{\epsilon_{B_0}}\right)^2\tau_{\rm dec}\left[\frac{r_{\rm A}^I + 1/4(\sigma_C^I)^2(r_{\rm A}^I+1)^2}{(r_{\rm A}^I+1)^3}\right.$$
$$\left. - \frac{1/6((r_{\rm A}^I)^{1/2} + 1/2\sigma_C^I(r_{\rm A}^I+1))^2}{(r_{\rm A}^I+1)^3}\right]\frac{1}{\epsilon_{B_0}}\left[\frac{4\pi}{3}\int_0^\infty dpp^4 v\frac{\partial f_0(p)}{\partial p}\right], \quad (190)$$

where in the third and fourth lines of $\gamma_{\rm INC}^{\rm stoch}(\langle f\rangle)$, $\overline{T}_{\mu p}^{\rm INC}(\epsilon_I) = (1/(r_{\rm A}^I+1))(\epsilon_I/\epsilon_{B_0})T_{\mu\mu}(\epsilon_I)$ and $\overline{T}_{pp}^{\rm INC}(\epsilon_I) = C_\delta(2/(r_{\rm A}^I+1)^2)(\epsilon_I/\epsilon_{B_0})^2 T_{\mu\mu}(\epsilon_I)$;

$$\gamma_{\rm ACC}^{\rm stoch}(\langle f\rangle) = \frac{2\pi}{\epsilon_I} 2\int_0^\infty dpp^3 \nu(\langle \nu_{\rm ACC}^I \nu_{\rm REF}^I\rangle + 2\langle(\delta\nu_{\rm ACC}^I)^2\rangle)\tau_{\rm dec} f_2(p)$$
$$+ \frac{2\pi}{\epsilon_I}\frac{2}{3}\int_0^\infty dpp^4 \nu \langle(\delta\nu_{\rm ACC}^I)^2\rangle \tau_{\rm dec}\frac{\partial f_0(p)}{\partial p}$$
$$= \frac{2\pi}{\epsilon_I} 2\int_0^\infty dpp^3\nu\left(\frac{V_{A0}}{v}\right)^2 C_\delta^{-1} r_{\rm A}^I \overline{T}_{\mu p}^{\rm ACC}(\epsilon_I)$$
$$\times\left[2f_2(p) + \frac{1}{3}p\frac{\partial f_0(p)}{\partial p}\right]$$
$$= C_\delta^{-1} r_{\rm A}^I \frac{14}{5} U_0 V_{A0}\left(\frac{L_I}{L_{\rm Ir}}\right)^2 \boldsymbol{b}_0\boldsymbol{b}_0 : \underline{\sigma}^{\rm sh}\frac{\epsilon_{B_0}}{\epsilon_I}\frac{1}{\epsilon_{B_0}}$$
$$\times\left[\frac{4\pi}{3}\int_0^\infty dp\frac{p^4}{v}\frac{U_0}{v}\frac{V_{A0}}{v}\frac{\partial f_0(p)}{\partial p}\right]$$
$$+ a\frac{r_{\rm A}^I}{r_{\rm A}^I+1}\frac{V_{A0}^2}{L_{\rm Ir}^2}U_0^2\frac{\tau_{\rm dec}}{\epsilon_{B_0}}\left[\frac{4\pi}{3}\int_0^\infty dp\frac{p^4}{v}\frac{\partial f_0(p)}{\partial p}\right], \quad (191)$$

where in the third and fourth lines of $\gamma_{\rm ACC}^{fluc}(\langle f\rangle)$, $\overline{T}_{p\mu}^{\rm ACC}(\epsilon_I) = C_\delta 4(U_0/v)^2(L_I/L_{\rm Ir})^2 T_{\mu\mu}(\epsilon_I)$;

$$\gamma_{\rm REC}^{\rm stoch}(\langle f\rangle) = \frac{2\pi}{\epsilon_I} 2\int_0^\infty dpp^3\nu(\langle\delta\nu_{\rm REC}^I\delta\nu_{\rm REF}^I\rangle$$
$$+ 2\langle(\delta\nu_{\rm REC}^I)^2\rangle)\tau_{\rm dec} f_2(p) + \frac{2\pi}{\epsilon_I}\frac{2}{3}\int_0^\infty dpp^4\nu\langle(\delta\nu_{\rm REC}^I)^2\rangle\tau_{\rm dec}\frac{\partial f_0(p)}{\partial p}$$
$$= -\frac{2\pi}{\epsilon_I}2\int_0^\infty dpp^2\nu\left(p\frac{V_{A0}}{v}\right)[(C_\delta^{-1/2}((r_{\rm A}^I)^{1/2}$$
$$+1/2\sigma_C^I(r_{\rm A}^I+1)) - 8a\frac{r_{\rm A}^I - 1/4(\sigma_C^I)^2(r_{\rm A}^I+1)^2}{(r_{\rm A}^I+1)^{1/2}}\frac{q}{|q|}$$
$$\times\frac{Z}{A}\left(\frac{V_{A0}}{v}\right)^2\frac{L_I}{d_{i/e}}\left(\frac{\epsilon_I}{\epsilon_{B_0}}\right)^{1/2}\overline{T}_{\mu p}^{\rm REC}(\epsilon_I)2f_2(p)$$
$$-\frac{1}{3}\left(p\frac{V_{A0}}{v}\right)(r_{\rm A}^I - 1\Big/4(\sigma_C^I)^2(r_{\rm A}^I+1)^2)\overline{T}_{pp}^{\rm REC}(\epsilon_I)\frac{\partial f_0(p)}{\partial p}\Bigg]$$
$$= -\frac{7}{5}\frac{1}{(r_{\rm A}^I+1)^{1/2}}\frac{q}{|q|}\frac{Z}{A}V_{A0}^2\frac{L_I}{d_{i/e}}\left(\frac{\epsilon_{B_0}}{\epsilon_I}\right)^{1/2}\boldsymbol{b}_0\boldsymbol{b}_0 : \underline{\sigma}^{\rm sh}$$
$$\times\frac{1}{\epsilon_{B_0}}\left[\frac{4\pi}{3}\int_0^\infty dp\frac{p^4}{v}(C_\delta^{-1/2}((r_{\rm A}^I)^{1/2} + 1/2\sigma_C^I(r_{\rm A}^I+1))\right.$$
$$- 8a\frac{r_{\rm A}^I - 1/4(\sigma_C^I)^2(r_{\rm A}^I+1)^2}{(r_{\rm A}^I+1)^{1/2}}\frac{q}{|q|}$$
$$\left.\times\frac{Z}{A}\left(\frac{V_{A0}}{v}\right)^2\frac{L_I}{d_{i/e}}\left(\frac{\epsilon_I}{\epsilon_{B_0}}\right)^{1/2}\right)\frac{\partial f_0(p)}{\partial p}\Bigg]$$
$$+ C_\delta\frac{4a^2}{(r_{\rm A}^I+1)^2}\left(\frac{Z}{A}\right)^2\frac{V_{A0}^2}{L_I^2}\left(\frac{L_I}{d_{i/e}}\right)^2$$
$$\times (r_{\rm A}^I - 1/4(\sigma_C^I)^2(r_{\rm A}^I+1)^2)V_{A0}^2\tau_{\rm dec}$$
$$\times\frac{1}{\epsilon_{B_0}}\left[\frac{4\pi}{3}\int_0^\infty dp\frac{p^4}{v}\frac{\partial f_0(p)}{\partial p}\right], \quad (192)$$

where in the fourth and fifth lines of $\gamma_{\rm REC}^{fluc}(\langle f\rangle)$, $\overline{T}_{p\mu}^{\rm REC}(\epsilon_I) = (2/(r_{\rm A}^I+1)^{1/2})(q/|q|)(Z/A)\quad(V_{A0}/v)(L_I/d_{i/e})$ $(\epsilon_I/\epsilon_{B_0})^{1/2}T_{\mu\mu}(\epsilon_I)$ and $\overline{T}_{pp}^{\rm REC}(\epsilon_I) = (16/(r_{\rm A}^I+1))\quad(Z/A)^2$ $(V_{A0}/v)^2(L_I/d_{i/e})^2\ (\epsilon_I/\epsilon_{B_0})T_{\mu\mu}(\epsilon_I)$. The final expressions presented for all the flux-rope damping rates in this section were derived assuming strong scattering $\tau_{\rm sc}^{\rm eff} \ll \tau_c$, fast diffusion ($\tau_D \ll \tau_c$), and that $\langle\nu_{\rm sc}^I\rangle \gg \langle\nu_{\rm sc}^A\rangle$. Accordingly, the energetic particle decorrelation timescale $\tau_{\rm dec}$ is defined by expression (179).

ORCID iDs

J. A. le Roux https://orcid.org/0000-0001-9199-2890
G. P. Zank https://orcid.org/0000-0002-4642-6192
O. V. Khabarova https://orcid.org/0000-0002-3230-2033

References

Adhikari, L., Zank, G. P., Hunana, P., et al. 2017, ApJ, 841, 85
Ambrosiano, J., Matthaeus, W. H., Goldstein, M. L., & Plante, D. 1988, JGR, 93, 14383
Antecki, T., Schlickeiser, R., & Zhang, M. 2013, ApJ, 764, 89
Bian, N. H., & Kontar, E. P. 2013, PhRvL, 110, 151101
Bieber, J. W., Matthaeus, W. H., Smith, C. W., et al. 1994, ApJ, 420, 294
Bieber, J. W., Wanner, W., & Matthaeus, W. H. 1996, JGR, 101, 2511
Birn, J., Hesse, M., & Schindler, K. 1989, JGR, 94, 241
Bogdan, T. J., Lee, M. A., & Schneider, P. 1991, JGR, 96, 61
Campeanu, A., & Schlickeiser, R. 1992, A&A, 263, 413
Cartwright, M. L., & Moldwin, M. B. 2010, JGRA, 115, A08102
Dahlin, J. T., Drake, J. F., & Swisdak, M. 2014, PhPl, 21, 092304
Dahlin, J. T., Drake, J. F., & Swisdak, M. 2016, PhPl, 23, 120704
Dahlin, J. T., Drake, J. F., & Swisdak, M. 2017, PhPl, 24, 092110
Dayeh, M. A., Desai, M. I., Dwyer, J. R., et al. 2009, ApJ, 693, 1588
de Gouveia dal Pino, E. M., & Lazarian, A. 2005, A&A, 441, 845
Dmitruk, P., & Matthaeus, W. H. 2006, JGR, 111, A12110
Dmitruk, P., Matthaeus, W. H., & Seenu, N. 2004, ApJ, 617, 667
Drake, J. F., Opher, M., Swisdak, M., & Chamoun, J. N. 2010, ApJ, 709, 963
Drake, J. F., Swisdak, M., Che, H., & Shay, M. A. 2006, Natur, 443, 553
Drake, J. F., Swisdak, M., & Fermo, R. 2013, ApJL, 763, L5
Dröge, W. 2005, AdSpR, 35, 532
Earl, J. A., Jokipii, J. R., & Morfill, G. 1988, ApJL, 331, L91
Eriksson, S., Lapenta, G., Newman, D. L., et al. 2015, ApJ, 805, 43
Eyink, G. L. 2015, ApJ, 807, 137
Fermo, R. L., Drake, J. F., & Swisdak, M. 2010, PhPl, 17, 010702
Fichthner, H., le Roux, J. A., Mall, U., & Rucinski, D. 1996, A&A, 314, 650
Fisk, L. A. 1976, JGR, 81, 4633
Fisk, L. A., & Gloeckler, G. 2006, ApJL, 640, L79
Fisk, L. A., & Gloeckler, G. 2008, ApJ, 686, 1466
Fisk, L. A., & Gloeckler, G. 2014, JGRA, 119, 8733
Fisk, L. A., Gloeckler, G., & Schwadron, N. A. 2010, ApJ, 720, 533
Forman, M. A., Wicks, R. T., & Horbury, T. S. 2011, ApJ, 733, 76
Gray, P. C., & Matthaeus, W. R. 1992, in AIP Conf. Proc. 261, Particle Acceleration in Cosmic Plasmas, ed. G. P. Zank & T. K. Gaisser (Melville, NY: AIP), 261
Giacalone, J. 2005, ApJL, 628, L37
Gleeson, L. J., & Axford, W. I. 1968, Ap&SS, 2, 431
Goldreich, P., & Sridhar, S. 1995, ApJ, 438, 763
Greco, A., Matthaeus, W. H., Servidio, S., Chuychai, P., & Dmitruk, P. 2009, ApJL, 691, L111
Guidoni, S. E., DeVore, C. R., Karpen, J. T., & Lynch, B. J. 2016, ApJ, 820, 60
Guo, F., Li, X., Li, H., et al. 2016, ApJL, 818, L9
Hill, M. E., & Hamilton, D. C. 2010, in AIP Conf. Proc. 1302, Pickup Ions throughout the Heliosphere and Beyond, ed. J. A. le Roux et al. (Melville, NY: AIP), 58
Horbury, T. S., Forman, M., & Oughton, S. 2008, PhRvL, 101, 17500
Hunana, P., & Zank, G. P. 2010, ApJ, 718, 148
Isenberg, P. A. 1987, JGR, 92, 1067
Khabarova, O. V., & Zank, G. P. 2017, ApJ, 843, 4
Khabarova, O. V., Zank, G. P., Li, G., et al. 2015, ApJ, 808, 181
Khabarova, O. V., Zank, G. P., Li, G., et al. 2016, ApJ, 827, 122
Kóta, J. 1977, Proc. ICRC (Plovdiv), 11, 186
Kóta, J., Manchester, W. B., Jokipii, J. R., de Zeew, D. L., & Gombosi, T. I. 2005, in AIP Conf. Proc. 781, The Physics of Collisionless Shocks, ed. G. Li, G. P. Zank, & C. T. Russel (Melville, NY: AIP), 201
Kulsrud, R. 1983, in Handbook of Plasma Physics, ed. M. N. Rosenbluth & R. Z. Sagdeev (New York: North-Holland), 115
le Roux, J. A., & Webb, G. M. 2007, ApJ, 667, 930
le Roux, J. A., & Webb, G. M. 2009, ApJ, 693, 534
le Roux, J. A., & Webb, G. M. 2012, ApJ, 764, 104
le Roux, J. A., Zank, G. P., Milano, L. J., & Matthaeus, W. H. 2004, ApJ, 602, 396
le Roux, J. A., Zank, G. P., Webb, G. M., & Khabarova, O. V. 2015a, ApJ, 801, 112
le Roux, J. A., Zank, G. P., Webb, G. M., & Khabarova, O. V. 2015b, J. Phys.: Conf. Series, 642, 012015

le Roux, J. A., Zank, G. P., Webb, G. M., & Khabarova, O. V. 2016, ApJ, 827, 47
Lee, M. A. 2005, ApJS, 158, 38
Li, G., Zank, G. P., & Rice, W. K. M. 2005, JGR, 110, A06104
Li, X., Guo, F., Li, H., & Birn, J. 2018, ApJ, 855, 80
Li, X., Guo, F., Li, H., & Li, G. 2015, ApJL, 811, L24
MacBride, B. T., Smith, C. W., & Vasquez, B. J. 2010, JGR, 115, A07105
Matthaeus, W. H., Goldstein, M. L., & Roberts, D. A. 1990, JGR, 95, 20673
Ng, C. K., & Reames, D. V. 2008, ApJL, 686, L123
Ng, C. K., Reames, D. V., & Tylka, A. J. 2003, ApJ, 591, 461
Northrop, T. G. 1963, RvGSP, 1, 283
Oka, M., Phan, T.-D., Krucker, S., Fujimoto, M., & Shinohara, I. 2010, ApJ, 714, 915
Oughton, S., Matthaeus, W. H., Wan, M., & Osman, K. T. 2015, RSPTA, 373, 20140152
Pritchett, P. L. 2008, PhPl, 15, 102105
Schlickeiser, R. 1989, ApJ, 336, 243
Schoeffler, K. M., Drake, J. F., & Swisdak, M. 2011, ApJ, 743, 70
Schwadron, N. A., Fisk, L. A., & Gloeckler, G. 1996, GeoRL, 23, 2871
Scudder, J. D., Karimabadi, H., Daughton, W., & Roytershteyn, V. 2015, PhPl, 22, 101204
Servidio, S., Greco, A., Matthaeus, W. H., Osman, K. T., & Dmitruk, P. 2011, JGR, 116, A09102
Shalchi, A., Bieber, J. W., Matthaeus, W. H., & Qin, G. 2014, ApJ, 616, 617
Shebalin, J. V., Matthaeus, W. H., & Montgomery, D. 1983, JPlPh, 29, 525
Smith, C. W., Isenberg, P. A., Matthaeus, W. H., & Richardson, J. D. 2016, ApJ, 638, 508
Song, H.-Q., Chen, Y., Li, G., Kong, Z.-L., & Feng, S.-W. 2012, PhRvX, 2, 021015
Tessein, J. A., Matthaeus, W. H., Wan, M., et al. 2013, ApJL, 776, L8
Tessein, J. A., Ruffolo, D., Matthaeus, W. H., & Wan, M. 2016, GeoRL, 43, 3620
Trenchi, L., Bruno, R., Telloni, D., et al. 2013, ApJ, 770, 11
Turner, A. J., Gogoberidze, G., & Chapman, S. C. 2012, PhRvL, 108, 085001
Vanio, R., & Schlickeiser, R. 1998, A&A, 331, 793
Verkhoglyadova, O. V., Zank, G. P., & Li, G. 2015, PhR, 557, 1
Webb, G. M., Martinic, M. J., & Moraal, H. 1981, Proc. ICRC (Paris), 10, 109
Weygand, J. M., Matthaeus, W. H., Dasso, S., et al. 2009, JGR, 114, A07213
Weygand, J. M., Matthaeus, W. H., Dasso, S., & Kivelson, M. G. 2011, JGR, 116, A08102
Yoon, P. H. 2017, PhPl, 25, 011603
Zank, G. P., Adhikari, L., Hunana, P., et al. 2017, ApJ, 835, 147
Zank, G. P., Dosch, A., Hunana, P., et al. 2012, ApJ, 745, 35
Zank, G. P., Hunana, P., Mostafavi, P., et al. 2015a, ApJ, 814, 137
Zank, G. P., Hunana, P., Mostafavi, P., et al. 2015b, J. Phys.: Conf. Series, 642, 012031
Zank, G. P., le Roux, J. A., Webb, G. M., Dosch, A., & Khabarova, O. 2014, ApJ, 797, 28
Zank, G. P., & Matthaeus, W. H. 1992, JPlPh, 48, 85
Zank, G. P., & Matthaeus, W. H. 1993, PhFlA, 5, 257
Zank, G. P., Rice, W. K. M., & Wu, C. C. 2000, JGR, 105, 25079
Zhang, M., & Lee, M. A. 2013, SSRv, 176, 133
Zheng, J. 2017, PhD thesis, Univ. Alabama
Zheng, J., & Hu, Q. 2016, JPhCS, 767, 0120
Zheng, J., & Hu, Q. 2018, ApJL, 852, L23
Zheng, J., Hu, Q., Chen, Y., & le Roux, J. A. 2017, JPhCS, 900, 012024
Zhou, Y., & Matthaeus, W. H. 1990, JGR, 95, 10291